



논문개요집

ISSN 2233-9485(Print)
ISSN 2233-9574(Online)

한국자기학회 2020년도 동계학술연구발표회

KMS 2020 Winter Conference

논문개요집



일시 2020. 11. 25.(수)~27.(금)

장소 여수 디오션리조트

주최 한국자기학회

후원   여수시  전라남도 관광재단

Digests of the KMS 2020 Winter Conference
The Korean Magnetism Society

사단법인 한국자기학회

한국자기학회 2020년도 동계학술연구발표회

KMS 2020 Winter Conference

논문개요집



일시

2020. 11. 25.(수)~27.(금)

장소

여수 디오션리조트

주최

한국자기학회

후원

KCFST
한국과학기술단체총연합회



여수시



전라남도 관광재단

“이 발표논문집은 정부재원(과학기술진흥기금 및 복권기금)으로 한국과학기술단체총연합회의 지원을 받아 발간되었음”

공지사항

1. 포스터발표를 하시는 회원은 아래의 사항을 지켜주시기 바랍니다.

1) 코로나19 확산에 따른 영향으로 포스터 현장게시는 취소되었고 직접 발표하는 시간은 없습니다.

포스터 질의응답(Q&A)은 11월 26일(목) 동계학술대회 온라인 홈페이지를 통한 비대면 개별 접촉으로 진행됩니다.

2. 일정

11월 25일(수)	13:00~	참가자 등록					
	14:30~18:00	Special Session I (그랜드볼룸A)					
	18:00~21:30	강습회 (그랜드볼룸A)					
11월 26일(목)	08:30~	참가자 등록					
	09:00~18:45	포스터 발표					
	09:00~12:30	09:00 ~ 12:20	Special Session II (그랜드볼룸A)	09:00 ~ 12:30	Oral Session I (그랜드볼룸C)	09:00 ~ 11:50	Special Session III (에메랄드AB)
	12:30~13:30	점심식사					
	13:30~17:00	Oral Session II (그랜드볼룸A)		Special Session IV (그랜드볼룸C)		Special Session V (에메랄드AB)	
	17:00~17:30	스핀트로닉스 초청강연 I (그랜드볼룸A)					
	17:30~18:00	총회초청강연 I (그랜드볼룸A)					
	18:00~18:30	총회초청강연 II (그랜드볼룸A)					
	18:30~19:00	한국자기학회 정기총회 및 시상식 (그랜드볼룸A)					
	19:00~	만찬취소					
11월 27일(금)	08:30~	참가자 등록					
	09:00~12:30	09:00 ~ 12:30	Oral Session III (에메랄드AB)	09:00 ~ 11:30	Special Session VI (그랜드볼룸C)	09:00 ~ 11:00	Special Session VII (그랜드볼룸A)

3. 11월 26일(목) 『포스터 최우수 및 우수발표상 시상』 및 저녁 만찬은 코로나19 확산에 따른 영향으로 부득이하게 취소되었습니다.



11월 25일[수]

시간	프로그램
13:00 ~	등록
	Special Session I (그랜드볼룸A) 'SOT 소자' (비공개 세션) 좌장: 김영근(고려대)
14:30 ~ 14:50	초S-I-1. Pd 굴곡 변화에 따른 자기적 특성과 iDMI의 변화 김영근(고려대)
14:50 ~ 15:10	초S-I-2. Orbital Hall effect induced spin-orbit torque via orbital-to-spin conversion 박병국(KAIST)
15:10 ~ 15:30	초S-I-3. Spin-Orbit Torque in Pd/Co/Pd(t) Heterostructure 홍종일(연세대)
15:30 ~ 15:50	초S-I-4. SOT-MRAM based crossbar array for Neural Network 박종선(고려대)
15:50 ~ 16:10	초S-I-5. Non-standard angular dependence of spin-orbit torques in ferromagnet/heavy metal bilayers 이경진(KAIST)
16:10 ~ 16:20	Coffee Break
16:20 ~ 16:40	초S-I-6. Pt계면 조절에 따른 Spin Orbit Torque의 향상 임상호(고려대)
16:40 ~ 17:00	초S-I-7. Spin Hall Conductivity of W-N alloys: A First Principles Study 임성현(울산대)
17:00 ~ 17:20	초S-I-8. Observation of stripe width variation, skyrmion formation, and spin pumping in trilayer structure Py/Ti/CoFeB 황찬용(KRISS)
17:20 ~ 17:40	초S-I-9. Spin-Hall-Effect-Modulation Skyrmion Oscillator 최석봉(서울대)
17:40 ~ 18:00	초S-I-10. Manipulation of Critical Switching Current and Effective Field of Spin-Orbit Torque by Interface Modulation 유천열(DGIST)
	강습회 (그랜드볼룸A) "대학원생 진행세션" 좌장: 임성현(울산대)
18:00 ~ 18:50	T-1. 자기센서의 원리와 응용 손대락((주)센서피아) 진행: 신정훈(한양대 박사과정)
18:50 ~ 19:40	T-2. Accelerating on the long way to magnetic materials design Stefano Sanvito(Tritiny College Dublin) 진행: Nguyen Thi Thanh Huong(DGIST/울산대 박사과정)
19:40 ~ 21:30	T-3. Topological Band Theory in a Nutshell 김영국(성균관대) 진행: 김석중(고려대학교 석사과정)

11월 26일[목]

시간	프로그램					
09:00 ~ 18:45	<div>포스터발표</div> <div>[1] Magnetic theory and calculation [2] Magnetization dynamics [3] Hard-magnetic Material</div> <div>[4] Soft-magnetic Material [5] Semiconductor spintronic [6] Spin orbit coupling and related phenomena</div> <div>[7] Nano-structured materials [8] Spin transfer torque for magnetic memory [9] Nanoscale Magnetis</div> <div>[10] Magnetic Oxides and Multiferroic [11] Biomedical Magnetic [12] Sensor and Application</div> <div>[13] 회원 참여 스페셜 세션 (자성소재, 부품, 장비핵심기술개발, 자기센서, 양자컴퓨팅, 산화물자성체, 의료 장비 및 소재 등)</div> <div>[14] Others</div>					
08:30 ~	등록					
09:00 ~ 12:30	Special Session II (그랜드볼룸A) ‘산화물 자성체 세션’		Oral Session I (그랜드볼룸C) “자기이론 및 의공학, 대학원생 세션”		Special Session III (에메랄드AB) ‘Hard & Soft Magnetic Materials’	
	좌장: 문은국(KAIST)		좌장: 제송근(전남대)/김상훈(울산대)		좌장: 최철진(재료연구소)	
	09:00 ~ 09:30	초S-II-1, Giant topological Hall response induced by spin chirality fluctuation in a ultraclean frustrated antiferromagnet	09:00 ~ 09:20	O-I-1, The study of planar Hall effect in CoFeB/MgO with various metal under layer structure	09:00 ~ 09:25	초S-III-1, Rare-Earth Permanent Magnets for the Fourth Industrial Revolution: Status and Prospects
		김준성(포항공대)	09:20 ~ 09:40	O-I-2, 기계학습과 인공지능 기법을 이용한 펄스와전류 신호해석		이우영(연세대)
	09:30 ~ 10:00	초S-II-2, First-principles study of magnetic van der Waals materials: from CrI3 and Fe3GeTe2 to VSe2 and VTe2	09:40 ~ 10:00	O-I-3, Unidirectional Transport of Magnetic Skyrmion through Symmetry- Breaking of Potential Energy Barriers	09:25 ~ 09:50	초S-III-2, Permanent magnets for high efficiency motor
		한명준(KAIST)		정대한(UNIST)		박지훈(재료연구소)
	10:00 ~ 10:30	초S-II-3, Terahertz Spectroscopy of Magnons in HoFeO3 and Detection of Rabi Splitting	10:00 ~ 10:20	O-I-4, Skyrmion calculator based on boundary annihilation	09:50 ~ 10:15	초S-III-3, Finite-element micromagnetic simulation study of NdFeB magnets
		김재훈(연세대)		송무준(KAIST)		김상국(서울대)
	10:30 ~ 11:00	초S-II-4, Random singlets in quantum magnets with frustration and disorder	10:20 ~ 10:40	O-I-5, Giant spin Seebeck effect (SSE) in two-dimensional ferromagnetic CrI3 monolayer	10:15 ~ 10:40	초S-III-4, Microstructure of Grain Boundary Diffusion Processed Nd-Fe-B Sintered Magnets : Microstructural Characteristics of HRE- rich Shells and Grain Boundary Phases
		최광용(중앙대)	10:40 ~ 10:50	Coffee Break		김태훈(재료연구소)



11월 26일[목]

시간		프로그램				
09:00 ~ 12:30	11:00 ~ 11:30	초S-II-5. An intermediate magnetic phase of a proximate Kitaev system in in-plane magnetic fields	10:50 ~ 11:10	O-I-6. 유연기판을 활용한 비정질 금속 박막의 연신저항특성 확인 김지호(고려대)	10:40 ~ 11:00	Coffee Break
		김범현(KIAS)	11:10 ~ 11:30	O-I-7. Educational a Pair of PET Detection System Based on 1D-RCD and Oscilloscope 이민호(전남대)	11:00 ~ 11:25	초S-III-5. Comparison of Soft magnetic composite cores from both Fe-based amorphous and crystalline powders 김휘준(KITECH)
	11:30 ~ 12:00	초S-II-6. Identification of a Kitaev Quantum Spin Liquid by Magnetic Field Angle Dependence 황규성(KIAS)	11:30 ~ 11:50	O-I-8. Nonvanishing anomalous Hall effect of the quaternary Heusler compound TiZrMnAl with compensated ferrimagnetism Thu-Thuy Hoang(울산대)	11:25 ~ 11:50	초S-III-6. Fabrication of Anisotropic Bulk Manget by Hot-deformation Process using Nd-lean Nd-Fe-B Melt-spun Powder 이정구(재료연구소)
	12:00 ~ 12:20	초S-II-7. Describing the magnetic structure and origin of band gap on Ba2CuOsO6 system; density functional theory approach 이창훈(포항공대)	11:50 ~ 12:10	O-I-9. Electric filed dependent valley polarization in 2D WSe2/CrGeTe3 heterostructure 브라힘마파(부경대)		
			12:10 ~ 12:30	O-I-10. A New Methods for Distinguishing Phoswich Detector consisting of LYSO and GAGG 양진규(전남대)		
	12:30 ~ 13:30	점심식사				
13:30 ~ 17:00	Oral Session II (그랜드볼룸A) “대학원생 및 신진과학자 세션” 좌장: 양승모(KRIS)/문경웅(KRIS)		Special Session IV (그랜드볼룸C) ‘Theoretical magnetism and experiments’ 좌장: 임성현(울산대)		Special Session V (에메랄드AB) ‘Electro-Magnetic Energy Convergence : MOTOR Session’ 좌장: 이정중(전자부품연구원)	
	13:30 ~ 13:50	O-II-1. Astroid in spin Hall current & Dzyaloshinskii-Moriya interaction 윤창진(고려대)	13:30 ~ 13:55	초S-IV-1. Physical Properties of Rare-Earth f-electron Systems: Past and Present 민병일(포항공대)	13:30 ~ 13:55	초S-V-1. Electromagnetic Force and Vibration Analysis of Outer Rotor Surface-Mounted Permanent Magnet Synchronous Motor 김재현(한양대)
	13:50 ~ 14:10	O-II-2. Gate-tunable large nonreciprocal charge transport in noncentrosymmetric LaAlO3/SrTiO3 interfaces 최대성(UNIST)				

11월 26일[목]

시간		프로그램				
13:30 ~ 17:00	14:10 ~ 14:30	O-II-3. Direct terahertz probing of the fundamentals of anisotropic magnetoresistance 박지호(KAIST)	13:55 ~ 14:20	초S-IV-2. MTG (Magnetism Theory Group) of Prof. B. I. Min at POSTECH and related academic genealogy 장영록(인천대)	13:55 ~ 14:20	초S-V-2. 토크밀도 향상을 위한 로봇 구동용 SPM 동기전동기 설계에 관한 연구 김성일(호서대)
	14:30 ~ 14:50	O-II-4. A large reduction in switching current in W/CoFeB heterostructures with W-N interfacial layers 이민혁(고려대)	14:20 ~ 14:45	초S-IV-3. Valley magnetic domain: A new pathway to valleytronics 이재동(DGIST)	14:20 ~ 14:45	초S-V-3. 시간 별 1일 부하변동을 고려한 에스컬레이터 시스템의 에너지 측정 및 추정 김해중(남해대)
	14:50 ~ 15:10	O-II-5. Electric-field control of deterministic spin-orbit torque switching via laterally modulated Rashba effect in Pt/Co/AlOx structures 강민구(KAIST)	14:45 ~ 15:10	초S-IV-4. Time-dependent density functional theory calculations of spin- phonon dynamics and band topology of two- dimensional materials 박노정(UNIST)	14:45 ~ 15:10	초S-V-4. A Design of Halbach Cylinder Shape Sintered Nd-Fe-B Magnets for Servo Motors 김효준(자화전자)
	15:10 ~ 15:30	O-II-6. Investigation of Weak Antilocalization Effect in Co- dusted Graphene films 도티나(이화여대)	15:10 ~ 15:20	Coffee Break	15:10 ~ 15:20	Coffee Break
	15:30 ~ 15:40	Coffee Break	15:20 ~ 15:45	초S-IV-5. Towards Rare-Earth and Rare-Earth-Free Permanent Magnets Designed Using First- Principles Dorj Odkhuu(인천대)	15:20 ~ 15:45	초S-V-5. 해석적방법을 이용한 표면부착형 영구자석 기기의 가진원 해석 최장영(충남대)
	15:40 ~ 16:00	O-II-7. Growth and analysis of novel A15 W3Ta Heavy metal layer 서정우(한양대)	15:45 ~ 16:10	초S-IV-6. Discovery of van der Waals magnets and beyond 박제근(서울대)	15:45 ~ 16:10	초S-V-6. A Study on the Electromagnetic Field Design of BLDC Motor For Electric Outboard Propulsion 이호준(청주대)
	16:00 ~ 16:20	O-II-8. Manipulation of spin-orbit torque in HM/FM/Oxide frame by external gate voltage 신정훈(한양대)	16:10 ~ 16:35	초S-IV-7. ARPES study of a Multifold Fermionic Semimetal PdSb2 노한진(전남대)	16:10 ~ 16:35	초S-V-7. Torque Improvement Design of Interior Permanent Magnet Synchronous Motor considering Saturation of Rotor Core 윤명환(KETI)
	16:20 ~ 16:40	O-II-9. Universality of stripe domain width change by an in-plane magnetic field 양승모(KRISS)	16:35 ~ 17:00	초S-IV-8. Textured Spin Singlets in an infinite layered nickelate 이관우(고려대)	16:35 ~ 17:00	초S-V-8. Rotor Design of Ultra- high-speed Motor for Electric Turbo Charger Considering Mechanical Stiffness 임명섭(한양대)
	16:40 ~ 17:00	O-II-10. Discovery of magnetoelectric coupling in a van der Waals compound CuCrP2S6 박창배(서울대)				



11월 26일[목]

시간	프로그램
	스핀트로닉스 초청강연 I (그랜드볼룸A) 좌장: 김갑진(KAIST)
17:00 ~ 17:30	초O-I-1. Thermoelectric energy conversion utilizing spin degree of freedom 진현규(포항공대)
	총회초청강연 I (그랜드볼룸A) 좌장: 정종율(충남대)
17:30 ~ 18:00	초O-I-1. 강일구박사님의 생애와 업적 김희중(KIST)
	총회초청강연 II (그랜드볼룸A) 좌장: 정종율(충남대)
18:00 ~ 18:30	초O-II-2. 2021년이후 소재 • 부품분야 과학기술정보통신부/연구재단 정책연구사업 소개 이영국(한국연구재단)
18:30 ~ 19:00	한국자기학회 정기총회 및 시상식 (그랜드볼룸A)
19:00 ~	만찬 취소

11월 27일[금]

시간	프로그램					
08:30 ~	등록					
09:00 ~ 12:30	Oral Session III (에메랄드AB) ‘Hard & Soft Magnetics’		Special Session VI (그랜드볼룸C) ‘Medical Magnetics’		Special Session VII (그랜드볼룸A) ‘Bio-Med-Magnetics convergence’	
	좌장: 임혜인(숙명여자대학교)		좌장 : 한만석(강원대)/안우상(울산의대)		좌장: 김철기(DGIST)	
	09:00 ~ 09:20	O-III-1. Coercivity improvement of Nd-Cu infiltrated Nd-Fe-B hot-deformed magnets by microstructure modification of initial HDDR powders 유재경(재료연구소)	09:00 ~ 09:20	초S-VI-1. Transcranial Magnetic Stimulation for the Treatment of Multiple Neurologic Conditions; Focused on Clinical Application 정중우(강원대)	09:00 ~ 09:30	초S-VII-1. FePt-Ferrite heterogeneous nanoparticles: One-pot synthesis with controlled phase and their enhanced biocompatibility
	09:20 ~ 09:40	O-III-2. Coercivity enhancement of (Nd, M)-Fe-B hot-deformed magnet by post-annealing treatment 김가영(재료연구소)	09:20 ~ 09:40	초S-VI-2. Image Quality Assessments According to the Angle of Tilt of a Flex Tilt Coil Supporting Device: An ACR MRI Phantom Study 장지성(서울아산병원)	09:30 ~ 10:00	엄윤지(DGIST)
	09:40 ~ 10:00	O-III-3. Phase transformation and magnetic properties of Sm(Fe0.8Co0.2)11Ti bulk magnets 천취동(재료연구소)	09:40 ~ 10:00	초S-VI-3. MRI 보어 구경에 따른 검사 시 실효 단면적 분석 정현근(HK리서치센터)		초S-VII-2. 생체기능화 된 자성입자의 프로그래밍 가능한 이송을 위한 다중 전송 게이트
	10:00 ~ 10:20	O-III-4. First-Principles Study of Magnetic Properties of MnBi with Bi-site Substitutes 톱신(인천대)	10:00 ~ 10:20	초S-VI-4. Feasibility of fast non-local means algorithm for T1-weighted MR images using BrainWeb: A simulation study 강성현(가천대)		10:00 ~ 10:30
	10:20 ~ 10:40	O-III-5. Control of magnetic properties of MnBi by elements doping 양양(재료연구소)	10:20 ~ 10:30	Coffee break	초S-VII-3. Label-free electrochemical biosensor for miRNA-122 biomarker detection based on naturally reduced rGO/Au nanocomposite Satish(DGIST)	
		10:30 ~ 10:50	초S-VI-5. A Study on the Evaluation of Dose Distribution Error According to the Spacing and Angle of Bolus in Electromagnetic Radiation 김정호(선린대)	10:30 ~ 11:00	초S-VII-4. Development of magnetic-based pressure sensor for pulse pattern detection 김미진(DGIST)	



11월 27일[금]

시간		프로그램			
09:00 ~ 12:30	10:40 ~ 10:50	Coffee break	10:50 ~ 11:10	초S-VI-6. Feasibility of Customized 3d Bolus for H&N cancer: Applied to Oral Cavity and Supraclavicular Area	
	10:50 ~ 11:10	O-III-6. Enhancement of magnetic properties of Fe-rich compounds with tetragonal ThMn12 structure by mixing non- magnetic materials 임정태(재료연구소)		백승협(강원대학교병원)	
	11:10 ~ 11:30	O-III-7. 모터용 연자성 복합재 분말코팅 기술개발 김영민(현대자동차)	11:10 ~ 11:30	초S-VI-7. The effect of patient size on radiation with size- specific dose estimates for computed tomography dose index 전필현(연세대병원)	
	11:30 ~ 11:50	O-III-8. Structural and magnetic properties of rare earth doped Fe by ion beam implantation 이준혁(부산대)			
	11:50 ~ 12:10	O-III-9. Spin-thermoelectric energy conversion based on molecule-based magnetic thin film 오인선(UNIST)			
	12:10 ~ 12:30	O-III-10. First-principles prediction of enhancing magnetic anisotropy and stability of α ''-Fe16N2 phase 어취르(인천대)			

CONTENTS

KMS 2020 Winter Conference

11월 25일(수) 14:30~18:00
Special Session I 'SOT 소자' (비공개 세션)

그랜드볼룸A

✽ 좌 장: 김영근(고려대)

초S-I-1	14:30	Pd 굴곡 변화에 따른 자기적 특성과 IDMI의 변화 3
		A. S. Samardak [†] , A. V. Davydenko, A. G. Kolesnikov, A. Yu. Samardak, A. G. Kozlov, Bappaditya Pal, A. V. Ognev, A. V. Sadovnikov ^{3,4} , S. A. Nikitov ^{3,4} , A. V. Gerasimenko, 차인호, 김용진, 김규원, Oleg A. Tretiakov, 김영근*
초S-I-2	14:50	Orbital Hall effect induced spin-orbit torque via orbital-to-spin conversion 4
		Soogil Lee, Min-Gu Kang, Dongwook Go, Taekhyeon Lee, Dohyoung Kim, Kab-Jin Kim, Sanghoon Kim, and Byong-Guk Park*
초S-I-3	15:10	Spin-Orbit Torque in Pd/Co/Pd(t) Heterostructure 5
		Keesung Kim, Jongill Hong*
초S-I-4	15:30	SOT-MRAM based crossbar array for Neural Network 6
		Yunho Jang*, Taehwan Kim, Jooyoon Kim, Jongsun Park*
초S-I-5	15:50	Non-standard angular dependence of spin-orbit torques in ferromagnet/heavy metal bilayers 7
		Kyung-Jin Lee*
초S-I-6	16:20	Pt계면 조절에 따른 Spin Orbit Torque의 향상 8
		김영래, 박경배, 임상호*
초S-I-7	16:40	Spin Hall Conductivity of W-N alloys: A First Principles Study 9
		Quynh Anh T. Nguyen, D. D. Cuong, S. C. Hong, and Sonny H. Rhim*
초S-I-8	17:00	Observation of stripe width variation and skyrmion formation and spin pumping in trilayer structure Py/Ti/CoFeB 10
		Kyoung-Woong Moon [†] , Seungmo Yang [†] , Tae-Seong Ju, Changsoo Kim, Byong Sun Chun, Chanyong Hwang*
초S-I-9	17:20	Spin-Hall-Effect-Modulation Skyrmion Oscillator 11
		Hyun-Seok Whang, Sug-Bong Choe*
초S-I-10	17:40	Manipulation of Critical Switching Current and Effective Field of Spin-Orbit Torque by Interface Modulation 12
		Ki-Seung Lee, Suhyeok An, Eunchong Baek, Jin-A Kim, Chun-Yeol You*

11월 25일(수) 18:00~21:30
강습회 '대학원생 진행세션'

그랜드볼룸A

✿ 좌 장: 임성현(울산대)

T-1	18:00	자기센서의 원리와 응용..... 15 손대락*
T-2	18:50	Accelerating on the long way to magnetic materials design..... 16 Stefano Sanvito*
T-3	19:40	Topological Band Theory in a Nutshell..... 17 Youngkuk Kim*

11월 26일(목) 09:00~18:45
Session : 포스터발표

그랜드볼룸B

○ Session MT [Magnetic theory and calculations]

MT01	Poster	Generalized Equation for Magnetic Domain Wall Chirality with Consideration of Domain Wall tilting 21 Jung-Hyun Park*, Dae-Yun Kim, Yune-Seok Nam, Hyun-Seok Whang, Sug-Bong Choe*
MT02	Poster	Influence of W Thickness on Perpendicular Magnetic Anisotropy in Pt/Co/W(111) Superlattices 22 Thi Huynh Ho*, Sanghoon Kim, S. H. Rhim†, S. C. Hong†
MT03	Poster	Emergence of the anomalous Hall effect from a compensated collinear ferrimagnetism..... 23 Minkyu Park*, Guihyun Han, S. H. Rhim
MT04	Poster	Local control of magnetization of CoO _x thin films by He ion irradiation 24 Jisu Kim*, Seongboo Park, Eunkang Park, Nyun Jong Lee, Taekhyeon Lee, Ji-Seok Yang, Ki-Seung Lee, Chun-Yeol You, Kab-Jin Kim, Young-Han Shin, Sanghoon Kim
MT05	Poster	Non-vanishing Anomalous Hall Effect in nearly Compensated Ferrimagnet Mn ₃ Al 25 Guihyun Han*, Minkyu Park, Su Yeon An, Soon Cheol Hong, S.H. Rhim
MT06	Poster	Two-dimensional Fe ₃ GeTe ₂ : strain effect on magneto-crystalline anisotropy ... 26 G Hye Kim*, Qurat ul Ain, Soon Cheol Hong, S. H. Rhim
MT07	Poster	Mn ₄ C의 자성: 제일원리 계산..... 27 이준규*, 임성현, 홍순철†
MT08	Poster	IPMSM의 출력밀도 개선을 위한 권선법 선정 및 회전자 형상 변경을 통한 영구자석의 감자 개선 설계 28 Ju-Hyeong Moon ^{1*} , Dong-Hwan Kim ² , Jong-Hwan Cho ³ , Sung-Gu Lee ⁴ , Dong-Woo Kang ¹
MT09	Poster	Unusual pressure-induced quantum phase transition from superconducting to charge-density wave state in LuPd ₂ In 29 Heejung Kim*, J. H. Shim, Sooran Kim, Jae-Hoon Park, Kyoo Kim, B. I. Min†

MT10	Poster	Structural Control of Demagnetizing Field in the Magnet 30 Namkyu Kim [*] , Hee-Sung Han, SooSeok Lee, and Ki-Suk Lee [†]
MT11	Poster	X-선 강자성공명으로 연구된 Py/Ti/CoFeB 구조에서의 스핀펄핑 현상 31 김창수 [*] , 최원창, 김현중, 문경웅, 양승모, 홍정일, 황찬용
MT12	Poster	Temperature and angle-dependence magnetization reversal behavior in a FePt-C granular thin film 32 Donghyeon Lee [*] , Suzuki Ippei, Seyeop Jung, Nyun Jong Lee, Heechan Jang, Eunkang Park, Takahashi Yukiko, Sanghoon Kim [†]
MT13	Poster	Three-dimensional dynamic mode of the magnetic vortex in a permalloy circular disk 33 Hee-Sung Han, Dae-Han Jung, Suyeong Jeong [*] , Namkyu Kim, Sooseok Lee, Ki-Suk Lee
MT14	Poster	The Practical Energy Product of Cylindrical Core/shell Consist of Soft- and Hard-magnetic Materials 34 Namkyu Kim [*] , Hee-Sung Han, SooSeok Lee, Ki-Suk Lee [†]
MT15	Poster	Breathing Modes of a Magnetic Skyrmion on a Defective Surface 35 Namkyu Kim [*] , Hee-Sung Han, Dae-Han Jung, Ki-Suk Lee [†]
MT16	Poster	Guided Motion of a Magnetic Skyrmion Confined in Spatially Modulated Dzyaloshinskii-Moriya Interaction 36 Dae-Han Jung [*] , Hee-Sung Han, Namkyu Kim, and Ki-Suk Lee [†]
MT17	Poster	Generative machine learning model guided by magnetic Hamiltonian 37 H. Y. Kwon [*] , H. G. Yoon, S. M. Park, D. B. Lee, J. W. Choi, and C. Won
○ Session MD [Magnetization dynamics]		
MD01	Poster	Development of ISHE-FMR system in extremely low temperature 38 Jungmin Park [*] , Seulgi Koo, Taiwoon Eom, Seung-Young Park, Younghun Jo [*]
MD02	Poster	Determination scheme for DMI based on chiral domain wall roughness measurement 39 Ji-Sung Yu [*] , Dae-Yun Kim, Joon Moon, Seong-Hyub Lee, Jun-Young Chang, Duck-Ho Kim, Sug-Bong Choe [†]
MD03	Poster	Magnetic properties tailoring by local interface engineering at Pt/Co/MgO structure 41 Suhyeok An [*] , Ki-Seung Lee, Jin-A Kim, Chun-Yeol You [†]
MD04	Poster	A 3-dimensional control of exchange bias by spin orbit torque in Pt/Co/IrMn heterostructure 42 Eunchong Baek [*] , Suhyeok An, Chan-Kang Lee, Ki-Seung Lee, Woo-Yeong Kim, Chun-Yeol you
MD05	Poster	Linear Dependence of Creep Scaling Constant on Co-Layer Thickness ... 43 Seong-Hyub Lee [*] , Joon Moon, Ji-Sung Yu, Sug-Bong Choe [†]
MD06	Poster	Magnetic and mechanical properties of 17-4PH stainless steel fabricated by Metal FDM additive manufacturing 44 최광수 [*] , 이승훈, 정효연 [†]

MD07	Poster	Re203 나노입자의 극저온 자기열량효과 45 Kiran Shinde, Tien Van Manh, 유성초, 김동현*
MD08	Poster	Dependence of magnetic properties and structural characteristics on low Boron concentration in CoFeB-MgO thin films 46 Jun-Su Kim*, Woo-Yeong Kim, Jaehun Cho, June-seo Kim, Gukcheon Kim, Jinwon Jung, Chun-Yeol You*
MD09	Poster	Investigating the structural magnetic and magnetocaloric properties in Ce-doped La_{1.4-x}Ce_xCa_{1.6}Mn₂O₇ (0 ≤ x ≤ 0.4) bilayer manganites 48 Akshay Kumar*, Min Ji Shin, Ji Eun Lee, Bon Heun Koo†
MD10	Poster	Current induced spin-orbit toques in two-dimensional Fe₃GeTe₂ nanoflakes 49 Sungyu Park*, Eun-su An, Junho Seo, Jun Sung Kim
MD11	Poster	Domain wall energy analysis in trapezoid shaped Hall bar with perpendicular magnetic anisotropy 50 Dongryul Kim, Suhyeok An, Eunchong Baek, Woo-yeoung Kim, Ki-seung Lee, Chun-yeol You†
MD12	Poster	Manipulating asymmetric domain wall motion by uniaxial realignment of antiferromagnet spins in exchange coupled system with Dzyaloshinskii-Moriya interaction effect 51 Hyun-Joong Kim*, Soong-Geun Je, Won-Chang Choi, Kyoung-Woong Moon, Seungmo Yang, Changsoo Kim, Jung-Il Hong, Chanyong Hwang
MD13	Poster	Spin-thermoelectric energy conversion for transparent thermoelectrics 52 HyeonJung Jung*, Inseon Oh*, Jung-Woo Yoo†
MD14	Poster	Direct Investigation of Lattice Expansion of Ni_xFe_{1-x} alloy films by Ultrafast Sagnac Interferometry 53 Yooleemi Shin, Ji-Wan Kim*
MD15	Poster	Large Spin-Orbit Torque and Strong Two Magnon Scattering in AuPt/Ferromagnet bilayers 54 D. J. Lee*, D. H. Yun, B. -C. Min, H. C. Koo, K.-J. Lee, O. J. Lee
MD16	Poster	Magnetic Oscillation on Indirectly Coupled Ferromagnetic Layers 55 D. H. Yun*, D. J. Lee, B. -C. Min, H. C. Koo, K.-J. Lee, O. J. Lee
MD17	Poster	Observation of magnetic field induced ferroelectricity in the poly- and single crystals of CaFe₃(PO₄)₃ 56 Kwang-Tak Kim, Aga Shahee, Joong-Woo Lee, Voma Uday Kumar, B. Koteswara Rao, Kee Hoon Kim

○ Session HM [Hard-magnetic Materials]

HM01	Poster	Designing the composition of the Fe-Ni-Si-B-Cu-P amorphous alloy based on Nanomet 57 JongHee Han*, Haein Choi-Yim
HM02	Poster	Fabrication of Epsilon Hard Ferrites for Electromagnetic Wave Absorption Application 58 Min-Ji Pyo*, Gi-Ryeon Jo, Hee-Lack Choi, Youn-Kyoung Baek†

HM03	Poster	Facile Synthesis of Al-Ca Substituted M-type Hexaferrites with a Gigantic Coercivity	59
		Gi-Ryeon Jo [*] , Min-Ji Pyo, Young-Guk Son, Youn-Kyoung Baek [†]	
HM04	Poster	Sm-Fe계 HDDR 분말의 결정구조에 따른 자기특성과 질화 거동	60
		노태성 [*] , 차희령, 김태훈, 김양도 [†] , 이정구 [†]	
HM05	Poster	Iron deficiency of La-Co substituted Sr M-type hexaferrites on the magnetic properties	61
		Kang-Hyuk Lee [*] , Junho Park, SungJoon Choi, Sang-Im Yoo [†]	
HM06	Poster	Preparation for qualified MnBi powder via process control	62
		Su Yeon Ahn [*] , Yang Yang, Jung Tae Lim, Jihoon Park, Jong-Woo Kim, Chul-Jin Choi	
HM07	Poster	Structural and Magnetic Property Modification of [111]-oriented Epitaxial CoFe₂O₄ Films	63
		Tae-Seong Ju [*] , Dooyong Lee, Chang-Woo Cho, Jisung Lee, Hyegyung Kim, Jong-Han Won, Kyoung Soon Choi, Se-Jeong Park, Jouhahn Lee, Seungmo Yang, Chanyong Hwang, Sungkyun Park	
HM08	Poster	Rare-Earth-Free MnBi Permanent Magnets	64
		Hyun-Sook Lee [*] , Sumin Kim, Hongjae Moon, Wooyoung Lee [*]	
HM09	Poster	Effect of sintering temperature on the formation of epsilon Fe₂O₃ nanoparticles encapsulated by SiO₂	65
		Phuoc Cao Van, Trinh Nguyen Thi, Ha Yeong Ahn, Jong-Ryul Jeong [*]	

○ Session SM [Soft-magnetic Materials]

SM01	Poster	Thermal and Soft Magnetic Properties of Fe-based Amorphous Ribbons according to Changes in Fe/Co Ratio	66
		Hyunsol Son [*] , Haein Choi-Yim [*]	
SM02	Poster	Controlled Switching of Asymmetric Bloch wall in a Rectangular Ferromagnetic disk	67
		Sooseok Lee [*] , Hee-Sung Han, Young-Sang Yu, Soong-Geun Je, Myeonghwan Kang, Hye-Jin Ok, Namkyu Kim, Weilun Chao, Mi-Young Im [†] , Ki-Suk Lee [†]	
SM03	Poster	Effect of magnetic field on the synthesis of Ni nanowires	68
		Min Ji Shin [*] , Ji Eun Lee, Bon Heun Koo [*] , Seok Hwan Huh [†]	
SM04	Poster	스프레이 코팅을 적용하여 절연 특성을 높은 연자성 금속 파워인덕터의 투자율 향상에 관한 연구	69
		공선호 [*] , 안지훈, 김상우, 강예빈, 이보화 [†]	
SM05	Poster	나노분말을 함유한 연자성-고분자 복합체의 투자율 향상에 관한 연구	70
		김예래 [*] , 이민영, 우혁준, 정우현, 이보화 [†]	
SM06	Poster	The interfacial Dzyaloshinskii-Moriya interaction change due to insertion of the ferromagnet-heavy metal alloy	71
		Jeong Kyu Lee [*] , Junho Park, Gyu Won Kim, V.B. Bessonov, A.V. Telegin, A.V. Ognev, A.S. Samardak, Young Keun Kim	

SM07	Poster	Symmetry breaking in the formation of asymmetric Bloch wall in ferromagnetic dots.....	72
		Sooseok Lee*, Hee-Sung Han, Young-Sang Yu, Soong-Geun Je, Myeonghwan Kang, Hye-Jin Ok, Namkyu Kim, Weilun Chao, Mi-Young Im†, Ki-Suk Lee†	
SM08	Poster	Study on the fabrication of Fe-Based Electric Conductivity Alloy for Semiconductor Test Socket.....	73
		Sang-Uk Kim*, In-Ho Kim, Je-An Yu, Tae-Haeng Lee, Chang-Bin Song	

○ Session SS [Semiconductor spintronics]

SS01	Poster	Pd/Co/Pd 삼층 구조에서 상위 Pd층의 두께에 따른 스핀-궤도 토크의 변화에 관한 연구(A study on the effect of top Pd thickness on the spin-orbit torques in a Pd/Co/Pd trilayer).....	74
		김기성, 강범승, 이상호, 홍종일*	
SS02	Poster	Charge-to-spin interconversion without ferromagnetic material using spin Hall and Rashba effects	75
		Jeehoon Jeon*, Seong Been Kim, Taeyueb Kim, OukJae Lee, Suk Hee Han, Hyung-jun Kim, Hyun Cheol Koo, Jinki Hong	
SS03	Poster	Magnetoresistance of ferromagnet-semiconductors hybrid structure in spin Hall and strong Rashba effect at room temperature.....	76
		Seong Been Kim*, Hyung-jun Kim, Joonyeon Chang, Hyun Cheol Koo†	
SS04	Poster	비대칭 [Co/Pd/Pt]10 다층박막에서의 스핀궤도토크	78
		김영래*, 임상호	
SS05	Poster	분자선 에피택시를 이용한 2D 반데르발스 자성체 Fe3+xGeTe2 (FGT) 성장	79
		김주란*, 이상선, 박창배, 황찬용†	
SS06	Poster	Observation of unconventional Hall signal in ferrimagnet/oxide/silicon structure	80
		Jun-Ho Kang*, Soogil Lee, Dohyoung Kim, Seyeop Jung, Sanghoon Kim, Byong-Guk Park, Kab-Jin Kim	
SS07	Poster	Study of electronic structure of Bi thin films grown on the MoS2 surface.....	81
		Sang Wook Han*, Seungho Seong, J.-S. Kang, Eunsook Lee, Won Seok Yun, Soon Cheol Hong	

○ Session SO [Spin orbit coupling and related phenomena]

SO01	Poster	Perpendicular Magnetic Anisotropy Control via Wedge-Type Oxide Layer.....	82
		Chan-Kang Lee†, Jaehun Cho, KwangHyun Lee, Joonwoo Kim, June-Seo Kim†, Chun-Yeol You†	
SO02	Poster	Study on magnon-contribution to unidirectional spin Hall magnetoresistance in HM/FM bilayer structures.....	84
		Heechan Jang, Eunkang Park, Seyeop Jeong, Donghyun Lee, Jisu Kim, Kwangsu Kim, Nyun Jong Lee, Chun-Yeol You, Sanghoon Kim†	

S003	Poster	Study on charge-to-spin conversion in Pt/Py/perovskite trilayers 85 SeYeop Jeong [*] , Jongmin Lee, Heechan Jang, Eunkang park, Nyun Jong Lee, Sanghan Lee, Tae Heon Kim, Sanghoon Kim [*]
S004	Poster	Study on spin Hall magnetoresistance in Cr-based heterostructure 86 Eunkang Park [*] , Min-gu Kang, Soogil Lee, Byong-Guk Park, Sanghoon Kim [*]
S005	Poster	Investigation of Unidirectional Spin Hall Magnetoresistance in Epitaxial Cr/Fe Bilayer Films on MgO Substrates 87 Nguyen Thi Thanh Huong [*] , Nguyen Van Quang, Seyeop Jung, Heechan Jang, Eunkang Park, Nyun Jong Lee, Sunglae Cho, Jung-Il Hong, Sanghoon Kim [†]
S006	Poster	Spatially-Resolved Phonon and Magnon Population in magnetic insulator TmIG 88 Geun-Hee Lee [*] , Phuoc Cao Van, Jong-Ryul Jeong, and Kab-Jin Kim
S007	Poster	Spin Hall Conductivity in W-Ta Alloy 89 Dong-Soo Han [*]
S008	Poster	Reduced spin-orbit torque switching current by electrical modulation of easy cone states in Ta/CoFeB/Pt/MgO structures 90 Jimin Jeong [*] , Min-Gu Kang, Byong-Guk Park
S009	Poster	Fast Magneto-Ionic Switching of Interface Anisotropy Using Yttria-Stabilized Zirconia Gate Oxide 92 Dongwon Choi [*] , Sujin Jo, Byeong-Kwon Ju, Seonghoon Woo, Ki-Young Lee [†]
S010	Poster	Current-driven Spin Modulation in a van der Waals Fe₅GeTe₂ 93 Kwangsue Kim, Hyo-bin Anh, Seyeob Jeong, Jungmin Park, Nyun Jong Lee, Trinh Thi Ly, Kyung Mee Song, Jung Dae Kim, Changgu Lee, Tae-Eon Park [*] , Sanghoon Kim [*]

○ Session NS [Nano-structured materials]

NS01	Poster	Study on stochasticity in the switching of Co/Pt nanodisks 94 Sooseok Lee [*] , Soong-Geun Je, Hee-Sung Han, Myeonghwan Kang, Hye-Jin Ok, Namkyu Kim, Weilun Chao, Mi-Young Im [*] , Ki-Suk Lee [†]
NS02	Poster	평면홀 저항 센서를 이용한 강자성 재료의 와전류 결함 신호 측정 95 김동영, 윤석수 [*]
NS03	Poster	Contribution of hydrogen irradiation-induced defects to the magnetic characterization of FeRh films 96 Sehwan Song [*] , Chang-woo Cho, Jiwoong Kim, Jisung Lee, Sungkyun Park [*]
NS04	Poster	Two-Dimensional Organic-Inorganic Hybrid Perovskite Ultrathin Magnets 97 Ki-Yeon Kim [*] , Garam Park, Jaehun Cho, Joonwoo Kim, June-Seo Kim, Jinyong Jung, Kwnojin Park, Chun-Yeol You, In-Hwan Oh
NS05	Poster	Temperature and field-dependent MFM measurements of MnAs/GaAs(001) 98 Jiseok Yang [*] , Jiyoung Jang, Kyung Jae Lee, Sanghoon Lee, Kab-Jin Kim
NS06	Poster	Observation of Current Induced Skyrmion Density Control in a Lorentz Transmission Electron Microscope 99 Albert M. Park [*] , Zhen Chen, Xiyue S. Zhang, Lijun Zhu, David Muller, Gregory D. Fuchs

○ Session ST [Spin transfer torque for magnetic memory]

- ST01 Poster Spin Hall Conductivity of W-N alloys: A First Principles Study 100**
 Quynh Anh T. Nguyen*, D. D. Cuong, S. C. Hong, Sonny H. Rhim

○ Session NM [Nanoscale Magnetism]

- NM01 Poster Torque magnetometry using circuit change of membrane-type surface stress sensor 101**
 Mariam Omran, Joonyoung Choi, Younjung Jo*

○ Session MO [Magnetic Oxides and Multiferroics]

- MO01 Poster Praseodymium substituted Bi-YIG film prepared by MOD method for magneto-optical isolators 102**
 Trinh Nguyen Thi, Viet Dongquoc, Duc Duong Viet, Phuoc Cao Van, Jong-Ryul Jeong*

○ Session BM [Biomedical Magnetics]

- BM01 Poster 자성마이크로비드를 이용한 펄스자기장 처리에 따른 혈액 내 산-염기 균형평가 103**
 최유경*, 방승환, 이현숙*

○ Session MM [Medical Magnetics]

- MM01 Poster Optimization of the Diverging Collimator for Thyroid Cancer Treatment Room Monitoring with I Isotopes Using Monte Carlo Simulation 105**
 Dong-Hee Han*, Jong-Seok Byeon, Kyung-Hwan Jung, Cheol-Ha Baek*
- MM02 Poster Performance Analysis of Comparison of Digital Dental Model Acquired using Electromagnetic Wave Projection (Dental Cone Beam Computerized Tomography) with 3D Printing Temporary Resin 106**
 Seen-Young Kang*, Ji-Min Yu, Jun-Seok Lee, Jae-Won Lee, Ho-Sang Jung, Seung-Youl Lee*
- MM03 Poster Performance Test Methods of Dental Materials(Magnetic Attachment, Dental Ceramic) Reflecting Latest International Standards 109**
 Ji-Min Yu*, Seen-Young Kang, Jun-Seok Lee, Jae-Won Lee, Ho-Sang Jung, Seung-Youl Lee†

○ Session SA [Sensor and Applications]

- SA01 Poster A Preliminary Experimental Study of Positioning System Using Multiple Radiation Spectroscopy Detectors 111**
 Seung-Jae Lee*, Cheol-Ha Baek*
- SA02 Poster Research on Polar Anisotropic Molding Yoke Shape to Reduce Dead Zone of Ring Type Bond Magnets 112**
 Jeong-Yeon Min*, Dong-Woo Nam, Hyun-Jo Pyo, Min-Jae Jeong, Seo-Hee Yang, Won-Ho Kim
- SA03 Poster Test Environment Construction of ITF in BLDC motor 115**
 Dong-yeol Lee*, Dong-Hwan Kim, Jong-Hwan Cho, Sung-Gu Lee, Dong-Woo Kang

SA04	Poster	LC공진을 이용한 OFG센서의 감도 향상 117
		김경원, 신광호*

11월 26일(목) 09:00~12:20
Special Session II ‘산화물 자성체 세션’

그랜드볼룸A

✽ 좌 장: 문은국(KAIST)

09:00	초S-II-1	Giant topological Hall response induced by spin chirality fluctuation in a ultraclean frustrated antiferromagnet 121
		Jun Sung Kim*
09:30	초S-II-2	First-principles study of magnetic van der Waals materials: from CrI₃ and Fe₃GeTe₂ to VSe₂ and VTe₂ 122
		Myung Joon Han*
10:00	초S-II-3	Terahertz Spectroscopy of Magnons in HoFeO₃ and Detection of Rabi Splitting 123
		Howon Lee, Kyung Ik Sim, Hyunjun Shin, Y. J. Choi, Jae Hoon Kim*
10:30	초S-II-4	Random singlets in quantum magnets with frustration and disorder 124
		Kwang-Yong Choi*
11:00	초S-II-5	An intermediate magnetic phase of a proximate Kitaev system in in-plane magnetic fields 125
		Beom Hyun Kim*, Shigetoshi Sota, Tomonori Shirakawa, Seiji Yunoki, Young-Woo Son
11:30	초S-II-6	Identification of a Kitaev Quantum Spin Liquid by Magnetic Field Angle Dependence 126
		Kyusung Hwang*, Ara Go, Ji Heon Seong, Takasada Shibauchi, Eun-Gook Moon
12:00	초S-II-7	Describing the magnetic structure and origin of band gap on Ba₂CuOsO₆ system; density functional theory approach 127
		Changhoon Lee, Ji Hoon Shim

11월 26일(목) 09:00~12:30
Oral Session I ‘자기이론 및 의공학, 대학원생 세션’

그랜드볼룸C

✽ 좌 장: 제송근(전남대)/김상훈(울산대)

09:00	O-I-1	The Study of Planar Hall Effect in CoFeB/MgO with various Metals under Layer Structure 131
		Mingu Kim*, Chang-Jin Yun, Jiho Kim, Kungwon Rhie
09:20	O-I-2	기계학습과 인공지능 기법을 이용한 펄스와전류 신호해석 132
		김재민*, 신정우, 서호건, 김경모, 박덕근
09:40	O-I-3	Unidirectional Transport of Magnetic Skyrmion through Symmetry-Breaking of Potential Energy Barriers 133
		Dae-Han Jung*, Hee-Sung Han, Namkyu Kim, Ganghwi Kim, Suyeong Jeong, Sooseok Lee, Myeonghwan Kang, Mi-Young Im, Ki-Suk Lee*

10:00	O-I-4	Skymion calculator based on boundary annihilation 134 Moojune Song*, San Ko, Sung Kyu Jang, Min Gyu Park and Kab-Jin Kim
10:20	O-I-5	Giant spin Seebeck effect (SSE) in two-dimensional ferromagnetic Cr₁₃ monolayer 135 Brahim Marfoua*, Imran Khan, Jisang Hong†
10:50	O-I-6	유연기판을 활용한 비정질 금속 박막의 연신저항특성 확인 136 김지호*, 윤창진, 김민구, 이궁원
11:10	O-I-7	Educational a Pair of PET Detection System Based on 1D-RCD and Oscilloscope 137 이민호*, 허희선, 권철민, 정지윤, 강지훈†
11:30	O-I-8	Nonvanishing anomalous Hall effect of the quaternary Heusler compound TiZrMnAl with compensated ferrimagnetism 138 Thu-Thuy Hoang*, Minkyu Park, Do Duc Cuong, S. H. Rhim, S. C. Hong
11:50	O-I-9	Electric filed dependent valley polarization in 2D WSe₂/CrGeTe₃ heterostructure 139 Brahim Marfoua*, Jisang Hong†
12:10	O-I-10	A New Methods for Distinguishing Phoswich Detector consisting of LYSO and GAGG 140 Jingyu Yang*, Songhyup Kang, Kanguk Jin, Joomin Kim, Jihoon Kang†

11월 26일(목) 09:00~11:50

Special Session III 'Hard & Soft Magnetic Materials'

에메랄드AB

❁ 좌 장: 최철진(재료연구소)

09:00	초S-III-1	Rare-Earth Permanent Magnets for the Fourth Industrial Revolution: Status and Prospects 143 Wooyoung Lee*
09:25	초S-III-2	Permanent magnets for high efficiency motor 144 Jihoon Park*, Jong-Woo Kim, Kwanghyun Chung, Soon Cheol Hong, Chul-Jin Choi†
09:50	초S-III-3	Finite-element micromagnetic simulation study of NdFeB magnets 145 Sang-Koog Kim*
10:15	초S-III-4	Microstructure of Grain Boundary Diffusion Processed Nd-Fe-B Sintered Magnets : Microstructural Characteristics of HRE-rich Shells and Grain Boundary Phases 146 Tae-Hoon Kim*, Jung-Goo Lee
11:00	초S-III-5	Comparison of Soft magnetic composite cores from both Fe-based amorphous and crystalline powders 147 Hwi-Jun Kim*, Min-Woo Lee
11:25	초S-III-6	Fabrication of Anisotropic Bulk Magnet by Hot-deformation Process using Nd-lean Nd-Fe-B Melt-spun Powder 148 Jung-Goo Lee*, Ga-Yeong Kim, Hee-Ryoung Cha, Dong-Kwan Kim, Hae-Woong Kwon

✿ 좌 장: 양승모(KRISS)/문경웅(KRISS)

13:30	O-II-1	Astroid in spin Hall current & Dzyaloshinskii-Moriya interaction ····· 151
		Chang-Jin Yun [*] , Jiho Kim, Kungwon Rhie
13:50	O-II-2	Gate-tunable large nonreciprocal charge transport in noncentrosymmetric LaAlO ₃ /SrTiO ₃ interfaces ····· 152
		Daeseong Choe [*] , Mi-Jin Jin, Shin-Ik Kim, Hyung-Jin Choi, Junhyeon Jo, Inseon Oh, Jungmin Park, Hosub Jin, Hyun Cheol Koo, Byoung-Chul Min, Suk-Min Hong, Hyun-Woo Lee, Seung-Hyub Baek, Jung-Woo Yoo [*]
14:10	O-II-3	Direct terahertz probing of the fundamentals of anisotropic magnetoresistance ····· 153
		Ji-Ho Park [*] , Hye-Won Ko, Jeong-Mok Kim, Byong-Guk Park, Se Kwon Kim, Kyung-Jin Lee, Kab-Jin Kim
14:30	O-II-4	A large reduction in switching current in W/CoFeB heterostructures with W-N interfacial layers ····· 154
		Min Hyeok Lee [*] , Yong Jin Kim, Gyu Won Kim, Taehyun Kim, In Ho Cha, Quynh Anh T. Nguyen, Sonny H. Rhim, Young Keun Kim [†]
14:50	O-II-5	Electric-field control of deterministic spin-orbit torque switching via laterally modulated Rashba effect in Pt/Co/AlO _x structures ····· 155
		Min-Gu Kang [*] , Jong-Guk Choi, Jimin Jeong, Jae Yeol Park, Hyeon-Jong Park, Jong Min Yuk, Kyung-Jin Lee, Byong-Guk Park
15:10	O-II-6	Investigation of Weak Antilocalization Effect in Co-dusted Graphene films ····· 156
		Thi-Nga Do [*] , Sehee Lee, Chanyong Hwang, Taehee Kim [*]
15:40	O-II-7	Growth and analysis of novel A15 W ₃ Ta Heavy metal layer ····· 157
		Jeongwoo Seo [*] , Jeonghoon Shin, Woojong Kim, Jungyup Yang, Jinpyo Hong
16:00	O-II-8	Manipulation of spin-orbit torque in HM/FM/Oxide frame by external gate voltage ····· 158
		Jeonghun Shin [*] , Jeongwoo Seo, Jungyup Yang, Jinpyo Hong
16:20	O-II-9	Universality of stripe domain width change by an in-plane magnetic field ····· 159
		Seungmo Yang [*] , Kyoung-Woong Moon, Tae-Seong Ju, Changsoo Kim, Byoung Sun Chun, Sungkyun Park, Chanyong Hwang
16:40	O-II-10	Discovery of magnetoelectric coupling in a van der Waals compound CuCrP ₂ S ₆ ····· 160
		Chang Bae Park [*] , Aga Shahee, Deepak R. Patil, Nikita Ter-Oganessian, Kee Hoon Kim

✿ 좌 장: 임성현(울산대)

13:30	초S-IV-1	Physical Properties of Rare-Earth f-electron Systems: Past and Present ····· 163
		Byung Il Min [*]

13:55	초S-IV-2	MTG (Magnetism Theory Group) of Prof. B. I. Min at POSTECH and related academic genealogy..... 164 Young-Rok Jang*, Kicheon Kang
14:20	초S-IV-3	Valley magnetic domain: A new pathway to valleytronics..... 165 J.D. Lee*
14:45	초S-IV-4	Time-dependent density functional theory calculations of spin-phonon dynamics and band topology of two-dimensional materials..... 166 Noejung Park*, Mahmut Okayay, Bum Seop Kim
15:20	초S-IV-5	Towards Rare-Earth and Rare-Earth-Free Permanent Magnets Designed Using First-Principles..... 167 Dorj Odkhuu*, T. Ochirkhuyag, D. Tuvshin, T. Tsevelmaa, S. C. Hong
15:45	초S-IV-6	Discovery of van der Waals magnets and beyond 168 Je-Geun Park*
16:10	초S-IV-7	ARPES study of a Multifold Fermionic Semimetal PdSb2 169 Woo-Ri Ju, Jinwon Jeong, En-Jin Cho, Han-Jin Noh*, Kyoo Kim, Byeong-Gyu Park
16:35	초S-IV-8	Textured Spin Singlets in an infinite layered nickelate..... 170 Kwan-Woo Lee*

11월 26일(목) 13:30~17:00

Special Session V 'Electro-Magnetic Energy Convergence : MOTOR Session'

에메랄드AB

✿ 좌 장: 이정중(전자부품연구원)

13:30	초S-V-1	Electromagnetic Force and Vibration Analysis of Outer Rotor Surface-Mounted Permanent Magnet Synchronous Motor 173 Jae-Hyun Kim*, Soo-Hwan Park, Min-Ro Park, Soo-Gyung Lee, Kyoung-Soo Cha, Myung-Seop Lim
13:55	초S-V-2	토크밀도 향상을 위한 로봇 구동용 SPM 동기전동기 설계에 관한 연구 175 김광용†, 김동욱, 이근호, 김성일*
14:20	초S-V-3	시간별 1일 부하변동을 고려한 에스컬레이터 시스템의 에너지 측정 및 추정 176 김해중*, 윤명환, 이정중
14:45	초S-V-4	A Design of Halbach Cylinder Shape Sintered Nd-Fe-B Magnets for Servo Motors 177 김효준*, 김상면
15:20	초S-V-5	해석적방법을 이용한 표면부착형 영구자석 기기의 가진원 해석 178 이훈기†, 최장영*
15:45	초S-V-6	A Study on the Electromagnetic Field Design of BLDC Motor For Electric Outboard Propulsion..... 179 Ho-Joon Lee*, Jae-Sung Woo, Dong-Hyun Kim
16:10	초S-V-7	Torque Improvement Design of Interior Permanent Magnet Synchronous Motor considering Saturation of Rotor Core..... 180 Myung-Hwan Yoon*, Ki-Deok Lee, Se-Hyun Rhyu, Jeong-Jong Lee

16:35	초S-V-8	Rotor Design of Ultra-high-speed Motor for Electric Turbo Charger Considering Mechanical Stiffness.....	181
Sung-Hyeok Wi [†] , Soo-Gyung Lee, [*] Jun-Yeol Ryu, Sung-Woo Hwang, Soo-Hwan Park, Myung-Seop Lim [*]			

11월 26일(목) 17:00~17:30
스핀트로닉스 초청강연 I

그랜드볼룸A

✽ 좌 장: 김갑진(KAIST)

17:00	초O-I-1	Thermoelectric energy conversion utilizing spin degree of freedom	185
Hyungyu Jin (진현규)			

11월 26일(목) 17:30~18:00
총회초청강연 I

그랜드볼룸A

✽ 좌 장: 정종율(충남대)

17:30	초O-I-1	강일구박사님의 생애와 업적	189
김희중			

11월 26일(목) 18:00~18:30
총회초청강연 II

그랜드볼룸A

✽ 좌 장: 정종율(충남대)

18:00	초O-II-1	2021년 이후 소재·부품분야 과학기술정보통신부/연구재단 국책연구사업 소개	193
이영국			

11월 27일(금) 09:00~12:30
Oral Session III 'Hard & Soft Magnetics'

에메랄드AB

✽ 좌 장: 임혜인(숙명여대)

09:00	O-III-1	Coercivity improvement of Nd-Cu infiltrated Nd-Fe-B hot-deformed magnets by microstructure modification of initial HDDR powders.....	197
Jae-Gyeong Yoo [*] , Hee-Ryoung Cha, Tae-Hoon Kim, Yang-Do Kim [†] , Jung-Goo Lee [†]			
09:20	O-III-2	Coercivity enhancement of (Nd, M)-Fe-B hot-deformed magnet by post-annealing treatment.....	198
Ga-Yeong Kim [*] , Hee-Ryoung Cha, Tae-Hoon Kim, Dong-Hwan Kim, Yang-Do Kim [*] , Jung-Goo Lee [†]			
09:40	O-III-3	Phase transformation and magnetic properties of Sm(Fe _{0.8} Co _{0.2}) ₁₁ Ti bulk magnets.....	199
Hui-Dong Qian [*] , Jung Tae Lim, Yang Yang, Jong-Woo Kim, Su Yeon Ahn, Hankuk-Jeon, Tian Hong Zhou, Kyung Mox Cho, Jihoon Park [*] , Chul-Jin Choi [†]			
10:00	O-III-4	First-Principles Study of Magnetic Properties of MnBi with Bi-site Substitutes.....	200
Dorjsuren Tuvshin [*] , Tumentsereg Ochirkhuyag, Soon Cheol Hong [†] , Dorj Odkhuu [†]			

10:20	O-III-5	Control of magnetic properties of MnBi by elements doping 201 Yang Yang*, Hui-Dong Qian, Jung Tae Lim, Jihoon Park, Jong-Woo Kim [†] , Chul-Jin Choi
10:50	O-III-6	Enhancement of magnetic properties of Fe-rich compounds with tetragonal ThMn₁₂ structure by mixing non-magnetic materials 202 Jung Tae Lim*, Hui-Dong Qian, Jihoon Park, Chul-Jin Choi [†]
11:10	O-III-7	A Development of the coating technique on Soft-magnetic Composite Powders for a motor device 203 Kim youngmin*, Kim shingyu, Chung yeonjun, Kim jongryul
11:30	O-III-8	Structural and magnetic properties of rare earth doped Fe by ion beam implantation 204 Joonhyuk Lee*, Jinhyung Cho, Hyoungjeen Jeon [†]
11:50	O-III-9	Spin-thermoelectric energy conversion based on molecule-based magnetic thin film 205 Inseon Oh*, Jungmin Park, Deaseong Choe, Junhyeon Jo, Hyeonjung Jeong, Mi-Jin Jin, Younghun Jo, Joonki Suh, Byoung-Chul Min, Jung-Woo Yoo
12:10	O-III-10	First-principles prediction of enhancing magnetic anisotropy and stability of α"-Fe₁₆N₂ phase 206 Tumentsereg Ochirkhuyag, Dorjsuren Tuvshin, Soon Cheol Hong [†] , Dorj Odkhuu [†]

11월 27일(금) 09:00~12:30
Special Session VI 'Medical Magnetics'

그랜드볼룸C

❀ 좌 장: 한만석(강원대)/안우상(울산의대)

09:00	초S-VI-1	Transcranial Magnetic Stimulation for the Treatment of Multiple Neurologic Conditions; Focused on Clinical Application 209 Jung-Woo Jeong*, Bo-Kyoung Song
09:20	초S-VI-2	Image Quality Assessments According to the Angle of Tilt of a Flex Tilt Coil Supporting Device: An ACR MRI Phantom Study 210 Ji-Sung Jang*, Ho-Beom Lee, Sung-min Kim
09:40	초S-VI-3	MRI 보어 구경에 따른 검사 시 실효 단면적 분석 212 유재원, 배규성, 배서현, 김성호, 유세종, 전민철, 고현철, 정현근*
10:00	초S-VI-4	Feasibility of fast non-local means algorithm for T1-weighted MR images using BrainWeb: A simulation study 214 Seong-Hyeon Kang*, Youngjin Lee
10:30	초S-VI-5	A Study on the Evaluation of Dose Distribution Error According to the Spacing and Angle of Bolus in Electromagnetic Radiation 215 Kim Jeong Ho*, Seo Jeong Min, Kim Gap Jung
10:50	초S-VI-6	Feasibility of Customized 3d Bolus for H&N cancer: Applied to Oral Cavity and Supraclavicular Area 216 Seunghyeop Baek*, Eunbin Ju, Woo Sang Ahn, Nuri Hyun Jung, Sohyun Ahn
11:10	초S-VI-7	The effect of patient size on radiation with size-specific dose estimates for computed tomography dose index 217 Pil-Hyun Jeon*, Cheol-Ha Baek

✻ 좌 장: 김철기(DGIST)

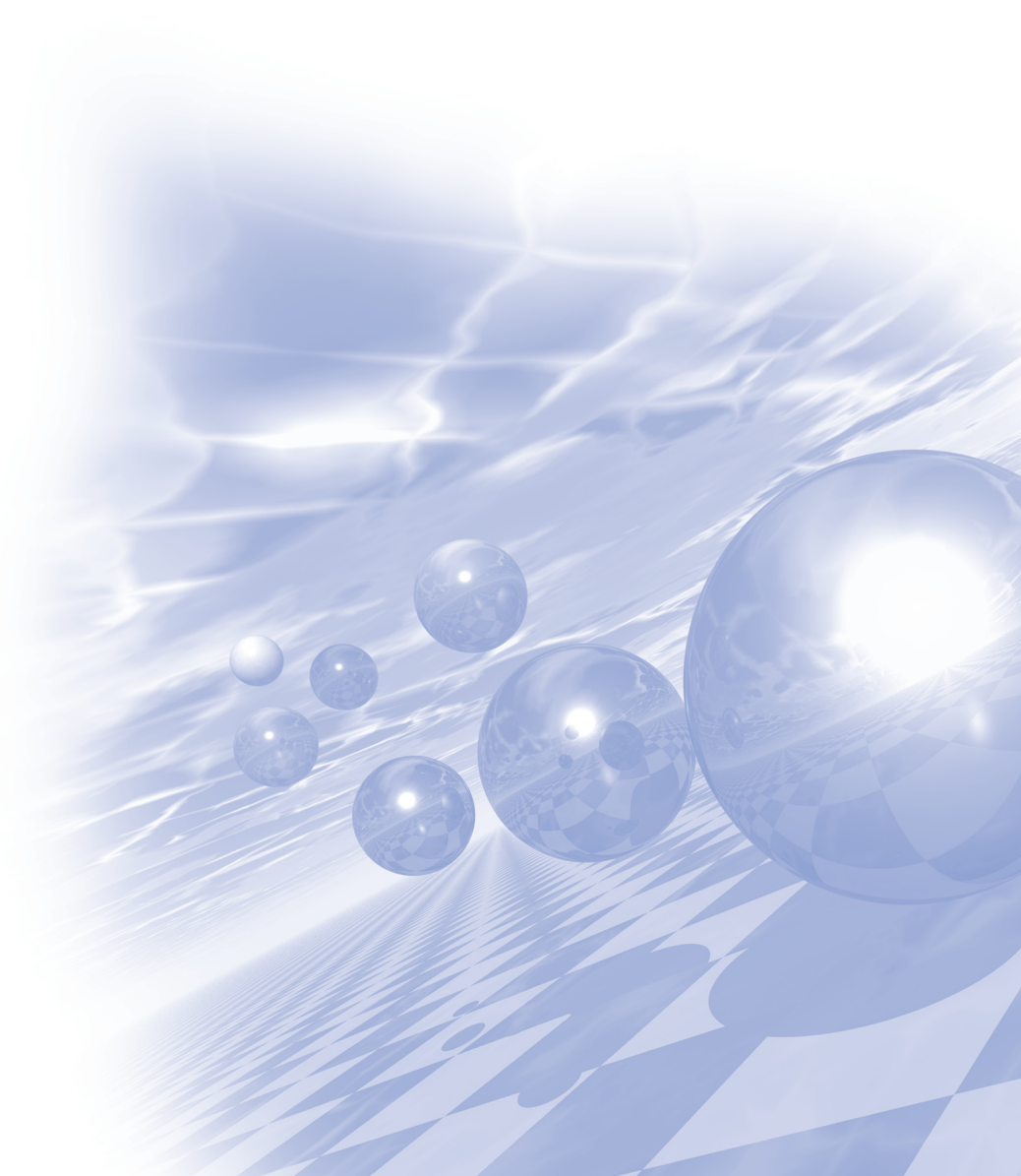
- 09:00 초S-VII-1 FePt-Ferrite heterogeneous nanoparticles: One-pot synthesis with controlled phase and their enhanced biocompatibility 221**
Yunji Eom^{*}, Yumin Kang, Satish Kasturi, Sri Ramulu Torati, CheolGi Kim[†]
- 09:30 초S-VII-2 생체기능화 된 자성입자의 프로그래밍 가능한 이송을 위한 다중 전송 게이트 222**
임병화^{*}, 후싱하오, 토라티라무, 김현설, 윤종환, 김철기[†]
- 10:00 초S-VII-3 Label-free electrochemical biosensor for miRNA-122 biomarker detection based on naturally reduced rGO/Au nanocomposite 223**
Satish Kasturi^{*}, Yun Ji Eom, Sri Ramulu Torati, CheolGi Kim[†]
- 10:30 초S-VII-4 Development of magnetic-based pressure sensor for pulse pattern detection 224**
Mijin Kim^{*}, Sang-Hoon Shin, Sunjong Oh[†], Cheolgi Kim[†]



KMS 2020 Winter Conference

Special Session I

‘SOT 소자’ (비공개 세션)



Pd 굴곡 변화에 따른 자기적 특성과 iDMI의 변화

A. S. Samardak^{1,2*}, A. V. Davydenko¹, A. G. Kolesnikov¹, A. Yu. Samardak¹, A. G. Kozlov¹,
Bappaditya Pal¹, A. V. Ognev¹, A. V. Sadovnikov^{3,4}, S. A. Nikitov^{3,4}, A. V. Gerasimenko⁵,
차인호⁶, 김용진⁶, 김규원⁶, Oleg A. Tretiakov^{7,8}, 김영근^{6*}

¹School of Natural Sciences, Far Eastern Federal University, Vladivostok 690950, Russia

²National Research South Ural State University, Chelyabinsk 454080, Russia

³Laboratory "Metamaterials", Saratov State University, Saratov 410012, Russia

⁴Kotel'nikov Institute of Radioengineering and Electronics, Russian Academy of Sciences, Moscow 125009, Russia.

⁵Institute of Chemistry, Far East Branch, Russian Academy of Sciences, Vladivostok 690022, Russia.

⁶Department of Materials Science and Engineering, Korea University, Seoul 02481, Republic of Korea

⁷School of Physics, The University of New South Wales, Sydney 2052 NSW, Australia.

⁸National University of Science and Technology "MISiS", Moscow 119049, Russia

중금속/강자성체 박막 이중층 구조에서 스핀 궤도 결합을 이용한 수직자기이방성과 [1] 스핀 궤도 토크에 [2] 관한 연구들이 활발하게 진행되고 있다. 최근에 중금속층과 강자성체층이 포함된 비대칭 구조에서는 스핀 궤도 결합에 의한 Dzyaloshinskii-Moriya Interaction (DMI) [3] 현상이 보고되었고, DMI를 조절하는 것이 비휘발성 메모리의 구현에 핵심 이론으로 급부상하였다. 그러나 원자 규모에서의 박막에 존재하는 굴곡이 높은 스핀 궤도 결합을 가지는 중금속 층에 영향을 주어 DMI까지 영향을 줄 수 있어 이와 관련된 연구가 필요하다. [4] 따라서, 중금속층에 굴곡을 형성하여서 DMI의 변화를 보는 실험을 진행하였다. Pd의 두께를 0 nm 에서 12.6 nm 까지 증가시키면 굴곡은 0.15 nm 에서부터 1.0 nm 까지 증가하였다. Pd 층 위에, Pt (2 nm) /CoFeSiB (1.5 nm)를 공통적으로 증착하고, 비대칭 구조에 필수적인 자성층 윗 계면의 재료를 MgO, Ta, Ru로 다르게 증착하여 실험을 진행하였다. Pd의 두께에 따라서 Ta의 굴곡이 세 경우에 모두 0.2 nm 에서 0.4 nm 까지 증가함을 보였다. 그리고 계면 품질 계수는 Pd의 두께가 증가함에 따라 세 경우에 모두 감소함을 보였고 이는 Pd에 의한 계면 굴곡이 중금속층에 전달됨을 의미한다. 또한 Pd의 두께가 없는 경우에는 자기 이방성 에너지가 조건에 따라서 $-3 \times 10^6 \sim -1 \times 10^6$ erg/cm³ 를 보이지만, Pd의 두께가 증가함에 따라서 $0 \sim 2 \times 10^6$ erg/cm³ 까지 증가하다가 -2×10^6 erg/cm³까지 감소하였고 이러한 결과는 Pd의 굴곡이 수직자기이방성을 강화시킨 것을 의미한다. BLS를 이용하여 DMI를 측정한 결과 Pd의 두께가 증가할수록 유효 DMI 에너지 밀도값이 -0.25 erg/cm³ 에서 -0.9 erg/cm³ 까지 증가함을 보였다. 이러한 실험결과는 계면에서 형성되는 굴곡의 크기가 자성 특성과 DMI에 영향을 미침을 보이면서 DMI 값을 제어할 때 계면의 굴곡 역시 중요한 요소로 고려해야 함을 알 수 있다.

References

- [1] Hellam, F et al., Interface-induced phenomena in magnetism. Rev. Mod. Phys. 89, 025006 (2017)
- [2] P. Gambardella et al., Current-induced spin-orbit torques. Philos. Trans. R. Soc. A 369, 3175-3197 (2011)
- [3] Park, Y.-K. et al. Experimental observation of the correlation between the interfacial Dzyaloshinskii-Moriya interaction and work function in metallic magnetic trilayers. NPG Asia Mater. 10, 995-1001 (2018)
- [4] Yang, H. X., Thiaville, A., Rohart, S., Fert, A. & Chshiev, M. Anatomy of Dzyaloshinskii-Moriya interaction at Co/Pt interfaces. Phys. Rev. Lett. 115, 267210 (2015).

Orbital Hall effect induced spin–orbit torque via orbital–to–spin conversion

Soogil Lee¹, Min–Gu Kang¹, Dongwook Go², Taekhyeon Lee³, Dohyoung Kim¹,
Kab–Jin Kim³, Sanghoon Kim⁴, Byong–Guk Park^{1*}

¹Department of Materials Science and Engineering, KAIST, Daejeon 34141, Korea

²Institute of Physics, FB 08 Physik, Mathematik und Informatik, Johannes Gutenberg–
University Mainz, Mainz 55128, Germany

³Department of Physics, KAIST, Daejeon 34141, Korea

⁴Department of Physics, University of Ulsan, Ulsan 44610, Korea

Electrical control of magnetization by spin-orbit torque (SOT) in nonmagnet (NM)/ferromagnet (FM) bilayers is regarded as an essential key to provide a low power operation for emerging spintronic devices. In order to efficient control of magnetization, searching for nonmagnetic materials with the large SOT efficiency have been desired. Thus, there were many efforts to enhance the SOT efficiency with strongly spin-orbit coupled heavy metals, such as Ta, W, and Pt, because spin-orbit coupling (SOC) of a NM was considered for a crucial source to generate the spin current via large spin Hall effect (SHE). However, further enhancement of the SOT efficiency is still required to realize the low power operation. Recently, newly proposed orbital torques suggested that the large SOT can be generated even in weakly spin-orbit-coupled NMs by the orbital current, as a consequence of the orbital Hall effect and subsequent orbital-to-spin conversion via SOC [1–5]. In this talk, we present that the orbital torque is efficiently tailored by orbital-to-spin conversion engineering. Here, we discuss the effect of different FMs or insertion layers at the NM/FM interface with varying SOC strength on the orbital torque. Our study suggests that the orbital current can be utilized to further enhance the magnetization switching efficiency in spin-orbit-torque-based spintronic devices.

References

- [1] Dongwook Go and Hyun–Woo Lee, Phys. Rev. Research 2 (2020) 013177.
- [2] T. Tananka et al., Phys. Rev. B 77 (2008) 165117.
- [3] H. Kontani, et al., Phys. Rev. Lett. 102 (2009) 016601.
- [4] Dongwook Go, et al., Phys. Rev. Lett. 121 (2018) 086602.
- [5] Daegeun Jo, et al., Phys. Rev. B 98 (2018) 214405.

Spin–Orbit Torque in Pd/Co/Pd(t) Heterostructure

Keesung Kim, Jongill Hong*

Department of Materials Science and Engineering, Yonsei University, Seoul 03722, Republic of Korea

Our study discusses how spin-orbit torques changes upon changing the top Pd thickness in metallic and hydrogen-irradiated, reduced Pd/Co/Pd(t) heterostructures. The spin-orbit torque originates from spin-orbit interaction (SOI), and its mechanisms have been understood with the spin accumulation at the interface, so-called Rashba effect, and the bulk spin Hall effect (SHE) as well. Due to those two mechanisms, a field-like torque (FLT) and a damping-like torque (DLT) arise. However, it is not clear which mechanism (or torque) dominates over another in Co/Pd/Co heterostructures. A way to answer such a question is to change only one Pd layer' s thickness while keeping other interfaces and layers untact to observe whether or not the bulk spin Hall effect indeed starts to play a role in generating the spin-orbit orque. In this talk, we report and discuss the effect of a change in top Pd thickness on the spin-orbit torque based on the two mechanism.

SOT-MRAM based crossbar array for Neural Network

Yunho Jang*, Taehwan Kim, Jooyoon Kim, Jongsun Park*

Department of Electrical Engineering, Korea University, Seoul 02481, Republic of Korea

Neural network hardware using emerging device has been actively studied since emerging device based synaptic weight array brings about energy and area efficient neural network hardware. Especially, crossbar array structure using emerging device can easily perform multiplication and accumulation (MAC) of activation and weight by current summation. For low cost and reliable implementation of crossbars, Spin-orbit torque (SOT) MRAM is promising candidate for implementing crossbar due to its non-volatility, high endurance, low write energy and CMOS compatibilities [1]. However, the hardware cost of ADC located in the interface of the crossbars mitigates the effectiveness of the crossbar. In [2], ADCs accounts for around 35% of area and 49% of power consumption in the crossbar design. Although many previous works have tried to reduce the ADC cost either by lowering the resolution [3] or by sharing ADC between crossbars [4], the ADCs still takes considerable hardware cost in the crossbar [3]. In case of SOT-MRAM based crossbar design, small R_{OFF}/R_{ON} ratio of SOT-MRAM [5] is another design bottleneck, which makes the SOT-MRAM crossbar sensitive to process variations. The problem is even exacerbated with large-scale crossbars, limiting the SOT-MRAM based crossbars to small size. In this paper, we present a low cost SOT-MRAM crossbar based binary CNN (BCNN) accelerator. First, we propose data dependent switch (DDS) for SOT-MRAM cell, which can effectively address the low R_{OFF}/R_{ON} ratio issue in the crossbar array. DDS controls the current flow of the read access transistor depending on stored data to enlarge the magnitude of difference between the currents generated by R_{OFF}/R_{ON} . In addition, in order to reduce the large ADC cost, we replace the conventional CMOS ADC with hybrid spin/CMOS based ADC. The proposed hybrid ADC exploits the SOT device as a current comparator to improve area and energy efficiencies. When implemented with 65nm CMOS process, the proposed BCNN accelerator shows the 22.7% area and 68.9% energy savings compared to the conventional design, while achieving comparable classification accuracy of 86.3% for the CIFAR-10 dataset.

References

- [1] G. Srinivasan, A. Sengupta, and K. Roy, "Magnetic Tunnel Junction Based Long-Term Short-Term Stochastic Synapse for a Spiking Neural Network with On-Chip STDP Learning," *Sci. Rep.*, vol. 6, p. srep29545, Jul. 2016.
- [2] A. Shafiee et al., "ISAAC: A Convolutional Neural Network Accelerator with In-Situ Analog Arithmetic in Crossbars," in *2016 ACM/IEEE 43rd Annual International Symposium on Computer Architecture (ISCA)*, Seoul, South Korea, 2016, pp. 14-26.
- [3] X. Sun, S. Yin, X. Peng, R. Liu, J. Seo, and S. Yu, "XNOR-RRAM: A scalable and parallel resistive synaptic architecture for binary neural networks," in *2018 Design, Automation & Test in Europe Conference & Exhibition (DATE)*, Dresden, Germany, 2018, pp. 1423-1428.
- [4] X. Qiao, X. Cao, H. Yang, L. Song, and H. Li, "AtomLayer: A Universal ReRAM-Based CNN Accelerator with Atomic Layer Computation," in *2018 55th ACM/ESDA/IEEE Design Automation Conference (DAC)*, San Francisco, CA, 2018, pp. 1-6.
- [5] B. Rajendran and F. Alibart, "Neuromorphic Computing Based on Emerging Memory Technologies," *IEEE J. Emerg. Sel. Top. Circuits Syst.*, vol. 6, no. 2, pp. 198-211, Jun. 2016.

Non-standard angular dependence of spin-orbit torques in ferromagnet/heavy metal bilayers

Kyung-Jin Lee^{*}

Department of Physics, KAIST, Korea

We investigate angular dependence of spin-orbit torques in ferromagnet (FM)/heavy metal (HM) bilayers. We find that non-standard angular dependence is observed in a FM/HM bilayer, which helps reduce the switching current in the presence of symmetry breaking effective fields. We show first-principles calculations that give a hint about the origin of the non-standard angular dependence.

Pt계면 조절에 따른 Spin Orbit Torque의 향상

김영래¹, 박경배², 임상호^{1*}

¹고려대학교 신소재공학부, 서울특별시 성북구 안암동 고려대학교, 136-713

²서강대학교 물리학과, 서울특별시 마포구 백범로, 35

수직자기이방성을 가지는 고효율, 비휘발성 스핀케도토크-MRAM (Magnetic Random Access Memory) 소자를 실현시키기 위하여 스핀케도토크 효율의 향상은 필수적이다. 최근 heavy-metal/ ferromagnet/ insulator 구조의 계면을 조절하여 스핀케도토크의 효율을 향상시키기 위한 많은 연구가 진행되었다. Pt/ Co/ MgO 구조에서 0.2nm 두께의 Hf 층을 다층으로 Pt 층에 삽입하게 되면 스핀 홀 각도가 증가한다[1]. 이는 같은 조성비의 Pt, Hf 합금과 비교하여도 상당한 값을 나타내고 있다. 따라서 본 연구에서는 heavy-metal/ ferromagnet/ insulator 구조에서 heavy-metal 층에 최소한으로 삽입된 0.2nm 두께의 Ti 층의 위치에 따른 스핀 홀 각도를 측정하였고, 불안정하게 증착된 ferromagnet 층의 구조를 안정화 시키기 위하여 ferromagnet/ heavy-metal/ insulator 구조의 PMA, IMA 특성을 가지는 샘플을 확보하여 0.2nm 두께의 Ti 층을 heavy-metal 층에 삽입하여 위치에 따른 스핀 홀 각도를 측정하였다. 또한 heavy-metal/ insulator 계면에서 Ti 이 삽입되었을 때 Ti에 의해 강화되는 스핀 홀 효과와 라쉬바 효과의 관계에 대하여 조사하였다.

References

- [1] R. A. Buhrman et al., Enhancing Spin-Orbit Torque by Strong Interfacial Scattering From Ultrathin Insertion Layers Phys. Rev. Appl. 11, (2019) 061004.

Spin Hall Conductivity of W–N alloys: A First Principles Study

Quynh Anh T. Nguyen, D. D. Cuong, S. C. Hong, Sonny H. Rhim*

Department of Physics and Energy Harvest Storage Research Center, University of Ulsan,
Ulsan 44610, Republic of Korea.

Efforts to enhance spin current generation, commonly quantified as spin Hall angle, have been major research in the past decade. Recent work has opened another opportunity in tungsten compounds, where β -W phase with A15 structure plays more role than stable α -W in body-center-cubic structure. As an extension, several fabrications have been performed, where W-N alloy is one of them. Motivated by recent experiment of W-N alloy, here ab initio investigation is done on some prototype W-N alloy, WN and W₂N with 1:1 and 2:1 ratio of W and N. We found that W₂N has spin Hall conductivity as large as -966 S/cm, enhanced by 29 % and 18 % over α - and β -W, respectively. On the other hand, WN with three structural phases gives -194 S/cm, thermodynamically averaged over their relative formation energies. Analysis of k resolved Berry curvature reveals that anti-crossing point near Fermi level in **FX** is distinct in W₂N, responsible for large spin Hall conductivity.

References

- [1] K.-U. Demasius, T. Phung, W. Zhang, B. P. Hughes, S.-H. Yang, A. Kellock, W. Han, A. Pushp, and S. S. P. Parkin, Nat. Commun. 7, 10644 (2016).
- [2] X. Sui, C. Wang, J. Kim, J. Wang, S. H. Rhim, and W. Duan, Phys. Rev. B 96, 241105(R) (2017).
- [3] Y. J. Kim, M. H. Lee, G. W. Kim, T. Kim, I. H. Cha, Q. A. T. Nguyen, S. H. Rhim, and Y. K. Kim, Acta Mater. 200, 551 (2020).

Observation of stripe width variation and skyrmion formation and spin pumping in trilayer structure Py/Ti/CoFeB

Kyoung-Woong Moon[†], Seungmo Yang[†], Tae-Seong Ju, Changsoo Kim, Byong Sun Chun, Chanyong Hwang^{*}

Quantum Spin Team, Korea Research Institute of Standards and Science, Daejeon 34113, Republic of Korea

In recent advances in magnetism, formation of Isolated domains in perpendicular magnetic anisotropy (PMA) systems draw great interest because the isolated domains can have a topologically protected magnetization texture known as a skyrmion [1]. Due to the topological properties of the skyrmion, it is treated as an ideal information carrier for memory, logic, and neuromorphic devices [2]. However, creation of skyrmion is still challenging problems. A well-known but only half successful method is using a stripe domain state which is filled with half-up and half-down magnetization [3,4]. What is evident is that the isolated bubble-filled state has slightly larger energy than the stripe-filled state at zero magnetic field. Furthermore, application of a proper perpendicular magnetic field makes the bubble-filled state the global minimum energy state [3,4]. So, the stripe domain is thought to be a precursor for creation of skyrmion states. However, generation of bubble domains from the stripe domains is not successful except for thin stripe domain cases, because the stripe domain has a well-defined local minimum energy up to large perpendicular field. Therefore, if the perpendicular field is increased from zero, the bubble state cannot be reached, and only the stripe domain is observed [4]. This is a main reason for “half successful”. The starting point of our discussion is that the isolated bubble magnetic domains can be formed using an in-plane magnetic field instead of the perpendicular magnetic field. We will discuss four effects of the in-plane magnetic field. Firstly, the in-plane field increases the stripe density. Secondly, the in-plane field changes from a random stripe to an aligned structure, which is parallel to the in-plane field direction. Thirdly, the in-plane field can generate bubble domains from stripe domains. Lastly, from the above findings, we demonstrate that there exists a critical stripe width for the formation of bubble domains (skyrmions), because the stripe width determines the energy barrier for the transition between a stripe domain and a skyrmion. We also want to emphasize that our finding will be a universal method for the skyrmion creation we can create bubble-filled states as a seed for skyrmion in arbitrary PMA samples.

X-ray Ferromagnetic Resonance (XFMR) is the unique tool studying interactions between two different magnetic atoms. Especially, we measured the precessional phases of CoFeB and Py in Py/Ti/CoFeB trilayer. The precessional phase of CoFeB was modulated by spin current generated from Py in resonance with Ti = 2, 5, 10 nm. However, without Ti, two magnetization of layers rotated with the same phase in magnetic field. With Ti above 20 nm, it seemed like that there was no coupling. We simulated the spin pumping effect using two LLG equations and compared the simulation with the experimental results.

References

- [1] N. Nagaosa, Y. Tokura, Topological properties and dynamics of magnetic skyrmions, *Nat. Nanotechnol.* 8 (2013) 899.
- [2] A. Fert, N. Reyren, V. Cros, Magnetic skyrmions: advances in physics and potential applications, *Nat. Rev. Mater.* 2 (2017) 17031.
- [3] N. Saratz, U. Ramsperger, A. Vindigni, D. Pescia, Irreversibility, reversibility, and thermal equilibrium in domain patterns of Fe films with perpendicular magnetization, *Phys. Rev. B* 82 (2010) 184416.
- [4] T. N. G. Meier, M. Kronseder, M. Zimmermann, C. H. Back, Quantification of thermal fluctuations in stripe domain patterns, *Phys. Rev. B* 93 (2016) 064424.

Spin–Hall–Effect–Modulation Skyrmion Oscillator

Hyun–Seok Whang, Sug–Bong Choe^{*}

Department of Physics and Institute of Applied Physics, Seoul National University, Seoul,
08826, Republic of Korea

The electric-current-induced spin torque on local magnetization allows the electric control of magnetization, leading to numerous key concepts of spintronic devices. Utilizing the steady-state spin precession under spin-polarized current, a nanoscale spin-torque oscillator tunable over GHz range is one of those promising concepts. Albeit successful proof of principles to date, the spin-torque oscillators still suffer from issues regarding output power, linewidth and magnetic-field-free operation. Here we propose an entirely new concept of spin-torque oscillator, based on magnetic skyrmion dynamics subject to lateral modulation of the spin-Hall effect (SHE) [1]. In the oscillator, a skyrmion circulates around the modulation boundary between opposite SHE-torque regions, since the SHE pushes the skyrmion toward the modulation boundary in both regions. A micromagnetic simulation confirmed such oscillations with frequencies of up to 15 GHz in media composed of synthetic ferrimagnets. This fast and robust SHE-modulation-based skyrmion oscillator is expected to overcome the issues associated with conventional spin-torque oscillators.

References

- [1] H.-S. Whang, S.-B. Choe, Spin-Hall-Effect-Modulation Skyrmion Oscillator, *Scientific Reports* 10 (2020) 11977.

Manipulation of Critical Switching Current and Effective Field of Spin–Orbit Torque by Interface Modulation

Ki-Seung Lee, Suhyeok An, Eunchong Baek, Jin-A Kim, Chun-Yeol You*

A Department of Emerging Materials Science, DGIST, Daegu, Korea

The control of magnetization with pure electrical current has been actively investigated because of perspective of various spin based devices. Among them, many researches have been carried out on the converting system from pure electric current to spin current, such as spin transfer torque (STT) and spin-orbit torque (SOT), owe to its potential of applications including magnetic random-access memory (MRAM), racetrack memory devices, and skyrmion-based logic devices [1]. Compared with STT, the SOT induced magnetization control is not only considered more efficient in both energy and time consumption, but also has structural advantages for the device applications. the SOT based devices consist of a heavy metal (HM) and ferromagnetic (FM) layers, in here, when the pure electrical current flows through the HM layer, transversal polarized spin current is generated by the spin Hall effect (SHE). Moreover, for more efficient SOT, spin Hall angle (SHA) at various HMs has been investigated: 0.15 for Ta, 0.33 for W, and 0.10 for Pt. [2, 3, 4]

However, instead of a higher SHA, for achieving more efficient SOT-based magnetic material devices than before, manipulation of the system itself. For this investigation, we employed the Helium Ion Microscope (HIM) for manipulated local magnetic properties and to observe the deformation characteristics by magnetization switching, harmonics measurement, magneto-optic Kerr effect (MOKE), and Brillouin light scattering (BLS).

Through this study, it was confirmed that the critical switching current decreased markedly by HIM irradiation, and HIM affect to the HM layer and its interface as well as the FM layer. Detailed results of this will be explained in the session.

References

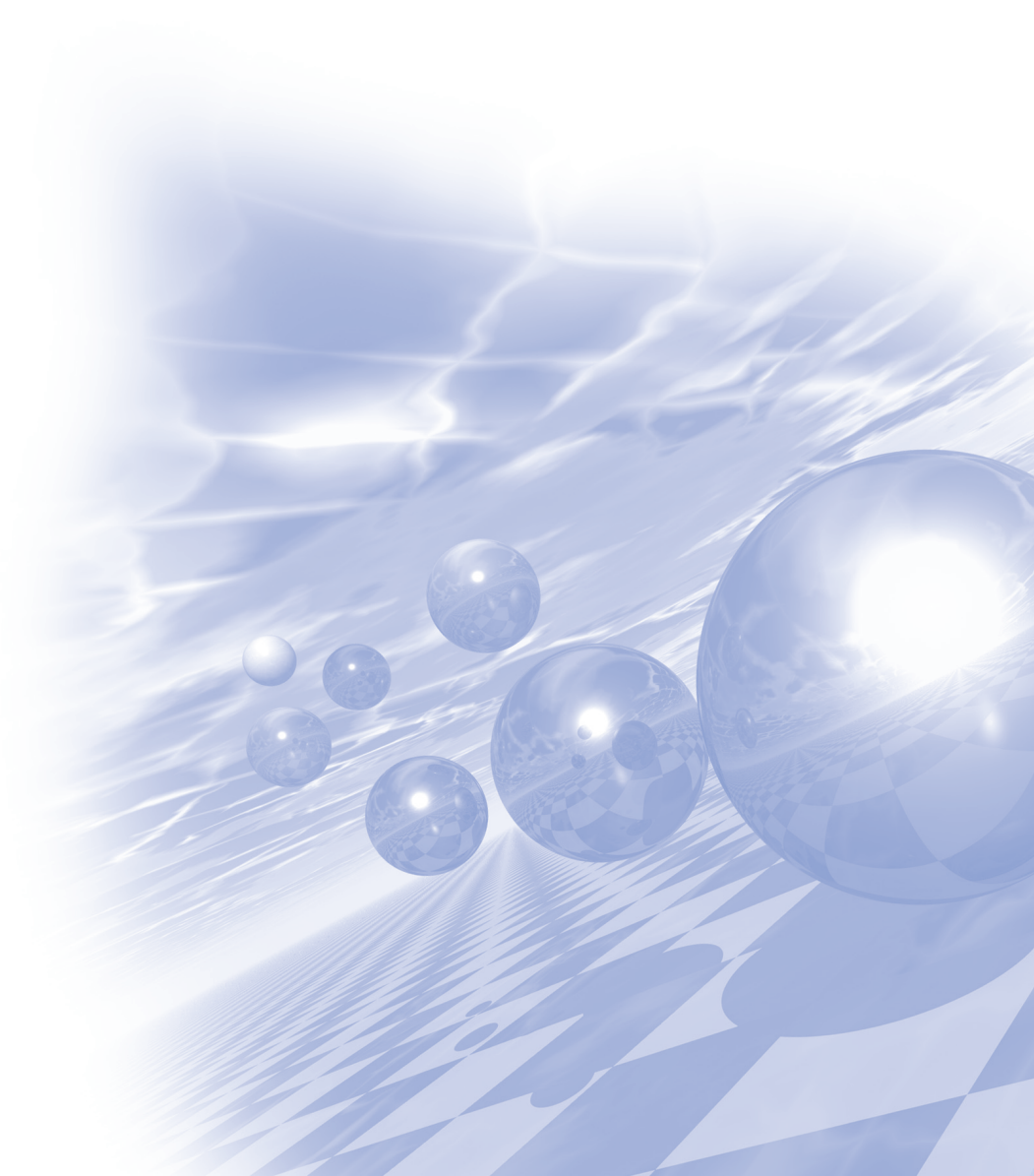
- [1] X. Zhao et al., Appl. Phys. Lett. 116, 242401, (2020).
- [2] Pai C. F. et al., Appl. Phys. Lett. 101, 122404, (2012)
- [3] Azevedo A. et al., Phys. Rev. B 83, 144402 (2011)
- [4] Pai C. F. et al., Appl. Phys. Lett. 104, 082407 (2014)



KMS 2020 Winter Conference

강습회

‘대학원생 진행세션’



자기센서의 원리와 응용

손대락*

주)센서피아

4차 산업과 AI기술이 중요하여 지면서 이에 필수적인 IoT기술이 모든 분야에 폭넓게 적용되고 있다. IoT 기술이 도입되기 위해서는 액추에이터와 센서가 무엇보다 더 중요시 되고 있다. 또한 이들이 가능한 전기로 구동되어야 편리하기 때문에 자기현상의 응용이 더 증가되고 있는 중이다. 특히 전기에너지를 기계적 에너지로 변환하기위해서 사용되는 모터나 솔레노이드 밸브 같은 장치는 대부분 에너지 변환과정에서 중간 과정이 자기에너지를 거쳐야 한다.

자기센서의 경우 자동차나 국방 분야에서와 같이 열악한 온도 환경에서도 높은 신뢰성이 요구되고 있는 분야에 폭넓게 사용되고 있다. 예를 들면 내연기관자동차에 사용 되었던 각종의 rpm 및 회전각 센서에서 오늘날 전기자동차에 사용되는 각종 전류센서에 이르기 까지 다양하게 사용되고 있고, 국방 분야의 경우 지구가 거대한 자석이고 합금이 철 구조물로 되어 있어 합금의 탐지분야 등에 전통적으로 사용되고 있다. 산업이 발전되면서 많은 분야에서 가장 경제적인 구조물 재료로 철강을 사용하고 있고 이들의 구조물의 안정성을 확인 하는 방법으로 Barkhausen효과 등 다양한 자기적 현상을 자기센서에 적용하고 있다. 인공위성 분야의 경우도 우주환경의 고 에너지 입자에 대하여 강한 내성을 가지고 있으며 질량을 최소화 하여야 되기 때문에 전류센서, 자기장센서 및 고주파용 코어가 광범위하게 사용되고 있다.

Accelerating on the long way to magnetic materials design

Stefano Sanvito*

School of Physics and CRANN Institute, Trinity College, Dublin 2, Ireland

The development of novel materials is a strong enabler for any technology, to the point that often technology and materials innovation cannot be separated. Unfortunately the process of finding new materials, optimal for a given application, is lengthy, often unpredictable and has a low throughput. Here I will describe a systematic pathway to the discovery of novel compounds, which demonstrates an unprecedented throughput and discovery speed. The method can be applied to any materials class and any potential application. I will use the example of magnetism to introduce the main features of the method, and I will demonstrate the discovery of several new high-performance magnets. Furthermore, I will highlight how such high-throughput schemes can be combined with machine-learning methods for data-mining to extract novel materials designing rules and for identifying new prototypes for further investigation.

Based on an extensive electronic structures library of Heusler alloys containing 236,115 prototypical compounds, we have filtered those alloys displaying magnetic order and established whether they can be fabricated at thermodynamical equilibrium [1]. Specifically, we have carried out a full stability analysis for intermetallic Heuslers made only of transition metals. Among the possible 36,540 prototypes, 248 are found thermodynamically stable but only 20 are magnetic. The magnetic ordering temperature, T_c , has then been estimated by a regression calibrated on the experimental T_c of about 60 known compounds. As a final validation we have attempted the synthesis of a few of the predicted compounds and produced two new magnets. One, Co_2MnTi , displays a remarkably high T_c in perfect agreement with the predictions, while the other, Mn_2PtPd , is a complex antiferromagnet.

In the second part of my talk I will discuss the use of machine-learning methods for predicting the Curie temperature of ferromagnets, based solely on their chemical composition (see figure) [2], and for sorting magnets into hard and soft. In particular I will discuss how to develop meaningful feature attributes for magnetism and how these can be informed by experimental and theoretical results. I will also show a potential promising scheme for extracting information from published literature. All these together can pave the way for the large-scale design of novel magnetic materials at unprecedented speed.

References

- [1] Stefano Sanvito, Corey Oses, Junkai Xue, Anurag, Tiwari, Mario Zic, Thomas Archer, Pelin Tozman, Munuswamy Venkatesan, J. Michael D. Coey and Stefano Curtarolo, Accelerated discovery of new magnets in the Heusler alloy family, *Science Advances* 3, e1602241 (2017).
- [2] James Nelson and Stefano Sanvito. Predicting the Curie temperature of ferromagnets using machine learning. *Phys. Rev. Mat.* 3, 104405 (2019).

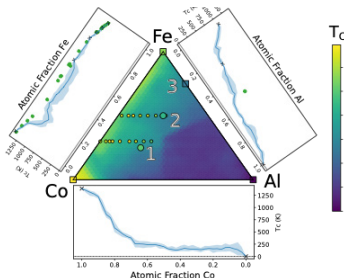


Fig. 1. T_c prediction as a function of composition for the ternary system Al-Co-Fe. Data are presented as a function of the atomic fraction of the three species and the T_c is expressed as a heat map. The figure also introduces a detailed analysis of the three relevant binary phase diagrams, where the blue line traces the ML prediction, black crosses (green dots) are experimental points included (not included) in the training set. The light-blue shadowed area in the binary plots corresponds to the range of predicted T_c 's, namely it indicates the uncertainty of the machine-learning model. The solid square (circles) included in the ternary T_c

diagram are for experimental data included (not included) in the training set, with the colour code describing the T_c . Numbers correspond to four known stoichiometric phases: 1) Co_2FeAl , $T_c = 1,000$ K, 2) Fe_2CoAl , $T_c > 873$ K, 3) Fe_4CoAl , $T_c = 420$ K, 4) Fe_3Al , $T_c = 573$ K.

Topological Band Theory in a Nutshell

Youngkuk Kim^{*}

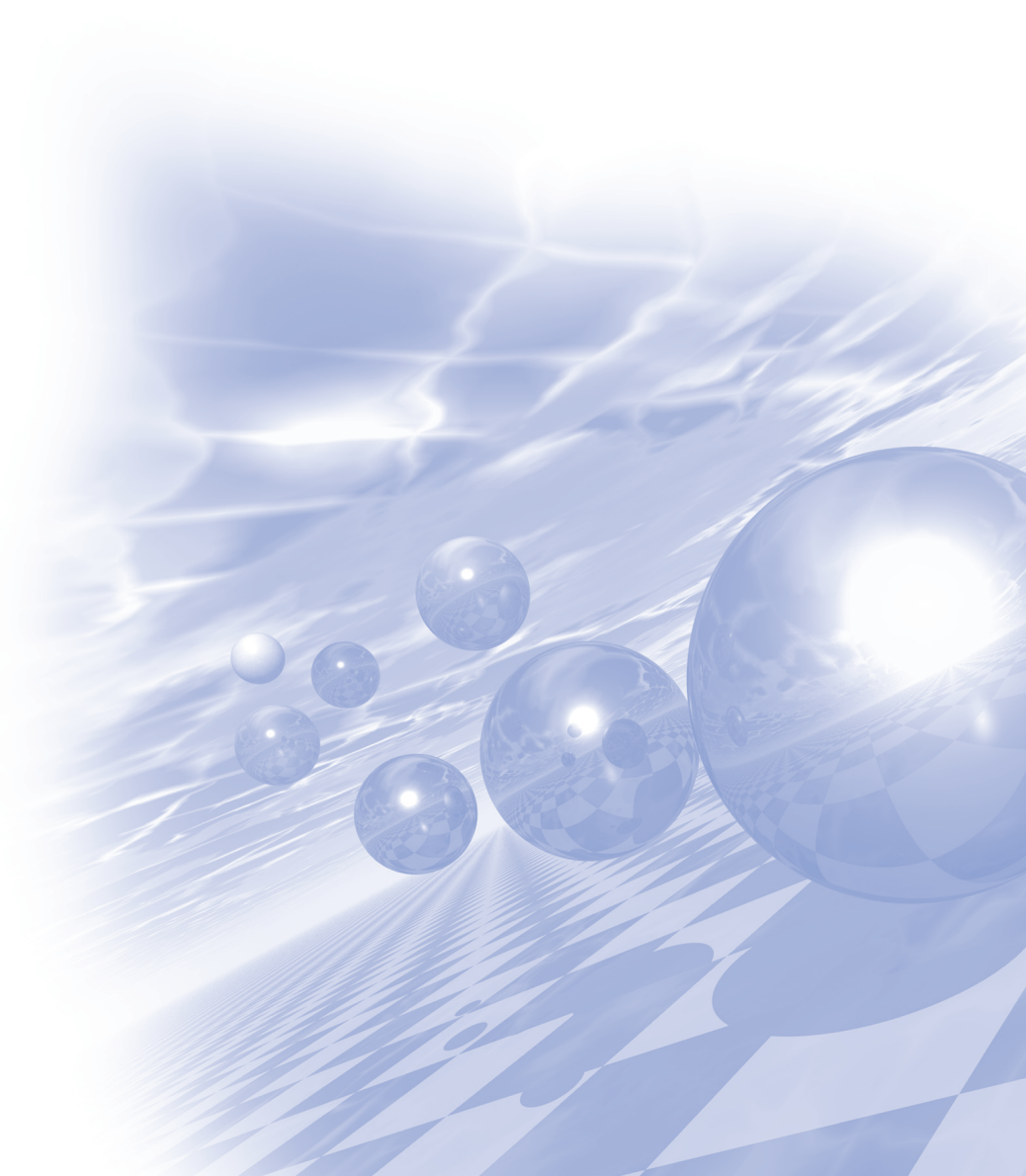
Department of Physics, Sungkyunkwan University, Suwon 16419, Korea

The purpose of this tutorial is to introduce the basic ideas and uses of topological band theory, which has been actively developed over the last decade to assess the topological properties of band structures. Following a brief introduction to the band theory and the role of topology in band theory, I will give several examples of topological analysis for archetypal topological phases, including quantum Hall insulators, Z_2 topological insulators, and Weyl semimetals. Practical methods for diagnosing topological invariants will be delineated, such as the Berry phase, Chern number, and Z_2 topological invariant. I will close with a discussion about the recent developments associated with magnetic topological materials.



KMS 2020 Winter Conference

포스터발표



Generalized Equation for Magnetic Domain Wall Chirality with Consideration of Domain Wall tilting

Jung-Hyun Park^{1*}, Dae-Yun Kim², Yune-Seok Nam¹, Hyun-Seok Whang¹,
Sug-Bong Choe^{1*}

¹Department of Physics, Seoul National University, Seoul, 08826, Korea

²Center for Spintronics, Korea Institute of Science and Technology (KIST), Seoul, 02792, Korea

The domain wall chirality is the key parameter in recent experimental schemes to measure the spin-orbit torque and Dyzloshinskii-Moriya interaction, both of which have recently been main research topics. These schemes, so far, are based on a model that the domain wall is placed transversely to magnetic wires without consideration of tilting. Here, we report that, in materials with Dyzloshinskii-Moriya interaction, an in-plane magnetic field longitudinal to the magnetic wires exerts a torque on domain walls and consequently, the domain walls have to be tilted. A generalized equation reveals that the tilting-angle dependence of the Zeeman energy is distinct to the other energies and thus, the equilibrium angle is determined by counterbalance between those energies. Due to the energy relaxation with tilting, the transition region of the domain wall chirality is broadened. Therefore, the present generalized equation provides a better realistic model to understand the experimental observations in measurement schemes of the spin-orbit torque and Dyzloshinskii-Moriya interaction

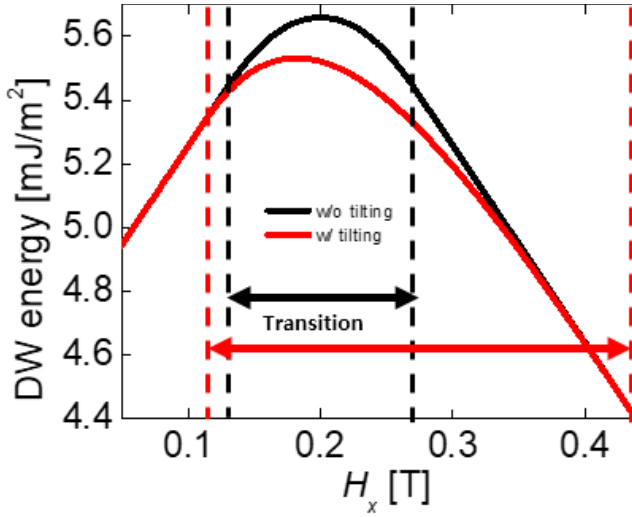


Fig. 1. Domain wall energy graph representing transition region broadening and energy difference in the region

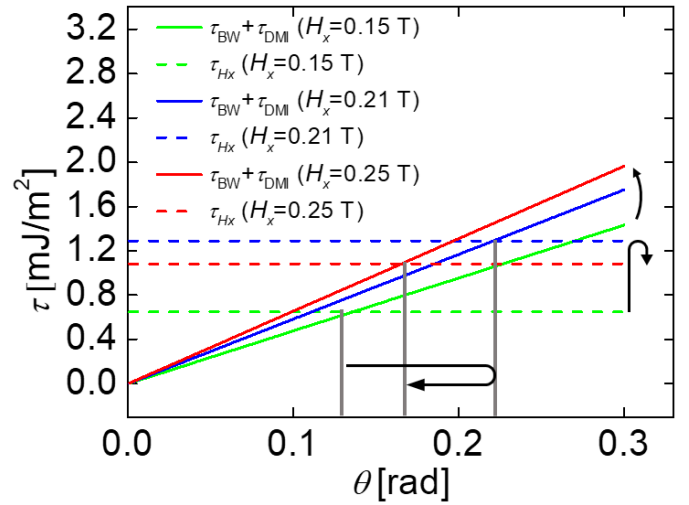


Fig. 2. Torques for each term for given in-plane fields

Influence of W Thickness on Perpendicular Magnetic Anisotropy in Pt/Co/W(111) Superlattices

Thi Huynh Ho^{*}, Sanghoon Kim, S. H. Rhim[†], S. C. Hong[†]

Department of Physics and Energy Harvest Storage Research Center, University of Ulsan,
Ulsan 44610, Republic of Korea.

Corresponding authors: ^{*}sonny@ulsan.ac.kr, [†]schong@ulsan.ac.kr

Recently, Pt/Co/W(111) systems with reflection asymmetry are reported to exhibit strong perpendicular magnetocrystalline anisotropy (PMA), which leads to great attractions for spintronics applications.^[1,2] However, the influence of the W-capping on PMA of Pt/Co have not been clearly revealed. In this work, ab initio calculations have been performed to investigate PMA of Pt/Co/W(111) superlattices. W thickness dependence of PMA is obvious, whose maximum occurs for three monolayers of W (Fig. 1). Orbital hybridizations at the interfaces play a significant role in PMA. In particular, PMA is proportional to orbital magnetic anisotropy ($m_{\text{orb}}^{\perp} - m_{\text{orb}}^{\parallel}$), which is in good agreement with the so-called Bruno relation.^[3] The analysis within the framework of second-order perturbation theory as well as k- and m-resolved PMA indicate that most contributions originate from the Γ point by the orbital coupling $\langle |m|=2 \mid L_z \mid |m|=2 \rangle$

Keywords: magnetocrystalline anisotropy, superlattices, thickness dependence

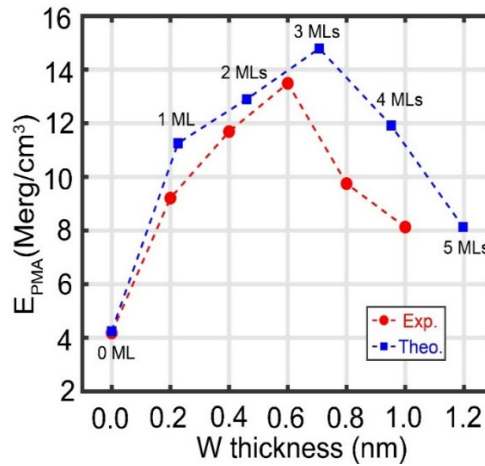


Fig. 1 PMA energy with respect to W thickness. The red circled-dashed line and blue squared-line indicate the experimental and theoretical results, respectively. The number of layers corresponds to the W thickness used in calculations.

References

- [1] Z. A. Bekele et al., Solid State Commun. 274, 41 (2018).
- [2] S. Mendisch et al., J. Magn. Magn. Mater. 485, 345 (2019).
- [3] P Bruno, Phys. Rev. B 39, 865 (1989).

Emergence of the anomalous Hall effect from a compensated collinear ferrimagnetism

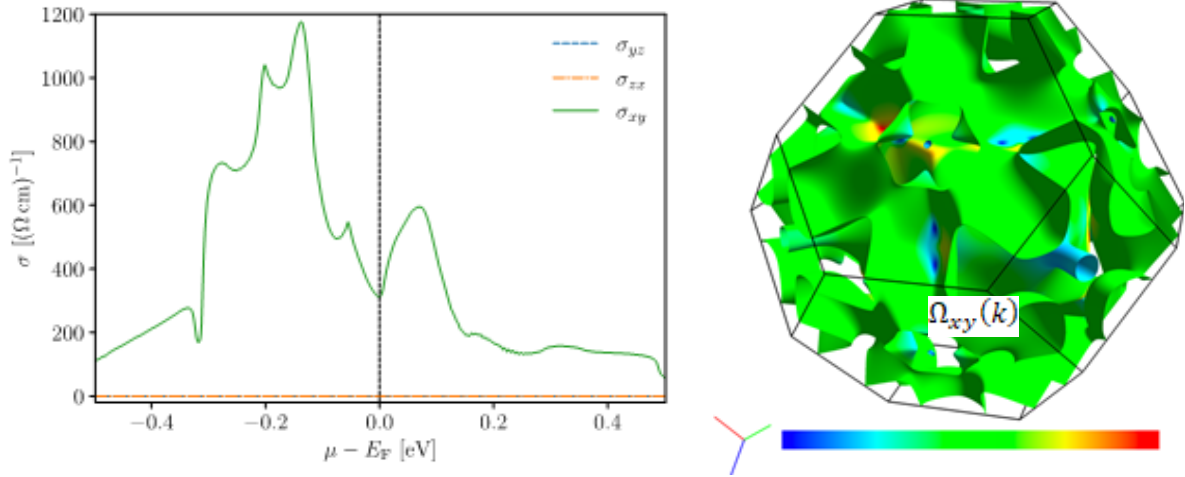
Minkyu Park^{1*}, Guihyun Han², S. H. Rhim²

¹Research Institute of Basic Sciences, University of Ulsan, 93, Daehak-ro, Nam-gu, Ulsan 44610, Republic of Korea

²Department of Physics, University of Ulsan, 93, Daehak-ro, Nam-gu, Ulsan, 44610, Republic of Korea

It has long been believed that the anomalous Hall effects can only be observed in ferromagnetic materials. It is clear, however, that any magnetic material can exhibit the anomalous Hall effects because the time-reversal symmetry is absent in those systems. In this work, we investigate the compensated collinear ferrimagnetic material Mn₃Al with the magnetization along \mathbf{z} axis. We found that the Hall conductivity σ_{xy} only survives under the constraint of the magnetic symmetry while the Berry curvature can be non-trivial even for \mathbf{yz} and \mathbf{zx} components. The explicit first-principles calculations reveal that σ_{xy} indeed has a quite large value about $300 (\Omega \text{ cm})^{-1}$ as shown in the figure below.

The Berry curvature $\Omega_{xy}(\mathbf{k})$ on the Fermi surface is shown below to illustrate non-trivial topological aspects of the band structure of Mn₃Al.



Local control of magnetization of CoO_x thin films by He ion irradiation

Jisu Kim^{1*}, Seongboo Park¹, Eunkang Park¹, Nyun Jong Lee^{1,2}, Taekhyeon Lee³, Ji-Seok Yang³,
Ki-Seung Lee², Chun-Yeol You², Kab-Jin Kim³, Young-Han Shin¹, Sanghoon Kim¹

¹Department of Physics, University of Ulsan

²Department of Emerging Materials Science, Daegu Gyeongbuk Institute of Science & Technology

³Department of Physics, Korea Advanced Institute of Science and Technology

Magnetic nanoscale patterning is one of the most important technology not only for high density of magnetic recording media, but also for developing spin logic devices or spintronic devices. It has been reported that when the magnetic oxide is reduced by proton irradiation, both the local phase and anisotropy of the magnetic thin film can be controlled in terms of the degree of reduction without defect formation. That is to say, such proton irradiation technique has advantages for the non-destructive nano patterning.

In this presentation, we demonstrate that such local phase control of the transition metal oxide, CoO_x for this study, can be done with He ion irradiation. Use of He ions also has advantage for the non-destructive nano patterning due to light mass. The reduction mechanism is also discussed based on the molecular dynamics study with ab initio calculation.

*corresponding author: sanghoon.kim@ulsan.ac.kr

This work was supported by NRF-2018R1A4A1020696, NRF-2019R1C1C1010345, NRF-2018R1A6A3A11041061, NRF-2017R1A2B3002621) and by the Samsung Research Funding Center of Samsung Electronics under project no. SRFC-IT1901-11.

Non–vanishing Anomalous Hall Effect in nearly Compensated Ferrimagnet Mn_3Al

Guihyun Han^{*1}, Minkyu Park², Su Yeon An¹, Soon Cheol Hong^{1,3}, S.H. Rhim^{1,3}

¹Department of Physics, University of Ulsan, Republic of Korea.

²Research Institute of Basic Sciences, University of Ulsan, Ulsan, Republic of Korea.

³Energy Harvest-Storage Research Center, University of Ulsan, Republic of Korea.
(schong@ulsan.ac.kr, sonny@ulsan.ac.kr,)

Anomalous Hall effect (AHE), discovered by Edwin H. Hall, has long been believed to occur only in ferromagnets with non-vanishing magnetization. Contrary to this conventional wisdom, AHE is reported in other magnetic systems such as noncollinear and collinear antiferromagnets [1–3] and compensated ferrimagnets [4].

In this work, using density functional theory, AHE is investigated for Mn_3Al with nearly compensated magnetization.

Hydrostatic volume changes from –5 to 5 % are taken into account, electronic structures near Fermi level are elucidated with Berry curvature analysis.

References

- [1] Hua Chen, Qian Niu and A. H. MacDonald, Phys. Rev. Lett. 112, 017205 (2014).
- [2] Yang Zhang, Yan Sun, Hao Yang, Jakub Zelezny', Stuart P. P. Parkin, Claudia Felser, and Binghai Yan, Phys. Rev. B 95, 075128 (2017).
- [3] Libor Smejkal, Rafael Gonzalez-Hernandez, T. Jungwirth, J. Sinova, Sci. Adv. 6 eaaz8809 (2020).
- [4] Wujun Shi, Lukas Muechler, Kaustuv Manna, Yang Zhang, Klaus Koepernik, Roberto Car, Jeroen van den Brink, Claudia Felser, and Yan Sun, Phys. Rev. B 97, 060406(R) (2018).

AHE for various volumes under hydrostatic limit

Volume-dependent AHE under hydrostatic limit is investigated. We consider from –5 to 5 % volume change whose AHC are 700 600 450 S/cm

Change of bands near Fermi level upon volume change are elucidated along with Berry curvature analysis

Two-dimensional Fe_3GeTe_2 : strain effect on magneto-crystalline anisotropy

G Hye Kim*, Qurat ul Ain, Soon Cheol Hong, S. H. Rhim

Department of Physics and Energy Harvest-Storage Research Center, University of Ulsan,
Republic of Korea.
(schong@ulsan.ac.kr, sonny@ulsan.ac.kr)

Magnetism in two-dimensional van der Waals materials [1][2] has attracted huge attention recently, where Fe_3GeTe_2 (FGT) is one of them with relatively high $T_c \sim 130\text{K}$ [3]. Here, using density-functional theory, strain ($-5\% \leq \eta \leq 5\%$) dependent magnetism and magneto-crystalline anisotropy (MCA) of FGT monolayer as well as bilayer are investigated. Firstly, without strain ($\eta = 0\%$), bilayer FGT (Fig. 1) of A-type antiferromagnetic (A-AFM) energetically favors over ferromagnetic (FM) ($\Delta E = 15.96\text{ meV}$). Moreover, A-AFM to FM transition occurs at strain of $+4.16\%$ (Fig. 2). Secondly, MCA is evaluated using force theorem with band analysis. While monolayer FGT exhibits perpendicular MCA for all η , bilayer shows perpendicular MCA for most of η but in-plane MCA for $\eta = -5\%$.

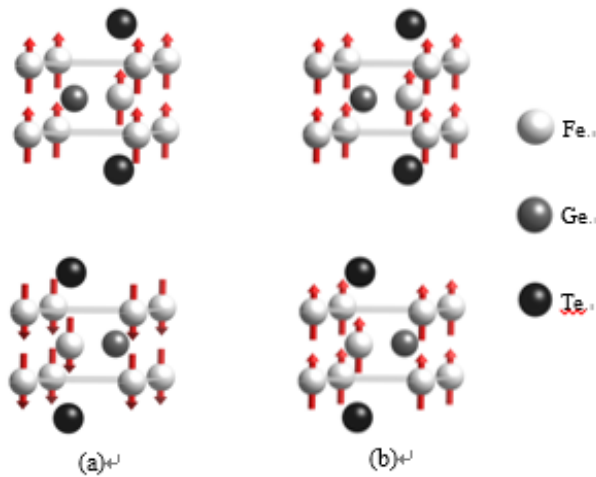


Fig. 1. Structure and spin state of bilayer Fe_3GeTe_2 .
(a) is AFM, and (b) is FM.

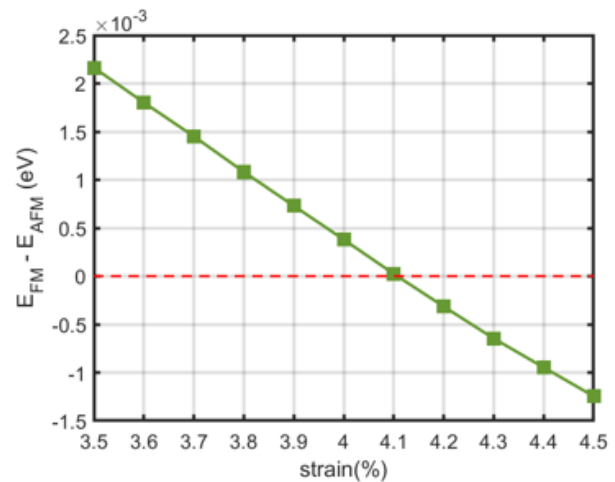


Fig. 2. Energy difference between FM and AFM state of bilayer FGT $\Delta E = E_{FM} - E_{AFM}$, with respect to strain.

Keywords

2D magnetic material; density-functional theory; magneto-crystalline anisotropy; strain

References

- [1] Kenneth S. Burch, David Mandrus and Je-Geun Park, Nat. 563, 47 (2018).
- [2] M. Giberini, M. Koperski, A. F. Morpurgo and K. S. Novoselov, Nat. Nanotechnol. 14, 408 (2019).
- [3] Zaiyao Fei, Jiun-Haw Chu and Xiaodong Xu et al, Nat. Mater. 17, 778 (2018).

Mn4C의 자성: 제일원리 계산

이준규*, 임성현, 홍순철†

울산대학교 물리학과, 울산시 남구 대학로 93, 44610

최근 새로운 자기 화합물 Mn4C을 최초로 합성하는데 성공하였고, XRD 실험을 통해 Mn4C의 결정구조는 그림 1과 같은 입방체이며 격자상수 $a=3.868 \text{ \AA}$ 인 것으로 확인되었다[1]. 이는 Mn4N의 결정구조와 유사하다 [2]. 또한 Mn4C의 포화자화가 온도가 올라감에 따라 590 K까지 증가하여 최고치에 도달한 이후 870 K(T_c)까지는 감소하는 특이한 M-T 곡선을 보여주었다. 포화자화가 590 K까지 온도에 따라 증가하는 현상은 일반적인 자성체에서는 보기 드문 특성이다.

본 연구에서는 Mn4C의 독특한 자성의 원인을 규명하기 위하여 Vienna Ab-initio Simulation Package를 이용하여 제일원리 계산을 수행하였다. 자체 층속 계산에는 $14 \times 14 \times 14$ Monkhorst-Pack k-point 그물을 사용하였고, 차단에너지는 500 eV을 사용하였다. 계산 결과, 입방상에서 안정한 Mn4C의 격자상수는 $a=3.782 \text{ \AA}$ 이었고, 안정된 자기구조는 그림 1과 같은 준강자성체로 확인되었다. Mn I 과 Mn II 의 자기모멘트는 각각 3.383 \mu B , 1.274 \mu B 로 계산되어 총 자기모멘트는 $0.239 \text{ \mu B/unit-cell}$ 이었다. 본 계산 결과들은 실험 값인 3.868 \AA 과 $0.26 \text{ \mu B/unit-cell}$ 와 비교적 잘 일치하였다[1]. Mn4C의 안정성을 점검하기 위해 형성에너지를 계산하고 그 결과에 대해 보고하고 논의할 계획이다.

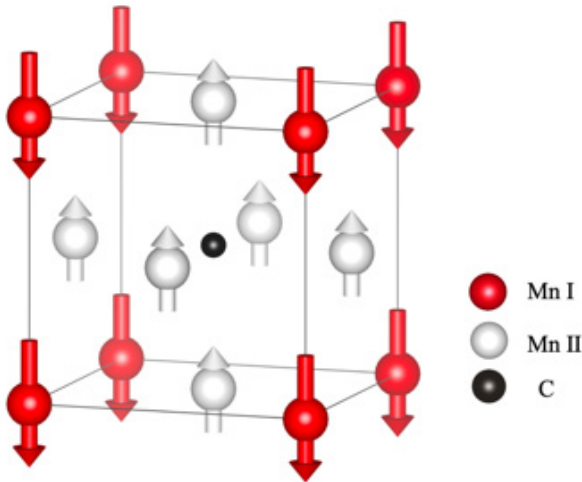


그림 1. Mn4C의 결정구조

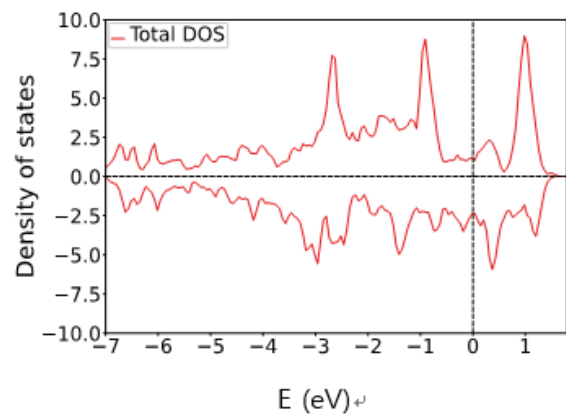


그림 2. Mn4C의 상태밀도

References

- [1] Ping-Zhan Si, Hui-Dong Qian, Hong-Liang Ge, Jihoon Park, and Chul-jin Choi, Appl. Phys. Lett. 113, 049903 (2018).
- [2] W. J. Takei, R. R. Heikes, and G. Shirane, Phys. Rev. 125, 1893 (1962).

IPMSM의 출력밀도 개선을 위한 권선법 선정 및 회전자 형상 변경을 통한 영구자석의 감자 개선 설계

Ju-Hyeong Moon^{1*}, Dong-Hwan Kim², Jong-Hwan Cho³, Sung-Gu Lee⁴, Dong-Woo Kang¹

¹Department of Electrical Energy Engineering, Keimyung University, Daegu 42601, South Korea

²STAR GROUP IND. Co., LTD, Daegu 42714, South Korea

³Valeo Pyeong Hwa co, LTD, Daegu 42921, South Korea

⁴Department of Electrical Engineering, Dong-A University, Busan 49315, South Korea

Currently, in many fields of research for miniaturization and high efficiency of electronic parts are being conducted in order to reduce the weight and improve efficiency of electric vehicles. Therefore, the research was conducted for the purpose of optimal design to improve the efficiency of the motor and reduce size of motor in this paper. We redesigned the distributed winding model into the concentrated winding model as first step of optimal design process by changing the winding method. The purpose of this research is to reduce the weight of the motor by reducing the end coil, improving the operation efficiency at the low speed section and increase the output by changing the winding method. In order to solve irreversible demagnetization problem, this paper analyzes the rotor design parameters that are a major factor in the irreversible demagnetization and design the structure to improve them. Since then, we have implemented the loss reduction and efficiency improvement design through the optimization of the stator design parameters. Finally, to verify the reliability of the simulation results, load experiments using dynamo test bench were conducted and analyzed.

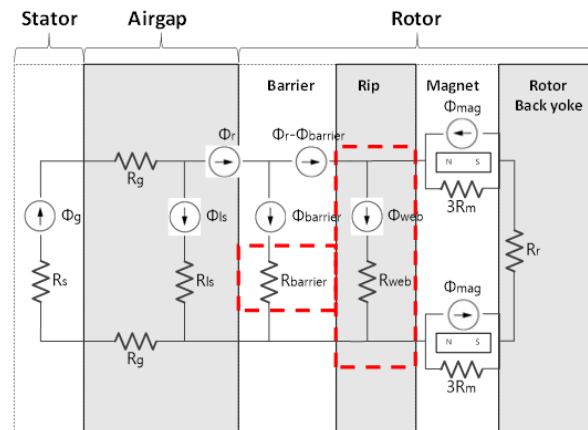


Fig. 4. Magnetic equivalent circuit of IPMSM type.

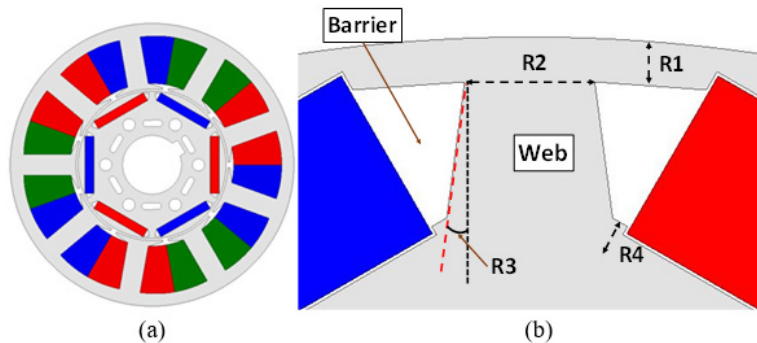


Fig. 6. Basic model of teeth concentrated winding. (a) Basic model. (b) Rotor shape and parameters.

Unusual pressure–induced quantum phase transition from superconducting to charge–density wave state in LuPd₂In

Heejung Kim^{1,2*}, J.H. Shim^{1,3}, Sooran Kim⁴, Jae–Hoon Park^{1,2,6}, Kyoo Kim^{1,2,5,*}, B.I. Min^{1,†}

¹Department of Physics, POSTECH, Pohang 37673, Korea

²MPPHC–CPM, Max Planck POSTECH/Korea Research Initiative, Pohang 37673, Korea

³Department of Chemistry, POSTECH, Pohang 37673, Korea

⁴Department of Physics Education, Kyungpook National University, Daegu 41566, Korea

⁵Korea Atomic Energy Research Institute (KAERI), 111 Daedeok-daero, Daejeon 34057, Korea

⁶Division of Advanced Materials Science, POSTECH, Pohang 37673, Korea

The charge density wave (CDW) is often competing with superconductivity because they originate commonly from the electron-phonon coupling. In typical metallic materials showing the CDW property, the pressure induces the phase transition from CDW to superconducting (SC) state due to the suppression of nesting feature. In this work, we have found the occurrence of intriguing phase transition from SC to CDW state in pressurized cubic-Heusler compound LuPd₂In, which is quite unusual in view of that the pressure is detrimental to the CDW state in usual systems. Based on *ab initio* density functional theory, we have demonstrated that this abnormal transition originates from the extraordinary softened-phonon mode, which first enhances the SC transition temperature, but eventually yields the phonon softening instability so as to bring about the CDW transition. This extraordinary transition originates from the occurrence of phonon softening instability at a special $q = M$ in the Brillouin zone. We have thus proposed that LuPd₂In is a quite unique material, in which the CDW quantum critical point is realized under the SC dome by applying the pressure.

Structural Control of Demagnetizing Field in the Magnet

Namkyu Kim^{*}, Hee-Sung Han, SooSeok Lee, Ki-Suk Lee[†]

School of Materials Science and Engineering, Ulsan National Institute of Science and Technology, Ulsan 44919, Republic of Korea

Devices such as electric vehicles and power generators utilize the magnetic energy of permanent magnet. To meet the increasing demand for such devices, researchers have actively been developing permanent magnets with higher efficiencies and lower cost [1-2]. Magnetic energy emitted by the magnet is represented by the energy product BH , which is twice the energy stored in the stray field outside the magnet. It can be obtained from the volume integral of the square of the stray field outside the magnet, or from the volume integral of the dot product between the demagnetizing field H_d and the internal magnetic flux density B . As noted by Skomski and Coey et al [3], BH is determined rigorously from the hysteresis loop by considering the exact working point because H_d is determined by the shape of the magnet, which results in the magnet of specific shape should be used in order to have the maximum energy product. In this work, controlling the demagnetizing factor by designing the internal structure of the magnet is investigated by micromagnetic solver [4]. As a model system, $\text{Sm}_2\text{Co}_{17}$ for hard-magnetic material and FeCo for soft-magnetic material are adopted [5-7] and arranged with periodicity. From the simulation results, the demagnetizing factor is successfully controlled, which results in reducing limit of the shape of the magnet for maximizing the energy product.

References

- [1] R.W. McCallum, L. Lewis, R. Skomski, M.J. Kramer, I.E. Anderson, *Annu. Rev. Mater. Res.* 44 (2014) 451-477.
- [2] N. Poudyal, J. Ping Liu, *J. Phys. D: Appl. Phys.* 46 (2013) 043301.
- [3] R. Skomski, J.M.D. Coey, *Scr. Mater.* 112 (2016) 3-8.
- [4] A. Vansteenkiste, J. Leliaert, M. Dvornik, M. Helsen, F. Garcia-Sanchez, B. Van Waeyenberge, *AIP Adv.* 4 (2014) 107133.
- [5] Liu, J. P., E. Fullerton, O. Gutfleisch, D.J. Sellmyer, *Nanoscale Magnetic Materials and Applications*, Springer US, 2009.
- [6] Y. Liu, D.J. Sellmyer, D. Shindo, *Handbook of Advanced Magnetic Materials*, Springer US, 2006.
- [7] G.C. Hadjipanayis, G.A. Prinz, A. Gary, *Science and Technology of Nanostructured Magnetic Materials*, Springer US, 2013.

X-선 강자성공명으로 연구된 Py/Ti/CoFeB 구조에서의 스핀펌핑 현상

김창수^{1*}, 최원창², 김현중¹, 문경웅¹, 양승모¹, 홍정일², 황찬용¹

¹양자기술연구소, 한국표준과학연구원

²신물질과학전공, 대구경북과학기술원

X-선 강자성공명은 XMCD (X-ray Magnetic Circular Dichroism) 의 원리를 이용하여 세차운동하는 자화의 위상을 측정하는 기법으로, 이중 자성원소 사이의 상호작용을 연구 하는데에 사용되고 있다.¹ 우리는 Py(50 nm)/Ti(0, 2, 5, 10, 20, 40 nm)/CoFeB (3 nm)의 구조에서 Py층에서 스핀펌핑에 의해 발생한 스핀전류를 Ti 층을 통하여 CoFeB 층에 전달시키는 과정에서 CoFeB층의 위상변화를 측정하였다. Ti 층이 2 nm 에서 10 nm 로 증가할수록 CoFeB층에 전달되는 스핀전류의 영향이 점진적으로 감소하는 것을 측정하였다. 또한 Ti 층이 없는 경우에는 두 자성층이 같은 위상으로 움직이는 것을 관찰하였고, Ti 층이 20 nm 이상일 때는 두 자성층이 분리되어 움직이는 것을 확인하였다. 스핀펌핑 및 스핀전류 현상이 고려된 LL (Landau-Lifshitz) 방정식을 이용해 실험을 모사하였고 두 결과를 비교하였다.

References

- [1] Synchrotron Radiation News, Vol. 33, No.2, 12-19 pages (2020)

Temperature and angle–dependence magnetization reversal behavior in a FePt–C granular thin film

Donghyeon Lee^{1*}, Suzuki Ippei², Seyeop Jung¹, Nyun Jong Lee¹, Heechan Jang¹, Eunkang Park¹, Takahashi Yukiko², Sanghoon Kim^{1*}

¹Department of Physics, University of Ulsan, Ulsan 44610, Korea

²National Institute for Materials Science (NIMS), Tsukuba 305-0047, Japan

Correspondence to: sanghoon.kim@ulsan.ac.kr

Magnetic thin films have been studied in a way that induces various phenomena such as perpendicular magnetic anisotropy and magneto-resistive effect through a change in the structure such as superlattice materials and multilayered materials. Among magnetic thin films, the granular thin films refer to the formation of magnetic particles of several nanometers in diameter in one magnetic layer. Such granular magnetic thin films have been studied a lot as a media material for hard disk drives.

Recently, for the development of ultra-high density HDDs, granular thin films made of magnetic materials having high magnetic anisotropy be studied. In this study, we discuss about the change in coercivity according to the angle and temperature of the FePt-C granular thin film with high magnetic anisotropy, and the thermal stability was evaluated using Shorrock equation applied Stoner-Wohlfarth model.[1]

Acknowledgments This work was supported by the Brain Korea 21 Plus Program (Human Resource Center for Novel Materials Research Experts) through the National Research Foundation of Korea (No. F19SR21D1101) and the National Research Foundation of Korea(NRF) grant funded by the Korea government(MSIT) (No. NRF-2018R1A4A1020696, 2017R1A2B3002621 and 2019R1C1C1010345).

References

- [1] M.P.Sharrock. "Time dependence of switching fields in magnetic recording media" Applied Physics Letters 76.10 (1994): 6413.

Three-dimensional dynamic mode of the magnetic vortex in a permalloy circular disk

Hee-Sung Han, Dae-Han Jung, Suyeong Jeong*, Namkyu Kim, Sooseok Lee, Ki-Suk Lee

School of Materials Science and Engineering, Ulsan National Institute of Science and Technology, Ulsan, Republic of Korea

The magnetic vortex has received a lot of attention owing to high stability and its tiny size. It is composed of the out-of-plane vortex core and in-plane curling magnetization [1]. The magnetic vortex has rich dynamic modes including the gyrotropic mode, azimuthal and radial spin wave modes, which can facilitate the development of the energy-efficient nano-oscillator [2,3]. It is well-known that the vortex core is rigid during dynamic motion. However, recently, it is reported that the magnetic vortex shows a flexible oscillation of the vortex core in thick ferromagnetic elements [4,5]. In this work, our micromagnetic simulation results show three-dimensional (3D) dynamic mode of vortex core in a permalloy circular disks by applying AC out-of-plane current. We found the size oscillation of the vortex core and it is closely associated with the spin-transfer torque and overstepped field effect. In addition, we found that the vortex core can be switched through the resonant excitation. We believe that our works contribute to design the vortex-based spintronic devices including neuromorphic device and logic device.

References

- [1] S.-K. Kim, K.-S. Lee, et al, Appl. Phys. Lett. 92, 022509 (2008).
- [2] M.-W. Yoo, and S.-K. Kim, Appl. Phys. Lett. 117, 023904 (2015)
- [3] M.-W. Yoo, et al, Appl. Phys. Lett. 100, 172413 (2012)
- [4] J. Ding et al., Sci. Rep. 4, 4796 (2014)
- [5] H.-S. Han et al., Appl. Phys. Lett. 117, 042401 (2020)

The Practical Energy Product of Cylindrical Core/shell Consist of Soft- and Hard-magnetic Materials

Namkyu Kim^{*}, Hee-Sung Han, SooSeok Lee, Ki-Suk Lee[†]

School of Materials Science and Engineering, Ulsan National Institute of Science and Technology, Ulsan 44919, Republic of Korea

The exchange-coupled soft-and hard-magnet has been considered as a good candidate for a future high-efficient permanent magnet since it can acquire high saturation magnetization and high coercivity from soft- and hard-magnets, respectively. However, to achieve such an ideal advantage from both magnets, very rigorous design of structures and mixing ratio are required. To do this, various types of exchange-coupled magnet has been investigated including multi-layer, mixture, core/shell structures. The cylindrical core/shell structure are particularly advantageous owing to large interface and versatility at controlling compositions and a demagnetization factor by dimensions.

Since the energy product corresponds to the energy stored in the stray field produced by the magnet itself, it should be measured from demagnetizing field, H_d and the flux density, B at the remanent state. In this study, we investigate the energy product of the cylindrical core/shell structure, which do not mean the maximum energy product estimated from a hysteresis loop for a single aspect ratio, but the energy product considering H_d of the system at the remanent state by using micromagnetic simulations. As a model system, we adopted cylindrical core/shell structure composed of the soft-magnetic shell and the hard-magnetic core. To estimate the energy product, the hysteresis loops were calculated by applying external magnetic field along with easy axis and H_d and B . The results reveal that the energy product basically depends on the ratio but the dimension of the whole system contribute dominantly in the high energy product range. By optimizing the dimension and the ratio, the energy product can reach to very high value of 90 MGOe. We finally expanded this model to iterative array structure of the cylindrical core/shell.

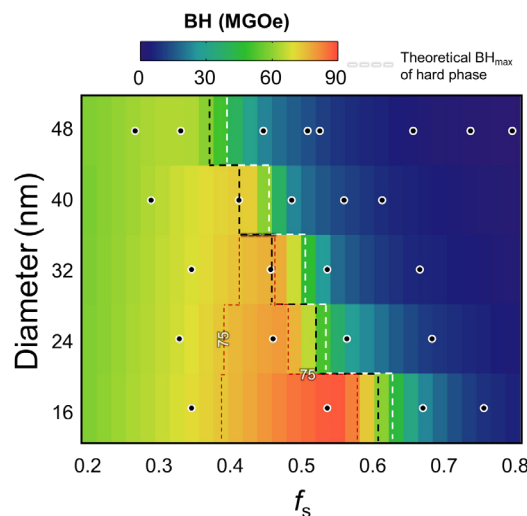


Fig. 1. The phase diagram of the energy product according to the ratio of the soft-magnetic shell and the diameters of the hard-magnetic core.

The energy product is plotted as black dots, and its color is linearly interpolated in each diameter. The black and white dashed line indicates that the calculated nucleation field is zero and the theoretical maximum energy product of the hard phase.

Breathing Modes of a Magnetic Skyrmion on a Defective Surface

Namkyu Kim^{*}, Hee-Sung Han, Dae-Han Jung, Ki-Suk Lee[†]

School of Materials Science and Engineering, Ulsan National Institute of Science and Technology, Ulsan 44919, Republic of Korea

Due to the tiny size of magnetic skyrmions with their unique topological robustness, they hold the promise of low-energy and high-density memory devices. To utilize the magnetic skyrmions for future spintronic devices, their atomistic nature should be studied because this topological spin structures formed physically on the atomic sites in the monolayer-scaled-thickness thin films. I.e., it is indispensable that the magnetic skyrmions are influenced by the surface roughness and the thermal fluctuation. To address those atomistic effects on the skyrmions, we adopt a numerical method based on atomic-scaled micromagnetic model. In this work, we focused on the effect of atomistic defects on the dynamics of skyrmions, particularly, the breathing mode. As a model system, monolayer Co nanodisk with 60 nm diameter was used. We assumed that the Co film has simple cubic (SC) structure with the lattice constant of 2.5 Å and the interfacial Dzyaloshinskii-Moriya interaction (DMI) appears only at the bottom surface. The DMI is considered as the tensor form of magnetic interaction between neighbor spins. To explore the effect of roughness, we assumed that the vacancies are formed randomly on the top surfaces of the Co film with various number of vacancies. Fig. 1(a) reveals clearly that the size of skyrmion in a steady state is affected sensitively by the surface roughness; the vacancies shrink the skyrmion. As shown in Fig. 1(b), the breathing mode is affected dramatically with the roughness. While its eigenfrequency was enhanced with increasing the roughness, its amplitude and the quality factor decreases. This reveals that the atomistic defects can significantly weaken the topological robustness.

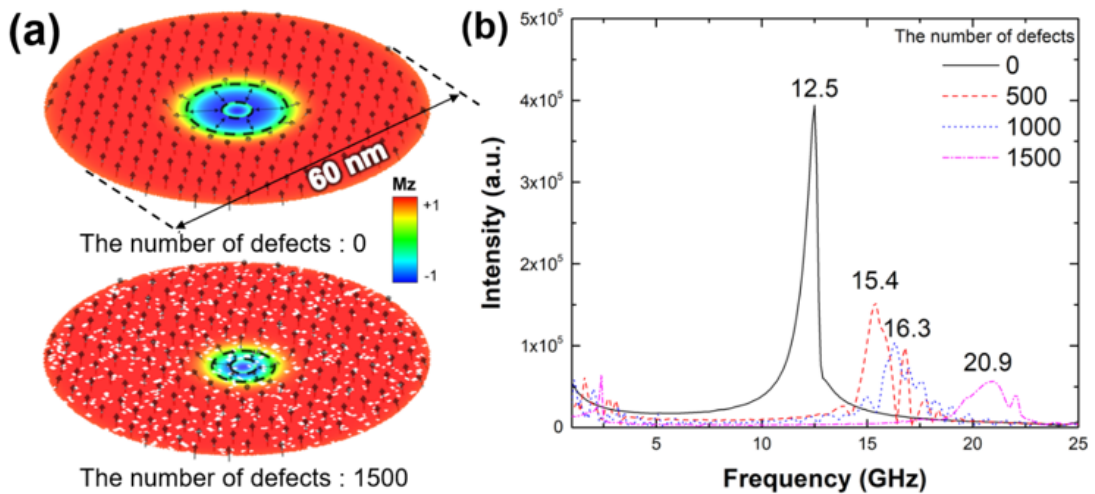


Fig. 1. (a) Expanding and contracting skyrmions with 0, 1500 atomistic defects. (b) Fast Fourier transformation (FFT) spectra for skyrmion breathing mode.

Guided Motion of a Magnetic Skyrmion Confined in Spatially Modulated Dzyaloshinskii–Moriya Interaction

Dae-Han Jung^{*}, Hee-Sung Han, Namkyu Kim, Ki-Suk Lee[†]

School of Materials Science and Engineering, Ulsan National Institute of Science and Technology, Ulsan 44919, Republic of Korea

Magnetic skyrmions can be ideally incorporated into the future spintronic devices, owing to their unique advantages such as extremely small sizes in the nanometre range and particle-like behaviors [1-3]. The prerequisite for developing such skyrmion-based potential devices relies on how stably and quickly guide the movement of the skyrmion propagated at the boundaries of a confined structure. However, there exists a threshold current density where the skyrmion can be annihilated from the boundary edges of the nanostructure, which places an upper limit for the speed of current-induced skyrmion propagation [4,5], if the system is not specially designed to suppress the skyrmion annihilation at the boundaries. Although several earlier studies have been presented by using curved nanowire structures [6] or electric-field-controlled magnetic anisotropy [7], there still exist practical difficulties to be applied to integrated circuits. In this work, we propose, via micromagnetic simulations, a simple planar track-type structure to stably confine and quickly guide the skyrmions by spatial modulations of Dzyaloshinskii-Moriya interaction (DMI). The boundaries located between highly- and lowly-modulated DMI regions can strongly suppress the skyrmion annihilation and significantly enhance the maximum speed of the skyrmion propagation. In such system, the skyrmion can be facilely guided on a curved track which has a 180° turning angle. These findings are expected to possibly utilize the skyrmions into race-track-like computation devices.

References

- [1] N. S. Kiselev, A. Bogdanov, R. Schäfer, and U. K. Rößler, *J. Phys. D* 44, 392001 (2011).
- [2] A. Fert, V. Cros, and J. Sampaio, *Nat. Nanotech.* 8, 152 (2013).
- [3] N. Nagaosa and Y. Tokura, *Nat. Nanotech.* 8, 899-911 (2013).
- [4] Xichao Zhang, G. P. Zhao, Hans Fangohr, J. Ping Liu, W. X. Xia, J. Xia, and F. J. Morvan, *Sci. Rep.* 5, 7643 (2015).
- [5] M. W. Yoo, V. Cros, and J. V. Kim, *Phys. Rev. B* 95, 184423. (2017).
- [6] I. Purnama, W. L. Gan, D. W. Wong, and W. S. Lew, *Sci. Rep.* 5, 10620 (2015).
- [7] P. Upadhyaya, G. Yu, P. K. Amiri, and K. L. Wang, *Phys. Rev. B* 92, 134411 (2015).

Generative machine learning model guided by magnetic Hamiltonian

H. Y. Kwon^{1*}, H. G. Yoon², S. M. Park², D. B. Lee², J. W. Choi¹, C. Won²

¹Center for Spintronics, Korea Institute of Science and Technology, Seoul 02792, South Korea

²Department of Physics, Kyung Hee University, Seoul 02447, South Korea

Abstract

Numerical generation of physical states has been an important task across all scientific research fields including magnetism not only to understand experimental results but also to predict or investigate the characteristics of the uncharted systems. We devised a variational autoencoder based machine learning model to generate magnetic states. In the model, the magnetic Hamiltonian calculation explicitly participates in the training process to generate magnetic states that is more energetically stable with less local noises and less deformation of magnetic structures compared to those without considering Hamiltonian. Another great benefit of this model is that the generator produces a ground state spin configuration when the influence of the Hamiltonian is increased, though the ground state is not included in the training process. Based on this study, we anticipate that the proposed Hamiltonian-guided generative model can bring about great advances in various scientific research fields conducted by numerical approaches.

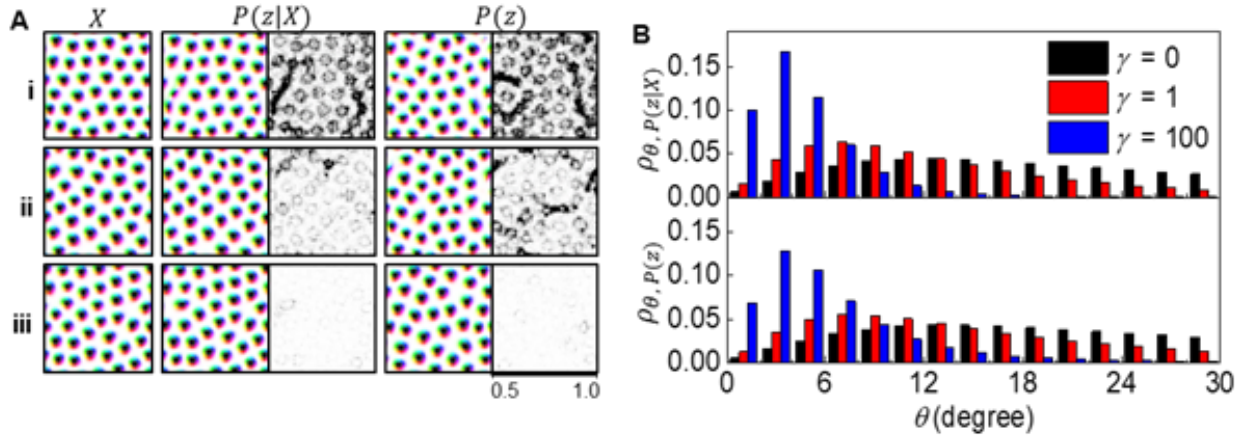


Figure. Sampled states from variational autoencoder.

Development of ISHE–FMR system in extremely low temperature

Jungmin Park^{1*}, Seulgi Koo², Taiwoon Eom², Seung–Young Park¹, Younghun Jo^{1*}

¹Center for Scientific Instrumentation, Korea Basic Science Institute, Daejeon, 34133 Korea

²RNDWARE Co., Ltd, Daejeon, 34133 Korea.

In spintronics, spin pumping with magnetization precession by ferromagnetic resonance (FMR) has received great attention because it facilitates an alternative method for generating pure spin current from ferromagnetic materials (FM) and injecting it into a normal metal (NM) at room temperature. The generated spin current could be converted into a transverse charge current in NM via the inverse spin Hall effect (ISHE). Also, the FMR is a useful method to analyze the spin dynamics of ferromagnetic material. Recently, there has been a many study for the spin dynamics and a spin-charge conversion of FM/NM heterostructure at the various range of temperature because of the T_c (Curie temperature) of ferromagnetic materials.

Now, the commercial FMR measurement system used in Korea is supplied by Quantum Design Incorporation (U.S.A.) with NanOsc instruments. This FMR system can only use in PPMS (physical property measurement system) chamber of Quantum Design, and it is very expensive excluding the price of PPMS.

For localization of the FMR system, we have developed a customizable ISHE-FMR system which is cheaper than the commercial FMR system (Quantum Design Inc.). The developed ISHE-FMR system can simultaneously measure the ISHE voltage and FMR signal in the various range of temperature (2 K ~ 300 K). From this ISHE-FMR system, we measured the FMR derivative absorption signals and ISHE voltage of molecule-based magnet (Cr-PBA, $T_c = 220\text{K}$) as well as Co (5 nm) and polycrystal YIG (20 nm) thin films in low temperature. In this poster section, we will show the design and manufacture process of ISHE-FMR system briefly, and discuss the Gilbert damping parameter of all the test samples compared with References value.

Determination scheme for DMI based on chiral domain wall roughness measurement

Ji-Sung Yu^{1*}, Dae-Yun Kim¹, Joon Moon¹, Seong-Hyub Lee¹, Jun-Young Chang¹,
Duck-Ho Kim², Sug-Bong Choe^{1*}

¹Department of Physics & Astronomy, Seoul National University, Seoul 151-742, Republic of Korea

²Spin Convergence Research Center, Korea Institute of Science and Technology, Seoul 136-791, Republic of Korea

Stabilization of chiral domain-walls (DWs) is a key issue to achieve high performance spintronic applications such as memory and data storage devices with high speed and high durability [1]. Such stabilization can be achieved by the Dzyaloshinskii-Moriya interaction (DMI) in structural inversion asymmetry systems [2-4]. It is therefore important to analyze the strength of DMI accurately and thus, there have been also numerous efforts devoted to quantifying the DMI [5-6]. However, many of the DMI measurement schemes have a trouble with severe artefact caused by additional asymmetries such as the chiral damping [7]. Here, we propose a new scheme to measure the strength of the DMI-induced effective field H_{DMI} , based on the DW roughness. According to the creep theory [8], the DW roughness w_{DW} follows a scaling law with the DW energy σ_{DW} as a form of $w_{\text{DW}} \sim \sigma_{\text{DW}}^{-4/9}$, where σ_{DW} is given by a function of the in-plane magnetic field H_x as

$$\sigma_{\text{DW}}(H_x) = \begin{cases} \sigma_0 - \frac{\pi^2 \lambda M_S^2}{8K_D} (H_x + H_{\text{DMI}})^2 & \text{for } |H_x + H_{\text{DMI}}| < \frac{4K_D}{\pi M_S}, \\ \sigma_0 + 2K_D \lambda - \pi \lambda M_S |H_x + H_{\text{DMI}}| & \text{otherwise} \end{cases} \quad (1)$$

at equilibrium. Here, σ_0 is the Bloch-type DW energy density, K_D is the DW anisotropy energy density, λ is the DW width, and M_S is the saturation magnetization [5]. The equation provides that $w_{\text{DW}}(H_x)$ has its minimum value at $H_x = -H_{\text{DMI}}$, where the maximum σ_{DW} also appears. Therefore, measurement of $w_{\text{DW}}(H_x)$ provides a way to determine H_{DMI} . The present scheme was then applied to determine H_{DMI} 's in Pt/Co/Pt ultrathin films, which exhibit both sizable DMI strength and strong perpendicular magneto anisotropy. To check the validity, H_{DMI} 's were again measured by other independent measurement schemes based on the DW velocity v_{DW} [5]. Figure 1 shows the plots of (a) w_{DW} and (b) v_{DW} with respect to H_x . It is clear from the plots that both experimental schemes show the same strength of H_{DMI} and therefore, we confirmed the validity of our present DMI measurement scheme based on the DW roughness.

References

- [1] Stuart S. P. Parkin,* Masamitsu Hayashi and Luc Thomas, Science 320 (5873), 190-194. (2008).
- [2] I. E. Dzialoshinskii, Sov. Phys. JETP 5, 1259 (1957).
- [3] T. Moriya, Phys. Rev. 120, 91 (1960).
- [4] Albert Fert, Vincent Cros and João Sampaio, Nat. Nanotechnol. 8, 152 (2013).
- [5] S.-G. Je, K.-J. Lee, and S.-B. Choe, Phys. Rev. B 88, 214401 (2013).
- [6] J. Cho, B. Koopmans, and C.-Y. You, Nat. Commun. 6, 7635 (2015).
- [7] E. Jué, I. M. Miron, and G. Gaudin, Nat. Mater. 15, 272 (2016).
- [8] S. Lemerle, T. Giamarchi, and P. Le Doussal, Phys. Rev. Lett. 80, 849 (1998).

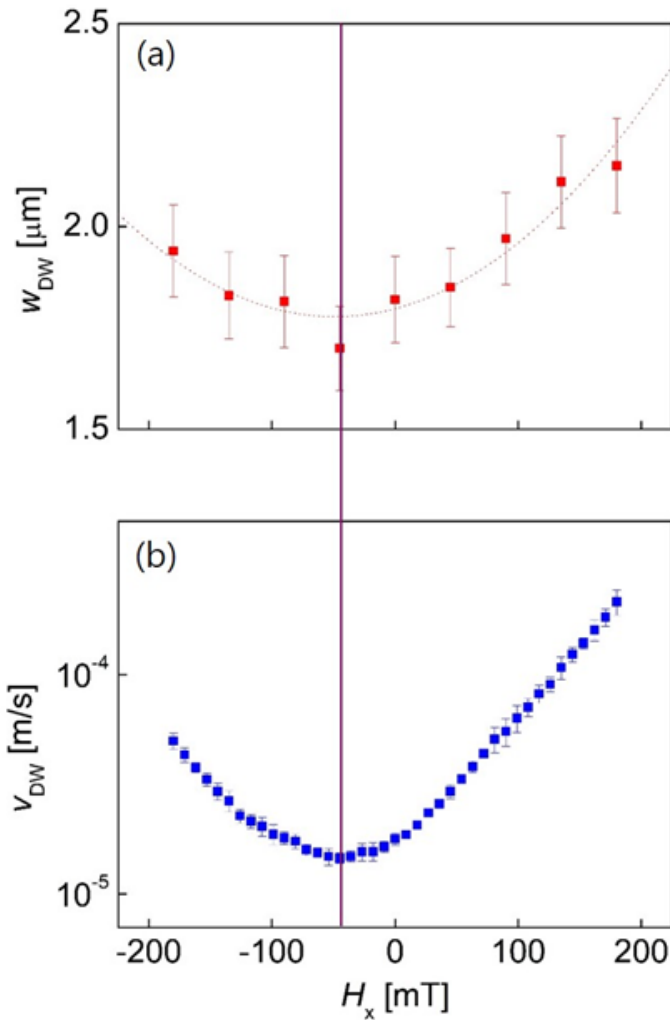


Figure 1. Plot of (a) w_{DW} and (b) v_{DW} with respect to H_x , respectively.

Magnetic properties tailoring by local interface engineering at Pt/Co/MgO structure

Suhyeok An^{*}, Ki-Seung Lee, Jin-A Kim, Chun-Yeol You[†]

A Department of Emerging Materials Science, DGIST, Daegu, Korea

The magnetic thin film with inversion symmetry breaking has been investigated because of its great potential for application of magnetic random access memory (MRAM) devices and scientific interests about spin-orbit coupling (SOC) phenomena. Especially because Heavy-metal (HM) / Ferromagnet (FM) / Oxide (MgO) structure has strong SOC at the HM/FM interface and inversion symmetry breaking system, resulting in strong perpendicular magnetic anisotropy (PMA) [1], spin-orbit torque (SOT) [2] and Dzyaloshinskii-Moriya interaction (DMI) [3,4], many researchers have been attracted and then many studies also carried out. Furthermore, not only phenomena itself, modulation research also has been conducted owe to its potential of applicating or improving magnetic material-based devices [5]. Although controlling interface induced magnetic properties is important for many reasons, these effects are directly related with the symmetry broken system itself and therefore manipulating and standardizing in sub-micron scale remain many challenges.

Here, we report that local magnetic properties are modulated by He⁺ ion irradiation at Pt/Co/MgO structure using Helium Ion Microscope (HIM). The Pt(5)/Co(0.8)/MgO(2) structure is irradiated by He⁺ ion with the dose range from 0 to 30 ions/nm², then effective PMA energy density, SOT switching critical current, and interfacial DMI energy density are investigated as function of irradiation dose. As a result, with the growing of dose values, changing of PMA energy density, SOT switching critical current, and interfacial DMI is observed but tendency is not simple. All of those phenomena depend on the interface state itself, but the reason for the different tendency is that the structural changes, resulting in the variation of SOC, degree of inversion symmetry breaking, and interface roughness caused by He⁺ ion irradiation, are working at each phenomena with different rates. From these results, we expect that low energy switching SOT devices and skyrmion-based logic devices also could be improved by light ion irradiation process.

References

- [1] Manchon, A. et al., J. Appl. Phys. 103, 07A912, (2008).
- [2] Miron, I. M. et al., Nature 476, 189-193 (2011)
- [3] Lee, J. M. et al., Nano Lett. 16, 62-67 (2015)
- [4] Cho, J et al., Nat. Comm. 6, 7635 (2015).
- [5] Zhao, X et al., Appl. Phys. Lett. 116, 242401, (2020).

A 3-dimensional control of exchange bias by spin orbit torque in Pt/Co/IrMn heterostructure

Eunchong Baek^{1*}, Suhyeok An¹, Chan-Kang Lee¹, Ki-Seung Lee¹, Woo-Yeong Kim^{1,2}, Chun-Yeol you¹

¹A Department of Emerging Materials Science, DGIST, Daegu, Korea

²A Department of Materials Science and Engineering, Korea University, Seoul 02841, Republic of Korea

Antiferromagnetic (AFM) materials are one of the future memory device candidates with the advantage of being robust to an external magnetic field and no fringing magnetic field [1]. However, for the same reason, it is difficult to manipulate magnetic states of an AFM. In recent years, there have been many reports of manipulating antiferromagnet by current injection [2,3]. In the AFM/heavy metal (HM) structure, the spin current due to the spin Hall effect of HM manipulates the AFM Neel vector. However, the difficulty of detecting AFM Neel vector limit relating researches. One of the ways to detect the AFM state is exchange bias (EB) in Ferromagnetic metal (FM)/AFM structure. Many studies reported that employ the EB to detect AFM switching by spin orbit torque in AFM/HM structure [4]. However, the underlying mechanism of how the spin torque act on EB has been unrevealed.

Here, we observe 3-dimensional control of EB by SOT in the Pt/Co/IrMn as a typical HM/FM/AFM heterostructure. The EB field is switched by applying a current pulse to the Hall bar and detected by anomalous Hall effect of Co. Injecting a single current pulse under an external magnetic field set the FM state arbitrarily and manipulate exchange bias field depending on FM state simultaneously. Furthermore, the multi-domain, 3-dimensional state can be imprinted on the AFM under various external magnetic fields. To exclude the Joule heating effect, the maximum temperature during current pulse injection is estimated from the change of resistance and confirmed that the maximum temperature is below the blocking temperature.

References

- [1] V. Baltz, et al., Antiferromagnetic spintronics. *Rev. Mod. Phys.* 90, (2018)
- [2] P. Wadley, et al., Electrical switching of an antiferromagnet. *Science* 351, 587-590 (2016)
- [3] X. Z. Chen, et al., Antidamping-Torque-Induced Switching in Biaxial Antiferromagnetic insulators. *Phys. Rev. Lett.* 120, 207204 (2018)
- [4] P.-H. Lin, et al., Manipulating exchange bias by spin-orbit torque. *Nat. Mater.* 18, 335 (2019)

Linear Dependence of Creep Scaling Constant on Co-Layer Thickness

Seong-Hyub Lee^{*}, Joon Moon, Ji-Sung Yu, Sug-Bong Choe[†]

Department of Physics & Astronomy, Seoul National University, Seoul 151-742, Republic of Korea

Despite apparently different phenomena, many of systems often follow unified dynamics laws such as fluid invasion of porous media, vortex lattices, charge-density waves, and contact lines during wetting of solids by liquids. Among these various disordered systems, magnetic multilayer systems provide test body to analyze the disordered media with their dynamics, especially through the behavior of magnetic domain wall motion under application of external field. Here we report the relation between the creep scaling constant α and the ferromagnetic layer thickness t_{Co} in various tri-layer magnetic systems. For this study, we prepared a series of magnetic ultrathin films using DC magnetron sputtering system. The detailed layer structure is Ta (5 nm) / X (2.5 nm) / Co (t_{Co}) / Pt (1.5 nm) on Si (525 μm) / SiOX (100 nm) substrates, with three different heavy metals X (=Au, Pd, and Pt) over the t_{Co} ranges (0.3-0.9 nm) with 0.1 increments. And then, creep motion was observed by use of a polar magneto-optical Kerr effect (MOKE) microscope. Under application of external magnetic field H , the domain wall speed v follows the creep scaling law $v=v_0\exp(-\alpha H-\mu)$ of elastic interfaces, where v_0 is the characteristic speed and μ ($=0.25$) is the creep exponent. Figure 1 plots α with respect to t_{Co} for different X. The figure clearly exhibits the linear proportionality between α and t_{Co} irrespective of different X. This clear linear proportionality provides us a way to predict the effective ferromagnetic layer thickness in perpendicular magnetic anisotropy ultrathin films.

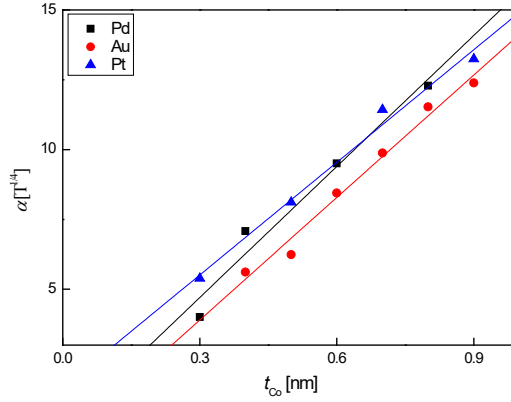


FIG. 1. Linear proportionality of the creep scaling constant α over the Co-layer thickness t_{Co} of Ta (5 nm) / X (2.5 nm) / Co (t_{Co}) / Pt (1.5 nm), where X (=Au, Pd, and Pt) over t_{Co} ranges (0.3-0.9 nm) with 0.1 nm increments.

References

- [1] D.-Y. Kim, M.-H. Park, and S.-B. Choe, Appl. Phys. Lett. 112, 062406 (2018).
- [2] P. J. Metaxas, J. P. Jamet, and R. L. Stamps, Phys. Rev. Lett, 99, 217208 (2007).
- [3] S. Lemerle, J. Ferre, and P. L. Doussal, Phys. Rev. Lett. 80, 849 (1998).
- [4] R. Chauve, T. Giamarchi, and P. L. Doussal, Phys. Rev. B, 62, 6241 (2000).
- [5] K.-W. Moon, D.-H. Kim, and S.-B. Choe, Phys. Rev. Lett. 110, 107203 (2013).
- [6] S. Bandiera, R. C. Sousa, and B. Dieny, IEEE Magn. Lett. 2, 3000504 (2011).

Magnetic and mechanical properties of 17–4PH stainless steel fabricated by Metal FDM additive manufacturing

최광수^{1,2*}, 이승훈¹, 정효연^{2*†}

금속 적층제조 공정(metal additive manufacturing)은 디지털 모델링이 된 부품을 형상 그대로 금속 재료로 한층 씩 쌓아 올려 형상을 제작하는 제작 공정이다. 이러한 적층제조 공정은 제작 가능한 형상의 자유도가 높아, 복잡한 형상의 부품 제작이 요구되는 고부가가치의 산업의 특수 부품 제작을 위한 공정으로 많은 주목을 받고 있다. 금속 적층제조 공정 중 Fusion Deposition Modeling (FDM)은 기존에 상용화 되고 있는 금속 적층 공정인 Powder bed fusion (PBF), Direct Energy deposition (DED) 보다 공정 비용과 산업적인 측면에서 우수한 특징이 있다. 본 연구에서는, 17-4PH 분말이 포함된 필라멘트를 사용한 FDM 공정으로 3차원 형상의 스테인리스 강 시편을 제작하여, Printing / Debinding / Sintering으로 구성된 각 제조 단계 및 적층 방향에 따른 자성 특성을 비교하였다. 또한, 인장시험을 통해 제작된 시편의 기계적 물성을 평가하고 파단면 분석을 진행하였다. 이를 통해, FDM 적층 공정으로 제작된 산업 부품의 활용 및 검토를 위한 기초 자료로 사용 할 수 있을 것으로 사료된다.

Keywords: Fusion Deposition Modeling, 17-4PH stainless steel, magnetic properties, tensile test

Re₂O₃ 나노입자의 극저온 자기열량효과

Kiran Shinde¹, Tien Van Manh¹, 유성초², 김동현^{*}

¹ 충북대학교 물리학과

² UNIST 물리학과

(*Email : donghyun@cbnu.ac.kr)

자기열량효과(MCE: Magnetocaloric effect)에 기반한 냉각기술은 친환경성 및 고효율 등의 성질로 인해 최근 많은 각광을 받고 있다. 상온에서의 응용뿐 아니라 수소의 끓는점 근처의 자기열량효과가 수소를 액화하여 저장 및 수송하는데 고려해야할 중요한 요소라는 것이 알려져 있다. 본 발표에서는 Re₂O₃ 구조의 희토류(Re) 산화물이 극저온 환경에서 갖는 자기열량효과를 보고한다. Re 원소로 Tb, Dy, Ho 등의 원소를 사용하여 먼저 질화물을 만든 후 안정적으로 산화물 나노입자를 제작하였고 구조적 특성을 체계적으로 분석하였다. 제작된 희토류 산화물 나노입자들이 10K 및 그 이하의 극저온에서 2차 상전이를 보이는 것을 확인하였고 상전이 부근에서 자기열량효과를 체계적으로 분석하였다.

Dependence of magnetic properties and structural characteristics on low Boron concentration in CoFeB–MgO thin films

Jun-Su Kim^{*}, Woo-Yeong Kim^{a,d}, Jaehun Cho^b, June-seo Kim^c,
Gukcheon Kim^e, Jinwon Jung^e, Chun-Yeol You^{a,*}

^a Department of Emerging Materials Science, DGIST, Daegu, Republic of Korea

^b Global Center for Bio-Convergence Spin System, DGIST, Daegu, Republic of Korea

^c Intelligent Devices and System Research Group, DGIST, Daegu, Republic of Korea

^d Department of Materials Science and Engineering, Korea University, Seoul, Republic of Korea

^e SK hynix Inc., Icheon, Republic of Korea

*Corresponding Author email: cyyou@dgist.ac.kr

CoFeB has been used as a ferromagnet layer of various magnetic memory devices since the discovery of high TMR and thermal stability (Δ), low critical current (I_c), and perpendicular magnetic anisotropy (PMA) characteristics required for spin torque MRAM (ST-MRAM). However, when scaling down required in the device stage, a decrease of Δ and an increase in I_c were inevitable according to the smaller cell size. For successful device engineering, the need for new modulators that can offset such changes has been raised. Here, we present the tendencies of fundamental magnetic properties, such as the saturation magnetization (M_S), exchange stiffness (A_{ex}), and gilbert damping constant (α) according to the Boron composition of the 22nm CoFeB stacked as MgO/CoFeB/MgO. This approach presents a significant change of M_S , A_{ex} , α according to Boron composition and a clear structural correlation of the phenomena.

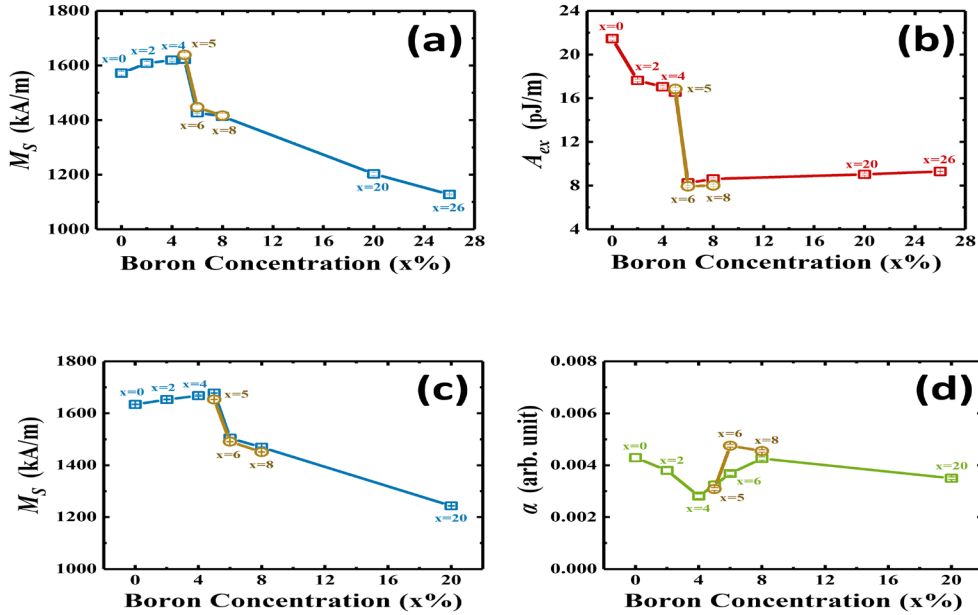


Fig. 1. BLS and FMR results. BLS results for the (a) saturation magnetization, and (b) exchange stiffness (A_{ex}) on Boron concentration. FMR results for the (c) saturation magnetization and (d) Gilbert damping constants on Boron concentration. Brown disks represents 18nm CoFeB for confirmation.

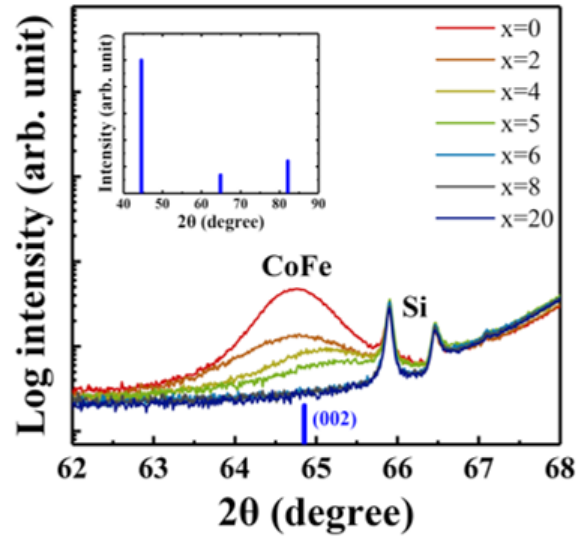


Fig. 2. XRD spectra. BCC (002) peak of CoFeB was observed and the peak intensity decreases according to increasing Boron concentration. The peak intensity disappears from 6% of the Boron composition.

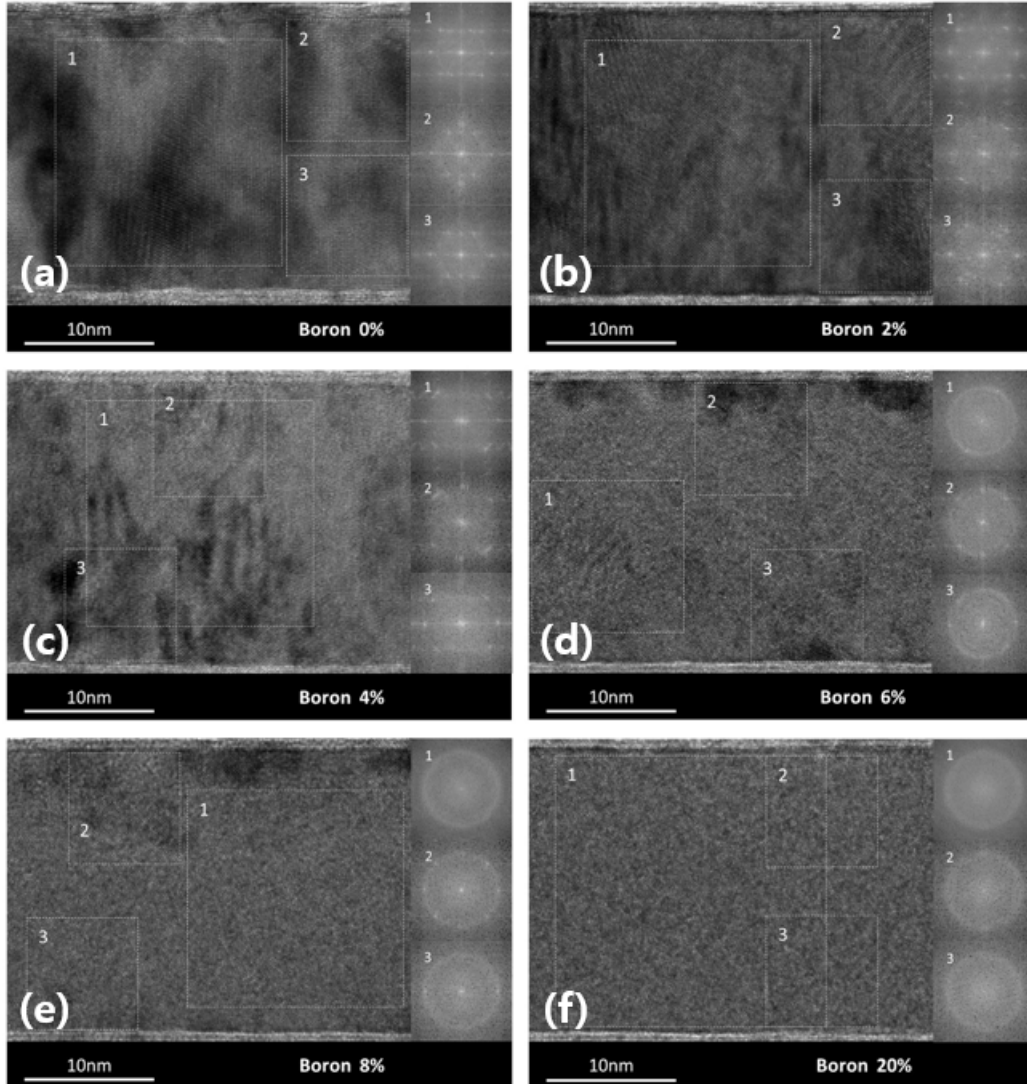


Fig. 3. TEM cross-section and FFT images. The dominant crystallinity of the CoFeB layer is BCC Crystalline up to 4% of the Boron composition, and then rapidly becomes amorphous as the Boron composition increases.

Investigating the structural magnetic and magnetocaloric properties in Ce-doped $\text{La}_{1.4-x}\text{Ce}_x\text{Ca}_{1.6}\text{Mn}_2\text{O}_7$ ($0 \leq x \leq 0.4$) bilayer manganites

Akshay Kumar^{*}, Min Ji Shin, Ji Eun Lee, Bon Heun Koo[†]

School of Materials Science and Engineering, Changwon National University,
Changwon, Gyeongnam, 51140, Republic of Korea

Abstract

Controlled substitution of Cerium (Ce) in place of Lanthanum (La) was performed in $\text{La}_{1.4-x}\text{Ce}_x\text{Ca}_{1.6}\text{Mn}_2\text{O}_7$ ($x = 0.0, 0.1, 0.2, 0.3$ and 0.4) to explore a possible enhancement in the magnetic and magnetocaloric properties of the material. The samples were produced following the solid-state reaction route. Rietveld refined XRD profiling was used that established the bilayer tetragonal structure ($I4/mmm$) of the Ruddlesden-Popper Phase in all compositions. Significant variations in the unit cell parameter were observed upon incorporation of Ce in place of La. All samples displayed well-defined ferromagnetic to paramagnetic transition at their transition temperature (TC). Against the pristine sample, the magnetic entropy change (ΔS_M) increased from $3.1 \text{ Jkg}^{-1}\text{K}^{-1}$ for the parent compound to $3.84 \text{ Jkg}^{-1}\text{K}^{-1}$ for $x = 0.1$ composition under 2.5 T applied field with controlled substitution of Ce. Highest relative cooling power (RCP) values of 102 Jkg^{-1} were obtained in the $x = 0.1$ samples at 2.5 T applied field. Our findings in this work suggest enhanced magnetic and magnetocaloric properties in the Ce-doped samples and support the possibility of further tailoring these materials for applications in magnetic refrigeration technology.

Keywords: Magnetocaloric properties, Ruddlesden-Popper Phase, transition temperature (TC), relative cooling power (RCP), magnetic refrigeration

Current induced spin–orbit toques in two–dimensional Fe₃GeTe₂ nanoflakes

Sungyu Park^{1*}, Eun–su An^{1,2}, Junho Seo^{1,2}, Jun Sung Kim^{1,2}

¹Center for Artificial Low Dimensional Electronic Systems, Institute for Basic Science, Pohang 790–784, Korea

²Department of Physics, Pohang University of Science and Technology, Pohang 790–784, Korea

Fe₃GeTe₂ (FGT) holds a unique position among ferromagnetic materials due to the hidden inversion-symmetry breaking and the topological band structure. Recent development on Al₂O₃-assisted exfoliation enables isolation of FGT nanoflake with thickness down to monolayer, which can be utilized for spintronic applications based on van der Waal heterostructures. Particularly, due to the broken inversion symmetry of the single layer, the current-induced spin-orbit torque(SOT) has been predicted to be effective to control the magnetization, which may remain robust even in a few layers of FGT. In this work, we will present experimental evidence for the current-induced manipulation of magnetization in FGT nanoflakes. Possible implication on the high-efficiency SOT based switching device will also be discussed.

Domain wall energy analysis in trapezoid shaped Hall bar with perpendicular magnetic anisotropy

Dongryul Kim^{*}, Suhyeok An, Eunchong Baek, Woo-yeoung Kim^b, Ki-seung Lee, Chun-yeol You[†]

^a Department of Emerging Materials Science, DGIST, Daegu, Republic of Korea

^d Department of Materials Science and Engineering, Korea University, Seoul, Republic of Korea

^{*}Corresponding Author email: cyyou@dgist.ac.kr

In the department of memory devices, there is a kind of requirements for storing performance such as non-volatility, storing volume and processing ability. Especially, the processing speed is an issue of the memory devices field. Similar to hard disk drive memory, Domain wall devices that utilize phenomena occurs in magnetic materials have been steadily developed such as racetrack memory. When it comes to domain wall memory devices, processing ability associate with domain wall speed. To achieve processing speed for comparison to other memory devices such as solid state device, dynamic random access memory or more than that, driving force such as a magnetic field or current should be higher, or we can adjust the width of the racetrack that affects to domain wall energy.

To identify shape is affect to domain wall energy, we choose a Pt(5)/Co(1.2)/Ta(2) multilayer film that has a perpendicular magnetic anisotropy with the trapezoid shape Hall bar system. In the narrow region of the trapezoid shape which has a lower domain wall energy, the velocity of the domain wall is increased. We designed three angles for trapezoid 30, 40 and 50 degree. Domain wall velocity is observed magneto-optical Kerr effect microscope imaging method. Consequently, effective field that caused by shape effect, is increased as trapezoidal angle is increased. And velocity increment percent is also proportional to angle.

By using Hall bar system, we can designate starting and end point of domain wall position. As you can see in the fig. 1., Hall resistance will be change whether domain wall pass through the line or not. The result is expected that domain wall energy can be controlled by shape effect so that enhancement of processing speed.

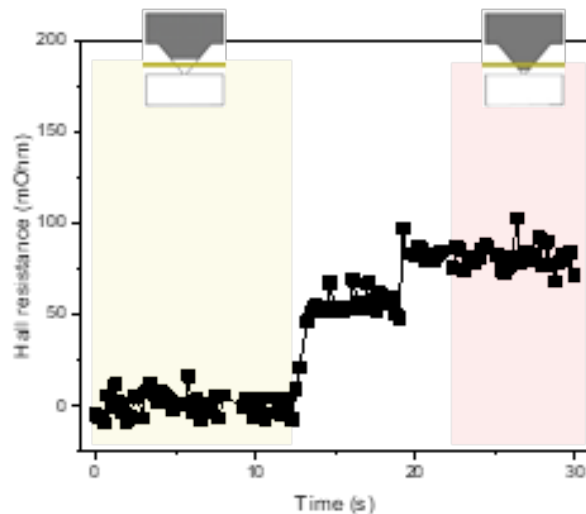


Figure 1. Voltage difference according to domain wall position

Manipulating asymmetric domain wall motion by uniaxial realignment of antiferromagnet spins in exchange coupled system with Dzyaloshinskii–Moriya interaction effect

Hyun–Joong Kim^{1*}, Soong–Geun Je², Won–Chang Choi³, Kyoung–Woong Moon¹,
Seungmo Yang¹, Changsoo Kim¹, Jung–Il Hong³, Chanyong Hwang¹

¹Quantum Technology Institute, Korea Research Institute of Standards and Science, Daejeon 34113, Republic of Korea

²Department of Physics, Chonnam National University, Gwangju 61186, Republic of Korea

³Department of Emerging Materials Science, DGIST, Daegu 42988, Republic of Korea

Recently, the current-induced domain wall (DW) motion as well as the field-driven DW motion in ultrathin ferromagnetic (FM) film with Dzyaloshinskii–Moriya interaction (DMI) effect has been mainly studied to examine unique behavior of DW motion. In general, it has been researched that asymmetric DW propagation with application of both out-of plane and in-plane external magnetic field (H_{ext}) was resulted from DMI effect in ultrathin film with perpendicular magnetic anisotropy (PMA). On the other hand, the DW motion of FM layer dependent on configuration of antiferromagnet (AFM) spins was not mainly researched and reported yet, even though the exchange-bias phenomenon due to an exchange coupled AFM/FM bilayers has been studied for a long time over several decades. Thus, we investigated field-driven DW motion of ultrathin FM layer with PMA, exchange coupled with AFM IrMn layer. Furthermore, it was realized that perpendicular field-driven asymmetric DW was propagated by uniaxial alignment of AFM spins at the interface between AFM/FM bilayer without in-plane H_{ext}. Additionally, it was possible to control asymmetric DW motion by manipulating configuration of AFM spins using injection of spin hall current.

Spin–thermoelectric energy conversion for transparent thermoelectrics

HyeonJung Jung^{*}, Inseon Oh^{*}, Jung-Woo Yoo[†]

Department of Materials Science and Engineering, Ulsan National Institute of Science and Technology, Ulsan, 44919, Korea

Spin Seebeck effect, in combination with the inverse spin Hall Effect, can be applied directly for the conversion from heat to electric energy. Spin Seebeck thermoelectric generator allows new approaches toward the improvement of thermoelectric generation efficiency. In general, the conventional thermoelectric generator has the limitation of the efficiency due to the trade-off relation among Seebeck coefficient (S), electrical conductivity (σ), and thermal conductivity (κ). In contrast, the application of ferrimagnet insulator in spin Seebeck effect has great advantages for enhancing thermoelectric efficiency. In particular, the magnetic insulators are generally optically transparent so that the spin-thermoelectric module also can be constructed to be transparent.

Here, we introduce the transparent and spin-thermoelectric device based-on YIG/Pt heterojunction with improved figure of merit (ZSSET). Using ultrathin Pt layer, the transmission of YIG/Pt heterojunction can be as high as 90 % in the visible range (400 to 700 nm). Furthermore, the observed longitudinal spin Seebeck coefficient ($S = ((\Delta V/L)/(\Delta T/L_z))$) increased exponentially with decreasing Pt thickness. For 0.8 nm of the Pt layer, the estimated longitudinal spin Seebeck coefficient $\sim 13 \mu\text{V/K}$, which is much higher than those obtained in previous studies. Our study showed that the spin-thermoelectric device could be utilized in ubiquitous recycling of waste heat thanks to its simple structure, relevant for keeping transparency.

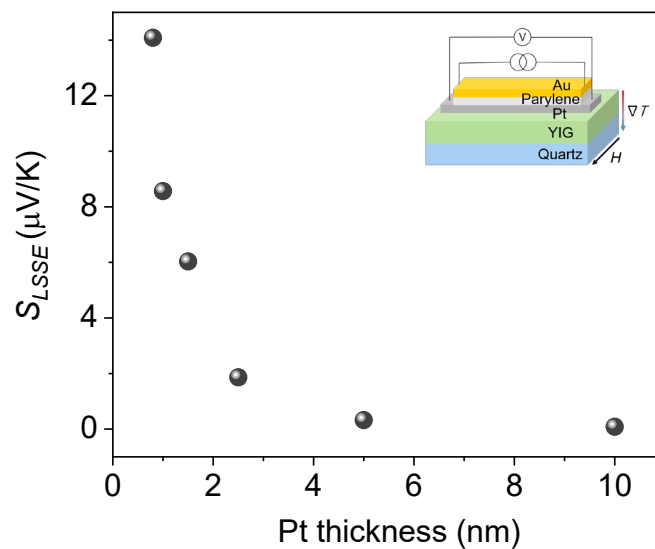


Fig. 1. Longitudinal spin Seebeck coefficient (S_{LSEE}) as a function of Pt thickness

Direct Investigation of Lattice Expansion of $\text{Ni}_x\text{Fe}_{1-x}$ alloy films by Ultrafast Sagnac Interferometry

Yooleemi Shin^{1,2}, Ji-Wan Kim^{1*}

¹Department of Physics, Kunsan National University, Kunsan 54150, South Korea

²Department of Physics, Chungbuk National University, Cheongju-si 28644, South Korea

Until now, in order to understand ultrafast dynamics of electron and lattice induced by femtosecond laser pulses, the differential reflectivity $\Delta R(t)/R$ needs to be analyzed. By assuming that $\Delta R(t)/R$ has only thermal-optic contribution, three-temperature model has been generally employed to obtain the time-dependent temperature profile of each subsystem. However, this is hypothetical because in fact, $\Delta R(t)/R$ contains a piezo-optic contribution as well as a thermo-optic one. The piezo-optic property occurs when a material dimension changes by a certain reason. In case of the pump-probe experiment, materials absorb the photon energy of femtosecond laser leading to ultrafast thermal expansion. Although the piezo-optic property are secondary effect induced by a change of temperature, the piezo-optic contribution is comparable to the thermo-optic one and should not be passed over.

To estimate the piezo-optic contribution to the differential reflectivity, it is definitely proceeded to quantitatively measure a change of dimension, that is the dynamics of lattice expansion after femtosecond laser excitation. Here, as shown in Fig. 1, we directly investigate the dynamics of lattice expansion of various ferromagnetic materials ($\text{Ni}_x\text{Fe}_{1-x}$ alloys, $x=0, 0.33, 0.36, 0.39, 0.42$) with ultrafast Sagnac interferometer [1]. They appear very different behaviors, but show in common that their lattice expansions complete in 5 ~ 10 ps and decay via thermal energy dissipation to substrates.

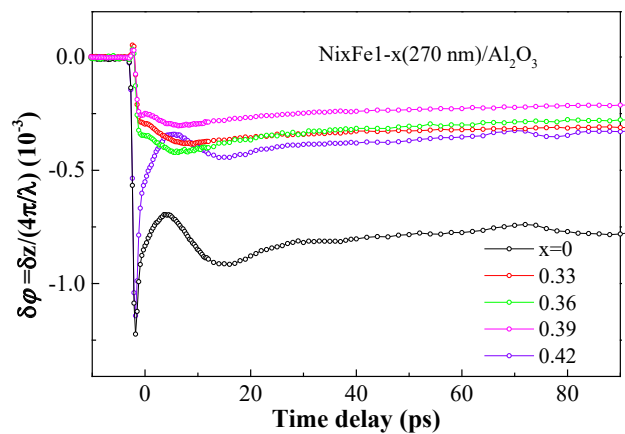


Figure 1. Measurement of the lattice expansion ($\delta \varphi$) with NiFe alloys using ultrafast Sagnac interferometry

[1] D. H. Hurley and O. B. Wright, Opt. Lett. 24, 1305 (1999).
email: hwoarang@kunsan.ac.kr

Large Spin–Orbit Torque and Strong Two Magnon Scattering in AuPt/Ferromagnet bilayers

D. J. Lee^{1,2*}, D. H. Yun^{1,3}, B. -C. Min¹, H. C. Koo¹, K.-J. Lee⁴, O. J. Lee¹

¹Center for Spintronics, Korea Institute of Science and Technology, Seoul 02792, Korea

²KU-KIST Graduate School of Converging Science and Technology, Korea University, Seoul 02841, Korea

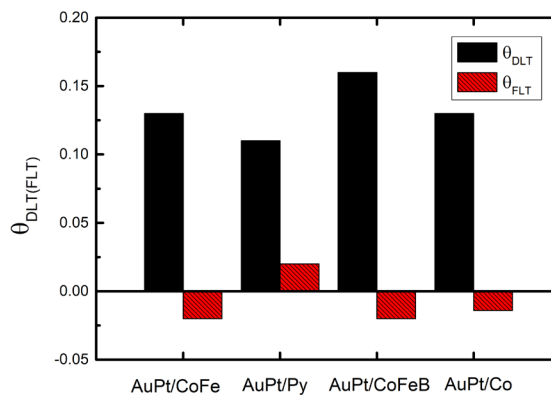
³Department of Electrical Engineering, Korea University, Seoul 02841, Korea

⁴Department of Physics, KAIST, Daejeon 34141, Korea

Current induced spin-orbit torques (SOTs) has attracted attention in spintronics due to their efficient manipulation of magnetization. Recently, several researches have reported that AuPt alloy has larger spin hall efficiency than Pt with lower resistivity than other heavy metals (W, Ta). [1] [2] [3] it means that the possibility of energy-efficient ultrafast SOT-MRAMs based on AuPt alloy. [4] Also magnetic damping (α) is key parameter which determine magnetic relaxation of magnetic dynamics. In general cases, magnetic damping mostly dominated by spin-pumping effect in ferromagnet (FM)/heavy metal (HM) bilayers system. However recent works suggest that two-magnon scattering (TMS) is major element of magnetic damping which related to interfacial spin-orbit coupling (ISOC). [5] We investigated spin-orbit torque and magnetic damping in AuPt/Ferromagnet (FM) bilayers with different FM materials (FM = CoFe, CoFeB, Py, Co) by using spin-torque ferromagnetic resonance (ST-FMR). We observed large spin Hall efficiency of AuPt, And the magnitude of damping-like spin hall efficiency depends on FM materials up to 50 %. Also we observed magnetic damping of AuPt/FM bilayer system critically depends on FM materials. This dependence supports that TMS is intimately related to interfacial spin orbit coupling.

References

- [1] M. Obstbaum, M. Decker, and C.H. Back et al., Phys. Rev. Lett. 117, 167204 (2016)
- [2] Yanjun Xu, Yumeng Yang, Hang Xie, and Yihong Wu, Appl. Phys. Lett. 115, 182406 (2019).
- [3] Lijun Zhu, D. C. Ralph, and R. A. Buhrman, Phys. Rev. Appl. 10, 031001 (2018).
- [4] Lijun Zhu, Lujun Zhu, Shengjie Shi D. C. Ralph, and R. A. Buhrman, Adv. Electron. Mater. 6, 1901131 (2020).
- [5] Lijun Zhu, Lujun Zhu, D. C. Ralph, and R. A. Buhrman, Phys. Rev. Appl. 13, 034038 (2020).



Magnetic Oscillation on Indirectly Coupled Ferromagnetic Layers

D. H. Yun^{1,2*}, D. J. Lee^{1,3}, B. -C. Min¹, H. C. Koo¹, K.-J. Lee⁴, O. J. Lee¹

¹Center for Spintronics, Korea Institute of Science and Technology, Seoul 02792, Korea

²Department of Electrical Engineering, Korea University, Seoul 02841, Korea

³KU-KIST Graduate School of Converging Science and Technology, Korea University, Seoul 02841, Korea

⁴Department of Physics, KAIST, Daejeon 34141, Korea

In spintronics, recent researches are attracting attention to radio frequency devices such as oscillator through magnetization manipulation. Spin-orbit torque are considered as mechanism of radio frequency devices using magnetization manipulation such as spin Hall nano-oscillator (SHNO) [1][2]. In this works, we observed higher order resonance mode in ferromagnet/normal metal/ferromagnet trilayers system which manipulated by inplane charge current. We inserted Pd to weaken exchange interaction at the CoFe/Py interface with varying Pd thickness. We performed spin-torque ferromagnetic resonance (ST-FMR) measurements in ferromagnet/normal metal/ferromagnet trilayers system. When Pd is very thin, measured FMR spectra shows one peak, and when Pd is thick, exchange interaction between two magnetic layers disappears, showing two peaks, and each peak represents FMR spectra of each magnetic layer[3]. However, when certain thickness of Pd inserted, we observed two peaks of FMR spectra, and the higher order mode appears in range of frequencies much higher than ferromagnetic resonance. We also performed conventional FMR measurements without inplane charge current. The higher order modes were vanished. The higher order modes induced by inplane current have potential to expand frequency range of magnetic oscillator. In this presentation, we shall show detailed results of measured FMR spectra, and will discuss about possible origins of higher order modes.

References

- [1] V. E. Demidov, S. Urazhdin, A. Zholud, A. V. Sadovnikov, and S. O. Demokritov, Appl. Phys. Lett. 105 172410 (2014).
- [2] R. H. Liu, W. L. Lim, and S. Urazhdin, Phys Rev. Lett. 110 147601 (2013)
- [3] S. Iihama, T. Taniguchi, K. Yakushiji, A. Fukushima, Y. Shiota, S. Tsunegi, R. Hiramatsu, S. Yuasa, Y. Suzuki, and H. Kuboto, Nat. Elec. 1, 120-123(2018).

Observation of magnetic field induced ferroelectricity in the poly- and single crystals of $\text{CaFe}_3\text{O}(\text{PO}_4)_3$

Kwang-Tak Kim¹, Aga Shahee¹, Joong-Woo Lee¹, Voma Uday Kumar², B. Koteswara Rao²,
Kee Hoon Kim^{1,2}

¹Center for Novel States of Complex Materials Research, Department of Physics and Astronomy, Seoul National University, Seoul 08826, Republic of Korea

²Department of Physics, Indian Institute of Technology Tirupati, TIRUPATI, Chittoor District, Andhra Pradesh- 517506, India

³Institute of Applied Physics, Department of Physics and Astronomy, Seoul National University, Seoul 08826, South Korea

email: khkim@phya.snu.ac.kr

A new type of magnetic oxyphosphate $\text{CaFe}_3\text{O}(\text{PO}_4)_3$ [1-2], consisting of chains of Fe^{3+} polyhedra (octa- and tetra-hedra) along the b axis and another axis in the ac-plane, forms a complex three-dimensional frustrated spin lattice. The polycrystal $\text{CaFe}_3\text{O}(\text{PO}_4)_3$ has been claimed to exhibit three structural transitions at $T_{C1} = 18.1$ K, $T_{C2} = 10.4$, and $T_{C3} = 7.9$ K, and spin transitions have been identified near T_{C1} and T_{C3} , which were interpreted as canted antiferromagnetic transitions CAF I and III, respectively. A reported large Curie-Weiss temperature $\Theta_{CW} = -260.5$ K compared with T_{C1} indicate moderate magnetic frustration. The various competing spin transitions and spin frustration in this material suggest a possibility of spin-ordering induced ferroelectricity [3-4]. Here, we report the observation of magnetic field (H) induced ferroelectric polarization (P) in both poly- and single-crystals of $\text{CaFe}_3\text{O}(\text{PO}_4)_3$ below T_{C2} and at $H > \sim 1.1$ T. In the $\text{CaFe}_3\text{O}(\text{PO}_4)_3$ single crystals, we found an experimental evidence of a new magnetic phase (named as CAF II) in the magnetization study below 1 T along the a-axis, being consistent with the previously known structural transition near T_{C2} . When the magnetic field is applied along the a-axis, a sharp field-induced first-order magnetic transition below T_{C2} occurring at $\mu_0 H = \sim 1.1$ T, which suggests a spin-flop transition. In the electric polarization measurements of the polycrystal $\text{CaFe}_3\text{O}(\text{PO}_4)_3$, we found first H-induced ferroelectricity at $\mu_0 H \geq 1.0$ T and below T^* . In the subsequent investigations with single crystal $\text{CaFe}_3\text{O}(\text{PO}_4)_3$, we find that P_b and P_c appear under a transverse $\mu_0 H_a \geq 1.0$ T, at which the spin-flop transition along a-axis occurs. As the three magnetic transitions existing below the spin-flop transitions are not observed at high fields according to the magnetization measurements at high fields, a new spin order seems to be stabilized at $\mu_0 H \geq 1.0$ tesla and below T^* . Based on the previous observation of magnetic phase competition between CAF and spiral phases in various compounds such as MnWO_4 [4], we argue that the H-induced ferroelectricity may stem from the spin spiral phase, competing with CAF orders but being stabilized under finite magnetic fields above ~ 1 T.

References

- [1] H. El Hafid et al., Eur. J. Inorg. Chem. 36 5486-5495 (2011)
- [2] H. El Hafid et al., Solid State Sci. 36, 52-61 (2014)
- [3] K. Yoo et al., npj Quantum Materials 3, 45 (2018).
- [4] K. Taniguchi et al., Phys. Rev. Lett. 97, 097203 (2006)

Designing the composition of the Fe–Ni–Si–B–Cu–P amorphous alloy based on Nanomet

JongHee Han^{*}, Haein Choi–Yim

Department of Physics, Sookmyung Women's University

The rare-earth-free hard magnetic L10-FeNi phase has excellent magnetic properties such as a high saturation magnetization ($M_s \sim 1270 \text{ emu/cm}^3$) and a large uniaxial magnetic anisotropy ($K_u \sim 1.3 \times 10^7 \text{ erg/cm}^3$). However, it is very difficult to artificially produce the L10-FeNi phase due to the low atomic diffusion coefficients of Fe and Ni near the order-disorder temperature ($\sim 320^\circ\text{C}$). Also, if the interval between the crystallization temperatures of each stage is increased, the effect of phase except the L10-FeNi phase can be minimized during in heat treatment, so the implementation of the L10-FeNi phase becomes easy. Therefore, the composition of Fe-Ni-Si-B-Cu-P amorphous alloys based on Nanomet were designed. The thermal properties of Fe-Ni-Si-B-Cu-P amorphous alloys were measured by using differential scanning calorimetry (DSC), including crystallization temperature (T_x). It exhibit T_x near the transition temperature. After measuring thermal properties, the amorphous alloys were annealed at T_x resulting in high atomic diffusion. The structural and micro structural characterizations of annealed ribbons revealed the formation of L10-FeNi phase through observation of the superlattice peak by using X-ray Diffraction (XRD). The magnetic property measured by a vibrating sample magnetometer (VSM), such as M_s and coercivity (H_c), also indicated the formation of L10 FeNi phase.

Fabrication of Epsilon Hard Ferrites for Electromagnetic Wave Absorption Application

Min-Ji Pyo^{1,2*}, Gi-Ryeon Jo^{1,3}, Hee-Lack Choi², Youn-Kyoung Baek^{1†}

¹ Powder and Ceramics Division, Korea Institute of Materials and Science, Chang-won, Korea

² Department of Materials Science and Engineering, Pukyong National University, Busan, Korea

³ School of Materials Science and Engineering, Pusan National University, Busan, Korea

Electromagnetic (EM) waves are beginning to be using in electronic devices for high-speed wireless communication such as in local-area networks and radars for the distance between cars. Ferrites with high coercive field (H_c) have been used as Electromagnetic wave shielding materials due to their ferromagnetic resonance. The epsilon iron oxide (ϵ -Fe₂O₃) has remarkable advantages in spectroscopic absorption with highest resonance frequency due to its gigantic coercive field ($> 20\text{kOe}$) at room temperature. However, it is difficult to produce high purity epsilon phase since that only can be obtained under the specific conditions such as nanometer sized particle and narrow annealing temperature. Thus, researchers have tried various synthesis methods to obtain ϵ -Fe₂O₃ nanoparticles such as reverse-micelle & sol-gel method and templating method, which have multiple steps and low yield. In this study, we have developed a facile and scalable method to fabricate high purity ϵ -Fe₂O₃ via an aerosol approach. In addition, the magnetic properties were controlled by replacing some Fe³⁺ ions with various non-magnetic elements such as Ga and Y. Thus, our strategy would pave the way for the practical application of ϵ -Fe₂O₃ as the electromagnetic wave absorber.

Acknowledgement: This research was supported financially by the Fundamental Research Program (PNK 6820 and PNK 6900) of Korea Institute of Materials Science.

Keywords: Epsilon Ferrite, Electromagnetic Wave, Millimeter Wave, Absorber, Aerosol,

Facile Synthesis of Al–Ca Substituted M–type Hexaferrites with a Gigantic Coercivity

Gi–Ryeon Jo^{1,2*}, Min–Ji Pyo^{1,3}, Young–Guk Son², Youn–Kyoung Baek^{1†}

¹ Powder & Ceramics Division, Korea Institute of Materials Science, Changwon, Korea

² School of Materials Science and Engineering, Pusan National University, Busan, Korea

³ Department of Materials Science and Engineering, Pukyong National University, Busan, Korea

Hard magnetic materials have applied in various applications ranging from permanent magnets and microwave absorbers. Especially, M-type hexaferrites (MFe₁₂O₁₉ (M=Pb, Sr, Ba)) with magnetoplumbite structure have been of considerable interest due to their high saturation magnetization (≈ 70 emu/g), chemical stability and low price. However, ferrites have relatively low coercivity (<7 kOe), resulting in the limitation for the application of hard magnet or millimeter wave absorber. Herein, to enhance the coercivity of M-hexaferrite, we have synthesized Sr-ferrite with elemental substitution of Ca and Al ions using aerosol - assisted. The resulting ferrites show the gigantic coercivity over 20 kOe, which may attributed to the lattice contraction of unit cell induced by replacing Al ions for octahedral Fe sites. This work would be one of the methods for industrial production of hard ferrite magnets for millimeter wave absorption.

This research was supported financially by the Fundamental Research Program (PNK 6900) of Korea Institute of Materials Science and National R&D Program through the National Research Foundation of Korea(NRF) funded by Ministry of Science and ICT(2020M3H4A308202811).

Keywords: M-type hexaferrite, EM wave absorption, Millimeter wave, Permanent magnet

Sm-Fe계 HDDR 분말의 결정구조에 따른 자기특성과 질화 거동

노태성^{1,2*}, 차희령¹, 김태훈¹, 김양도^{2*†}, 이정구^{1*†}

¹한국기계연구원 부설 재료연구소, 기능분말연구실

²부산대학교, 재료공학과

최근 Nd-Fe-B계 자석은 우수한 자기특성으로 하이브리드/전기자동차 구동모터에 핵심소재로 이용되고 있다. 이러한 친환경 자동차 모터는 작동 중에 약 200℃까지 온도가 상승할 수 있지만, Nd-Fe-B계 자석은 높은 온도에서 보자력이 급격히 감소하는 중대한 문제점이 있다. 이와 같은 문제를 해결하기 위해 Nd-Fe-B계 자석에 Dy와 같은 중희토류를 첨가하여 보자력을 개선하고 있지만, Dy와 같은 중희토류 자원은 대부분 중국에서 생산되고 있기 때문에 수급 불안정 및 가격 문제가 지속적으로 발생하고 있는 실정이다. 따라서 현재 Nd-Fe-B계 자석에 이용되고 있는 Dy를 줄이기 위해 Dy저감 기술과 Dy-free 자석의 개발연구가 주목받고 있다. 한편, Sm-Fe-N계 자석은 Nd-Fe-B계 자석과 비슷한 높은 자성특성을 가지고, Nd-Fe-B계 자석보다 약 150℃ 높은 큐리 온도를 가지고 있다. 특히 이방성자계가 26T로 Nd-Fe-B계 자석의 약 3배이기 때문에 Dy와 같은 중희토류를 사용하지 않으면서도 높은 보자력을 가질 수 있어 Nd-Fe-B계 자석을 대체할 수 있는 자석으로 알려져 있다. Sm-Fe-N계 영구자석을 제조하는 방법으로 분말 야금법, 급속응고법, Hydrogenation-Disproportionation-Desorption-Recombination (HDDR), 기계적합금법, 환원확산법이 있다. 이 중 HDDR 공정은 결정립을 수소화 반응, 상분해, 수소방출 및 재결합 과정을 통해 Sm-Fe-N계 자석의 단자구 크기인 300nm까지 미세화 할 수 있는 공정이다. 특히 Sm-Fe 합금의 경우 HDDR 공정온도를 제어함으로써 육방정계 결정구조와 능면체의 결정구조 형성이 가능하다고 보고되어 있고, 이러한 결정구조 차이는 제조된 분말의 자기 특성에 영향을 줄 수 있다. 한편, HDDR 처리된 Sm-Fe 합금분말은 질화를 통해 자기 특성을 향상시킬 수 있는데, 이러한 결정구조 차이에 따른 질화 거동에 대한 연구는 보고되지 않았다.

본 연구에서는 TbCu7 상의 육방정계 결정구조와 Th2Zn17 상의 능면체 결정구조를 가진 자성 분말을 제조하기 위해 Sm2Fe17 (at.%) 조성의 합금과 Sm2.4Fe17 (at.%) 조성의 합금을 600℃와 900℃에서 HDDR처리하였다. 제조된 HDDR 분말은 질소 분위기에서 12시간 질화 처리하여 Sm-Fe-N계 분말로 제조하였다. 실험 결과 TbCu7 상에서 질화가 비교적 내부까지 균일하게 이루어진 반면에 Th2Zn17 상에서는 표면에서만 균일한 질화가 이루어졌다. 하지만 TbCu7 상을 가진 분말의 경우 질화가 균일하게 이루어졌음에도 불구하고 자기 특성은 크게 향상되지 않았는데, 이러한 결과는 낮은 온도에서의 HDDR 공정 중에 재결합이 완전하게 이루어지지 않아 분말 내부에 다량의 α -Fe를 함유하고 있었기 때문이다. 한편, Th2Zn17 상을 가진 HDDR 분말의 내외부의 불균질한 질화를 해결하기 위해 입자 크기를 25-53 μ m까지 분쇄한 후 질화 처리하였는데, 이때 10.3 kOe의 가장 높은 보자력을 보였다. 본 연구에서는 이러한 결과를 바탕으로 Sm-Fe계 HDDR 분말의 결정구조에 따른 자기 특성과 질화 거동을 논의하고자 한다.

Keywords: Sm-Fe-N, HDDR, crystal structure

Iron deficiency of La–Co substituted Sr M–type hexaferrites on the magnetic properties

Kang-Hyuk Lee^{*}, Junho Park, SungJoon Choi, Sang-Im Yoo[†]

Department of Material Science and Engineering, Research Institute of Advanced Materials (RIAM), Seoul National University, Seoul, Korea

The Sr M-type hexaferrites (SrFe₁₂O₁₉) are one of the most widely used magnetic material due to their cost efficiency, strong uniaxial magnetic anisotropy along the c-axis, and excellent chemical stability. Recently, many studies have improved the intrinsic magnetic properties of M-type hexaferrites by substitution, such as saturation magnetization and crystalline anisotropy. Previous reports have been mainly focused on La³⁺ substitution for the Sr²⁺ site and Co²⁺ substitution for the Fe³⁺ sites of M-type hexaferrites. La-Co substituted Sr M-type indicated that intrinsic coercivity increased continuously with the substitution content. In addition, there is generally requires a non-stoichiometric of iron ratio between 10 and 12 on Ba M-type hexaferrites. While iron deficiency is known to be helpful for the grain growth and the structure formation of NiZn spinel ferrites. However, the effect of La-Co substitution and iron deficiency on magnetic properties of the Sr-La-Co M-type hexaferrites remains unexplored. In this study, therefore, we tried to investigate La-Co substituted Sr M-type hexaferrites Sr_{1-x}La_xFe_{12-x}Co_yO₁₉, (0 ≤ x ≤ 0.5) and the effect of iron deficiency on the magnetic properties of Sr_{1-x}La_xFe_yCo_{12-y}O_{19-δ} (x = 0.15, 10 ≤ y ≤ 12-x) hexaferrites prepared by solid state reaction. The raw materials were ball-milled for 24 h with SiO₂ additive and calcined at 1280 °C for 2 h in air. as-calcined powder was pressed into pellets and sintered at 1230 °C for 1 h in air with SiO₂ and CaCO₃ additives. Samples were characterized by powder X-ray diffraction (XRD), vibrating sample magnetometer (VSM), and scanning electron microscope (SEM). In case of Iron deficient Sr-La-Co M-type hexaferrites, Powder XRD analyses revealed that M-type single phase were obtained with all Fe contents at sintering temperature. The saturation magnetization (M_s) of the Sr-La-Co M-type hexaferrite samples was around 72 emu/g. The maximum M_s was obtained for Fe content of 11.85 at 74.4 emu/g. However, the coercivity (H_c) decreased with higher Fe content because the grain size was larger than the single domain size. The V_{cell} change due to substitution and iron deficiency seems to be inversely related to H_a obtained by magnetic hysteresis loops calculation. Detailed microstructures and magnetic properties of Sr-La-Co M-type hexagonal ferrites will be presented for a discussion

This research was supported by Future Materials Discovery Program through the National Research Foundation of Korea (NRF) funded by the Ministry of Science and ICT (2016M3D1A1027835)

Keywords: Hexaferrite, magnetic property, iron deficiency, M-type hexaferrite

Preparation for qualified MnBi powder via process control

Su Yeon Ahn*, Yang Yang, Jung Tae Lim, Jihoon Park, Jong-Woo Kim, Chul-Jin Choi

Korea Institute of Materials Science (KIMS), Republic of Korea

Rare-earth free permanent magnets are current emerging issues of industry for the growing market demands. Among the rare-earth free permanent magnets, MnBi has attracted attention for its strong magnetocrystalline anisotropy, positive temperature coefficient of coercivity and high energy product. In addition, MnBi shows higher coercivity as compared with other rare-earth magnets at the elevated temperature range. Therefore, MnBi is one of the potential candidates for high-temperature applications.

In this study, a precise process control for high performance MnBi powders will be discussed. A detailed optimization process and mass synthetic process of MnBi powder which has advantages for industrial applications will be presented. In addition, effective post processing method for control of crystal structure, microstructure, and finally, enhancement of magnetic property will also be discussed. With the optimized process of MnBi powder, remarkably high maximum energy product, (BH)max was recorded of 14.2 MGOe at room temperature, which is reasonable value for industrial permanent magnet applications as next generation permanent magnets.

Structural and Magnetic Property Modification of [111]–oriented Epitaxial CoFe₂O₄ Films

Tae-Seong Ju^{1,6*}, Dooyong Lee^{1,2}, Chang-Woo Cho¹, Jisung Lee³, Hyegyoung Kim⁴, Jong-Han Won³, Kyoung Soon Choi³, Se-Jeong Park⁵, Jouhahn Lee³, Seungmo Yang⁶, Chanyong Hwang⁶, Sungkyun Park¹

¹Department of Physics, Pusan National University, Busan, 46241, Korea

²Department of Chemical Engineering & Materials Science, University of Minnesota, Minneapolis, NM, 55455, USA

³Korea Basic Science Institute, Daejeon, 34133, Korea

⁴Core Research Facilities, Pusan National University, Busan, 46241, Korea

⁵R&D Center, Application Group, Korea I. T. S. Co Ltd., Seoul, 06373, Korea

⁶Quantum Spin Team, Korea Research Institute of Standards and Science, Daejeon, 34113, Korea

Physical properties of an oxide film grown by physical vapor deposition process are dominantly affected by the deposition environment. Here, we have grown an epitaxial magnetic oxide CoFe₂O₄ film on Al₂O₃(0001) substrate with various deposition environment using the RF magnetron sputtering system and studied the correlation between magnetic, structural, and chemical properties of films. As a result, relatively strong perpendicular magnetic anisotropy (PMA) with a large value of saturation magnetization was identified in the CoFe₂O₄ film deposited under Ar+O₂ environment while the film deposited under only Ar environment showed the magnetically isotropic property. We have proved that the PMA in the CoFe₂O₄ film deposited under the Ar+O₂ environment is the consequence of a significant structural difference. The film deposited under Ar+O₂ environment had about 3 times larger crystallite size and more compressive strain along the in-plane direction, and smoother surface and interfacial roughness than that of the film deposited under Ar environment. It was identified that oxygen in the deposition environment suppressed the deposition rate and increased the electron density of the film, resulting in better crystallinity, which directly influences the anisotropic magnetic properties. Thus, oxygen in the deposition process should be considered one of the essential parameters for enhancing the structural and magnetic properties of CoFe₂O₄ films.

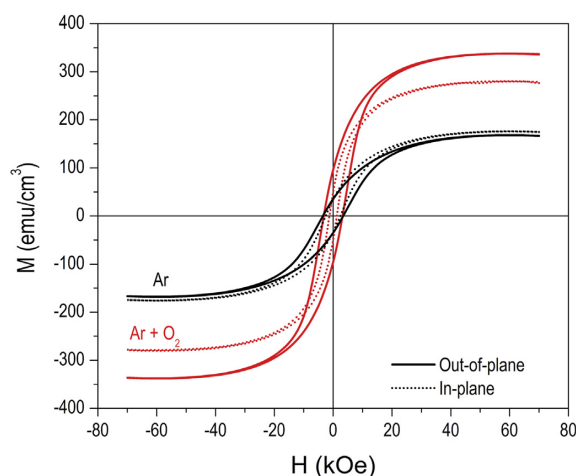


Figure. Room-temperature magnetic hysteresis loop of the CoFe₂O₄ films deposited under Ar (black) and Ar + O₂ (red) environment. External field was applied along its out-of-plane (solid line) and in-plane (dotted line) direction.

Rare–Earth–Free MnBi Permanent Magnets

Hyun–Sook Lee*, Sumin Kim, Hongjae Moon, Wooyoung Lee*

Department of Materials Science and Engineering, Yonsei University,
50 Yonsei-ro, Seodaemun-gu, Seoul, 03722, Republic of Korea

*Corresponding Authors Email: wooyoung@yonsei.ac.kr (W. Lee), h-slee@yonsei.ac.kr (H.-S. Lee)

Low-temperature phase (LTP) of MnBi has attracted much attention due to its larger coercivity than that of Nd-Fe-B at high temperature. Moreover, according to the theory of exchange-coupled core-shell magnet, when the LTP-MnBi is used as a hard magnetic core and combined with soft magnetic shell, the maximum energy product (BH)_{max} is estimated to overcome that of Nd-Fe-B. In this regards, there have been many efforts to obtain the LTP-MnBi bulks and thin films for the exchange-coupled magnets. We report on the magnetic properties of low-temperature-phased (LTP) MnBi bulks synthesized by arc-melting and melt-spinning, and LTP-MnBi thin films grown by a UHV sputtering system. First of all, we found that MnBi bulks shows $iH_c = 5.60$ kOe, $B_r = 6.00$ kG, and $(BH)_{max} = 7.27$ MGOe for 1 h milling (low-energy planetary ball milling) in the synthesis process, indicating that anisotropic precursor powders are crucial in achieving high-performance MnBi bulk magnets. On the other hand, we found that the ratio of Bi/Mn strongly has an effect on the magnetic properties of LTP-MnBi films. The highest value of $(BH)_{max}$ of LTP film was obtained to be ~ 8.6 MGOe at room temperature when the thicknesses of Bi and Mn were adjusted in 36nm and 14nm, respectively. The magnetic properties of exchange-coupled MnBi with various soft layers such as FeCo and Fe will be discussed in detail.

Keywords: Permanent magnet, rare-earth free permanent magnet, MnBi, bulk, multilayer film,

Effect of sintering temperature on the formation of epsilon Fe_2O_3 nanoparticles encapsulated by SiO_2

Phuoc Cao Van¹, Trinh Nguyen Thi¹, Ha Yeong Ahn¹, Jong-Ryul Jeong^{1,2*}

¹Department of Material Science and Engineering,

²Graduate School of Energy Science and Technology, Chungnam National University,
Daejeon, 34134, Republic of Korea.

Fax: +82-(42)-833-3206 E-mail: jrjeong@cnu.ac.kr (J.-R. Jeong)

The synthesis of $\epsilon\text{-Fe}_2\text{O}_3$ has long been attractive within the scientific community due to its giant coercive field at room temperature, high-frequency millimeter-wave absorption, and the coupling of its magnetic and dielectric properties. This work investigated the effect of sintering temperature on the formation of $\epsilon\text{-Fe}_2\text{O}_3/\text{SiO}_2$ composites which were fabricated by a combination of the reverse micelle and sol-gel methods. We performed sintering at various temperatures to determine the optimal temperature for obtaining the $\epsilon\text{-Fe}_2\text{O}_3$ phase and the highest coercive field. The optimal conditions were sintering at 1150°C to achieve a giant coercive field up to 21.57 KOe. Base on X-ray powder diffraction (XRD), the crystal structure $\epsilon\text{-Fe}_2\text{O}_3$ was analyzed. TEM images show a wide size distribution of iron oxide nanoparticles (from 10 to 20nm). Our study illustrated that the $\epsilon\text{-Fe}_2\text{O}_3$ are a promising candidate for a recording medium and unlock the door to possible applications in electronic devices intended for high-speed wireless communication.

Keywords: $\epsilon\text{-Fe}_2\text{O}_3$; sintering temperature; coercivity; reverse micelle and sol-gel

Thermal and Soft Magnetic Properties of Fe–based Amorphous Ribbons according to Changes in Fe/Co Ratio

Hyunsol Son^{*}, Haein Choi–Yim

Department of Physics, Sookmyung Women' s University, Seoul 04310, Korea

Fe-based amorphous alloy systems have attracted the interest in the remarkable soft magnetic properties, high saturation magnetization, and low cost of manufacture. We added Cobalt to improve glass forming ability(GFA) and soft magnetic properties such as high saturation magnetization and permeability with good thermal stability. We investigated the Fe-based amorphous soft magnetic alloys of $(\text{Fe}_{1-x}\text{Co}_x)_{72}\text{B}_{19.2}\text{Si}_{4.8}\text{Nb}_4$ prepared by arc-melting system with high purity metals under Ti-gettered Argon atmosphere. Then, with these samples, we produced rapidly solidified ribbons with 2-3mm widths and 20-30 μm thicknesses by using melt spinning technique. After processing these ribbons, we analyzed the alloys' structural, thermal and magnetic properties. $(\text{Co}_{1-x}\text{Fe}_x)_{72}\text{B}_{19.2}\text{Si}_{4.8}\text{Nb}_4$ alloy system was verified as fully amorphous by using X-ray diffraction (XRD). The thermal properties including crystallization temperature (T_x) were measured by differential scanning calorimetry (DSC). Lastly, magnetic properties of the amorphous ribbons were measured by a vibrating sample magnetometer (VSM).

Controlled Switching of Asymmetric Bloch wall in a Rectangular Ferromagnetic disk.

Sooseok Lee, Hee-Sung Han, Young-Sang Yu, Soong-Geun Je, Myeonghwan Kang,
Hye-Jin Ok, Namkyu Kim, Weilun Chao, Mi-Young Im[†], Ki-Suk Lee[†]

School of Materials Science and Engineering, Ulsan National Institute of Science and
Technology, Ulsan 44919, Republic of Korea.

Advanced Light Source, Lawrence Berkeley National Laboratory, Berkeley, CA, 94720, USA

Department of Physics, Chonnam National University, Gwangju 61186, Korea.

Center for X-ray Optics, Lawrence Berkeley National Laboratory, Berkeley, CA94720, USA.

Patterned magnetic elements have been studied extensively due to fundamental issues and their potential for developing practical ultrahigh density memory devices. In the small magnetic element, the magnetization tends to be stabilized in magnetic vortex states to minimize the magnetostatic interaction. [1] such configuration can be characterized by an in-plane (chirality) and an out-of-plane (polarity) magnetization. Controlling these degrees of freedom have been performed in various geometry by external magnetic field and electrical current. [2,3] Recently, the discovery of the additional degree of freedom can be controllably switched in three-dimensional (3D) system opened up new possibility in developing multi-bit memory device. [4] In this system, two degenerated asymmetric Bloch walls (ABWs) exist with same energy and probability. To control them, it is necessary to break the symmetry of those state. For example, an asymmetric geometry was utilized for control the ABW states. In this presentation, we suggest another way to control the ABWs efficiently without significant changing of other degrees of freedom by magnetic field using micromagnetic simulation. We also successfully verified our method experimentally by using the magnetic transmission soft x-ray microscopy (MTXM). [5]

References

- [1] A. Hubert and R. Schäfer. Magnetic Domains. (Springer, Berlin, 1999)
- [2] B. Van Waeyenberge, A. Puzic, H. Stoll, K. W. Chou, T. Tylliszczak, R. Hertel, M. Faehnle, H. Brueckl, K. Rott, G. Reiss, I. Neudecker, D. Weiss, C. H. Back and G. Schuetz. Magnetic vortex core reversal by excitation with short bursts of an alternating field. *Nature*. 444, 461-464 (2006)
- [3] M. Jaafar, R. Yanes, D. Perez de lara, O. Chubykalo-Fesenko, A. Asenjo, E. M. Gonzalez, J. V. Anguita, M. Vazquez and J. L. Vicent. *Phys. Rev. B*. 81, 054439 (2010)
- [4] F. Cheynis, A. Masseboeuf, O. Fruchart, N. Rougemaille, J. C. Toussaint, R. Belkhou, P. Bayle-Guillemaud and A. Marty. Controlled Switching of Néel Caps in Flux-Closure Magnetic Dots. *Phys. Rev. Lett.* 102, 107201 (2009).
- [5] P. Fischer, D.-H. Kim, W. L. Chao, J. A. Liddle, E. H. Anderson and D. T. Attwood. *Mater. Today* 9, 26-33 (2006).

Effect of magnetic field on the synthesis of Ni nanowires

Min Ji Shin^{1*}, Ji Eun Lee¹, Bon Heun Koo^{1*}, Seok Hwan Huh^{2†}

¹Department of Materials Science and Engineering, Changwon National University,
Changwon, Gyung-sangnam-do 51140, Republic of Korea

²Department of Mechatronics Conversion Engineering, Changwon National University,
Changwon, Gyung-sangnam-do 51140, Republic of Korea

Abstract

Recently, due to the development of nanoscale electronic devices, the necessity of preparing one-dimensional nanomaterials is increasing. Nanowires have excellent crystallinity and have various properties that conventional bulk materials do not have, such as high chemical reactivity and stress relaxation properties due to a large specific surface area. Therefore, Ni, a soft magnetic material was synthesized in the form of nanowires, and shape magnetic anisotropy was provided through a magnetic field to enhance magnetic properties. In this study, nanowires were prepared using $\text{NiCl}_2 \cdot 6\text{H}_2\text{O}$, NaOH , $\text{N}_2\text{H}_4 \cdot \text{H}_2\text{O}$, etc. through a solution synthesis method, and the effect of shape magnetic anisotropy was observed by dividing the sample with a magnetic field and a sample without applying a magnetic field during heating. Crystal structure and microstructure were observed through XRD and FE-SEM, and magnetic properties were measured through PPMS. Through the evaluation of properties, Ni powder was synthesized and it was confirmed that it exists in the form of nanowires. In addition, in the case of a sample prepared by applying a magnetic field, the diamagnetic field was reduced due to the effect of shape magnetic anisotropy, thereby improving magnetic properties.

Keywords: Soft magnetic, Nanowires, magnetic field, shape magnetic anisotropy, magnetic properties

스프레이 코팅을 적용하여 절연 특성을 높인 연자성 금속 파워인덕터의 투자율 향상에 관한 연구

공선호*, 안지훈, 김상우, 강예빈, 이보화†

한국외국어대학교 물리학과, 산화물 연구센터

*bwlee@hufs.ac.kr

파워인덕터 소재로 사용되는 Fe-Si, Fe-Ni, Fe-Si-Al 금속 분말을 고분자로 절연 코팅하여 코어 손실을 낮추고 투자율을 향상시킬 수 있는 연구를 진행하였다.

인덕터 소재의 절연 특성을 향상하여 코어의 투자율을 향상하는 연구는 많이 진행되어 왔다. 본 연구에서는 금속 분말에 간단한 공정과정이며 경제적이고 효율적인 스프레이코팅 공정을 적용하였다. 표면에 고분자를 코팅 시킴으로써 host 분말 표면에 guest분말이 치밀하게 형성될 수 있도록 볼밀링 방법으로 표면을 코팅하였다.

절연 코팅된 분말을 SEM/EDS 측정하여 표면에 효과적으로 코팅이 되었음을 확인하였고, VSM 을 측정하여 히스테리시스 루프의 변화를 통하여 코팅의 효과를 증명하였다.

효과적으로 절연 코팅이 확인된 분말을 토로이달 형태로 코어 성형하여 임피던스 분석기를 통해 투자율이 향상되었음을 확인하였다. B-H 측정을 통해서도 코팅 분말의 사용 주파수 영역이 증가하고 투자율이 향상되어 고주파 인덕터 소재로 사용이 가능함을 확인하였다.

나노분말을 함유한 연자성-고분자 복합체의 투자율 향상에 관한 연구

김예래*, 이민영, 우혁준, 정우현, 이보화†

한국외국어대학교 물리학과, 산화물 연구센터

*bwlee@hufs.ac.kr

나노분말을 첨가하여 미세구조를 변형시킨 연자성 금속 분말 코어의 투자율 향상에 미치는 영향을 연구하였다. 본 연구에서 사용된 인덕터 코어는 높은 전기저항과 높은 포화자화값을 갖는 Fe-6.5Si 분말을 사용했다. 미세구조를 변형시키기 위한 나노 철 분말은 Pulsed Wire Evaporation(PWE) 장비로 제조하였으며 나노 분말이 첨가될수록 고밀도 구조로 변형되었다. 밀도와 충전율이 최대인 비율에서 투자율은 최대가 되었으며, 실험적으로, 20 wt% 나노 철 분말을 함유한 코어에서 가장 높은 충전율과 투자율을 보였다. 이 사실은 올렌도르프 방정식의 충전율-투자율의 관계와 일치함을 보였다. 인덕터 코어는 연자성 재료의 본래 특성에 영향을 받지만, 미세구조 변형과 같은 2차적 처리를 통해서도 투자율을 비롯한 자기-전기적 특성들도 향상시킬 수 있음을 보여준다.

The interfacial Dzyaloshinskii–Moriya interaction change due to insertion of the ferromagnet–heavy metal alloy

Jeong Kyu Lee^{1*}, Junho Park¹, Gyu Won Kim¹, V.B. Bessonov², A.V. Telegin²,
A.V. Ognev³, A.S. Samardak³, Young Keun Kim¹

¹A Department of Materials Science and Engineering, Korea University, Seoul 02841, Korea

²M.N. Miheev Institute of Metal Physics, Ural Branch of Russian Academy of Sciences,
Yekaterinburg 620990, Russia

³School of Natural Sciences, Far Eastern Federal University, Vladivostok 690950, Russia

Magnetic skyrmions can be stabilized in thin films with perpendicular magnetic anisotropy (PMA) by the interfacial Dzyaloshinskii–Moriya interaction (DMI) are interesting information carriers that meet the conditions. The interfacial DMI is induced due to the strong spin-orbit coupling (SOC) between ferromagnet (FM) and nonmagnet (NM) and inversion symmetry breaking (ISB). The competition between Heisenberg exchange coupling and DMI makes neighboring spins tilt. This results in skyrmions tending to form Néel type domain walls. Many research groups mainly focused on different combinations of various materials to obtain a considerable value of DMI. Furthermore, various structures with modified interfaces have been recently studied [2]. In this study, we increased the interfacial contact area and observed the change in interface DMI that followed.

We fabricated three types of structures to gradually change the interface and observe its effect on the interfacial DMI energy density (D). Si/Ta(2)/Pt(3)/Co(1.2)/Ta(2) structure (sample A) was used as a References structure in nm. We modified the Pt/Co interface by co-sputtering Co–Pt alloys with various compositions. The first structure is Ta/Pt/Co50Pt50(1.2)/Co(1.2)/Ta (sample B) and the other structure which has a gradual interface is Ta/Pt/Pt75Co25(0.4)/Co50Pt50(0.4)/Co75Pt25(0.4)/Co(1.2)/Ta (sample C). The bottom Ta layer was deposited to help the growth of crystalline Pt(111) [3]. The capping layer of Ta was used to prevent oxidation. All samples were deposited in a DC magnetron sputtering system with a base pressure of 5×10^{-9} Torr at room temperature and post-annealed at 300 °C for 1 hour in the vacuum of 1×10^{-6} Torr. We studied magnetic properties using a vibrating sample magnetometer, and the IDMI value and sign (D -constant) were measured by Brillouin Light scattering spectroscopy.

While sample A with no Co–Pt alloys showed distinct PMA, both samples B and C exhibited in-plane magnetic anisotropies. We were able to obtain the effective saturation magnetization (M_s) value excluding the magnetic dead layer by using samples with different thicknesses. As alloys were added, samples B (803.1 kA/m) and C (857.9 kA/m) showed M_s values decreased by about 25~30% compared to sample A (1139.7 kA/m). This led to a decrease in DMI by about 15% for sample B ($D = -0.69$ mJ/m²). On the other hand, sample C ($D = -0.82$ mJ/m²) showed similar to sample A ($D = -0.81$ mJ/m²) due to the increased frequency shift despite the decrease in M_s . We, in turn, were able to find out that the interfacial DMI can increase or decrease depending on how the interfacial area was increased. Interface change leading to DMI change in this study can lead to other spin-related phenomena such as spin Hall effect, spin-orbit torque.

This work was supported by the National Research Foundation of Korea (2015M3D1A1070465) and by the Samsung Electronics' University R&D program.

A.S. Samardak and A.V. Ognev acknowledge the financial support of RFBR grant (19-02-00530).

V.B. Bessonov and A.V. Telegin acknowledge the financial support of the FASO of Russia ("Spin" No A A A A – A 18-118020291004-2)

Symmetry breaking in the formation of asymmetric Bloch wall in ferromagnetic dots

Sooseok Lee^{*}, Hee-Sung Han, Young-Sang Yu, Soong-Geun Je, Myeonghwan Kang,
Hye-Jin Ok, Namkyu Kim, Weilun Chao, Mi-Young Im[†], Ki-Suk Lee[†]

School of Materials Science and Engineering, Ulsan National Institute of Science and
Technology, Ulsan 44919, Republic of Korea.

Advanced Light Source, Lawrence Berkeley National Laboratory, Berkeley, CA, 94720, USA

Department of Physics, Chonnam National University, Gwangju 61186, Korea.

Center for X-ray Optics, Lawrence Berkeley National Laboratory, Berkeley, CA94720, USA.

Recently, the particle-like swirling magnetic configurations such as magnetic Skyrmions and vortices characterized by a topological number, have attracted considerable research attention due to highly promising properties in spintronic device applications [1-3]. To utilize them, it is essential to understand the three-dimensional (3D) magnetic configuration and their topological properties which can provide not only the detailed mechanisms of controlling magnetic structures but also an efficient method. In the present work, we show symmetry breaking in the one of peculiar 3D magnetic configuration, the asymmetric Bloch walls (ABWs) in the circular and square shaped ferromagnetic patterned discs using the magnetic transmission soft X-ray microscopy (MTXM). [4] In these systems, the point-like configuration, magnetic vortex is stabilized due to competition between short-range exchange interaction and long-range magnetostatic interaction. The top and bottom surface vortex are separated when applying horizontal external magnetic field creating ABWs either $(-,+)$ type or $(+,-)$ type. [5,6] The type of ABWs are determined by sample geometry. In this presentation, we will discuss about the detailed transformation process of ABWs.

References

- [1] S. Das et al. Nature. 568, 368-372 (2019)
- [2] Shinjo et.al. Science 289, 930 (2000)
- [3] T. Tanigaki et.al. Nano Lett, 15, 1309-1314 (2015)
- [4] P. Fischer et al. Mater. Today 9, 26-33 (2006).
- [5] F. Cheynis et al., Phys. Rev. Lett. 102, 107201 (2009)
- [6] A. Masseboeuf et al., Phys. Rev. Lett. 104, 127204 (2010)

Study on the fabrication of Fe-Based Electric Conductivity Alloy for Semiconductor Test Socket

Sang-Uk Kim^{1*}, In-Ho Kim¹, Je-An Yu², Tae-Haeng Lee³, Chang-Bin Song³

¹R&D Center NATM Co. Ltd., Korea

²NTECHNE Co., Ltd., Korea

³Div. of Materials Eng., Kongju National University, Korea

최근 IC 반도체 소자는 스마트폰/태블릿PC 등 각종 모바일 통신용 기기는 물론, IT, BT, 자동차 및 가정용/산업용/의료용/국방용 등의 각종 다양한 전기·전자부품이 증가함에 따라 그 수요 또한 증가하고 있다.

한편 IC 반도체 공정에 의해 완성된 반도체 패키지는 출하 전 최종적으로 전기적 및 성능 테스트를 위해 반도체 패키지 회로와 검사장비의 회로단자와 연결하는 테스트 소켓을 사용하고 있으며, 용도 및 제조사에 따라 다양한 제품이 제조되어 사용되고 있다.

특히 이러한 테스트 소켓의 전기적 회로의 소재로 사용되는 전도성 분말은 소켓의 전기적 특성 향상을 위해 우수한 전도성뿐만 아니라, 소켓 제조의 용이성 및 수명 향상을 위해 적당한 자성 및 경도가 요구된다. 그러나 현재 전도성 분말소재로 사용되는 순 니켈분말은 원래 경도(Hv=100정도)가 낮아 테스트 소켓의 수명이 저하하는 단점이 있다.

따라서 본 연구에서는 이러한 니켈분말을 대체할 수 있는 경도가 우수한 새로운 Ni기 합금의 조성설계, 전기저항, 자성 및 경도 특성을 조사하였다.

Keywords : Zn Bath Process, Waste Cemented Carbide, Tungsten, Cobalt, Zinc

Pd/Co/Pd 삼층 구조에서 상위 Pd층의 두께에 따른 스핀-궤도 토크의 변화에 관한 연구 (A study on the effect of top Pd thickness on the spin-orbit torques in a Pd/Co/Pd trilayer)

김기성, 강범승, 이상호, 홍종일*

연세대학교 신소재공학과

자기저항메모리(magnetoresistive random-access memory, MRAM)는 쓰기 속도가 빠르고, 전력 소모는 적은 특징이 있어 차세대 메모리로써 많은 주목을 받고 있다. 자기저항메모리의 기본 단위 소자인 자기터널접합(magnetic tunnel junction, MTJ)은 두 개의 강자성체층 사이에 절연체인 산화물이 있는 구조이며, 두 강자성체의 자화 방향이 평행일 때는 낮은 터널저항을, 반 평행일 경우 높은 터널저항을 나타내게 된다. 최근에는 전류만으로 강자성체의 자화 방향을 바꾸는 current-induced magnetization switching (CIMS) 방식을 이용하여 정보를 저장하고, 이렇게 저장된 정보를 터널 저항값을 통해 읽을 수 있게 되어 자기저항메모리에 대한 관심이 더욱 높아졌다. CIMS방법으로는 크게 스핀-전달 토크(spin-transfer torque, STT)와 스핀-궤도 토크(spin-orbit torque, SOT) 두 가지 방법이 있다. STT는 정보를 쓰기 위해 터널 배리어(tunnel barrier)에 큰 전류를 주게 되므로 break down이 일어날 수 있으며, 쓰고 읽는 과정에서 read disturbance라는 문제가 발생할 수 있다. 위의 문제점들을 해결 방법으로 최근에는 SOT가 많이 연구되고 있다.

본 연구에서는 Pd/metallic Co/Pd과 양성자를 조사하여 Pd/Co₃O₄/Pd를 Pd/Co₃O₄/Pd로 환원시킨 3층 구조에서 상위 Pd층의 두께를 바꿨을 때 SOT가 어떻게 달라지는지에 대하여 살펴보았다. SOT의 근원은 스핀-궤도 결합(spin-orbit interaction, SOI)으로 구체적인 메커니즘으로는 계면에서 나타나는 라쉬바 효과(Rashba effect)와 벌크 효과인 스핀 홀 효과(spin Hall effect, SHE)가 있다. 이 두 가지 메커니즘에 의해 field-like torque(FLT)와 damping-like torque(DLT)가 발생한다. 하지만 각각의 메커니즘이 어떠한 토크발생에 더 우세한지는 아직도 더 연구가 필요한 실정이다. 이를 연구하기 위하여 Pd 한 층의 두께만 바꿔서 계면을 최대한 일정하게 유지하면서 벌크 효과를 보는 방법을 택하였다. 또한 스핀 홀 효과와 라쉬바 효과의 특성 상 반전 대칭성(inversion symmetry)이 깨져야만 SOT가 나타날 수 있게 된다. 이에 따라 하위 Pd(7 nm)층을 기준으로 상위 Pd층의 두께를 3, 5, 7, 9 그리고 11 nm로 바꿔가면서 구조 반전 대칭성(structural inversion symmetry)을 만들 때 SOT가 구체적으로 어떻게 달라지는지에 대하여 조화측정법(harmonic measurement)을 통하여 살펴보았다. 측정한 결과 상위 Pd층의 두께가 증가함에 따라서 FLT가 증가하는 경향이 발견되었다. 그 이유에 대해서는 Pd의 스핀전달거리(spin diffusion length), Pd와 Ta의 스핀 홀 각도(spin Hall angle)의 부호가 다른 점, 그리고 스핀 홀 효과의 효율성을 고려하여 설명할 수 있다.

Keywords : Pd/Co/Pd, 양성자 조사, 스핀-궤도 토크(spin-orbit torque), 스핀 홀 효과(spin Hall effect), 라쉬바 효과(Rashba effect), 조화측정법(harmonic measurement)

Charge-to-spin interconversion without ferromagnetic material using spin Hall and Rashba effects

Jeehoon Jeon^{1*}, Seong Been Kim^{1,2}, Taeyueb Kim¹, OukJae Lee¹, Suk Hee Han¹,
Hyung-jun Kim¹, Hyun Cheol Koo^{1,2}, Jinki Hong³

¹ Spin Convergence Research Center, Korea Institute of Science and Technology, Seoul, 02792, Korea

² KU-KIST Graduate School of Converging Science and Technology, Korea University, Seoul, 02792, Korea

³ Department of Applied Physics, Korea University, Sejong, 30019, Korea

The importance of semiconductor spintronics is quantum mechanical spin phenomena with a focus on electrical operation that may add the functionality of electronic device. In conventional spin-based device, spin information is injected from a ferromagnetic source into a semiconductor channel. Spintronic device requires electric field control of the spin orientation; therefore, the most viable channel is a InAs quantum well channel with strong Rashba spin splitting, which enables spin modulation [1-4]. In a ferromagnet/semiconductor interface, despite its potential for use as a spin transistor, spin injection and detection efficiency from the ferromagnetic material to the semiconductor channel is very low due to the conductance mismatch. Thus, many researchers pay attention to charge-to-spin interconversion without a ferromagnetic material to realize an all-electrical spin device because this design obviates the need for magnetic field control of magnetization.

In this work, the spin is injected from a platinum electrode via the direct spin Hall effect and is subsequently detected in a strong Rashba channel via the inverse spin Hall effect [5]. Before being detected, the spin state is modulated by gate bias; the signal observed with various channel length and gate voltage demonstrates this Rashba precessional modulation. In addition, the addition of Zeeman precession induced by an external magnetic field provides the signal-elucidating definite spin motion in the channel. A theoretical model for our device is proposed in which all parameters are composed of experimentally measured ones. The spin signal from the device are quantitatively consistent with this model, which provides a clear understanding of interplay between the Rashba and Zeeman precessions. Our approach opens a fascinating possibility for realizing a ferromagnet-free system for use in low-power and high-temperature spin transistors.

References

- [1] S. Datta and B. Das, Appl. Phys. Lett. 56, 665 (1990)
- [2] A. Manchon, H. C. Koo, J. Nitta, S. M. Frolov, and R. A. Duine, Nat. Mater. 14, 871 (2015)
- [3] H. C. Koo, J. H. Kwon, J. Eom, J. Chang, S. H. Han, and M. Johnson, Science 325, 1515 (2009)
- [4] W. Y. Choi, H. Kim, J. Chang, S. H. Han, H. C. Koo, and M. Johnson, Nat. Nanotechnol. 10, 666 (2015)
- [5] J. Jeon, et al. Appl. Phys. Lett. 117(4), 042403 (2020)

Magnetoresistance of ferromagnet–semiconductors hybrid structure in spin Hall and strong Rashba effect at room temperature

Seong Been Kim^{1, 2*}, Hyung-jun Kim², Joonyeon Chang², Hyun Cheol Koo^{1, 2*}

¹Korea University, Korea

²Korea Institute of Science and Technology, Korea

Spin field effect transistor is considered as promising spin semiconductor device, however it has a lot of obstacles such as spin injection efficiency, and low operation temperature. The spin injection and detection efficiency from ferromagnet electrode to semiconductor channel are quite low because the most of spin information decayed at the interface. Adapting spin Hall effect as spin injection and detection can be the one of solutions to increase operation temperature of semiconductor spin devices since the spin Hall angle is larger than the spin injection efficiency using ferromagnet electrode.

In this work, we measured the channel resistance, R_{xx} and Hall voltage, R_{xy} of the ferromagnet–semiconductor Hall-bar structure. Figs. 1(a) is measurement geometry as a strong Rashba semiconductor channel, we fabricated the InAs based quantum well heterostructure. In_{0.52}Al_{0.48}As buffer (300 nm), n+ In_{0.52}Al_{0.48}As carrier supplier (7 nm), In_{0.52}Al_{0.48}As (6 nm), In_{0.53}Ga_{0.47}As (2.5 nm), InAs channel layer (2 nm), In_{0.53}Ga_{0.47}As (13.5 nm), In_{0.52}Al_{0.48}As (20 nm), and InAs (2 nm) were grown by molecular beam epitaxy on InP substrate.

While the magnetoresistance of ferromagnet materials and a quantum well channel have a conventional magnetoresistance behavior, the angle dependence of magnetoresistances measurement results in hybrid structure is totally different from the curves, ΔR_{xx1} , shown in Figs. 1(b) black line. This unconventional magnetoresistances such as black line curves can be explained by the spin Hall effect and the Rashba spin precession

To confirm the relationship between spin precession and spin Hall effect. The channel lengths are $L1 = 3.125$ and $L2 = 3.325$ respectively. We measured the spin Hall voltage as a function of the applied magnetic field for various magnetic field directions as shown in Figs. 2. when $\phi = 0^\circ$ or 180° , the injected spins are polarized along the direction which is perpendicular to the Rashba field, injected spins precess around the Rashba field and the spin Hall voltages is detected. On the other hand, when $\phi = 90^\circ$ or 270° , because the injected spins is parallel to the Rashba field, so the spin precession doesn't occur and the spin Hall voltages isn't observed.

Magenta line in Figure 1 (b) shows the spin Hall voltage as a function of the various applied field direction, ϕ . We demonstrate two curves, ΔR_{xx1} and $(\Delta R_{H1} - \Delta R_{H2})$, which are obtained from the experimental results, have the similar shape. These results also can be explained by the spin Hall effect in a strong Rashba system.

Figure 1

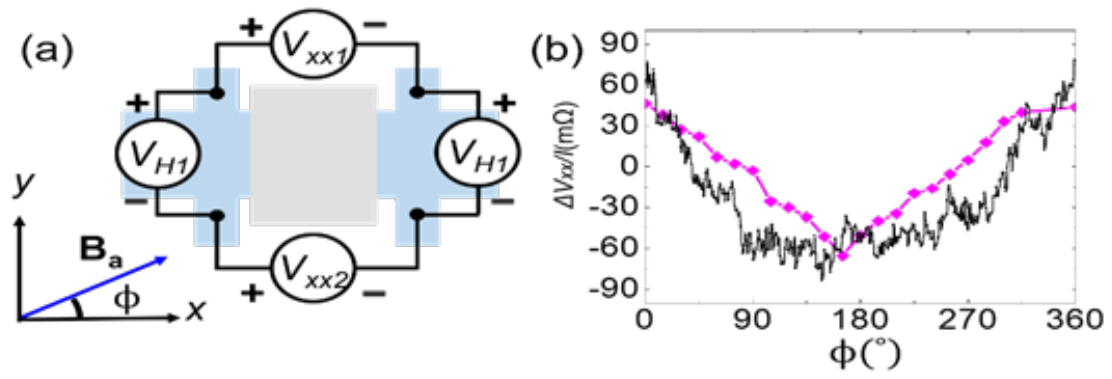
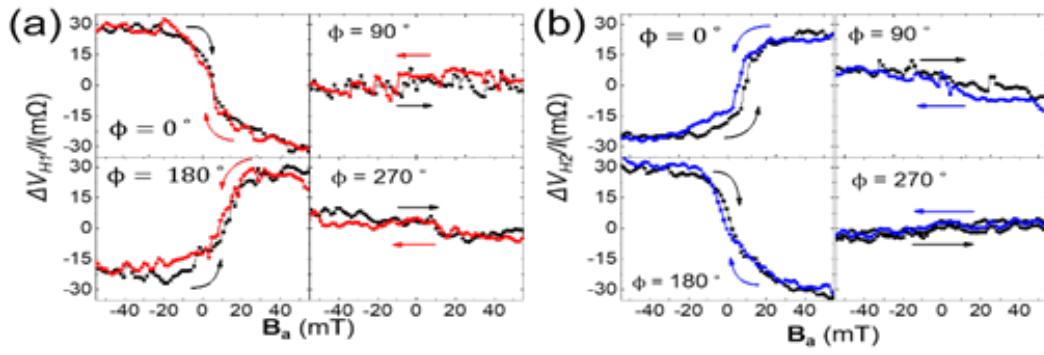


Figure 2



비대칭 [Co/Pd/Pt]10 다층박막에서의 스핀궤도토크

김영래*, 임상호

고려대학교 신소재공학부

최근 스핀궤도토크-MRAM (Magnetic random access memory) 소자를 실현하기 위한 스핀궤도토크와 수직자기이방성의 향상을 위한 연구가 진행되고 있다. 높은 효율의 스핀궤도토크와 강한 수직자기이방성은 자화를 반전시키기 위한 조건으로 필수적이고 이 메커니즘을 이해하기 위한 방법으로 ferro-magnetic metal/non-magnetic metal/insulator 구조에서의 계면에 대한 연구가 활발하게 진행되고 있다. [Co/Pt]10와 [Co/Pd]10 다층박막에 비해서 비대칭 [Co/Pd/Pt]10 다층박막구조에서 수직자기이방성의 크기가 크다는 결과가 발표되었다 [1]. 또한 [Co/Pd]10 다층박막에서 스핀 홀 각도의 크기가 상당히 큰 값을 보인다 [2]. 따라서 본 연구는 Co, Pd, Pt 원자들이 매우 얇은 두께로 10번 반복되어 증착되었을 때 [Co/Pd]10, [Co/Pt]10 다층박막과 [Co/Pd/Pt]10 비대칭 다층박막 구조에서 서로 다른 원자들의 계면 사이에서 발생하는 수직자기이방성과 스핀궤도토크에 대해 연구하였다. 샘플은 8×10^{-8} Torr 진공도의 초고진공DC 마그네트론 스퍼터링 장비를 통해 상온 증착하였고, 만들어진 샘플들의 자기적 특성은 VSM (vibrating sample magnetometer)를 통해 측정되었다. 또한 스핀궤도토크는 Harmonic Hall voltage measurements를 이용하여 측정하였다.

References

- [1] Pradipto, A. et al., phys. Rev. B 99, 180410 (2019)
- [2] M. Jamali et al., Phy. Rev. Lett. 111, 246602 (2013)

분자선 에피택시를 이용한 2D 반데르발스 자성체 Fe_{3+x}GeTe₂ (FGT) 성장

김주란^{1*}, 이상선¹, 박창배², 황찬용^{1†}

¹양자기술연구소, 한국표준과학연구원, 대전, 대한민국

²물리학과, 서울대학교, 서울, 대한민국

차세대 2차원 강자성 물질은 원자층 수준의 얇은 두께와 우수한 계면 특성을 가지고 있어 이를 이용한 저차원 자기 및 스핀트로닉 소자 개발이 큰 관심을 끌고 있다. 특히 단일층의 2차원 강자성체도 자기 특성을 보임에 따라 벌크 특성과 구별되는 물리적 특성을 밝혀내는 것이 중요하다. 그러나 2차원 자성체는 낮은 큐리 온도 (TC)를 가지고 있으며, 두께를 제어하여 대면적으로 성장시키기 어렵다는 단점이 있다. 본 연구에서는 분자선 에피택시 (Molecular Beam Epitaxy; MBE)를 이용하여 (0001) 사파이어 기판 위에 2차원 반데르발스 자성체인 Fe_{3+x}GeTe₂ (FGT)를 박막으로 성장하였다. 또, Fe의 비율을 조절하여 ($x = 5$) 낮은 큐리 온도를 상온으로 증가시켜 개선하고자 하였다. FGT 박막의 결정성은 X-ray diffraction (XRD)로 확인하였으며, 물질의 큐리 온도와 강자성체 성질을 확인하기 위해 시료진동식자속계 (vibrating sample magnetometer; VSM)를 이용하였다. 박막의 원소 조성은 X-ray photoelectron spectroscopy (XPS) 측정을 통해 확인하였다. 해당 연구 결과를 통해 두께가 조절된 2차원 FGT 박막의 대면적 성장이 가능하고, 2차원 강자성 물질에 기초한 고성능 스핀트로닉 소자 구현의 가능성을 제시할 것으로 기대한다.

Observation of unconventional Hall signal in ferrimagnet/oxide/silicon structure.

Jun-Ho Kang^{1*}, Soogil Lee^{1,2}, Dohyoung Kim², Seyeop Jung³, Sanghoon Kim³,
Byong-Guk Park², Kab-Jin Kim¹

¹Department of Physics, KAIST, Daejeon 34141, Korea

²Department of Materials Science and Engineering, KAIST, Daejeon 34141, Korea

³Department of Physics, University of Ulsan, Ulsan 44610, Korea

Unconventional behaviors emerging at the interface of materials have been spotlighted in many research fields. In spintronics, it has been regarded as a reasonable assumption that a signal coming from the interface between metal (M) and intrinsic silicon(i-Si) substrate would be negligibly small, because the resistivity of i-Si is extremely larger than that of metallic thin films. Therefore, i-Si has commonly been used in spintronics studies where the high electric current is essential, for example, the spin-orbit-torque (SOT)-driven magnetization switching. However, here we found that the interface effect is non-negligible in M/i-Si structure and generates an unconventional Hall signal. In particular, the observed unconventional Hall signal shows the same detection symmetry with the damping-like SOT measurement, suggesting that the unconventional Hall signal can be possibly permeated in SOT measurement. Our result shows that the electrical signal in the M/i-Si structure has to be analyzed more carefully in spintronic research.

Study of electronic structure of Bi thin films grown on the MoS₂ surface

Sang Wook Han^{1*}, Seungho Seong², J.-S. Kang², Eunsook Lee³, Won Seok Yun⁴,
Soon Cheol Hong¹

¹Department of Physics and EHSRC, University of Ulsan, Republic of Korea

²Department of Physics, The Catholic University of Korea, Republic of Korea

³Beamline Research Division, Pohang Accelerator Laboratory, Republic of Korea

⁴Convergence Research Institute, DGIST, Republic of Korea

Bulk Bi is topologically trivial in theory. However, Bi bilayers are expected to be a two-dimensional (2D) topological insulator with a large bulk bandgap due to the strong spin-orbit coupling. Although the epitaxial growth of Bi thin films has been intensely exploited on various substrates, it remains a significant challenge to construct free-standing Bi film experimentally. We investigate Bi thin films by employing low-energy electron diffraction, transmission electron microscopy, and angle-resolved photoemission spectroscopy. Bi thin films epitaxially grow on the MoS₂ surface without interfacial interaction. Bi thin films favor the Bi(111) facet on the MoS₂ surface as a Bi coverage increases. More interestingly, the air exposure of the Bi thin films induces a large bandgap. The characteristic of the topologically nontrivial or trivial phase transition through surface oxidation is discussed. Our study might provide a comprehensive understanding of the emergent electronic properties of the 2D topological insulator.

Perpendicular Magnetic Anisotropy Control via Wedge-Type Oxide Layer

Chan-Kang Lee^{1*}, Jaehun Cho², KwangHyun Lee^{2, 3}, Joonwoo Kim²,
June-Seo Kim^{2†}, Chun-Yeol You^{1†}

¹Department of Emerging Material and Science, DGIST, Daegu 42988, Republic of Korea

²Division of Nanotechnology, DGIST, Daegu 42988, Republic of Korea

³Department of Materials Engineering, Keimyung University, Daegu 42601, Republic of Korea
email: *spin2mtj@dgist.ac.kr and **cyyou@dgist.ac.kr

Since the magnetic thin film was applied to the memory device, it has become important to manipulate the magnetic anisotropy of the magnetic thin films [1]. It is important to control the magnetic anisotropy energy to implement a magnetic device. So, many studies have been done to make a magnetic device by controlling the magnetic anisotropy. A new way of magnetization operation was recently discovered by varying the thicknesses of the individual layers and choosing appropriate materials. It has been shown a possibility to manipulate the magnetic anisotropy. Many researches have mainly been conducted to control magnetic anisotropy by using various materials to change the structures of magnetic thin films. In particular, a lot of research controlling perpendicular magnetic anisotropy (PMA) has been conducted for its potential for application of magnetoresistive random access memory.

In this study, we investigated the PMA at the interface between ferromagnetic layer and oxide layer [2]. The structure of Pt/Co/Ta sample (Fig. 1 (a)) is deposited on SiO₂ on Si substrate using a magnetron sputtering system. The Ta capping layer thickness(0~3nm) is varied by using a linearly motorized shadow mask (so-called "Wedge Mask") as shown in Fig. 1 (a). After deposition, the top Ta layer is oxidized using an in-situ oxygen plasma system. Depending on the Ta layer thickness and various oxidation conditions, Ta layers are partially oxidized for thicker Ta cases. On the other hand, Ta layers are fully oxidized or top Co layer may be partially oxidized for thin Ta cases. The degree of Co layer oxidation and magnetic properties depending on the Ta capping layer thickness are measured through the magneto optic Kerr effect (MOKE) and Brillouin light scattering (BLS). A significant change of the perpendicular magnetic anisotropy is observed through systematic MOKE measurements (Fig. 1(b)) and the magnetic anisotropy field (H_k) is deduced through BLS measurements (Fig. 2(b)) with changing Ta wedge thickness. In Fig. 1 (b) the coercivity and remanence sharply decrease around of the Ta thickness 1.9 nm. And in Fig. 2 (a) PMA decrease from 1.5nm to 1.95nm in Ta thickness and it increase from 1.95nm to 2.7nm. The reason of the significant anisotropy change is originated from the competition of PMA due to spin orbit coupling at the interface between Pt and Co layer, shape anisotropy and magnetostriction (stress-induced anisotropy) due to strain caused by oxidized Ta capping layer. Because of volume change during the oxidation process, the strength of strain applied to the magnetic layer and change of magnetic anisotropy are depend on the oxidation. We carefully speculated that the interaction at the interface between the Ta and Co layers would have effect on reducing the perpendicular magnetic anisotropy energy at the Pt and Co interface [3, 4].

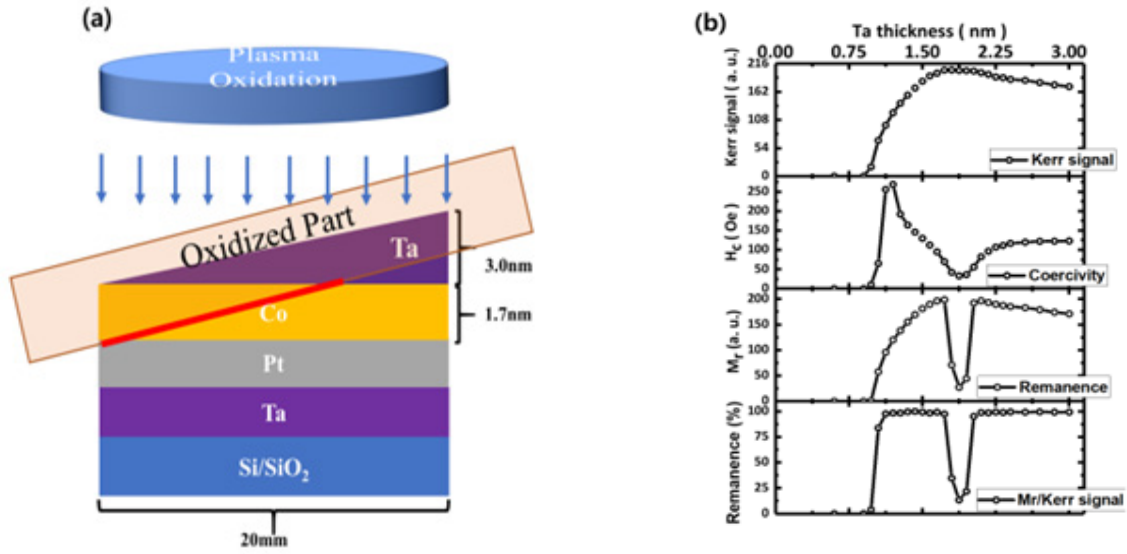


Fig. 1 (a) Schematic of sample structure and sample oxidation process. (b) MOKE signal (Kerr signal, coercivity (H_c), remanence magnetization (M_r) and Remanence)

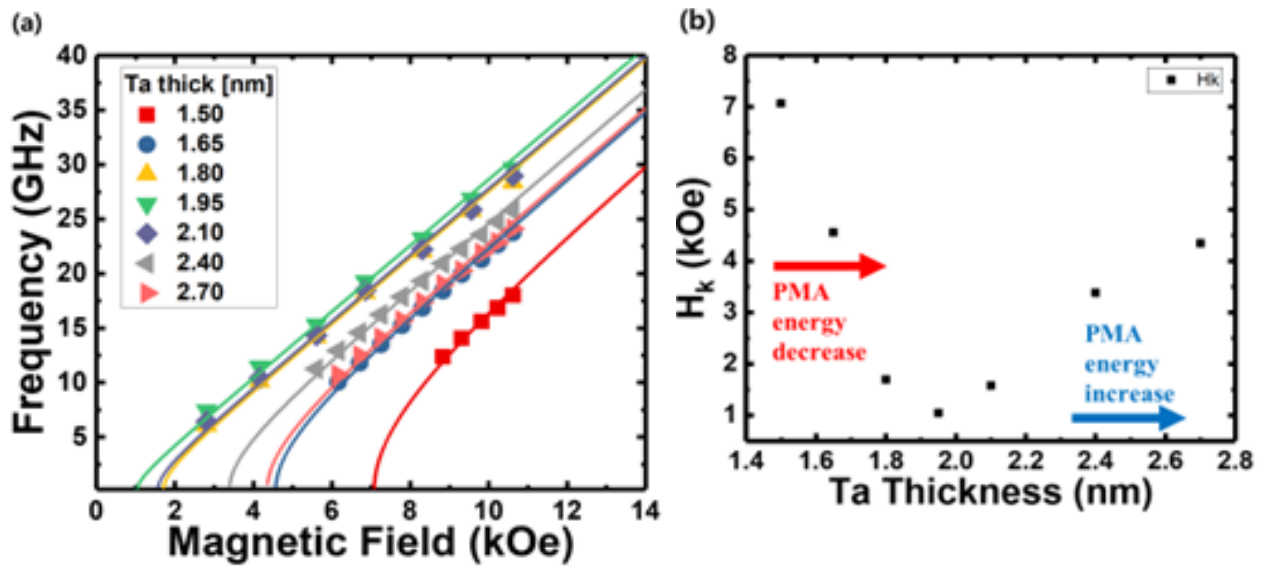


Fig. 2 (a) Spin-wave frequencies as a function of Ta thickness measured by using BLS. (b) The anisotropy

References

- [1] M. T. Johnson et al., Rep. Prog. Phys. 59, 11 (1996).
- [2] B. Dieny and M. Chshiev, Rev. Mod. Phys. 89, 025008 (2017).
- [3] C. Xu and W. Gao, Mat. Res. Innovat. 3, 231-235 (2000).
- [4] A. Manchon et al., J. Appl. Phys. 104, 043914 (2008).

Study on magnon–contribution to unidirectional spin Hall magnetoresistance in HM/FM bilayer structures

Heechan Jang¹, Eunkang Park¹, Seyeop Jeong¹, Donghyun Lee¹, Jisu Kim¹, Kwangsu Kim¹,
Nyun Jong Lee^{1,2}, Chun–Yeol You², Sanghoon Kim^{1†}

¹Department of Physics, University of Ulsan, Ulsan 44610, Korea

²Emerging Materials Science, Daegu Gyeongbuk Institute of Science & Technology, Daegu 42988, Republic of Korea

Correspondence to: sanghoon.kim@ulsan.ac.kr

Unidirectional spin Hall magnetoresistance (USMR) is a new member of the magnetoresistance family arising from the spin current generation in ferromagnet (FM)/non-magnetic heavy metal (HM) bilayers. Because the USMR shows asymmetric behavior with respect to the current or external magnetic field directions, it is easy to quantify not only amount of charge-to-spin conversion in a system, but also a sign of spin current. This can be utilized for quantitative analysis of spin current generation. Though it is well known that spin current generation gives rise to the USMR, its mechanism is still debating. C. O. Avci et al. firstly report the USMR and explain the mechanism using spin accumulation concept [1], while electron-magnon scattering has been also reported as a considerable mechanism of the USMR [2,3]. In this study, we try to derive an analysis model of USMR including the electron-magnon scattering as well as spin accumulation by applying the two current model used in GMR system.[4] And we find that magnitude of the USMR strongly depends on choice of FM with a fixed HM. Details about our observations will be discussed in this presentation.

Acknowledgments This work was supported by the Brain Korea 21 Plus Program (Human Resource Center for Novel Materials Research Experts) through the National Research Foundation of Korea (No. F19SR21D1101) and the National Research Foundation of Korea(NRF) grant funded by the Korea government(MSIT) (No. NRF-2018R1A4A1020696, 2017R1A2B3002621 and 2019R1C1C1010345).

References

- [1] Can Onur Avci, et al, Nature Physics, 11, 570 (2015).
- [2] Kab-Jin Kim, et al Applied Physics Express 12, 063001 (2019).
- [3] K. Yasuda, et al, Physical Review Letters, 117, 127202 (2016).
- [4] Dieny. B, et al, Physical Review B, 45(2), 806-813 (1992).

Study on charge-to-spin conversion in Pt/Py/perovskite trilayers

SeYeop Jeong^{1*}, Jongmin Lee², Heechan Jang¹, Eunkang park¹, Nyun Jong Lee¹,
Sanghan Lee², Tae Heon Kim¹, Sanghoon Kim^{1†}

¹Department of Physics, University of Ulsan, Ulsan, 44610 Korea.

²School of Materials Science & Engineering, Gwangju Institute of Science and Technology, Gwangju, 62005, Korea

Charge-to-spin (CS) conversion phenomenon in various systems composed of a ferromagnet (FM) and a non-magnet (NM) has been intensively studied for last a decade [1][2]. The phenomenon leads spin current within a transverse direction to charge current flowing in a system, thereby spin accumulation at the interface. Consequently, such accumulation generates the angular momentum dissipation, giving rise to spin-torque to the magnetization of the FM. That is to say, we can control the magnetization using the phenomena. The CS conversion has two origins; spin-Hall effect and Rashba effect. [4][5] Various metallic systems, such as Pt/FM, W/FM and topological insulator/FM, have been reported to have large CS conversion. In this work, we discuss CS conversion in a HM/FM/perovskite trilayer nano-device observed by unidirectional spin Hall magnetoresistance [USMR] and Spin-Orbit torque [SOT] using a harmonic measurement technique.

References

- [1] Miron, et al. "Perpendicular switching of a single ferromagnetic layer induced by in-plane current injection." *Nature* 189-193 (2011);
- [2] Lee, Hae-Yeon, et al. "Enhanced spin-orbit torque via interface engineering in Pt/CoFeB/MgO heterostructures." *APL Materials* 7, 031110 (2019);
- [3] Luqiao Liu., et al. "Spin-Torque Switching with Giant Spin Hall Effect of Tantalum" *Science* 336, 04.5 (2012): 1218197.
- [4] Miron, et al. "Fast current-induced domain-wall motion controlled by the Rashba effect" *Nature materials* 419-423 (2011);
- [5] Xuepeng Qiu, et al. "Spin-orbit-torque engineering via oxygen manipulation" *Nature Nanotechnology* 10, 333-338 (2015);

*corresponding author: sanghoon.kim@ulsan.ac.kr

Acknowledgments

This work was supported by the Brain Korea 21 Plus Program (Human Resource Center for Novel Materials Research Experts) through the National Research Foundation of Korea (No. F19SR21D1101) and the National Research Foundation of Korea(NRF) grant funded by the Korea government(MSIT) (No. NRF-2018R1A4A1020696 and 2019R1C1C1010345).

Study on spin Hall magnetoresistance in Cr-based heterostructure

Eunkang Park^{1*}, Min-gu Kang², Soogil Lee², Byong-Guk Park², Sanghoon Kim^{1*}

¹Department of Physics, University of Ulsan, Korea

²Department of Materials Science and Engineering, KAIST, Korea

Correspondence to: sanghoon.kim@ulsan.ac.kr

Spin-orbitronics devices based on spin Hall effect is a strong candidate for new generation memory devices. Here, the bilayer structure composed of a ferromagnet and a heavy metal layers should show sizable spin-orbit torque to manipulate magnetization of the devices. Even though a lot of research have been done so far, there are still many difficulties to find suitable materials. For example, although W generates a large spin current, the conductivity of W is known to be small for the energy efficient devices [1]. In case of Pt, it is so expensive that it does not suitable for industry in spite of its superior characteristics. In this presentation, we discuss spin transport in Cr-based heterostructures, which has sizable spin Hall angle and good conductivity. We found that spin Hall magnetoresistance (SMR) shows strong Cr-thickness dependence, showing the diffusion length ~2nm. This is much smaller value than other spin Hall materials such as W, Ta and Pt.[2][3]

References

This work was supported by the Brain Korea 21 Plus Program (Human Resource Center for Novel Materials Research Experts) through the National Research Foundation of Korea (No. F19SR21D1101) and the National Research Foundation of Korea(NRF) grant funded by the Korea government(MSIT) (No. NRF-2018R1A4A1020696, 2017R1A2B3002621 and 2019R1C1C1010345).

[1] Luqiao Liu, et al, Science 04, May 2012: Vol. 336, Issue 6081, pp. 555-558

[2] Min-gu Kang, et al, Nature communications 11, 3619 (2020)

[3] Sanghoon Kim, et al, Japanese Journal of Applied Physics, 55, 8

Investigation of Unidirectional Spin Hall Magnetoresistance in Epitaxial Cr/Fe Bilayer Films on MgO Substrates

Nguyen Thi Thanh Huong^{1*}, Nguyen Van Quang², Seyeop Jung², Heechan Jang²,
Eunkang Park², Nyun Jong Lee², Sunglae Cho², Jung-Il Hong¹, Sanghoon Kim^{2,†}

¹ Emerging Materials Science Department, Daegu Gyeongbuk Institute of Science and Technology

² Department of Physics, University of Ulsan

*corresponding email: sanghoon.kim@ulsan.ac.kr

Unidirectional spin Hall magnetoresistance (USMR) is universally observed in bilayer systems consisting of a non-magnetic layer with strong spin orbit coupling (SOC) and a ferromagnetic layer. The USMR is known to have two major origins; electron-magnon scattering and the spin accumulation at the interface between the two layers. Here, we report that USMR can be observed in epitaxial Cr/Fe bilayers of which the Cr has small SOC. Interestingly, we found that the USMR of the Cr/Fe bilayer strongly depends on which crystalline direction electric current flows. Correlation between USMR and magnetic anisotropy is also discussed in this presentation.

References

- [1] Avci, C. O., et al. (2015). "Unidirectional spin Hall magnetoresistance in ferromagnet/normal metal bilayers." *Nature Physics* 11(7): 570-575.
- [2] Avci, C. O., et al. (2018). "Origins of the Unidirectional Spin Hall Magnetoresistance in Metallic Bilayers." *Phys Rev Lett* 121(8): 087207.
- [3] Jo, D., et al. (2018). "Gigantic intrinsic orbital Hall effects in weakly spin-orbit coupled metals." *Physical Review B* 98(21): 214405.

Acknowledgement

This work was supported by the National Research Foundation of Korea (No. F19SR21D1101) and the National Research Foundation of Korea(NRF) grant funded by the Korea government(MSIT) (No. NRF-2018R1A4A1020696 and 2019R1C1C1010345).

Spatially–Resolved Phonon and Magnon Population in magnetic insulator TmIG

Geun–Hee Lee^{1*}, Phuoc Cao Van², Jong–Ryul Jeong², Kab–Jin Kim¹

¹Department of Physics, Korea Advanced Institute of Science and Technology, Daejeon 34141, Republic of Korea

²Department of Materials Science and Engineering, Chungnam National University, Daejeon 34141, Republic of Korea

Magnons, quanta of spin waves, are receiving of great interest because of its potential for long-distance spin transport which can be generally achieved in magnetic insulators due to their small magnetic damping [1, 2]. In magnetic insulator, the magnon relaxation is caused by the dissipation channel between spin and lattice [3], via spin orbit coupling. Therefore, the understanding of magnon and phonon relaxation is important not only for the fundamental point of view but also for the magnonic applications. In this work, we present spatially-resolved measurement of magnon and phonon population by measuring magneto-optic Kerr effect (MOKE) and thermo-reflectance (TR) in TmIG microwire under the temperature gradient. The MOKE signal, which represents the magnon-induced effect, is strongly affected by magnetic field, while the TR signal, which corresponds to the phonon-induced effect, is irrespective to the magnetic field. Both the MOKE and TR signals show exponential decay from the position of heat source. The decay length of MOKE shows different feature from that of TR, suggesting that the magnon and phonon temperature can be different in non-equilibrium condition.

References

- [1] Y. Kajiwara, et al., Nature, 464, 2623 (2010).
- [2] L.J. Cornelissen, et al., Nat. Phys. 11, 1022 (2015)
- [3] T. Kasuya and R. C. LeCraw, Phys. Rev. Lett. 6, 223 (1961)

Keywords: Magnetic Insulator, Magnonics, Magnon-Phonon Interaction

Spin Hall Conductivity in W–Ta Alloy

Dong–Soo Han^{*}

Korea Institute of Science and Technology, Seoul 02792, Republic of Korea

For the last decade, charge to spin conversion [1] and the magnetization control [2,3] via spin currents in magnetic multilayers consisting of ferromagnet/heavy elements have been an active topic of research in the field of spintronics. Particularly, with the respect of the energy efficiency for magnetization switching using spin-orbit torques, not only the charge-to-spin conversion efficiency but also the longitudinal resistivity of the channel materials are of importance. In this regard, we investigate the spin Hall conductivity in $W_{1-x}Ta_x/CoFeB/MgO$ ($x = 0 - 0.2$) using spin torque ferromagnetic resonance measurements (ST-FMR) [2,4,5] and discuss the switching efficiency of the given materials. Alloying W with Ta leads to a factor of two change in both the damping-like effective spin Hall angle (from -0.15 to -0.3) and longitudinal resistivity ($60 - 120 \ \Omega \text{ cm}$). In particular, at 11% Ta concentration, a remarkably high spin Hall angle value of -0.3 is achieved with a low longitudinal resistivity $\sim 100 \ \mu\Omega \text{ cm}$, which might be useful for a highly-efficient device operation using this W-based alloy [6]. Our findings suggest sputter-deposited W-Ta alloys could be a promising channel material for the next-generation spintronic devices [6–8].

References

- [1] J. Sinova, S. O. Valenzuela, J. Wunderlich, C. H. Back, and T. Jungwirth, *Rev. Mod. Phys.* 87, 1213 (2015).
- [2] L. Liu, et al. *Science* 336, 555 (2012)
- [3] I. M. Miron, et al. *Nature* 476, 189 (2011).
- [4] L. Liu, T. Moriyama, D. C. Ralph, and R. A. Buhrman, *Phys. Rev. Lett.* 106, 036601 (2011).
- [5] T. Nan, et al. *Phys. Rev. B* 91, 214416 (2015).
- [6] J.-Y. Kim et al., *Appl. Phys. Lett.* 117, 142403 (2020)
- [7] E. Derunova, et al. *Sci. Adv.* 5, eaav8575 (2019).
- [8] X. Sui, et al. *Phys. Rev. B* 96, 241105 (2017).

Reduced spin–orbit torque switching current by electrical modulation of easy cone states in Ta/CoFeB/Pt/MgO structures

Jimin Jeong^{*}, Min–Gu Kang, Byong–Guk Park

Department of Materials Science and Engineering, KAIST, Daejeon 34141, Korea

Gate voltage is a promising approach to control the magnetic properties because it consumes less energy compared with the magnetic field or spin torque induced by electrical current [1]. In particular, when the voltage-controlled magnetic anisotropy (VCMA) effect is applied to the magnetic memory device, the magnetization switching current can be lowered while maintaining the thermal stability. Furthermore, Implementation of spin logic operation by introducing the VCMA effect to the spin orbit torque device was reported recently [2]. Therefore, various studies have been conducted to enhance the VCMA efficiency in order to utilize the VCMA effect in spintronic applications [3].

In this study, we control the easy cone state by gate voltage and reduce the spin-orbit torque switching current accordingly in Ta (5 nm)/CoFeB (1.1 nm)/Pt (0.15 nm)/MgO (1.6 nm)/ZrO₂ (25 nm) structures, where the Pt layer is inserted at the CoFeB/MgO interface to enhance the VCMA effect. Fig 1.a shows the change of R_{H-H_z} curve when -7.5V gate voltage pulse is applied repeatedly. At virgin state, the device has perpendicular magnetic anisotropy. When -7.5 V pulses are applied with the pulse width 150 ~ 500 ms, it changes to easy cone state and easy cone angle gradually changed as the number of negative gate voltage pulse increases (Fig 1.b) which was confirmed by analyzing the Generalized Sucksmith-Thompson method. Fig 1.c shows the spin-orbit torque switching measurements at each easy cone state. Interestingly, As the easy cone angle increases, the spin-orbit torque switching current decreases (Fig 1. d). Reversely, when +8V pulses are applied with the pulse width 800 ms, the easy cone angle decreases and the spin-orbit switching current increases. The device recovers to the perpendicular magnetic anisotropy when +8V pulse is applied repeatedly. we experimentally demonstrate the reduction of spin-orbit torque switching current via controlling the easy cone state by gate voltage. These gradual and reversible manner of spin-orbit torque switching current and easy cone state control technique can be utilized for the multilevel spintronic device.

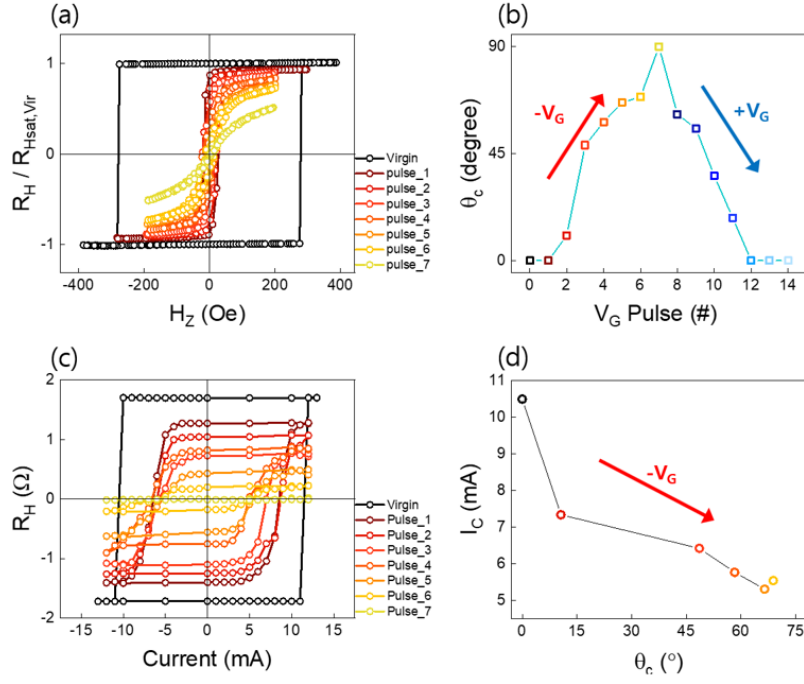


Fig 1. (a) Normalized anomalous Hall resistance curves measured after negative gate voltage pulses in Ta/CoFeB/Pt/MgO structures. (b) easy cone angle (θ_c) as a function of the number of gate voltage pulses. (c) SOT switching measurements after negative gate voltage pulses. (d) SOT switching current (I_C) as a function of easy cone angle (θ_c). All measurement is carried out at room temperature after the gate voltage pulse is applied at 125°C.

References

- [1] Takayuki Nozaki et al., Micromachines, 10, 327 (2019)
- [2] Baek, S.C. et al., Nat Electron 1, 398-403 (2018).
- [3] Jibiki, Y., Miwa, S., & Suzuki Y et al., Appl. Phys. Lett. 114, 082405 (2019)

Fast Magneto–Ionic Switching of Interface Anisotropy Using Yttria–Stabilized Zirconia Gate Oxide

Dongwon Choi^{1,2*}, Sujin Jo¹, Byeong–Kwon Ju², Seonghoon Woo^{1,3}, Ki–Young Lee^{1*}

¹Spin Convergence Research Center, Post–Silicon Semiconductor Institute, Korea Institute of Science and Technology (KIST),

Hwarang-ro 14-gil 5, Seongbuk-gu, Seoul 02792, Korea

²Display and nanosystem Laboratory, School of Electrical Engineering, Korea University
Anam-ro 145, Seongbuk-Gu, Seoul 02841, Korea

³IBM Thomas J. Watson Research Center
1101 Kitchawan Rd, Yorktown Heights, New York 10598, USA
*kylee80@kist.re.kr

Voltage control of magnetic anisotropy has attracted significant attention in spintronics research, due to the much reduced switching energies in devices. Voltage control of magnetism through solid-state electrochemical switching of the interfacial oxidation state in thin metallic ferromagnets was discovered [1–3]. Early works utilized voltage-induced oxygen ion (O^{2-}) migration in ferromagnetic heterostructures. In ultrathin ferromagnet/oxide bilayers, perpendicular magnetic anisotropy (PMA) arises from interfacial hybridization between the ferromagnetic 3d and oxygen 2p orbitals. However, such a scheme relying on reactive and relatively large oxygen ions suffered from slow switching speed, irreversible oxidation damage, and high operation temperature. Recently, proton (H^+)-based magneto-ionic devices has been suggested owing to nondestructive magnetization switching speed.

In this work, Yttria-stabilized zirconia (YSZ) is used as a gate oxide [4]. This oxide is stable under electrochemical reactions (i.e., reduction or oxidation) and present large ionic conductivities. These characteristics make them particularly suitable as proton conductors in proton-based magneto-ionic devices. We demonstrate reversible 90° magnetization switching in a thin Co film at room temperature by either inserting proton at its interface with an oxide or loading hydrogen into an adjacent heavy metal (Pt or Pd) layer. Moreover, a host of spin-orbit induced phenomena at heavy metal/ferromagnetic interfaces becomes accessible to voltage gating despite the fact that electric fields cannot be applied directly. This work establishes that gate oxide material engineering may be a key pathway for achieving fast and reliable switching in magneto-ionic devices, highlighting the significant potential of this approach toward future spintronic applications.

References

- [1] U. Bauer, et al., *Nature Nano.* 8, 411 (2013).
- [2] U. Bauer, et al., *Nature Mater.* 14, 174 (2015).
- [3] S. Emori, et al., *Appl. Phys. Lett.* 105, 222401 (2014).
- [4] Lee, K-Y, et al., *Nano Lett.* 20, 5, 3435–3441 (2020)

Current-driven Spin Modulation in a van der Waals Fe_5GeTe_2

Kwangsue Kim^{1, 2}, Hyo-bin Anh³, Seyeob Jeong¹, Jungmin Park⁴
 Nyun Jong Lee^{1, 5}, Trinh Thi Ly¹, Kyung Mee Song², Jung Dae Kim¹, Changgu Lee³,
 Tae-Eon Park^{2*}, Sanghoon Kim^{1*}

¹Department of Physics, University of Ulsan, Ulsan, Korea

²Center for spintronics, Korea Institute of Science and Technology (KIST), Seoul, Korea

³School of Mechanical Engineering, Sungkyunkwan University, Seoul, Korea

⁴Center for Scientific Instrumentation, Division of Scientific Instrumentation & Management, Korea Basic Science Institute (KBSI), Daejeon, Korea

⁵Energy Harvest Storage Research Center, University of Ulsan, Ulsan, Korea

Two dimensional (2D) systems are paving a new avenue towards understanding physical phenomena related to dimensionality. For example, 2D electron gas has already shown outstanding electron transport properties under the boundary condition.^[1] In this respect, the phenomena using spin polarized electrons in 2D systems also prospect similar capacity. However, spintronic devices have required heterostructures for using spin information, and the fabrication of heterostructures using 2D ferromagnetic materials is difficult generally because of its surface condition. Consequently, the difficulties hinder scientific endeavor, despite the promising expectation.

Recently discovered Fe_5GeTe_2 shows relatively high Curie temperature among 2D ferromagnets ($T_c \sim 310$ K). Furthermore, its complicated crystal and spin structures lead non-trivial magnetic behaviors.^[2, 3] Here, we discuss about that current-driven spin modulation can be observed in the single Fe_5GeTe_2 layer. We also discuss that the observed spin current generation can be attributed to broken inversion symmetry in the Fe_5GeTe_2 crystal.

References

- [1] Berger, C. et al. J. Phys. Chem. B 108, 19912-19916 (2004).
- [2] May, A. F. et al. ACS Nano 13, 4436-4442 (2019).
- [3] May, A. F., Bridges, C. A. & McGuire, M. A. Phys. Rev. Materials 3, 104401 (2019).

Study on stochasticity in the switching of Co/Pt nanodisks

Sooseok Lee^{*}, Soong-Geun Je², Hee-Sung Han¹, Myeonghwan Kang¹, Hye-Jin Ok¹,
Namkyu Kim¹, Weilun Chao³, Mi-Young Im^{*,3}, Ki-Suk Lee^{*,1}

¹School of Materials Science and Engineering, Ulsan National Institute of Science and Technology, Ulsan 44919, Republic of Korea.

²Department of Physics, Chonnam National University, Gwangju 61186, Korea.

³Center for X-ray Optics, Lawrence Berkeley National Laboratory, Berkeley, CA94720, USA.

Understanding the stochastic switching behavior in the magnetic elements is important not only for fundamental physics but also developing related applications. [1-4] In particular, the stochastic character can be potentially utilized as the probabilistic computing based on random fluctuation unit called probabilistic bit (p-bit). [5-6] The well-defined array of magnetic tunnel junctions (MTJs) is highly considered as suitable candidate for hardware implementation because the intrinsic stochastic feature of MTJs during switching process. In this presentation, we show the stochastic behavior in switching process of a perpendicularly magnetized Co/Pt disk within an array was directly observed utilizing full-field soft X-ray microscopy (MTXM). [7] we found the switching field for individual disks is stochastically fluctuated due to thermal agitation and the stochasticity considerably depends on the disk size. The stochasticity decreases as the disk radius gets bigger from 125 nm to 375 nm. We also observed that the trend of stochasticity is reversed with further enlarging disk radius from 375 nm to 625 nm because the multi-level switching in a disk. This work provides the way for controlling the stochasticity in the switching of nanopatterned elements, which is a key aspect for MTJ-based probabilistic computing.

References

- [1] Sethna, J. P.; Dahmen, K. A.; Myers, C. R. Crackling noise. *Nature*, 2001, 410, 242-250.
- [2] Ryu, K.-S.; Akinaga, H.; Shin, S.-C. Tunable scaling behaviour observed in barkhausen criticality of a ferromagnetic film. *Nat. Phys.*, 2007, 3, 547-550.
- [3] Devolder, T.; Chappert, C.; Katine, J. A.; Carey, M. J.; Ito, K. Distribution of the magnetization reversal duration in subnanosecond spin-transfer switching. *Phys. Rev. B*, 2007, 75, 064402.
- [4] Petta, J. R.; Weissman, M. B.; Durin, G. Dependence of Barkhausen pattern reproducibility on hysteresis loop size. *Phys. Rev. E*, 1997, 56, 2776.
- [5] Camsari, K. Y.; Faria, R.; Sutton, B. M.; Datta, S. Stochastic p-Bits for Invertible Logic. *Phys. Rev. X*, 2017, 7, 031014.
- [6] Mizrahi, A.; Hirtzlin, T.; Fukushima, A.; Kubota, H.; Yuasa, S.; Grollier, J.; Querlioz, D. Neural-like computing with populations of superparamagnetic basis functions. *Nat. Comm.*, 2018, 9, 1533.
- [7] Fischer, P.; Kim, D.-H.; Chao, W.L.; Liddle, J.A.; Anderson, E.H.; Attwood, D.T. Soft X-ray microscopy of nanomagnetism. *Materials Today*, 2006, 9, 26-33

평면홀 저항 센서를 이용한 강자성 재료의 와전류 결함 신호 측정

김동영, 윤석수*

안동대학교 물리학과

비파괴 검사용 와전류 센서는 현재까지 코일 센서가 주로 사용하고 있다. 전자기 유도 법칙을 이용하는 코일 센서는 저주파수 신호가 작은 단점이 있다. 한편 자기저항(magnetoresistance) 센서는 주파수 의존성이 없으므로 저주파수에서 사용이 가능하며[1,2], 마이크로 크기로 제조할 수 있으므로 결함의 공간 분해능을 향상할 수 있는 장점이 있다[3]. 따라서 코일 센서의 저주파수 단점을 보완할 수 있는 자기저항 센서를 이용한 와전류 결함 측정 연구가 세계적으로 활발히 진행되고 있다.

본 연구에서는 초소형으로 제작한 평면홀 저항 센서를 사용하여 10Hz-100kHz의 주파수 범위에서 강자성체 표면 결함에 의해 유도된 와전류 신호의 세기와 위상을 측정하였다. 와전류 결함 신호의 세기는 1kHz 이하의 주파수에서는 일정한 값으로 측정되었으며, 이는 강자성체 표면 결함의 가장자리에서 여기 자기장에 의해 유도된 일정한 자극의 영향으로 해석되었다. 한편, 1kHz 이상의 주파수에서는 와전류의 침투 깊이와 유사한 $f^{1/2}$ 에 비례하는 주파수 의존성을 보였다. 또한, 와전류 결함 신호의 위상은 10Hz-10kHz의 주파수 범위에서 와전류의 침투 깊이에 비례하는 $f^{1/2}$ 의 주파수 의존성을 보였으며 10 kHz 이상에서는 감소하는 특성을 보였다. 초소형 평면홀 저항 센서는 결함을 검출하는 공간 분해능이 우수할 뿐만 아니라 저주파수에서 강자성체 표면에 형성된 결함 검출 성능이 매우 우수하였다. 이러한 평면홀 저항 센서는 강자성체 내부에 형성된 결함을 검출하기 위한 비파괴 검사용 와전류 센서로 활용 가능하다.

References

- [1] J. W. Park, et.al., J. Magn. 22, 531 (2017).
- [2] G. M. Javier, et.al., Sensors 11, 2525 (2011).
- [3] M. Pelkner, et.al., AIP Conf. Proc. 1949, 040001 (2018)

Contribution of hydrogen irradiation–induced defects to the magnetic characterization of FeRh films

Sehwan Song^{1*}, Chang-woo Cho¹, Jiwoong Kim¹, Jisung Lee², Sungkyun Park^{1,†}

¹Department of Physics, Pusan National University, Busan 46241, Korea

²Korea Basic Science Institute, Daejeon 34133, Korea

B2-phase FeRh is well known as magnetic phase transition material from antiferromagnetic to ferromagnetic around 370 K. During the transition, it shows the volume expansion of about 1% with reducing the electrical resistivity. Although the origin of the magnetic phase transition is unclear, many studies have been conducted to modify transition characteristics by strain, doping, stoichiometry, etc. But studies on the correlation between defect (Fe or Rh vacancies) and magnetic properties are insufficient. In this study, we intentionally created defects by using hydrogen irradiation with different amounts of dose (1×10^{15} H/cm² and 1×10^{16} H/cm²) to understand the correlation between defects and phase transition characteristics. As a result, the residual ferromagnetic state below the magnetic phase transition temperature (i.e., antiferromagnetic region) increases with increasing dose concentration. Further, the transition temperature decreases and the lattice parameter both in-plane and out-of-plane increases with the increment of hydrogen dose. From the X-ray photoelectron spectroscopy measurement, we confirm that Fe vacancies dominantly increase with hydrogen dose. Therefore, the Fe vacancies induced by hydrogen irradiation increase lattice parameter and affect the breaking antiparallel spin configuration of (001) orientation of Fe-sublattice.

This work is supported in part by NRF Korea (NRF-2018R1D1A1B07045663 and NRF-2020K1A3A7A09077715).

Two-Dimensional Organic-Inorganic Hybrid Perovskite Ultrathin Magnets

Ki-Yeon Kim^{1*}, Garam Park¹, Jaehun Cho², Joonwoo Kim², June-Seo Kim²,
Jinyong Jung², Kwnojin Park², Chun-Yeol You², In-Hwan Oh¹

¹Korea Atomic Energy Research Institute, Korea

²Daegu Gyeongbuk Institute of Science and Technology, Korea

Organic-Inorganic hybrid perovskites (OIHPs) have been expanding into a very broad spectrum of research fields beyond perovskite solar cells. Specially, it is noteworthy that two dimensional Ruddlesden-Popper (RP) OIHPs with a general chemical formula of $(R-NH_3)_2MX_4$ (R = a monovalent organic moiety such as C_nH_{2n+1} and $C_6H_5(CH_2)_n$, M = a divalent transition metal cations such as Mn^{2+} , Fe^{2+} , Cu^{2+} , X =a monovalent halide ions such as I^- , Cl^- , Br^-) was considered as an ideal two-dimensional Heisenberg model in 1970s.[1] Interestingly, there is no successful experimental report on intrinsic magnetic order of atomically thin or few-layered RP-OIHP vdW magnets although Langmuir-Blodgett technique as well as theoretical calculation have been attempted for thin film preparation. [2,3] Here, we present the compelling evidence on the robust magnetic order of two-dimensional RP-OIHP ultrathin magnets chemically exfoliated from bulk single crystals by a combination of solvent-engineering and spin coating technique.

References

- [1] D. L. Cortie, G. L. Causer, K. C. Rule, H. Fritzsche, W. Kreuzpaintner, and F. Klose, *Adv. Func. Mater.* 1901414 (2019).
- [2] N. Akhtar, A. O. Polyakov, A. Aqeel, P. Gordiichuk, G. R. Blake, J. Baas, H. Amenitsch, A. Herrmann, P. Rudolf, and T. T. M. Palstra, *Small* 23, 4912 (2014).
- [3] D. Nafday, D. Sen, N. Kaushal, A. Mukherjee, and T. Saha-Dasgupta, *Phys. Rev. Research* 1, 032034(R) (2019).

Temperature and field–dependent MFM measurements of MnAs/GaAs(001)

Jiseok Yang^{1*}, Jiyoung Jang², Kyung Jae Lee², Sanghoon Lee², Kab–Jin Kim¹

¹Department of Physics, Korea Advanced Institute of Science and Technology, Daejeon 34141, Republic of Korea

²Department of Physics, Korea University, Seoul 02841, Republic of Korea

Epitaxial ferromagnetic MnAs films have received great attention because of their unique magnetic domain structures [1] and distinct phase transition from the ferromagnetic α phase to the paramagnetic β phase near the room temperature [2]. These characteristics allow to study the scaling phenomena of magnetic noise [3] as well as to study the topological spin structures [4]. To fully utilize the potential of MnAs in spintronic research, microscopic spin textures in various conditions must be better understood.

In this study, we investigate the temperature-dependent and the field-dependent magnetic domain structure of MnAs/GaAs(001) films using magnetic force microscopy (MFM). The topographic image clearly shows the hexagonal crystal structure and magnetic contrasts exhibits the in-plane magnetic anisotropy along the easy axis of MnAs[11 $\bar{2}$ 0] [5]. The magnetic field dependence shows the formation of alternating antiparallel in-plane magnetization in stripe-type domain structures and the temperature-dependence clearly demonstrates that the magnetic phase transition occurs at about 40°C. In particular, we found that Bloch line-like topological spin structures with a size of 100 nm start to appear at 15°C. These results suggest that the MnAs would be a good platform to study the dynamics of topological spin structures.

References

- [1] F. Schippan et al., Appl. Phys. Lett. 88, 2766 (2000)
- [2] T. Plake et al., Appl. Phys. Lett. 82, 2308 (2003)
- [3] Kwang–Su Ryu et al., Nat. Phys. 3, 547 (2007)
- [4] JinBae Kim et al., Appl. Phys. Lett. 98, 052510 (2011)
- [5] R. Engel–Herbert et al., J. Appl. Phys. 98, 063909 (2005)

Observation of Current Induced Skyrmion Density Control in a Lorentz Transmission Electron Microscope

Albert M. Park^{1,2*}, Zhen Chen¹, Xiyue S. Zhang¹, Lijun Zhu¹, David Muller^{1,3}, Gregory D. Fuchs¹

¹School of Applied and Engineering Physics, Cornell University, Ithaca, New York 14853, USA

²Department of Physics, Korea Advanced Institute of Science and Technology, Daejeon 34141, Republic of Korea

³Kavli Institute at Cornell for Nanoscale Science, Ithaca, New York 14853, USA

Recent advances in understanding of the skyrmion in ferromagnetic multilayers with interfacial DMI indicated a realistic possibility of using skyrmions for the device applications [1,2]. The increasing urge to utilize skyrmion in the device led to research seeking ways to create smaller, faster, and more stable skyrmions. We develop a technique for operando electrical current pulsing of chiral magnetic devices in a Lorentz transmission electron microscope to enable the investigation of nanoscale skyrmions and their response to external stimuli. Using the repeated multilayer stack of Pt/Co/Ru, we observe strongly pinned skyrmions that can be nucleated or annihilated with electric current but are strongly bound to pinning sites. Also, we control the skyrmion density using a thermally assisted nucleation and annihilation process via current induced Joule heating. Micromagnetic simulations clarify that the nucleation and annihilation of skyrmions are consistent with a thermally assisted process in which the spin texture finds its energetic minimum of configuration space. Finally, using the skyrmion density controllability, we demonstrate that high-density skyrmion states are more stable than low-density states or isolated skyrmions, resisting annihilation from magnetic field perturbations.

References

- [1] X. Zhang et al., J. Phys. Condens. Matter 32, 143001, (2020).
- [2] C.H. Back, et al., J. Phys. D: Appl. Phys. 53, 363001 (2020).

Spin Hall Conductivity of W–N alloys: A First Principles Study

Quynh Anh T. Nguyen*, D. D. Cuong, S. C. Hong, Sonny H. Rhim

Department of Physics and Energy Harvest Storage Research Center, University of Ulsan,
Ulsan 44610, Republic of Korea.

Currently, comprehensive studies about W alloys have attracted attentions, which purpose to enhance spin Hall angle (SHA) and spin Hall conductivity (SHC) [1–3]. Here, SHC of W–N alloys are investigated using first principles calculations. Among various N compositions of W–N alloys, W_2N and WN are taken into account. W_2N , with 50% N vacancy in NaCl structure, exhibits SHC of -966 S/cm, enhanced by 29 % and 18 % over α -W (-744 S/cm) and β -W (-817 S/cm), respectively. WN, on the other hand, thermodynamic average of three structures (NaCl, NbO and hexagonal) gives much smaller SHC of around -194 S/cm. In particular, the large SHC of W_2N is elucidated by large Berry curvature in Γ X.

Keywords: Spin Hall effect; spin Hall conductivity; spin Hall angle; first principles calculations

References

- [1] K.-U. Demasius, T. Phung, W. Zhang, B. P. Hughes, S.-H. Yang, A. Kellock, W. Han, A. Pushp, and S. S. P. Parkin, Nat. Commun. 7, 10644 (2016).
- [2] X. Sui, C. Wang, J. Kim, J. Wang, S. H. Rhim, and W. Duan, Phys. Rev. B 96, 241105(R) (2017).
- [3] Y. J. Kim, M. H. Lee, G. W. Kim, T. Kim, I. H. Cha, Q. A. T. Nguyen, S. H. Rhim, and Y. K. Kim, Acta Mater. 200, 551 (2020).

Torque magnetometry using circuit change of membrane-type surface stress sensor

Mariam Omran, Joonyoung Choi, Younjung Jo*

Department of Physics, Kyungpook National University, Daegu 41566, Korea

We present a new method for torque measurement by using a membrane-type surface stress sensor (MSS). This sensor has a silicon membrane supported by four beams with integrated piezoresistive paths [1]. We modified the on-chip aluminum interconnect on the MSS to obtain more magnetic information and used it for the torque measurement. We verified the angle-dependent magnetic torque measurement of magnetic material by rotating the device with a respect to the applied magnetic field. Instead of the existing one Wheatstone Bridge, on-chip aluminum interconnects have been modified to have two Wheatstone bridges. Using this experimental setup, it was possible to simultaneously investigate magnetic responses along different crystallographic directions in a two-dimensional plane.

References

- [1] H. Takahashi et al., J. Phys. Soc. Jpn. 86, 063002 (2017).

Praseodymium substituted Bi–YIG film prepared by MOD method for magneto–optical isolators

Trinh Nguyen Thi, Viet Dongquoc, Duc Duong Viet, Phuoc Cao Van, Jong–Ryul Jeong^{*}

Department of Materials Science and Engineering, Graduate School of Energy Science and Technology, Chungnam National University, Daejeon 34134, South Korea

In this study, we have investigated a praseodymium substituted Bi–YIG films ($\text{PrxBi}_{1-Y}\text{Fe}_{5012}$) for optical isolator applications. Magneto-optical (MO) thin films can be used for applications in various ways such as MO microscopy, optical isolators, and information storage devices. Although it is widely investigated, growth of high Faraday rotation magnetic thin films on glass substrate is still considered as a primary issue in MO thin films. Here, we have investigated enhancement of MO properties in praseodymium-substituted bismuth yttrium iron garnet ($\text{PrxBi}_{1-Y}\text{Fe}_{5012}$) thin film on a glass substrate by using a metallo-organic decomposition (MOD) method. To improve the MO performance of the as-prepared $\text{PrxBi}_{1-Y}\text{Fe}_{5012}$ thin film, different concentrations of Pr-substituted bismuth yttrium iron garnet were prepared. It shows that $\text{PrxBi}_{1-Y}\text{Fe}_{5012}$ thin film with an optimal concentration of $x=1$ exhibited high crystallinity, high saturation magnetization and the highest Faraday rotation (FR) angle of $-6.50/\mu\text{m}$ at a wavelength of 510 nm as shown in figure below. The $\text{PrBi}_{1Y}\text{Fe}_{5012}$ thin film fabricated by the modified MOD method displayed excellent MO performance and is a potential candidate for application in optical devices.

자성마이크로비드를 이용한 펄스자기장 처리에 따른 혈액 내 산-염기 균형평가

최유경*, 방승환, 이현숙†

상지대학교 보건과학대학 한방의료공학과, 강원 원주시 상지대길 84, 26339

I. 서론

인체 내 세포의 모든 활동은 체온, 삼투압, pH, 생화학물질의 혈중 농도 등의 항상성을 유지하는 것이 필수적이다. 특히 혈액 내 산-염기 불균형은 각종 질병을 유발한다. 혈액 내 H^+ 이온이 증가하여 산성화되면 급성폐질환, 심장마비, 질식 등 호흡성산증과 급성신부전증, 당뇨병성 케톤산증 등의 대사성산증이 나타난다. 심각한 산증은 쇼크나 사망으로 이어지기 때문에 혈액 내 산-염기 균형 유지는 매우 중요하다.[1]

혈액 내 pH 불균형 치료는 우선적으로 장애를 유발하는 원인에 대한 치료가 이루어진다. 그렇지만 산증이 심각한 경우에는 정맥 내에 중탄산염을 투여하는데 이는 모든 산증 치료에 적용할 수 없으며 부작용을 동반할 뿐만 아니라 침습적인 방법으로 각종 감염 문제가 있다고 한다.[2]

최근 비침습적인 방법으로 펄스자기장이 혈액에 미치는 영향에 대한 연구가 활발하게 이루어지고 있다. 펄스자기장 자극을 인체에 인가하면 자기장이 인체 깊숙이 투과하여 체내에 있는 이온전해물질에 영향을 준다고 알려져 있으며, 펄스자기장의 순간적인 자속변화율이 적혈구막의 음전하를 변화시켜 제타포텐셜이 증가함으로써 응집성이 개선되는 연구결과도 보고되었다.[3-4] 따라서 펄스자기장이 혈액내 H^+ 농도를 변화시켜 pH에도 영향을 미칠 것이라고 판단되어 본 연구를 진행하고자 한다.

II. 실험 방법 및 결과

실험을 위해 필요한 혈액은 IRB면제 심의 후 강원혈액원에서 공급받아 혈장과 적혈구를 분리하기 위해 혈액을 원심분리(3000 rpm, 5 min)한 후 PBS를 사용하여 인체와 동일한 적혈구용적률(HT) 45%로 맞추었다. pH 변화는 온도에 영향을 받으므로 모든 혈액의 온도를 같은 조건으로 맞추기 위하여 인큐베이터(37 °C, 10 min)에 보관 후 실험을 진행하였다. pH meter(HORIBA, LAQUA twin)를 이용하여 0.27 T세기의 펄스자기장을 3분간 인가 전후의 혈액 pH 수치를 비교하였다. 펄스자기장의 pH 치료 효과를 규명하기 위하여 혈액에 인위적으로 산화스트레스(tBHP 0.4mM) 처리하였고 자기장 유무에 따른 혈액의 pH 수치 변화를 혈장에서의 결과와 비교하였다.

대조군의 혈액보다 펄스자기장 인가 후 혈액의 pH 수치가 평균적으로 0.26% 증가하였다. 또한 산화스트레스 처리한 혈액의 pH 수치도 펄스자기장 인가 후 0.68% 증가한 것을 관찰하였다. 이러한 pH 변화는 혈장뿐만 아니라 PBS에서도 관측되었는데, 이는 펄스자기장의 자극으로 높아진 적혈구의 막전하와 양이온의 증가로 인해 나타나는 것으로 판단된다. 따라서 적혈구 주변의 양이온의 증가를 관찰하기 위하여 OH기를 가진 Magnetic bead(MB)를 투여한 후 MB가 부착된 적혈구를 관찰하여 간접적으로 펄스자기장과 산화스트레스에 따른 적혈구 주변 양이온의 변화를 확인하였다.

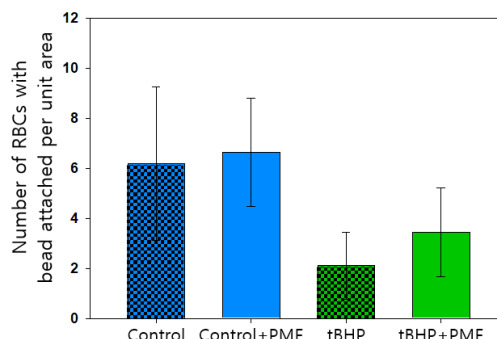


Fig. Comparison number of RBCs with beads attached.

III. 결론

본 연구에서는 펄스자기장 유무에 따른 혈액의 pH 수치 변화에 대해 연구하였다. 펄스자기장 인가 후 혈액의 pH 수치가 0.26% 증가하는 것과 인위적으로 산화스트레스처리한 혈액에서도 pH 수치가 0.68% 증가한 것을 확인하였다. 이는 펄스자기장의 순간적인 자속변화률이 적혈구의 막전하에 영향을 미쳐 막전하가 증가함으로써 혈장 내 양이온인 H^+ 이온과의 결합이 증가하여 혈장 내에 H^+ 이온의 수가 줄어들어 혈액의 pH 수치가 올라가는 것으로 판단된다. 또한 적혈구 주변 양이온의 증가로 인하여 Magnetic bead 부착 개수가 증가하는 것을 관찰하였다.

이 결과로 본 연구는 펄스자기장이 불균형이었던 혈액의 pH 항상성을 빠르게 회복할 수 있으며 여러 부작용을 동반하는 약물요법보다는 비침습적 방법인 대체요법으로의 가능성을 제시한다.

References

- [1] J. A. Kellum, Critical care 4, 1 (2000).
- [2] S. Sabatini, J Am Soc Nephrol 20, 4 (2009).
- [3] D. G. Hwang, J. Korean Magn. Soc. 23, 1 (2014).
- [4] S. H. Bang, J. Korean Magn. Soc. 30, 4 (2020).

Optimization of the Diverging Collimator for Thyroid Cancer Treatment Room Monitoring with ^{131}I Isotopes Using Monte Carlo Simulation

Dong-Hee Han^{1*}, Jong-Seok Byeon², Kyung-Hwan Jung², Cheol-Ha Baek^{1,2†}

¹Department of Medical Health Science, Kangwon National University, Samchoek, Republic of Korea

²Department of Radiological Science, Kangwon National University, Samcheok, Republic of Korea

In the field of nuclear medicine, ^{131}I , a radioactive isotope, is used for the treatment of residual tissues after respective surgery, and the number of treatments is increasing every year. The ^{131}I has a half-life of about eight days and emits β -rays up to 606 keV and 364 keV γ -rays. In order to prevent safety accidents such as exposure to the open air during treatment, patients are placed in the hospital room for a certain period of time, and radioactive contaminants are likely to be exposed to the outside through various channels, such as vomiting or excrement, which are typical side effects, and exposure to medical workers and the public occurs to deal with them. Gamma cameras can be used to visualize and monitor the distribution of ^{131}I isotopes in the room, where the collimator has previously used pinhole collimators to secure a wide range of field-of-view(FOV), but this requires new alternatives due to drawbacks such as variation in detection efficiency and poor performance at the edges. Although there were limitations in the development of diverging collimators due to their physically complicated structure, diverging collimators of metal materials are drawing attention as precision processing technology using 3D printers has recently become possible. The purpose of this study was to optimize the design parameters of the diverging collimator of tungsten for the imaging of ^{131}I isotopes by using GATE(Geant4 application for tomographic emission), a Monte Carlo simulation tool. The scintillator is GAGG, which has a relatively high density of 6.63 g/cm³, which has an efficient stopping power and high fluorescence yield. As a result of the simulation, the slit height of the collimator was raised to remove the penetration and scattering rays due to the structural features of the diverging collimator. By obtaining optimal sensitivity and spatial resolution for image formation, the design parameters for hole size and septal thickness were derived through trade-off, and the performance comparison with pinhole collimator was also carried out at the same magnification factor. In the future, it is necessary to study optimized collimator study according to the energy range of the monitored target and it is judged that experiments with actual sources should be conducted based on the simulation results.

Acknowledgement

This work was supported by a National Research Foundation of Korea (NRF) grant funded by the Korea Government (MSIT) (No. 2020R1C1C1004584)

Performance Analysis of Comparison of Digital Dental Model Acquired using Electromagnetic Wave Projection (Dental Cone Beam Computerized Tomography) with 3D Printing Temporary Resin

Seen-Young Kang*, Ji-Min Yu, Jun-Seok Lee, Jae-Won Lee, Ho-Sang Jung, Seung-Youl Lee*

Medical Device Research Division, National Institute of Food and Drug Safety Evaluation,
Chungcheong buk-do, Cheongju-si 28159, Korea

1. Introduction

In the field of digital dentistry, interest in dental treatment using digital technology has increased rapidly with the development of science and technology. Currently, one of the areas of interest in digital dentistry is the dental CAD/CAM (Computer-aided Design/ Computer-aided Manufacturing) system. Digital work flow is replacing the method of fabricating dental prosthesis by taking impressions in the mouth and fabricating dental models through Dental hard stone [1].

In the digital work flow, not only the method of obtaining an impression in the oral cavity using an intraoral scanner, but also the oral cavity is radio-graphed using a dental CBCT (Cone Beam Computed Tomography) which is an electromagnetic wave projection, and then DICOM File is converted into STL file for digital dentistry. Techniques for making prostheses have been introduced [2]. The digital model based on the CBCT scan can acquire data without the need to equip it with a high-rigidity optical scanner, and the possibility of utilizing it has been presented [2].

In addition, in order to manufacture dental prosthesis, the introduction of 3d printing method makes it possible to manufacture dental prosthesis with high accuracy and convenience [3]. The fabrication of dental prostheses using 3D printing is diverse, such as ceramic, metal, and polymer materials, but currently the most commonly used material in clinical practice is temporary crown resin material. Temporary crown material is a material that temporarily restores mastication and aesthetic functions in the oral cavity for a certain period of time before completion of the oral treatment during dental treatment or prosthesis treatment [4].

In the end, the most important thing for manufacturing a dental prosthesis with high accuracy in a digital method is that the digital file of the dental model and the accuracy according to the manufacturing method play a very important role. However, even if the accuracy of making a dental prosthesis is high, the strength to withstand mastication in the oral cavity plays a very important role.

The purpose of this study is to analyze the accuracy of a digital dental model using a dental CBCT (electromagnetic wave method), and the 3-point flexural strength of printed specimens for each angle (0° , 45° , 90°) of 3D printed temporary crown resin.

The first purpose of this study is to analyze the accuracy of a digital dental model using a dental CBCT and the second purpose is to analyze the printed flexural strength by each angle (0° , 45° , 90°) of 3D printed temporary crown resin.

2. material and method

In the first study, a single preparation dental model (AG 3Frasaco, GmbH, Tettrang, Germany) and a

3-unit preparation dental model (1 (AG 3Frasaco, GmbH, Tettrang, Germany)) were used to analyze the performance of a digital dental model using dental CBCT. After taking a tooth model using dental CBCT, the acquired tooth model DICOM FILE was converted to an STL file. The converted STL file was superimposed with References CBCT data and experiment CBCT data through a 3D superimposition program (Geomagic verify, Geomagic GmbH, Hill, USA), and then analyzed the accuracy and error of the digital dental model through 3D analysis (fig. 1).



Fig. 1. Procedure of experiment (CBCT dental digital model analysis)

In the second study, 3d printing temporary crown resin specimens were up-loaded to a 3d printing program (to find and put) an STL file of 25 ± 1 mm in length, 2 ± 0.1 mm in height, and 2 ± 0.1 mm in width. After that, the output conditions were set by setting the specimen angle to 0, 45, 90 angle, the layer thickness to 50 μ m, and the support thickness to 0.25 mm.

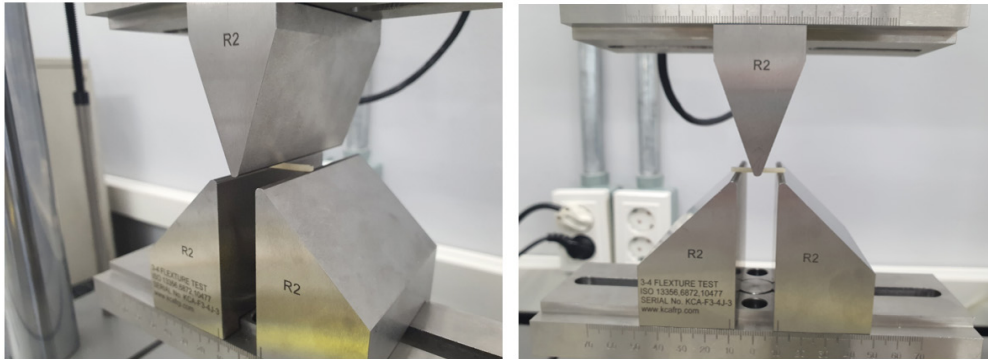


Fig. 2. Procedure of experiment (3-Point flexural strength)

After that, the universal tester (ElectroPuls E3000, Instron, Norwood, USA) is combined with a 3-point flexural strength jig required by ISO 10477. After that, the specimen was placed on the support so that the flat surface was symmetric, and the load was uniformly increased from the zero point until the specimen fractured at a rate of 1 ± 0.3 mm to apply fracture (fig. 2).

The maximum flexural strength was calculated in MPa from the following equation.

$$\delta_B = \frac{3FI}{2bh^2}$$

F: Maximum load applied to the specimen (N)

I: distance between supports

b: width of the specimen
h: thickness of the specimen

3. Results and discussion

As a result of the accuracy study of dental CBCT, the single preparation digital dental model and the 3-unit bridge digital dental model have a common surface distortion. In particular, there was a distortion of the positive shape in the margin of the preparation tooth, and it is considered that it would be difficult to manufacture a digital dental prosthesis due to the distortion of the surface of the negative and positive shape between adjacent teeth.

In the second study, there was no statistically significant difference in the flexural strength of the specimens printed by 3d printing angle (0, 30, 90 angle) of 3d printing temporary crown resin.

In the case of temporary crown resin, chemical bonds appear through photo-curing, so the physical strength does not seem to change depending on the 3d printing additive angle.

4. Conclusion

In the first study, the accuracy of a digital dental model using dental CBCT is still unreasonable to fabricate a dental prosthesis due to surface distortion, but it is believed that it will be possible if the resolution is improved.

In the second study, since there is no significant difference in the strength of 3d printing temporary crown resin according to the stacking angle, it is desirable to manufacture a dental prosthesis by setting the condition with the highest accuracy according to the 3d printing operator.

acknowledgement

The research was supported by a grant(20171MFDS346) from Ministry of Food and Drug Safety in 2020.

References

- [1] Kang SY, Park JH, Kim JH, Kim WC. Three-dimensional trueness analysis of ceramic crowns fabricated using a chairside computer-aided design/manufacturing system: An in vitro study. J Prosthodont Res 2020;64:152-158.
- [2] Na JY, Cha JY, woo CW, Kim YH, Lee JH, Hwang JJ, Jeong HG, Han SS. Comparative Accuracy of STL Conversion Digital Model of DICOM Files according to CBCT Scanning Protocol. J Korean Acad Adv Gene Dent, 2017- 6: 1-7.
- [3] Kim MS, Kim WG, Kang W, Evaluation of the accuracy of provisional restorative resins fabricated using dental 3d printer. J Korean Soc Dent Hyg. 2019.19:1089-97
- [4] Kang SY, Park JH, Kim JH, Kim WC. Accuracy of provisional crowns made using stereolithography apparatus and subtractive technique. J Adv Prosthodont 2018-10:354-60.

Performance Test Methods of Dental Materials (Magnetic Attachment, Dental Ceramic) Reflecting Latest International Standards

Ji-Min Yu^{*}, Seen-Young Kang, Jun-Seok Lee, Jae-Won Lee, Ho-Sang Jung, Seung-Youl Lee[†]

Medical Device Research Division, National Institute of Food and Drug Safety Evaluation,
Chungcheong buk-do, Cheongju-si 28159, Korea

This study is about the evaluation of the mechanical properties of the prosthesis used when a removable denture needs to be restored due to partial loss of teeth. If the tooth is partially lost and the tooth is restored using dentures, a device called a dental attachment is used. The attachment helps the removable dentures to be placed in a stable state without being separated from the gums when chewing food. When the removable local denture is not properly placed, not only functionalities such as mastication, but also aesthetics and pronunciation problems etc., cause considerable discomfort during use. There are various types of dental attachments, such as stud type, bar type, and magnetic type. Among these, magnetic attachments are actively used for advantages such as reducing lateral pressure applied to an implant by using the force of magnetic force, convenient attachment and detachment of dentures, and excellent vertical holding power. The retaining force of the upper and lower magnetic forces has a great influence on the attachment and detachment of the dentures. This study is about the holding power performance test of magnetic attachment. What is a magnetic attachment, the magnetic assembly with a built-in magnet is attached to the denture, and the keeper of the metal plate is embedded in the tooth, and the denture is fixed to the root of the tooth using the suction force acting on both the magnet structure and the keeper [1]. The method for testing the holding power of the magnetic attachment complies with ISO 13017. After attaching the magnetic attachment assembly and the keeper to the upper and lower portions of the mechanical property tester equipped with a low friction ball bearing slider jig, respectively, a cross head speed of 2 mm/min is applied. The retentive force is measured by applying a load until the upper magnetic assembly and the lower keeper are completely separated. The retentive force test of ISO 13017 was recently revised in 2020 after the standard was established in 2012. The crosshead speed of the retentive force test was changed from 5mm/min to 2mm/min, and an analysis method for the retentive force graph curve was added.

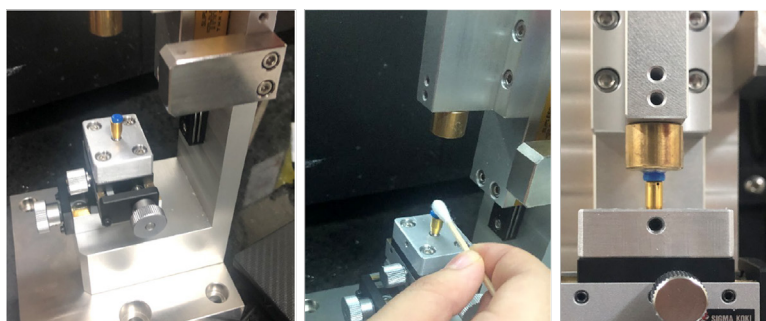


Fig. 1 Fixing of specimen for retentive force test of magnetic attachment

Dental ceramic, which is a material for tooth-shaped prostheses used in removable dentures, is very promising due to its mechanical strength comparable to metals and excellent esthetics [2]. Reflecting the changes in the international standard revised in 2015, the mechanical properties of dental ceramics made of zirconia according to firing condition were studied. For mechanical

properties, a three-point bending strength test was performed, and the effect of the firing time on the strength was analyzed. As the firing conditions, a comparative experiment was conducted by 3 groups such as 3hr 57min, 6hr 28min, and 10hr 51min at 1530 ° C. (n=15). The flexural strength test was performed in a universal testing machine (crosshead speed 1mm/min). The experimental results were 771 MPa in group 1, 796 MPa in group 2, and 753 MPa in group 3. All three groups showed similar strength, but it was the best at 6hr 28min, and the mechanical strength of zirconia ceramic was found to be affected by the firing time. By reflecting the newly revised international standard test method, performance evaluation on the mechanical properties of removable dentures was conducted to keep pace with the latest research trends.

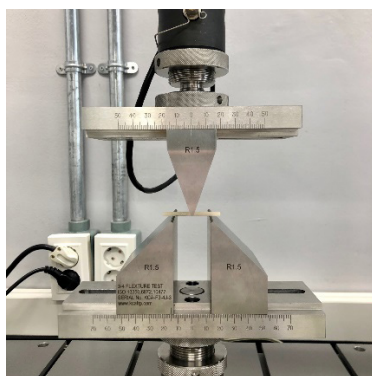


Fig. 2 3-point bending strength test of zirconia material ceramic

Acknowledgements

The research was supported by a grant (18171MFDS301, 20171MFDS346) from Ministry of Food and Drug Safety in 2018, 2020.

References

- [1] M. Hasegawa, Y. Umekawa, E. Nagai, T. Ishigami, Retentive force and magnetic flux leakage of magnetic attachment in various keeper and magnetic assembly combinations, *J Prosthet Dent* 2011;105:266-271.
- [2] M. Kelch, J. Schulz, D. Edelhoff, B. Sener, B. Stawarczyk, Impact of different pretreatments and aging procedures on the flexural strength and phase structure of zirconia ceramics, *Dent Mater*, 35 (2019), pp. 1439-1449.

A Preliminary Experimental Study of Positioning System Using Multiple Radiation Spectroscopy Detectors

Seung-Jae Lee^{1*}, Cheol-Ha Baek^{2†}

¹Department of Radiological Science, Dongseo University, Korea

²Department of Radiological Science, Kangwon National University, Korea

In order to detect a radiation source, a system using a position measurement method was constructed using a radiation spectroscopy detector. It is a method that can measure a two-dimensional position by using three detectors. For this, a basic system was constructed using three scintillators and three optical sensors. The actual location of the radiation source and the radiation emitted from each location were measured, and the error between the location calculated through the radiation location measurement algorithm was evaluated. A picture with coordinates was used to specify the exact location of the radiation source, and the location of the radiation source was calculated using the radiation coefficient measured at each location. As a result of the error measurement, the error was 2.23% at the X position, 3.26% at the Y position, and an average of 2.75%. This basic experiment is expected to play a role as basic data for many system configurations in developing a system that can quickly detect a radiation source without using a collimator when a system is constructed using a radiation spectroscopy detector.

Research on Polar Anisotropic Molding Yoke Shape to Reduce Dead Zone of Ring Type Bond Magnets

Jeong–Yeon Min*, Dong–Woo Nam, Hyun–Jo Pyo, Min–Jae Jeong, Seo–Hee Yang, Won–Ho Kim

Department of Electrical Engineering, Gachon University, Korea

Introduction

Recently, as the demand for robots and the supply ratio of renewable energy have increased, the usage of electric motors and generators has increased. Therefore, sensors required for detecting the position of the rotor has also increased. Of these, the safety window motor for preventing accidents in which an automobile window is pinched is based on the principle that a ring type bond magnet is attached to the lower part of the rotor of the motor to detect the magnetic flux and detect the position. At this time, a dead zone, which is a section where the magnetic flux is very weak, is generated between the N pole and the S pole of the ring-type bond magnet and the hall sensor does not detect the magnetic flux in this section. When the range of this dead zone is large, the region where the magnetic flux can be detected is limited, so that accurate position detection is impossible. In this paper, we provide the optimum model of a polar anisotropic molding yoke with a magnetic flux-concentrated structure for the dead zone reduction plan of ring type bond magnets for accurate control of electric motors and generators [1].

Equation

In order to concentrate the magnetic flux generated from the permanent magnet of the molding yoke, a structure having a high magnetic flux concentration factor is required. And it can be expressed by the following equation (1).

$$C_{\phi} = \frac{A_m}{A_g} \quad (1)$$

A_m is the cross-sectional area of the magnet, and A_g is the cross-sectional area of the air gap. This indicates that the more magnetic flux passing through the magnet than the air gap, the more the magnetic flux is concentrated. Therefore, if the magnetic flux-concentrated structure is used, when a magnetic field is applied, the air gap flux density can be higher than that of the conventional model,

Analysis & Result

In the case of the conventional model, the structure is such that a magnetic field is directly applied to a very different ring type bond magnet with a permanent magnet. Therefore, the magnetic flux does not penetrate deeply into the magnet, and a large Dead Zone is generated. To reduce this dead zone, this paper designed a model that could be molded with a high air gap flux density by inserting a magnetic flux concentration core. As shown in Fig. 1, the thickness of the inner and outer teeth and the direction of the magnetic field applied to the permanent magnet were used as the design variable. In this paper, the results were analyzed through finite element analysis. The design variable of inner and outer teeth thickness was set range of 0mm to 12mm and the angle degree of the magnetic field applied to the permanent magnet was set the range of 0° to 90°.

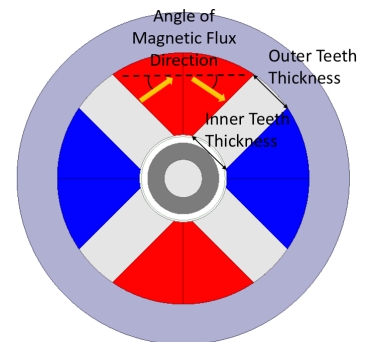
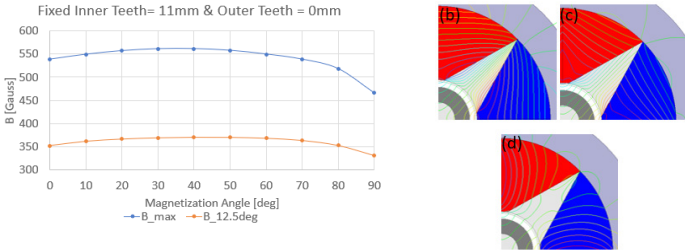


Figure 1: Variable Setting

and the dead zone of the ring type bond magnet can be reduced.

A. Air gap flux density according to magnetization angle

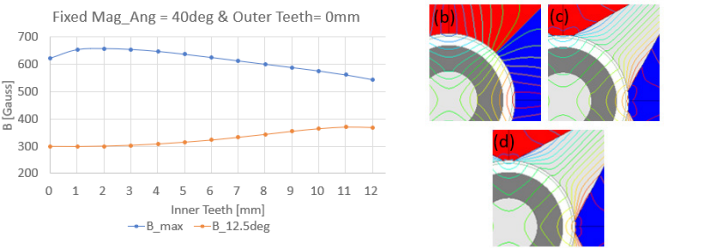


(a) Air gap flux density according to magnetization direction

(b) 0° (c) 40° (d) 90°

Figure 2 : Air Gap Flux Density according to Magnetization Angle

B. Air gap flux density according to the thickness of the inner teeth

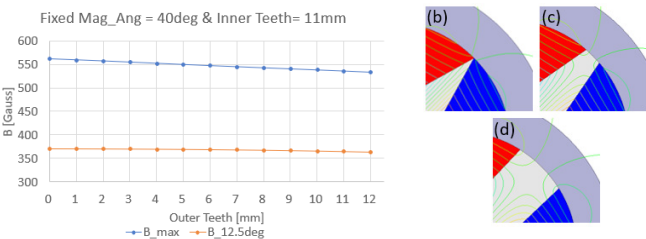


(a) Air gap flux density according to inner teeth

(b)0mm (c)11mm (d)12mm

Figure 3 : Air Gap Flux Density according to Inner Teeth Thickness

C. Air gap flux density according to the thickness of the outer teeth



(a) Air gap flux density according to outer teeth

(b)0mm (c)4mm (d)12mm

Figure 4 : Air Gap Flux Density according to Outer Teeth Thickness

Fig. 2 shows the change in air gap flux density according to the magnetization direction when the inner teeth thickness is 11mm and the outer teeth thickness is 0mm. Analyzing this result, when the angle of the magnetization direction is too large or too small, the magnetic flux leaks to the permanent magnet and the outside. So it can be confirmed that the maximum air gap flux density is generated around 40° .

Fig. 3 shows the change in air gap flux density according to the thickness of the inner teeth when the angle of the magnetization direction is 40° and the thickness of the outer teeth is 0mm. Analyzing the results at 12.5° where the dead zone occurs in a ring type bond magnet, the magnetic flux leaks to the adjacent core when the thickness of the inner teeth is too large. So it can be confirmed that the magnetic flux is most concentrated on the pole of the ring type bond magnet when the thickness of the inner teeth is 11mm.

Fig. 4 shows the change in air gap flux density according to the thickness of the outer teeth when the angle of the magnetization direction is 40° and the thickness of the inner teeth is 11mm. Analyzing the result, it is confirmed that when the thickness of the outer teeth is 0mm, the magnetic flux leaked to the outside is minimized and the maximum air gap flux density is generated.

Fig. 5 is the optimum model that can be molded to the highest air gap flux density.

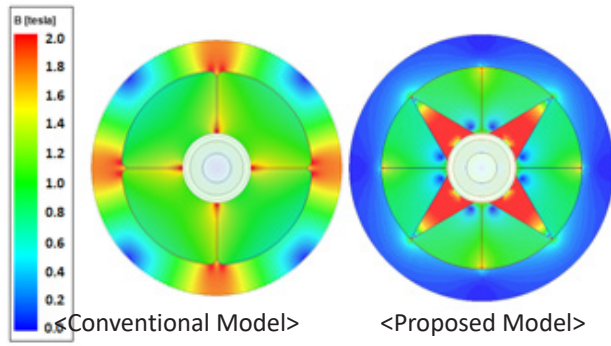


Figure 5 : Air Gap Flux Density of Conventional & Proposed Model

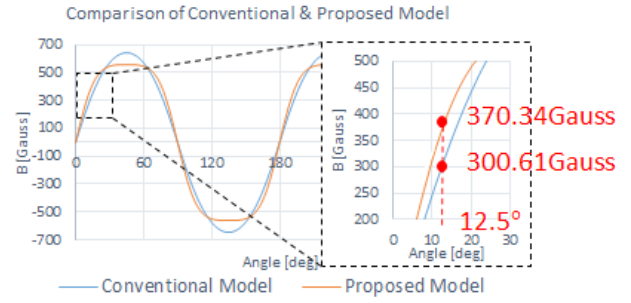


Figure 6 : Waveform Comparison of Conventional & Proposed Model

Fig. 6 is a comparison waveform of the air gap flux density of the proposed model and the conventional model. The proposed model has a 23% increase in air gap flux density compared to the conventional model. As a result, dead zone decreased by about 22%.

Conclusion

In this paper, a flux-concentrated core was inserted to reduce the dead zone range of the ring type bond magnet. As a result, it is possible to reach a higher air gap flux density than the conventional model. Finally, the validity of this paper was verified through the finite element analysis method. Based on this, it is expected that the market share of the safety window can be expanded, and further, the technological competitiveness of domestic sensor industries can be improved.

Acknowledgment

This work was supported by the National Research Foundation of Korea(NRF) grant funded by the Korea government(MSIT). (No. 2020R1A2C1013724) NRF - 2020R1A2C1013724

References

- [1] H. J. Kim et al, IEEE Trans. Magn., vol. 46, no. 6, pp. 2314-2317, Jun. 2010

Test Environment Construction of ITF in BLDC motor

Dong-yeol Lee^{1*}, Dong-Hwan Kim², Jong-Hwan Cho³, Sung-Gu Lee⁴, Dong-Woo Kang¹

¹Department of Electrical Energy Engineering, Keimyung University, Daegu 42601, South Korea

²STAR GROUP IND. Co., LTD, Daegu 42714, South Korea

³Valeo Pyeong Hwa co, LTD, Daegu 42921, South Korea

⁴Department of Electrical Engineering, Dong-A University, Busan 49315, South Korea

BLDC motors are widely used in electric vehicle systems such as actuators, traction motors, and steering motors due to their high power density and efficiency. PM BLDC motors have an armature winding wound around a stator and a permanent magnet attached to the rotor. Rotating force is generated by the interaction between the magnetic flux of the armature and the magnetic flux of the rotor by the armature current. The stator winding is a structure coated with an insulating material to prevent short circuits between windings. However, there are cases in which the insulation is destroyed due to voltage and current stress of the winding, driving temperature, vibration, and the like. In this case, a closed circuit is formed between adjacent windings, which is called ITF. When ITF occurs, a circulating current flows in the closed circuit, which causes the efficiency of the motor to decrease and the temperature to rise. In addition, heat is generated in proportion to the square of the circulating current, destroying the insulating material of the adjacent winding and spreading the fault at a high speed. Therefore, researches such as ITF characteristic analysis and fault diagnosis are actively in progress. However, further research is needed for research on establishing a test environment for research. Therefore, in this paper, we model and simulate the insulation breakdown of the stator winding of a SPM (Surface permanent magnet) type BLDC motor.

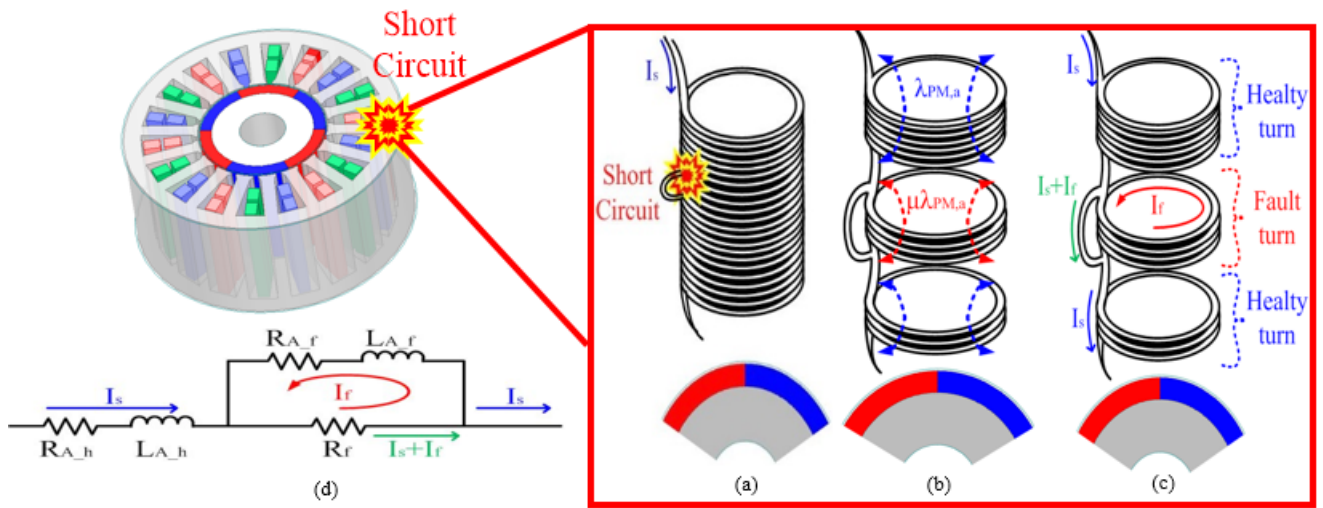


Fig. 1. Schematic drawing of the ITF winding. (a) ITF occurred, (b) Linkage flux when ITF occurred, (c) Current when ITF occurred (d) Equivalent circuit

LC공진을 이용한 OFG센서의 감도 향상

김경원*, 신광호†

경성대학교 정보통신공학과

센서는 A.I, 빅데이터와 더불어 4차 산업혁명의 핵심산업으로 주목받고 있다. 센서 중 한 종류인 자기 센서는 스마트폰, 자동차, 가전, 항공우주 등 여러 분야에서 사용되고 있고, 사용처가 계속 늘어남에 따라 고속성장 할 것으로 예측되는 고성장 산업 중 하나이다. 이러한 자기 센서의 종류 중 하나인 직교 플럭스게이트 센서는 센서의 입력전류를 연자성 코어에 직접 인가하는 것이 주요 특징이다. 직교 플럭스게이트 센서는 연자성체로 이루어진 코어와 코어를 둘러싼 솔레노이드 형태의 검출 코일로 구성되며, 외부자기장의 인가 시 센서 출력이 외부자기장에 의존하는 패러데이 법칙에 의해 출력이 결정된다. 이러한 센서의 형태는 검출 코일 측에서 바라보았을 때 솔레노이드 인덕터와 유사한 구조를 띄고 있으며 이는 회로 이론을 통해 적절한 공진주파수를 선정하고 LC공진을 통해 센서의 감도를 추가로 올릴 수 있다는 것을 의미한다. 왜냐하면 공진주파수는 임피던스의 허수부, 즉 리액턴스가 최소가 되는 주파수이며 외부 캐패시터를 추가로 연결했을 때 리액턴스는 외부 캐패시터의 리액턴스로 인해 달라지게 된다. 그로인해 공진주파수도 바뀌므로 이를 이용해 공진주파수를 선정할 수 있다. 그리고 공진 시에는 검출코일의 임피던스 또한 최소가 되어 동일신호대비 더 큰 전압이 검출되기 때문에 감도의 향상도 이루어지게 된다. 따라서 본 연구에서는 OFG센서의 LC공진에 의한 센서 구동주파수 조정 및 감도 향상에 대한 실험 결과를 보고한다.

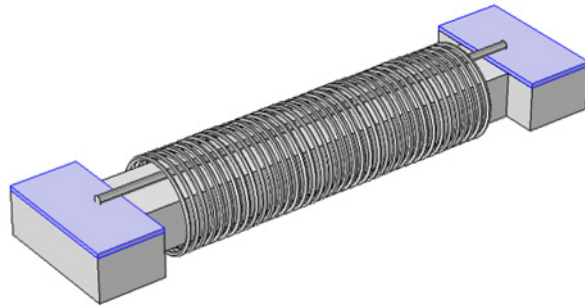


Fig 1. The structure of orthogonal fluxgate sensor

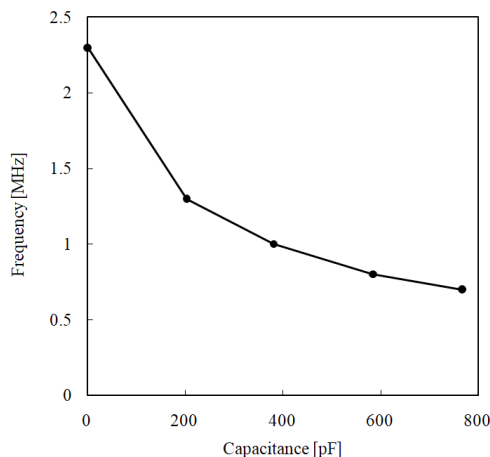


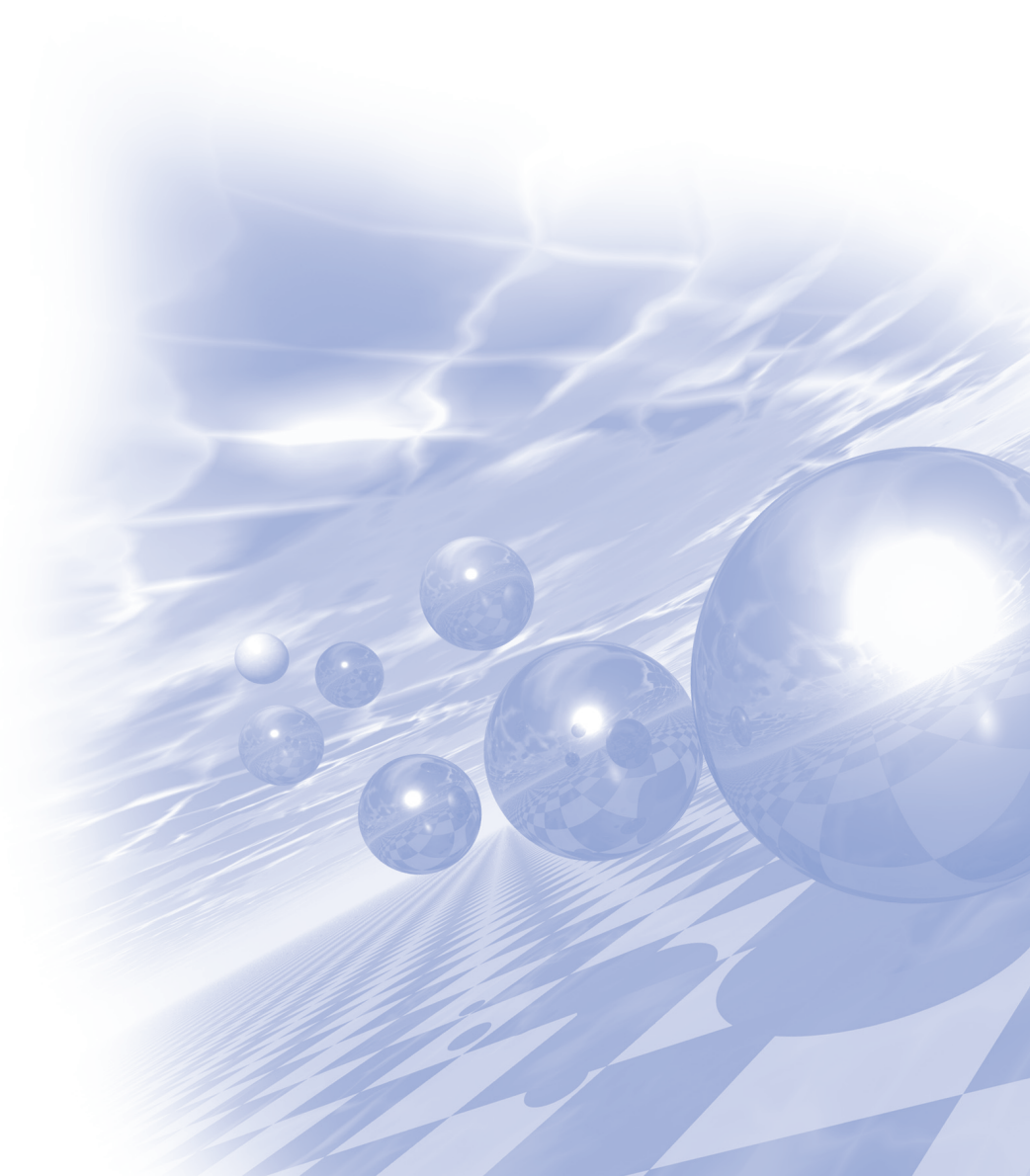
Fig 2. Resonance frequency dependence external capacitor



KMS 2020 Winter Conference

Special Session II

‘산화물 자성체 세션’



Giant topological Hall response induced by spin chirality fluctuation in a ultraclean frustrated antiferromagnet

Jun Sung Kim^{*}

Center for Artificial Low Dimensional Electronic Systems, Institute for Basic Science (IBS), Pohang 37673, Korea
Department of Physics, Pohang University of Science and Technology (POSTECH), Pohang 37673, Korea

Quantum nature of electrons' wave-functions manifests itself as Berry phase and emergent magnetic fields when coupled to various types of chiral spin textures in itinerant magnets. This spin Berry phase effect mainly works with a static spin order, which limits the magnitude of the resulting topological Hall conductivity (THC) close to quantum conductance e^2/h , and the effective temperature range below the magnetic transition. Here taking a ultraclean triangular antiferromagnet PdCrO_2 as a model system, we show that a giant Hall response can be induced with a THC much larger than e^2/h and maintained far above the Neel temperature up to $\sim 5 T_N$. This drastic enhancement of THC above T_N is attributed to the skew scattering of highly mobile Pd electrons to fluctuating but locally-correlated Cr spins with a finite spin chirality. Our findings highlight the chirality fluctuations as an effective source for topological Hall response in ultraclean itinerant magnets.

First-principles study of magnetic van der Waals materials: from CrI_3 and Fe_3GeTe_2 to VSe_2 and VTe_2

Myung Joon Han^{*}

Department of Physics, KAIST, Daejeon, Korea

Magnetism in 2-dimensional van der Waals materials attracts lots of research attention, and simultaneously, poses a challenge to the capability of our state-of-the-art measurement/simulation techniques. Here in this talk, I will try to present a brief overview of how first-principles-based theoretical methods can elucidate this intriguing material class when the experimental information is limited. By combining several different levels of approximations with the advanced magnetic force response theory, we try to understand the van der Waals superexchange (or, ‘super-super’ exchange), the role of defects, and other magnetic properties. The materials that we previously studied include Mott insulating CrI_3 [1], metallic Fe_3GeTe_2 [2], and two different transition-metal dichalcogenides [3, 4]. I will also try to outline the remaining open problems.

References

- [1] S. W. Jang et al., Phys. Rev. Mater. 3 031001 (R) (2019).
- [2] S. W. Jang et al., Nanoscale 12 13510 (2020).
- [3] T. J. Kim et al., 2D Materials 5 035023 (2020).
- [4] D. Won, D. H. Kiem et al., Adv. Mater 32 1906578 (2020).

Terahertz Spectroscopy of Magnons in HoFeO₃ and Detection of Rabi Splitting

Howon Lee, Kyung Ik Sim, Hyunjun Shin, Y. J. Choi, Jae Hoon Kim*

Department of Physics, Yonsei University, 50 Yonsei-Ro, Seoul 03722 Republic of Korea

Orthorhombic HoFeO₃ single crystals were studied via terahertz time-domain spectroscopy (THz-TDS) in the spectral range of 3-100 cm⁻¹ at 1.5 K under a magnetic field up to 7 Tesla. Three different classes of excitations were found: quasi-ferromagnetic resonance (qFMR) modes, quasi-antiferromagnetic resonance (qAFMR) modes, and the rare-earth (R) modes. The latter is due to an electron paramagnetic resonance (EPR) transition between the two states belonging to the ground quasi-doublet of Ho³⁺ ions further split by the crystal field and the Fe³⁺ exchange field. A strong interaction between the resonance modes and the R modes lead to a hybridization, which yields a Rabi splitting between the magnon-like branch and the EPR-like branch. Thus, HoFeO₃ can serve as a model solid-state system to study matter-field interactions in a cavity QED (quantum electrodynamics) setting, which traditionally focused on atom-photon interactions in the context of the Jaynes-Cummings model (JCM).

Random singlets in quantum magnets with frustration and disorder

Kwang-Yong Choi*

Department of Physics, Chung-Ang University, Korea

Conventional wisdom says that quenched disorders in magnetic insulators often lead to spin freezing or spin glass. Recently, however, exchange randomness has been proposed as an alternative to quantum-spin-liquid (QSL)-like states such as valence-bond glass and random-singlet states. Counterintuitively, quenched randomness seems to promote competing magnetic interactions and quantum fluctuations as long as a certain degree of disorder and frustration is present irrespective of their spatial dimensionality, type of exchange interactions (Heisenberg and Kiteev), and lattice geometry (triangular, Kagome, honeycomb, and square lattice).

Random singlets entail quasi-universal characteristics: quantum scalings of thermodynamic quantities, a T-linear dependence of magnetic specific heat in the strong disorder limit, and spinonlike behavior of orphan spins. However, little is known about the nature of this gapless QSL-like state. The related question is whether such a state is a simple quantum paramagnet or a disorder-driven QSL entailing many-body entanglement.

In this talk, I will briefly review recent theoretical and experimental progress in the research of random singlets and then present our activities. First, we will address this issue in the diluted Kitaev candidate material α - $\text{Ru}_{1-x}\text{Ir}_x\text{Cl}_3$ ($x \approx 0.2$). Combined thermodynamic and spectroscopic studies unveil that α - $\text{Ru}_{1-x}\text{Ir}_x\text{Cl}_3$ is a proximate realization of a bond-disordered Kitaev model harboring randomly hopping Majorana fermions. Second, we will discuss the $s=1/2$ J_1 - J_2 square-lattice Heisenberg antiferromagnets $\text{Sr}_2\text{Cu}(\text{Te}_{1-x}\text{W}_x)\text{O}_6$ ($x = 0.05 - 0.1$). The random Te-for-W substitution generates exchange randomness, thereby leading to a suppression of the Néel order. Our magnetic resonance and thermodynamic data show many of QSL phenomenology with some indication of a random-singlet state. Third, we will address the three-dimensional frustrated magnet $\text{Re}_3\text{Sb}_3\text{Mn}_2\text{O}_{14}$ (Re = La, Lu), where the Mn^{2+} magnetic ions ($S=5/2$) constitute a rhombohedral lattice. The thermodynamic quantities display quantum scalings and the magnetic resonance data show a dynamically fluctuating state down to 20 mK. All these results are consistent with a random-singlet picture.

An intermediate magnetic phase of a proximate Kitaev system in in-plane magnetic fields

Beom Hyun Kim^{1*}, Shigetoshi Sota², Tomonori Shirakawa², Seiji Yunoki^{2,3,4}, Young-Woo Son¹

¹Korea Institute for Advanced Study, Seoul 02455, South Korea

²Computational Materials Science Research Team,
RIKEN Center for Computational Science (R-CCS), Kobe, Hyogo 650-0047, Japan

³Computational Condensed Matter Physics Laboratory,
RIKEN Cluster for Pioneering Research (CPR), Saitama 351-0198, Japan

⁴Computational Quantum Matter Research Team, RIKEN,
Center for Emergent Matter Science (CEMS), Wako, Saitama 351-0198, Japan

α -RuCl₃ is an antiferromagnetic insulator with a zigzag long order. Observed magnetic continuum excitation and

fractionalized magnetic entropy have supported that it is proximate to the Kitaev system which can host the quantum spin liquid (QSL) interpreted with free Majorana fermions in a static Z_2 gauge field. The zigzag order can be suppressed and an intermediate phase (IP), possibly QSL, can emerge in between the zigzag spin order and the spin polarized order when an external magnetic field is applied. A few theories have attempted to explain the origin of IP in the presence of magnetic field. However, they have failed to show the IP in in-plane fields observed by some experiments. In this study, we introduce the simplest but essential quantum spin model with a ferromagnetic nearest neighboring (NN) Kitaev interaction and antiferromagnetic third NN Heisenberg interaction (K-J₃ model). Employing both exact diagonalization and density matrix renormalization group methods, we demonstrate that the model shows the magnetic phase transition from the zigzag order phase to the spin polarized phase through an IP in both cases when an in-plane magnetic field is applied perpendicular to the NN bond direction and when an out-of-plane field is applied, in good agreement with experimental observations. Furthermore, we verify that additional symmetric off-diagonal Γ interaction and ferromagnetic Heisenberg interaction between NN spins can both suppress the IP in in-plane fields.

Identification of a Kitaev Quantum Spin Liquid by Magnetic Field Angle Dependence

Kyusung Hwang^{1*}, Ara Go^{2,3}, Ji Heon Seong⁴, Takasada Shibauchi⁵, Eun-Gook Moon⁴

¹School of Physics, Korea Institute for Advanced Study, Seoul 02455, Korea

²Center for Theoretical Physics of Complex Systems, Institute for Basic Science, Daejeon 34126, Korea

³Department of Physics, Chonnam National University, Gwangju 61186, Korea

⁴Department of Physics, Korea Advanced Institute of Science and Technology, Daejeon 34141, Korea

⁵Department of Advanced Materials Science, University of Tokyo, Kashiwa, Chiba 277-8561, Japan

We argue that a non-abelian quantum spin liquid may be detected by magnetic field angle dependence of physical observables. A spin model with the Kitaev, Heisenberg, and off-diagonal symmetric terms on a honeycomb lattice is analyzed by using exact diagonalization, spin-wave theory, and parton mean-field theory. Characteristic field angle dependence of a non-abelian Kitaev quantum spin liquid is uncovered. The angle dependence is strikingly sensitive to the off-diagonal symmetric terms in drastic contrast to its insensitivity to the Heisenberg term. We further demonstrate the existence of critical lines on a plane of magnetic field direction, associated with topological natures of a non-abelian quantum spin liquid. Thus, we propose that the angle dependence may be used to identify a non-abelian Kitaev quantum spin liquid and discuss its smoking-gun signatures which are applicable to candidate materials such as α -RuCl₃.

Describing the magnetic structure and origin of band gap on $\text{Ba}_2\text{CuOsO}_6$ system; density functional theory approach

Changhoon Lee, Ji Hoon Shim

Max Planck POSTECH Center for Complex Phase of Materials, Pohang 790-784, Korea
Department of Chemistry, Pohang University of Science and Technology, Pohang 790-784, Korea

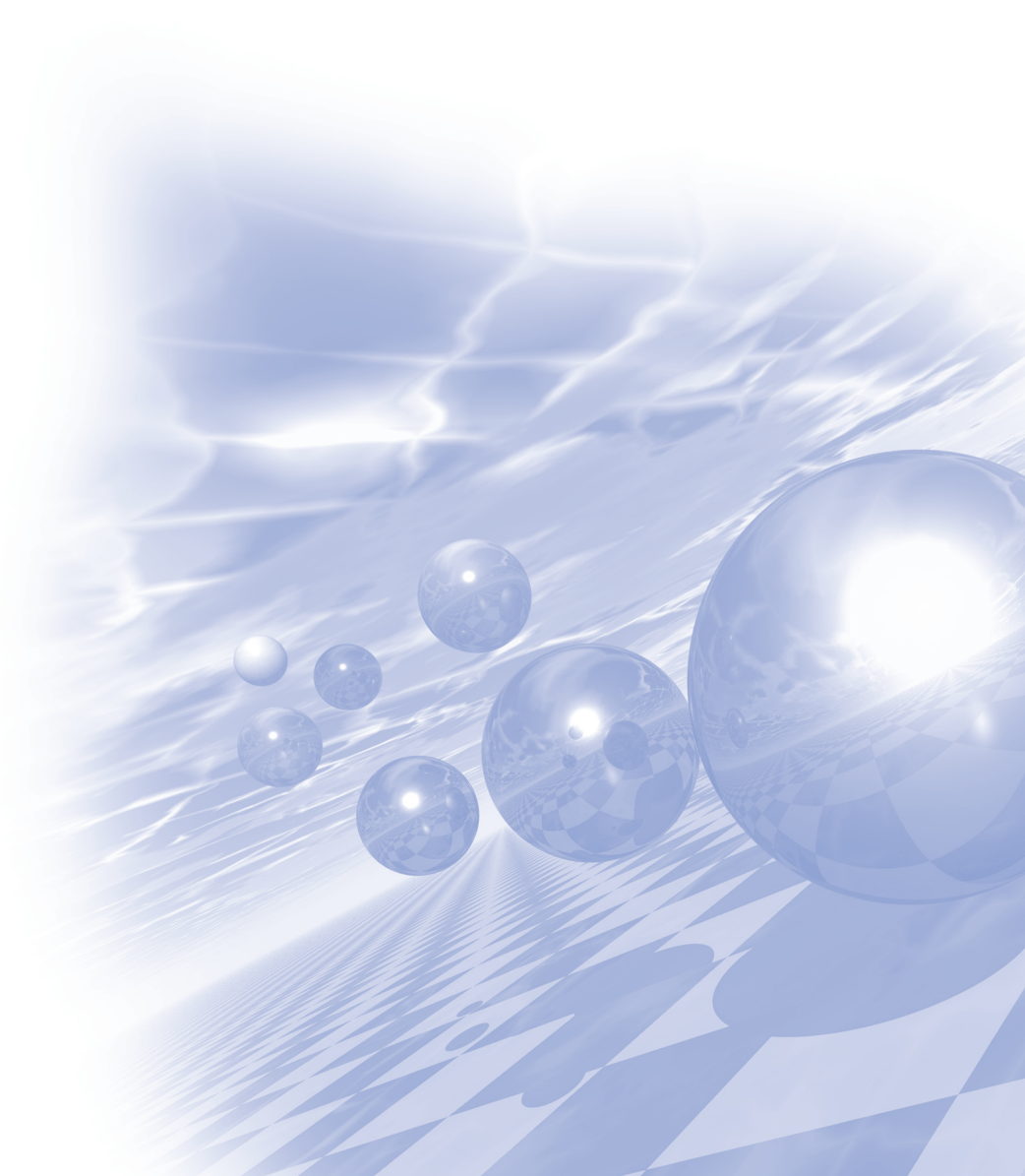
We examine the magnetic structure and origin of band gap opening for $\text{Ba}_2\text{CuOsO}_6$ by extracting spin exchange interaction and by adopting spin-orbit coupling effect. The ordered double-perovskites $\text{Ba}_2\text{CuOsO}_6$ which consist of 3d and 5d transition-metal magnetic ions (Cu^{2+} and Os^{6+} , respectively) is magnetic insulators; the magnetic susceptibilities of $\text{Ba}_2\text{CuOsO}_6$ obey the Curie-Weiss law with dominant antiferromagnetic interactions and the estimated Weiss temperature is -13.3 K. Solid-state osmium oxides can exhibit a variety of magnetic and electronic phenomena associated with their electron correlation. There are two important issues on solid-state osmium oxides; one is origin of band gap inducing metal to insulator transition. Other one is variety of oxidation state of Os ion. This wide spectrum of oxidation state of Os atom on osmium compounds is directly attributable to a large a spatial extension of Os 5d orbital. From the results of density functional study, the spin exchange interaction between Cu atoms is mainly responsible for antiferromagnetic ordering on $\text{Ba}_2\text{CuOsO}_6$ system. To describe the magnetic insulating states of $\text{Ba}_2\text{CuOsO}_6$, it is necessary adopting an electron correlation effect as well as spin-orbit coupling effect.



KMS 2020 Winter Conference

Oral Session I

‘자기이론 및 의공학, 대학원생 세션’



The Study of Planar Hall Effect in CoFeB/MgO with various Metals under Layer Structure

Mingu Kim^{1*}, Chang-Jin Yun¹, Jiho Kim¹, Kungwon Rhie^{1,2}

¹Department of Applied Physics, Korea University, Sejong, 30019, Korea

²Department of Display and Semiconductor Physics, Korea University, Sejong, 30019, Korea

The heavy metal/CoFeB/MgO is well known perpendicular magnetic anisotropy (PMA) thin film structure. The structure of samples were Ta(2)/Pt(5)/CoFeB(0.8)/MgO(3)/Ta(2), Ta(2)/W(5)/CoFeB(0.8)/MgO(1)/Ta(2) and Ta(5)/CoFeB(0.8)/MgO(2)/Ta(2) with thickness in nm. The thin films were deposited on Si substrate by magnetron sputtering system. After sputtering, Ta/W/CoFeB/MgO/Ta and Ta/CoFeB/MgO/Ta were annealed at 300 °C for 30 min. Meanwhile Ta/Pt/CoFeB/MgO/Ta samples were annealed at 450 °C for 30min.

The φ is the angle between in-plane magnetic field and injected current to samples. The measurement of anomalous Hall effect (AHE) was done rotating φ from 0° to 360°. The Hall resistance we obtained is explained by the contribution of AHE and the planar Hall effect (PHE). Since the PHE is dependent of φ , the PHE can be described as function of $\sin 2\varphi$. Thus, the Hall resistance is contributed only AHE when the $\varphi = 0^\circ$.

The PHE of W under layer samples exhibits larger magnitude than those of Ta or Pt under layer samples. The difference of PHE between W and the other samples shows that PHE is changed by heavy metal under the CoFeB layer.

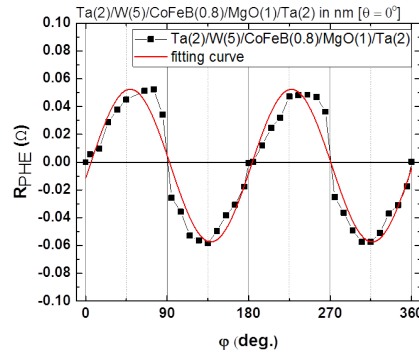


Fig. 1. Planar Hall resistance (R_{PHE}) measured in Ta(2)/W(5)/CoFeB(0.8)/MgO(1)/Ta(2) sample using rotating in-plane magnetic field.

기계학습과 인공지능 기법을 이용한 펄스와전류 신호해석

김재민^{*1, 3}, 신정우², 서호건¹, 김경모¹, 박덕근^{1,2}

¹한국 원자력 연구원, 덕진동 유성 34057, 대전

²주식회사 AIPIT, 덕진동 유성 34057, 대전

³신형원자력시스템공학과, 과학기술연합대학원대학교, 217 가정로, 대전

본 연구에서 다루고자 하는 펄스 와전류를 이용한 비파괴 검사는 도체에 전류를 펄스 형태로 가할때 생기는 와전류의 변화량을 통해 검사 대상을 분석하는 방법이다. 펄스 와전류 비파괴 검사는 배관 외부 보온재 피복 제거 없이 내부 결함 검사를 가능하게 하나 비접촉식 비파괴 검사이기에 정확도 개선을 위해서 많은 연구가 필요하다. 실험 장비로 아이피트 사가 개발한 펄스 와전류 방출 및 측정 장치를 이용하였으며, 이 측정 장비를 통해 내부에 계단 모양의 두께 차이가 있도록 제작된 배관 형태의 시험편을 측정하였다. 시험편의 재료인 합금 제조 공정 특성상 재료의 불균일성 때문에 생긴 측정 오차 탓에 동일한 두께에서도 측정치에 오차가 발생하였으며, 두께 차이로 인한 측정치의 변화량을 재료의 불균일성 때문에 생긴 측정치의 차이와 그 외 요인으로 생긴 오차와 구분하기 어려워 통계적 신호 처리 방법으로는 실험 결과를 분석하기 어려웠다. 펄스 와전류 비파괴 검사의 개선을 위해서는 측정 결과의 변화 요인중 시험편의 두께 차이 때문에 생긴 변화량만을 추출해 낼 필요가 있으며, 이를 위해 기계학습 기법인 Support Vector Machine (SVM) 과 딥러닝 기법중 CNN 기법을 적용하였다. SVM을 통해 두께에 따른 측정치 변화량을 구분해 낼 수 있었으나 측정치의 편차가 작은 시험편의 얇은 곳에서 정확도가 낮아졌다. CNN을 이용한 딥러닝 알고리즘은 SVM 이 구분에 어려움을 겪은 구간에서도 작동하는 결과를 보여주었다.

Unidirectional Transport of Magnetic Skyrmion through Symmetry-Breaking of Potential Energy Barriers

Dae-Han Jung^{1*}, Hee-Sung Han¹, Namkyu Kim¹, Ganghwi Kim¹, Suyeong Jeong¹,
Sooseok Lee¹, Myeonghwan Kang¹, Mi-Young Im², Ki-Suk Lee^{1*}

¹School of Materials Science and Engineering, Ulsan National Institute of Science and Technology, Ulsan 44919, Republic of Korea.

²Center for X-ray Optics, Lawrence Berkeley National Laboratory, Berkeley, CA 94720, USA.

Magnetic skyrmions, topologically protected chiral spin textures, are envisioned as the promising information bit carriers due to their particle-like nature with topological stability, high mobility, and small size [1-3]. Here, the unidirectional control of skyrmion transport is a crucial prerequisite for developing skyrmion-based spintronic devices. We show that, by means of symmetry-breaking of potential energy for a confined skyrmion within an asymmetric geometry, the current-driven motion of a skyrmion can be manipulated in a preferred direction. We develop the method makes use of an equipotential path and the location of the saddle point, which is time-efficiently applicable to know the final state of the transition in situations where the conventional equation of skyrmion motions are too costly or too tedious to evaluate it. From the method, we identified the underlying mechanism that the directionality of the potential energy barrier perpendicular to the external driving force plays a crucial role in the unidirectional control of skyrmion motions. These findings have important implications for an efficient way to design skyrmion-based logic devices such as a diode or a transistor element.

References

- [1] N. S. Kiselev, A. Bogdanov, R. Schäfer, and U. K. Rößler, *J. Phys. D* 44, 392001 (2011).
- [2] A. Fert, V. Cros, and J. Sampaio, *Nat. Nanotechnol.* 8, 152 (2013).
- [3] N. Nagaosa and Y. Tokura, *Nat. Nanotechnol.* 8, 899-911 (2013).

Skyrmion calculator based on boundary annihilation

Moojune Song^{*}, San Ko, Sung Kyu Jang, Min Gyu Park, Kab-Jin Kim^{a)}

Department of Physics, Korea Advanced Institute of Science and Technology, Daejeon 34141, Republic of Korea
^{a)}kabjin@kaist.ac.kr

Magnetic skyrmion has been receiving huge attention as an information carrier for next-generation memory/computing devices, because of its small size, fast speed, low-current motion, and especially the topological protection [1]. In that respect, many ideas to realize the skyrmion-based devices have been proposed in the belief that the skyrmion is robust. However, during a decade, the mass of experiments showed that the topological protection of skyrmion is debatable in a real system, but rather the skyrmion can easily be annihilated at the film edge. The skyrmion annihilation (SA), in respect of the data preservation of a memory device, was regarded as a detrimental phenomenon, and therefore the majority of researches devoted to avoid it. On the contrary, here we report that the SA can be used in a positive way, developing a new functionality of skyrmion logic device named as a skyrmion calculator. Previously proposed skyrmion logic gates [2, 3] could not directly realize the XOR operation, which is essential for the Boolean adding calculation. By modifying the previous skyrmion logic gate [3] and utilizing the SA properly we propose SA adder devices. Using MuMax3 micromagnetic simulations, we demonstrate the operation of SA half adder, SA full adder, arbitrary n-bit SA ripple-carry adder, and furthermore a parallel computing operation using them. Comparing the power consumption, our device showed about 15% level of previously proposed device [3], due to the cell density and structural simplicity. Based on the scalability and extensibility of our device, we suggest that the skyrmion annihilation is no more detrimental phenomenon, but is a beneficial for logic device applications.

References

- [1] Sampaio, J. et al. Nat. Nanotechnol. 8, 839 (2013).
- [2] Zhang, X. et al. Sci. Rep. 5, 9400 (2015).
- [3] Luo, S. et al. Nano Lett. 18, 1180 (2018).

Giant spin Seebeck effect (SSE) in two-dimensional ferromagnetic CrI_3 monolayer

Brahim Marfoua^{*}, Imran Khan, Jisang Hong[†]

Department of Physics, Pukyong National University, Busan 48513, Korea

The spin Seebeck effect (SSE) was discovered a decade ago, and it is one of the key factors in the spin caloritronics field which refers to the coupling electron spin and charge transport [1-3]. One of the many promising device applications using the SSE is the spin thermoelectric generator. Most of previous experimental and theoretical studies have investigated the SSE in bulk materials [4-6]. Nonetheless, the efficiency of the SSE is still insufficient compared the conventional Seebeck effect, and only a magnitude of a few $\mu\text{V/K}$ has been generated. To fabricate working device in realistic condition, it is highly desirable to find materials or structures which produce high SSE. However, no one has ever reported the SSE in the pure 2D ferromagnetic materials. Thus, using the first principle calculation, we investigated the SSE of the 2D ferromagnetic CrI_3 system in this study. An indirect bandgap of 1.08 eV was obtained from the spin majority contribution. However the spin minority had a large bandgap of 3.07 eV. The spin dependent thermoelectric properties using the Boltzmann equation theory were calculated at 20K and 40K. The spin dependent Seebeck coefficient ($S^{\uparrow\downarrow}$) and electrical conductivity (σ^{\uparrow} and σ^{\downarrow}), we found a similar magnitude (maximum values of 1450 $\mu\text{V/K}$) for both spin and charge Seebeck effect at 40K. To the best of our knowledge, such a giant SSE performance has never been reported in the 2D ferromagnetic materials. This finding may offer a new dimension in the generation of the spin current efficiency and a potential magnetic material in the thermoelectric generator based on magnetic/metal heterostructure in order to improve its performances.

Acknowledgment

This research was supported by the Basic Science Research Program through the National Research Foundation of Korea (NRF) funded by the Ministry of Science, ICT and Future Planning (2019RA21B5B01069807).

References

- [1] K. Uchida, S. Takahashi, K. Harii, J. Ieda, W. Koshibae, K. Ando, S. Maekawa, E. Saitoh, Observation of the spin Seebeck effect, *Nature*, 455 (2008) 778.
- [2] G.E. Bauer, E. Saitoh, B.J. Van Wees, Spin caloritronics, *Nat. Mater.*, 11 (2012) 391.
- [3] S.T. Goennenwein, G.E. Bauer, Spin caloritronics: Electron spins blow hot and cold, *Nat. Nanotechnol.*, 7 (2012) 145.
- [4] M. Schreier, A. Kamra, M. Weiler, J. Xiao, G.E. Bauer, R. Gross, S.T. Goennenwein, Magnon, phonon, and electron temperature profiles and the spin Seebeck effect in magnetic insulator/normal metal hybrid structures, *Phys. Rev. B*, 88 (2013) 094410.
- [5] D. Qu, S. Huang, J. Hu, R. Wu, C. Chien, Intrinsic spin Seebeck effect in Au/YIG, *Phys. Rev. Lett.*, 110 (2013) 067206.
- [6] S. Rezende, R. Rodríguez-Suárez, R. Cunha, A. Rodrigues, F. Machado, G.F. Guerra, J.L. Ortiz, A. Azevedo, Magnon spin-current theory for the longitudinal spin-Seebeck effect, *Phys. Rev. B*, 89 (2014) 014416.

유연기판을 활용한 비정질 금속 박막의 연신저항특성 확인

김지호^{1*}, 윤창진¹, 김민구¹, 이금원^{1,2}

¹고려대학교 디스플레이반도체물리학과

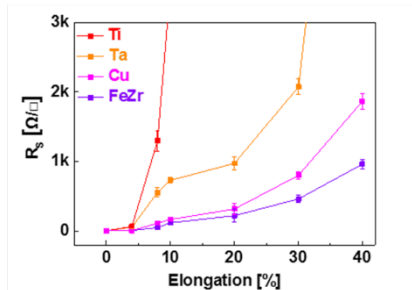
²고려대학교 응용물리학과

비정질 금속은 일반 금속과 다르게 결정 구조를 가지고 있지 않는다. 이러한 구조적 특성으로 인해 비정질 금속은 일반 금속 보다 연성이 좋아 더 큰 연신에서도 손상이 없을 것이라 예상하였다. 본 실험에서는 PDMS(Polydimethylsiloxane) 유연기판을 활용하여 비정질 금속 박막의 연신특성을 확인해 보았다.

비정질 금속 박막은 DC 마그네톤 스퍼터링으로 제작하였으며 증착 시 박막 내부에 void 구조가 형성되는 것을 막기 위해 SiO₂ 기판 위에 분압을 조절하여 증착 후, TEM(transmission electron microscope)을 이용하여 최적의 막질을 확인하였다. 그 후 최적의 조건으로 비정질 금속을 유연기판에 증착 하였으며 기판이 온도에 의해 열팽창후 이후 수축하여 박막에 wrinkle 발생하는 것을 편광현미경과 AFM(Atomic Force Microscope)로 분석하였다. 더 나아가 metal mask를 사용하여 박막 증착 시 길이방향에 수직하게 wrinkle 이 발생하는 것을 확인하여 연신방향과 평행한 wrinkle을 갖는 시료를 제작하여 연신 특성을 비교하였다.

실험은 PDMS기판을 연신하면서 비정질 박막의 저항을 측정하여 박막의 손상여부를 확인하였다. 연신 시 저항변화율이 일반금속에 비해 비정질 박막이 더 낮아 비정질 금속의 연신특성이 일반금속에 비해 더 뛰어난 것을 알 수 있다. 비정질 박막 전면 증착 시료는 일정 연신까지 저항이 안정적 이었으며 그 이상에서는 yield strength가 넘는 힘이 가해져 박막에 crack이 발생하였다. 그리고 원복 후 박막의 판상이 서로 겹쳐짐을 SEM(Scanning Electron Microscope)으로 확인하였다. Metal mask로 증착 된 시료는 전면 증착 보다 더 큰 연신에서도 손상되지 않았으며 여러 차례의 원복에도 연결을 유지하였다.

결론적으로 비정질 구조의 특성으로 인해 일반 금속보다 연신특성이 뛰어나며 증착 시 발생하는 wrinkle 이 연신특성에 영향을 주고 추가적으로 wrinkle을 조절하여 연신특성에 더욱 긍정적인 효과를 줄 수 있다.



2 cm x 2 cm 기판, 전면 증착, 박막 두께 50nm, 연신 시 면저항 그래프

Educational a Pair of PET Detection System Based on 1D-RCD and Oscilloscope

이민호^{1*}, 허희선¹, 권철민¹, 정지윤¹, 강지훈^{1, 2†}

¹전남대학교 의공학과

²전남대학교 헬스케어의공학연구소

양전자방출단층촬영기(PET, Positron Emission Tomography)는 대표적인 분자영상시스템으로 임상용 및 전임상용 시스템과 PET-CT 및 PET-MRI와 같은 융합영상시스템들이 개발되어 널리 활용되고 있다. 본 연구에서는 PET 동작 원리 및 기술적 특성을 쉽게 이해할 수 있는 1차원 저항분배회로 및 저가의 오실로스코프 기반 교육용 한 쌍 PET 검출기 시스템을 개발하고, 기초성능평가와 원리검증용 PET 영상획득을 수행하였다.

DS1104Z(RIGOL, Beijing, China)은 저가형 오실로스코프로 100 MHz 대역폭, 1 GSPS 샘플링 속도, 12 Mpts 메모리, 4 채널을 내장하고 있다. 오실로스코프와 PC는 USB Device를 이용하여 물리적으로 연결 하고, 'MATLAB' 을 이용한 데이터 획득 및 제어용 프로그램을 개발하였다. 오실로스코프에 의해 디지털화된 아날로그 신호는 데이터 후처리 프로그램을 이용하여 유효 신호 추출 및 저장하였다. 방사선모사파형 및 사각파를 이용하여 데이터획득장치로서의 기초적인 성능을 평가하였다.

$3 \times 3 \times 10 \text{ mm}^3$ LYSO (Lutetium-yttrium oxyorthosilicate) 섬광결정과 $3 \times 3 \text{ mm}^2$ GAPD(Geiger-Mode Avalanche Photodiode)는 광학 그리즈를 이용하여 한 쌍 PET 검출기를 구성하였다. 또한, 섬광결정의 위치를 정확하게 구별하고 분리하기 위해 1D-RCD의 저항을 동일하게 설계하였다. 아날로그 출력신호는 증폭기(AD8012, Analog Devices Inc, Norwood, USA)를 이용하여 신호의 모양 수정과 서밍 시스템이 가능한 전치증폭기를 구성했다. Na-22 표준 선원을 PET 검출기에 조사하였으며, 오실로스코프의 Coincidence Mode를 이용하여 PET 검출기에 적용 가능성을 평가하였다. 회전데이터를 얻기 위해서 아두이노와 서보모터를 이용하여 간단한 회전 장치를 설계하였고, 이는 3도씩 60단계로 10분동안 데이터를 획득하여 영상을 재구성하였다.

아날로그 입력신호의 진폭이 증가함에 따라 양자화된 변환 신호는 선형적으로 증가하였고, 선형회귀분석의 결정계수(R^2)는 0.999로 측정되었다. 1000 mV부터 5000 mV 진폭변화에 의한 반치폭(FWHM, Full Width at Half Maximum)은 평균 1.4% 수준이었다. PET 검출기로부터 획득한 평면영상에서는 50 ohm으로 구성된 1D-RCD에 의해 4개의 섬광결정 픽셀 간격이 평균 28로 측정되었고, 픽셀들이 완전히 분리되었으며 명확하게 구분되었다. 또한, 평균 PVR(Peak to Valley Ratio)은 18.9 수준이었다 추출한 픽셀별 에너지 스펙트럼에서 511 keV 에너지에 대한 반치폭은 평균 9.5%로 분석되었다. Coincidence Mode를 이용하여 신호를 획득하였고, 샘플링 기반 LED(Leading Edge Discriminator) 시간추출방법을 이용하여 시간스펙트럼을 획득하였다. 반치폭은 5.4 ns 수준이었다. 한 쌍 PET 시스템으로 획득한PET 영상의 공간스펙트럼의 반치폭은 평균 3.2 mm 수준이었다.

본 연구는 PET 동작 원리 및 기술적 특성을 쉽게 이해할 수 있는 교육용 한 쌍 PET 검출기 시스템 개발 및 성능평가를 수행하였다. 저가의 오실로스코프를 이용하여 방사선 검출기용 데이터획득장치를 성공적으로 개발하고 우수한 성능을 검증하였다. 또한, 오실로스코프에 간단한 회전장치를 추가함으로써 아날로그 회로 측정 및 교육용 PET 시스템을 선택적으로 사용할 수 있다. 더 나아가 필터링을 통한 영상 재구성 및 시스템 최적화를 진행할 것이며 응용 분야 교육 및 실험에 사용될 것으로 기대된다.

Nonvanishing anomalous Hall effect of the quaternary Heusler compound TiZrMnAl with compensated ferrimagnetism

Thu-Thuy Hoang^{1*}, Minkyu Park², Do Duc Cuong¹, S. H. Rhim¹, S. C. Hong¹

¹Department of Physics and Energy Harvest-Storage Research Center, University of Ulsan

²Research Institute of Basic Sciences, University of Ulsan
(sonny@ulsan.ac.kr, schong@ulsan.ac.kr)

Recently, nonzero anomalous Hall conductivity is predicted in full-Heusler compounds[1] with compensated ferrimagnetism despite vanishing magnetization. This finding has drawn a lot of attentions to achieve spintronic device with no stray field. In this work, a quaternary Heusler compound TiZrMnAl is studied, whose space group is $F\bar{4}3m$. Among two possible structures (Fig. 1) due to the equivalency of Ti and Zr, type I is energetically more stable by energy difference of 0.34 eV. Both types are spin-gapless semiconductors, where valence band maximum and conduction band minimum touch at the Fermi level [2,3]. Furthermore, compensated ferrimagnetic TiZrMnAl satisfies Slater-Pauling rule. We find non-negligible intrinsic anomalous Hall conductivity (AHC) of 641 ($\Omega^{-1}\text{cm}^{-1}$) and 200 ($\Omega^{-1}\text{cm}^{-1}$) for Type I and Type II, respectively. In particular, the dominant contribution to AHC in type I comes from the point between L - W, which can be enhanced to 1650 ($\Omega^{-1}\text{cm}^{-1}$) by an upward shift of the Fermi level by 27meV.

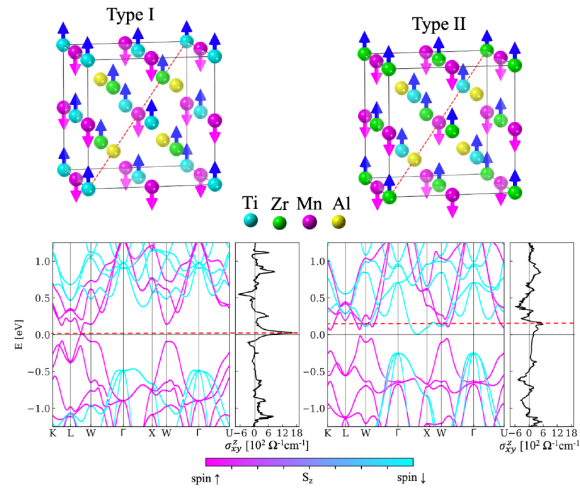


Fig 1. Crystal structure, band structure (soc), and calculated anomalous Hall conductivity of quaternary Heusler compounds TiZrMnAl Type I (left panel) and Type II (right panel).

Keywords: Heusler compounds, anomalous Hall conductivity

References

- [1] Wujun Shi, Lukas Muechler, Kaustuv Manna, Yang Zhang, Klaus Koepf, Roberto Car, Jeroen van den Brink, Claudia Felser, and Yan Sun. Phys. Rev. B 97, 060406(R) (2018)
- [2] X. L. Wang. Phys. Rev. Lett. 100, 156404 (2008)
- [3] Ersoy Şaşıoğlu, Thorsten Aull, Dorothea Kutschabsky, Stefan Blügel, and Ingrid Mertig. Phys. Rev. Applied 14, 014082 (2020)

Electric field dependent valley polarization in 2D WSe₂/CrGeTe₃ heterostructure

Brahim Marfoua^{*}, Jisang Hong[†]

Department of Physics, Pukyong National University, Busan 48513, Korea.

Valleytronic has received an extensive interest as a promising field for the information processing, storage and logic operation applications. It is necessary to break inversion symmetry in the semiconductors which has energetically degenerate valley to achieve valley-contrasting phenomenon [1–3]. An external magnetic field can manipulate the valley polarization[4]. However, it requires a huge magnetic field to induce a sizable valley polarization. Thus, the magnetic heterostructures via proximity has been proposed as an alternative approach[5]. For instance, 2D WSe₂/CrI₃ van der Waals heterostructure has been considered to investigate the valley polarization[6]. Along with the CrI₃, it is known that the 2D CrGeTe₃ also shows the ferromagnetic state with a finite band gap. Nonetheless, no report is available for the valley polarization induced by 2D CrGeTe₃ layer. Thus, we have investigated the electric field dependent valley polarization of 2D WSe₂/CrGeTe₃ heterostructure. The WSe₂/CrGeTe₃ system has an indirect band gap of 0.253 eV without spin orbit coupling (SOC), and this is reduced to 21 meV with SOC. The WSe₂/CrGeTe₃ system has a weak perpendicular magnetic anisotropy of 0.05 meV/cell, and the critical temperature is 38 K. The magnitude of the valley polarization is 3 meV without an electric field. For instance, we obtain the valley polarization of 9 meV if the electric field of 0.4 V/Å is applied from the CrGeTe₃ to the WSe₂, but it becomes 0.5 meV if the electric field direction is reversed even at the same intensity. We have found that the charge redistribution happens depending on the electric field direction. So, we attribute this feature to the electric field dependent valley polarization of the 2D WSe₂/CrGeTe₃ heterostructure. We may suggest that the WSe₂/CrGeTe₃ heterostructure can be a potential candidate for valleytronics device application.

ACKNOWLEDGMENT

This research was supported by the Basic Science Research Program through the National Research Foundation of Korea (NRF) funded by the Ministry of Science, ICT and Future Planning (2019RA21B5B01069807).

References

- [1] A. Srivastava, M. Sidler, A.V. Allain, D.S. Lembke, A. Kis, A. Imamoglu, Valley Zeeman effect in elementary optical excitations of monolayer WSe₂, *Nat. Phys.*, 11 (2015) 141–147.
- [2] Z.-M. Yu, S. Guan, X.-L. Sheng, W. Gao, S.A. Yang, Valley-Layer Coupling: A New Design Principle for Valleytronics, *Phys. Rev. Lett.*, 124 (2020) 037701.
- [3] J.R. Schaibley, H. Yu, G. Clark, P. Rivera, J.S. Ross, K.L. Seyler, W. Yao, X. Xu, Valleytronics in 2D materials, *Nat. Rev. Mater.*, 1 (2016) 1–15.
- [4] S.A. Vitale, D. Nezich, J.O. Varghese, P. Kim, N. Gedik, P. Jarillo-Herrero, D. Xiao, M. Rothschild, Valleytronics: Opportunities, challenges, and paths forward, *Small*, 14 (2018) 1801483.
- [5] G. Binasch, P. Grünberg, F. Saurenbach, W. Zinn, Enhanced magnetoresistance in layered magnetic structures with antiferromagnetic interlayer exchange, *Phys. Rev. B*, 39 (1989) 4828.
- [6] D. Zhong, K.L. Seyler, X. Linpeng, R. Cheng, N. Sivadas, B. Huang, E. Schmidgall, T. Taniguchi, K. Watanabe, M.A. McGuire, Van der Waals engineering of ferromagnetic semiconductor heterostructures for spin and valleytronics, *Sci. Adv.*, 3 (2017) e1603113.

A New Methods for Distinguishing Phoswich Detector consisting of LYSO and GAGG

Jingyu Yang^{*}, Songhyup Kang, Kanguk Jin, Joomin Kim, Jihoon Kang[†]

Department of Biomedical Engineering, College of Engineering, Chonnam National
University, Jeonnam 59626, Korea

This study introduces a phoswich detector consisting of widely used LYSO:Ce and recently newly developed GAGG:Ce without additional distinguishing methods. This proposed detector design induces light loss of scintillation photons by difference in refractive index and light transmission between the crystal layers. The light loss generate a pattern diagram of the 2D flood histogram that allows the extraction of 3-dimensional position (X, Y, and depth position). An experimental study was performed to acquire the flood histograms of the DOI detectors that consists of 4 x 4 LYSO arrays and 4 x 4 GAGG arrays with an individual size of 3.17 x 3.17 x 10 mm³ arranged with a 3.37 mm pitch and GAPD array with a pixel size of 3.16 x 3.16 mm². Experimental studies were performed twice by reversing crystal layers of proposed detector. Experimental results revealed that all crystal pixels were clearly identified in the 2D flood histogram when LYSO crystal layer was in bottom-layer. The mean energy resolutions of LYSO and GAGG crystals were 13.8% and 14.2%, respectively. These results demonstrate that phoswich detector can extract 3-dimensional interaction of gamma-ray without additional distinguishing methods. The important advantage of the proposed methods is that only simple anger logic is needed for providing the depth-of-interaction information. Also, additional distinguishing methods or pulse shape discriminating information were not needed.

This work was supported by the National Research Foundation of Korea (NRF) grant funded by the Korea government (MSIT) (NRF-????????????????????)

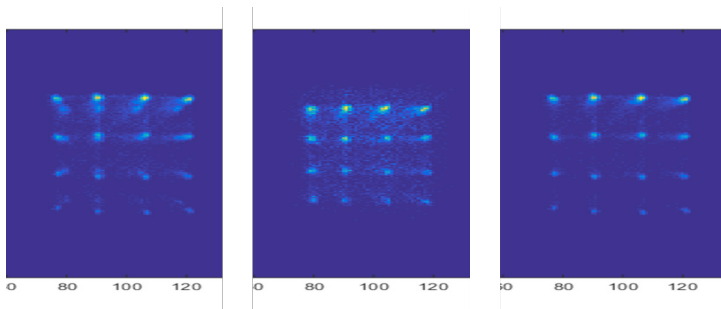


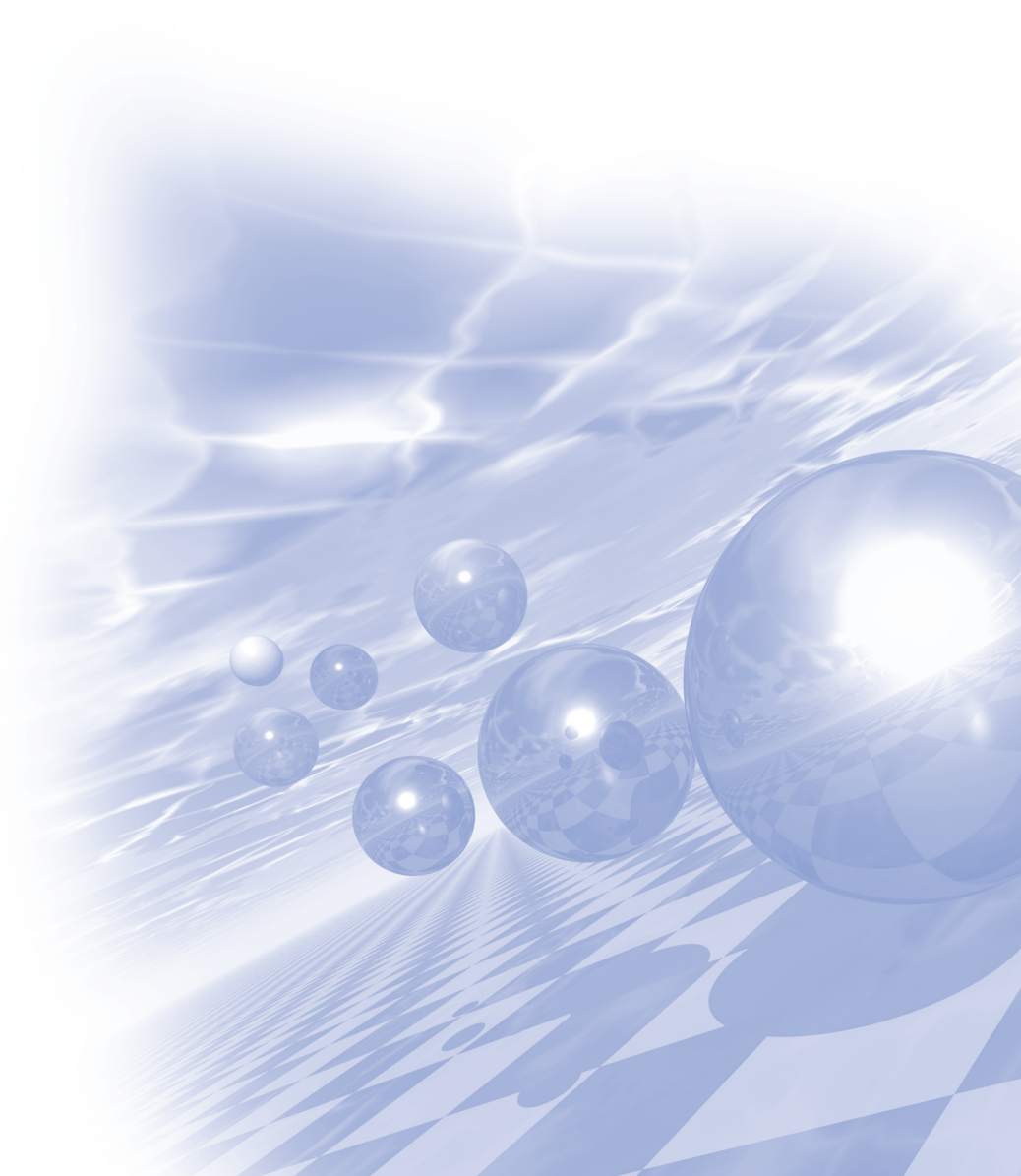
Fig 1. The obtained flood histograms of all layers (left), GAGG-layer (middle), and LYSO-layer (right).



KMS 2020 Winter Conference

Special Session III

‘Hard & Soft Magnetic Materials’



Rare–Earth Permanent Magnets for the Fourth Industrial Revolution: Status and Prospects

Wooyoung Lee*

Department of Materials Science and Engineering, Yonsei University, Seoul 03722, Republic of Korea

A compelling need for high magnetic properties led to active consideration of rare-earth permanent magnets, which have been used in various applications such as communication, memory, and audio equipment. Since their discovery in 1984, high-coercivity sintered Nd-Fe-B magnets have found numerous practical and industrial applications, e.g., as components of actuators, motors, generators, robots, and wind power plants due to the rise of the fourth industrial revolution and problematic issues of air pollution and fine dust generation. In particular, demand for high-performance permanent magnets is rapidly increasing to meet the ever growing interest in the industry of environment-friendly automobiles (hybrid / electric vehicles). However, since the rare-earth magnets are expensive and have limitation in high-temperature applications such as an automobile motor, it is essential to develop a permanent magnet with reduced rare-earth concentration that can bear high temperatures. Consequently, several major corporations have established a high-performance permanent magnet research team and are pursuing new businesses. At this point of view, the present article reviews a summary of the history and the R & D trends of rare-earth permanent magnets that have been developed in the past.

Keywords: Permanent Magnet, Rare Earth, Nd-Fe-B, Motor, Automobile

Permanent magnets for high efficiency motor

Jihoon Park^{a,*}, Jong-Woo Kim^a, Kwanghyun Chung^b, Soon Cheol Hong^c, Chul-Jin Choi[†]

^aPowder & Ceramic Division, Korea Institute of Materials Science, Changwon, Gyeongnam, 51508, Republic of Korea

^bDepartment of Physics, University of Ulsan, Ulsan 44610, Republic of Korea

^cKyungwon Industry Co., Ltd., Siheung, Gyeonggi, Republic of Korea

Electric motors are responsible for about 45% of the total consumption of electric energy, and the percentage ascribable to motors rises to around 66% for the most energy-eating ambits, i.e., manufacturing companies in the industry [1]. Considering that a large number of the motors currently in operation are obsolete, it is clear that replacing them with more efficient motors would lead to important advantages for the energy conservation and environment. For instance, enhancing motor efficiency by 3.3% could reduce the electric power of 2.7 nuclear power plants generating 1 GW, as well as a large amount of greenhouse gases. For these reasons, the leading countries, such as the United States, European Union, etc., are in force regulatory plans providing for the mandatory compliance with gradually increasing efficiency requisites for new installations.

Among all types of motors, the permanent magnet motor exhibits the best efficiency, and its efficiency can be further improved by enhancing magnetic properties of the permanent magnets. Rare earth Nd-Fe-B magnets exhibit the highest maximum energy product of 59 MGOe at room temperature [2]. However, its restricted supply, high cost and a large negative temperature coefficient of coercivity limit its usage for motor applications. In these reasons, developing new permanent magnets with moderate performance would be worth enough for the motor applications. Therefore, in this talk, we will introduce the magnetic properties of newly developed novel rare earth free/lean permanent magnets, such as ThMn₁₂-type Fe-rich compound, Mn-Bi, and grain boundary diffused heavy rare earth element-free Nd-Fe-B for the motor applications.

References

- [1] P. Waide and C. U. Brunner, “Energy-Efficiency Policy Opportunities for Electric Motor-Driven Systems” , International Energy Agency, Working paper (2011).
- [2] S. Sugimoto, “Current status and recent topics of rare-earth permanent magnets” J. Phys. D: Appl. Phys. 44, 064001-064011 (2011).

Finite–element micromagnetic simulation study of NdFeB magnets

Sang–Koog Kim^{*}

National Creative Research Initiative Center for Spin Dynamics and Spin-Wave Devices,
Nanospinics Laboratory, Research Institute of Advanced Materials, Department of Materials
Science and Engineering, Seoul National University, Seoul 151-744, South Korea

Permanent magnets of high remanence and coercivity have been intensively studied for their promising applications in environmentally friendly hybrid vehicles and wind turbines. Sintered NdFeB is the most widely utilized hard magnet, due to its high maximum-energy product, $BH)_{\max} \sim 64$ MGOe, as obtained by theoretical prediction. The microstructures of the NdFeB magnet remarkably modify the value of $BH)_{\max}$. In order to understand the correlations of $BH)_{\max}$ and coercivity with the microstructures of NdFeB magnets (e.g., grain size, grain boundary, crystallographic orientation of grains), a finite-element micromagnetic computational simulation approach is one of most optimal tools to elucidate magnetization reversals in three-dimensional granular magnets. In this talk, we show how finite-element micromagnetic simulations are useful in studies of the effects of a rich variety of microstructures on $BH)_{\max}$ and coercivity[1,2].

References

- [1] J.-H. Lee, J. Choe, S. Hwang, and S.-K. Kim, J. Appl. Phys. 122, 073901 (2017).
- [2] S.-K. Kim, S. Hwang, and J.-H. Lee, J. Magn. Mater. 486, 165257 (2019).

Microstructure of Grain Boundary Diffusion Processed Nd-Fe-B Sintered Magnets : Microstructural Characteristics of HRE-rich Shells and Grain Boundary Phases

Tae-Hoon Kim* Jung-Goo Lee

Powder and Ceramics Division, Korea Institute of Materials Science (KIMS), 797 Changwondaero, Changwon-city, 51508, South Korea.

In this presentation, we report recent microstructure analysis works revealing the microstructural characteristics of HRE (Heavy Rare-earth)-rich shells and Nd-rich grain boundary phases in grain boundary diffusion processed Nd-Fe-B sintered magnets. A different diffusion behavior of HRE within the magnets depending on the form of diffusing materials (HRE-vapor or HRE-compounds) was characterized [1-3], the systematic changes in structure and chemistry of the Nd-rich grain boundary phases during the grain boundary diffusion process were analyzed [1-3]. Through the detailed microstructure observation using the SEM and HAADF-STEM combined with the EDS and WDS, the formation mechanisms of HRE-rich shells could be established from two perspectives: i) solid diffusion of HRE and ii) solidification of HRE-dissolved liquid [4, 5]. Thereby, the origin of the asymmetric feature of HRE-rich shells along the grain boundary phases was also clarified [4, 5]. Based on the results from microstructure characterization, a method to further improve the coercivity of Nd-Fe-B sintered magnets by the grain boundary diffusion process will be proposed.

References

- [1] Tae-Hoon Kim et al., Acta Mater. 172, 139(2019).
- [2] Tae-Hoon Kim et al., Acta Mater. 93, 95(2015).
- [3] Tae-Hoon Kim et al., J. Appl. Phys. 115, 17A763(2014).
- [4] Tae-Hoon Kim et al., Scripta Mater. 178, 433(2020).
- [5] Tae-Hoon Kim et al., Acta Mater. 112, 59(2016).

Comparison of Soft magnetic composite cores from both Fe-based amorphous and crystalline powders

Hwi-Jun Kim*, Min-Woo Lee

Korea Institute of Industrial Technology, Korea

Whether we realize it or not, we use soft magnets, directly and indirectly, every hour of the day. Soft magnetic materials are used for power generation, transfer, and conversion, and are extensively used in electric machines, power electronics, sensors, and electromagnetic interference (EMI) shielding. They play a vital role in today's energy-use sectors of the economy.

A combination of emerging trends in demand for key end products, combined with the availability of new, more efficient and more effective soft magnet materials, is driving markets more rapidly than ever. Key factors include increasing demand for high-efficiency electric motors, particularly in the global automotive industry as electric vehicles (EVs) finally begin to make a meaningful push into global markets.

The properties of soft magnets rely on multiple diverse manufacturing technologies and materials that are used for a wide array of applications and end uses. The development of new materials and novel applications for the electric motors, high frequency power conversion parts and telecommunications industries during the past two decades has immensely broadened the scope and altered the nature of soft magnetic materials in Korea.

To meet the growing need for energy efficiency in power electronics and electric machines, we have been studying on a number of new soft magnetic composite cores with different structure like crystalline, amorphous and nano crystalline. Compared to the currently most widely used crystalline SMCs, the amorphous SMCs possess more favorable properties, including high electrical resistivity, good saturation magnetization, low coercivity and near-zero magnetostriction.

This presentation will introduce the results on frequency dependence of the soft magnetic SMC cores manufactured from crystalline and amorphous powders using conventional powder metallurgy processes. While crystalline SMC cores showed useful soft magnetic characteristics in low frequency ranges, amorphous SMC cores exhibited valuable properties in high frequency ranges.

Furthermore, effects of microstructural factors like grain boundary area fraction, porosity and grain size on soft magnetic properties of those SMC cores.

Keywords: soft magnetic property, soft magnetic composites, powders, microstructural factor, powder metallurgy process.

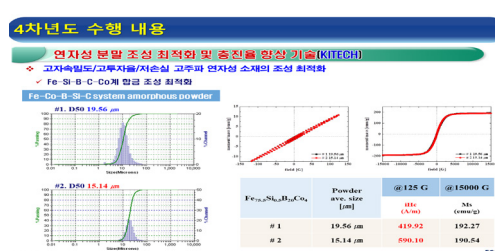


Fig. 1. Soft magnetic properties of FeSiBCo amorphous SMC Core

Fabrication of Anisotropic Bulk Magnet by Hot-deformation Process using Nd-lean Nd-Fe-B Melt-spun Powder

Jung-Goo Lee^{1,*}, Ga-Yeong Kim¹, Hee-Ryoung Cha¹, Dong-Kwan Kim², Hae-Woong Kwon²

¹Powder and Ceramics Division, Korea Institute of Materials Science (KIMS)

²R&D Center, Star Group Ind. Co.

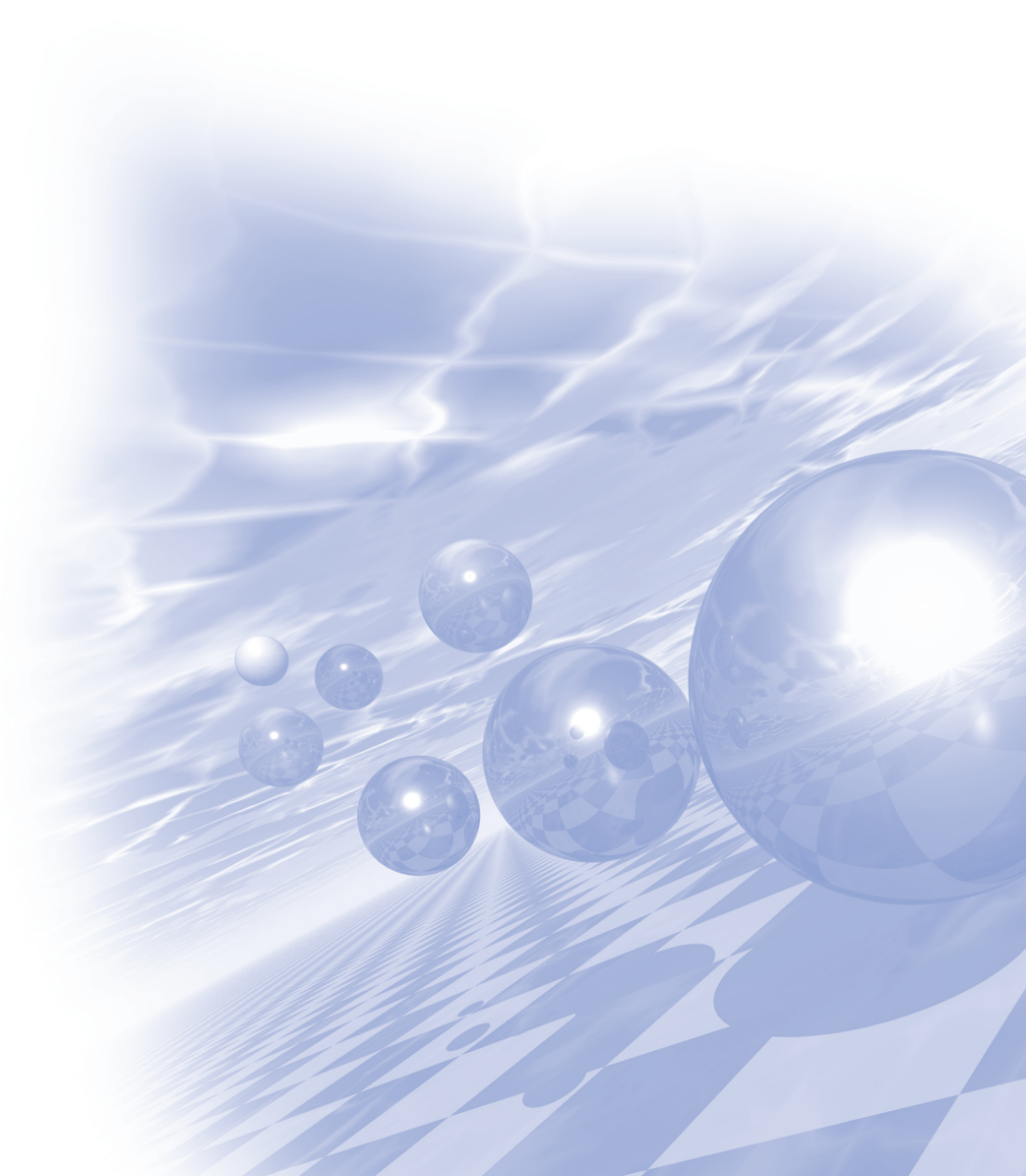
It is technologically interesting challenge to develop the high performance Nd-lean RE-Fe-B magnets by substitution of Ce and La for Nd, which is also quite important from an industrial viewpoint. Actually, many efforts have been made to substitute Ce and La for Nd in sintered Nd-Fe-B magnets. Despite of the inferior intrinsic magnetic properties of $\text{Ce}_2\text{Fe}_{14}\text{B}$ and $\text{La}_2\text{Fe}_{14}\text{B}$ compared to $\text{Nd}_2\text{Fe}_{14}\text{B}$, it is reported that deterioration of magnetic properties due to Ce and La substitution could be largely suppressed by constructing a multi-main-phase (MMP) structure in Nd-lean RE-Fe-B sintered magnets. On the other hand, most of the studies has been concerned with sintered magnets and studies on hot-deformed Nd-lean RE-Fe-B magnet are quite limited. In this study, therefore, Nd in hot-deformed Nd-Fe-B was partially substituted by Ce and La for the purpose of reducing the materials cost and balancing the utilization of rare earth resources. Initial melt-spun ribbons with the nominal compositions of $(\text{Nd}_{1-x}\text{M}_x)_{13.6}\text{Fe}_{61}\text{B}_{5.6}\text{Ga}_{0.6}\text{Co}_{6.6}$ ($x=0$, $x=0.2/\text{M}=\text{Ce}$, $x=0.3/\text{M}=\text{Ce}$, $\text{Ce}+\text{La}$, wt.%) were prepared by a single-roller melt-spinning method, and pulverized into powders. The powders were then hot-pressed at 973K under 100MPa and deformed at 973K until 75% of height reduction is achieved. The magnetic properties of hot-deformed magnets were decreased with the substitution of Ce for Nd in Nd-Fe-B magnets. In addition, simultaneous substitution of Ce and La for Nd resulted in much lower magnetic properties, which was almost the same tendency as initial melt-spun powders. Although the magnetic properties were deteriorated, the cost performance was largely enhanced from 2.32 to 2.62 MGOekg/\$ by 13% when increasing the content of Ce substituted for Nd from 0 to 30 wt.%. Based upon these results, the magnetic properties and microstructure of M(Ce, La)-substituted (Nd, M)-Fe-B hot-deformed magnets will be discussed.



KMS 2020 Winter Conference

Oral Session II

‘대학원생 및 신진과학자 세션’



Astroid in spin Hall current & Dzyaloshinskii–Moriya interaction

Chang-Jin Yun^{2*}, Jiho Kim², Kungwon Rhie¹

¹Display and Semiconductor Physics, Korea University, Sejong, 30019, Korea

²Applied Physics, Korea University, Sejong, 30019, Korea

Pt/Co/Pt and Ta/CoFeB/MgO/Ta multilayer with perpendicular magnetic anisotropy were fabricated with $30 \times 30 \mu\text{m}^2$ square pattern. To measure the astorid, y-directional magnetic field was set multiple fields and z-directional magnetic field (H_z) was varied in parallel with electro-magnet and Helmholtz coil. Hysteresis shows the value of unstable point that becomes a point of the astroid of the Stoner-Wohlfarth model. The astroids rotate with spin torque. This rotation pattern shows proportional relationship between spin torque and H_z at the range of few Oe. That is, if the linear relationship between H_z and spin torque makes it possible to measure an exact spin torque by measuring shifts of H_z . Furthermore, this astroid contains two important pieces of information. First, the direction of the rotation shows the sign of spin Hall angle. Second, flat part of the astorid gives the H_{DMI} value. Not only sign of spin Hall angle but also value of the H_{DMI} can be determind by astroid.

Gate-tunable large nonreciprocal charge transport in noncentrosymmetric $\text{LaAlO}_3/\text{SrTiO}_3$ interfaces

Daeseong Choe^{1*}, Mi-Jin Jin¹, Shin-Ik Kim², Hyung-Jin Choi², Junhyeon Jo¹, Inseon Oh¹, Jungmin Park¹, Hosub Jin³, Hyun Cheol Koo^{4,5}, Byoung-Chul Min⁴, Suk-Min Hong⁴, Hyun-Woo Lee⁶, Seung-Hyub Baek^{2,7} & Jung-Woo Yoo^{1*}

¹School of Materials Science and Engineering-Low dimensional Carbon Materials Center, Ulsan National Institute of Science and Technology, Ulsan, 44919, Korea.

²Center for Electronic Materials, Korea Institute of Science and Technology, Seoul, 02792, Korea.

³Department of Physics, Ulsan National Institute of Science and Technology, Ulsan, 44919, Korea.

⁴Center for Spintronics, Korea Institute of Science and Technology, Seoul, 02792, Korea.

⁵KU-KIST Graduate School of Converging Science and Technology, Korea University, Seoul, 02481, Korea

⁶Department of Physics, Pohang University of Science and Technology, Pohang, 37673, Korea.

⁷Division of Nano & Information Technology, KIST School, Korea University of Science and Technology, Seoul, 02792, Korea

The electrons confined at the interfacial quantum well of $\text{LaAlO}_3/\text{SrTiO}_3$ (LAO/STO) displays diverse exotic condensed matter phases and rich spin-orbitronic functionalities associated with broken inversion symmetry. This two-dimensional polar conductor may exhibit directional propagation of itinerant electrons, i.e. the rightward and leftward currents differ from each other, when the time-reversal symmetry is further broken by applying a magnetic field. This potential rectification effect generally was displayed to be very weak due to the fact that kinetic energy is much higher than energies related to symmetry breakings producing weak perturbation. Here, we present large gate-tunable nonreciprocal charge transport in the LAO/STO conductive oxide interface, where the electrons are confined at two-dimension with low Fermi energy. Moreover, the Rashba spin-orbit interaction owing to a sub-band hierarchy of this system allows powerfully tunable nonreciprocal response by applying a gate voltage. Upon increasing gate voltage, the ratio of resistance change between rightward and leftward currents was increased up to 2.7%. The coefficient γ indicating the strength of the magnetochiral anisotropy, was measured to be as high as $\sim 10^2 \text{ T}^{-1} \text{ A}^{-1}$, which is about three order of magnitude higher than those estimated for typical noncentrosymmetric conductors [1]. In addition, the magnitude of the directional response exhibits additional higher order magnetic field dependence. The overall behavior of nonreciprocal response in LAO/STO can be attributed to the competing energy scales among kinetic energy, spin splitting energy due to broken inversion symmetry, and Zeeman energy due to time-reversal symmetry breaking. The observed behavior of the large directional response in our study inspires a promising channel to enhanced nonreciprocal charge transport in polar materials.

Direct terahertz probing of the fundamentals of anisotropic magnetoresistance

Ji-Ho Park^{1*}, Hye-Won Ko¹, Jeong-Mok Kim², Byong-Guk Park², Se Kwon Kim¹,
Kyung-Jin Lee¹, Kab-Jin Kim¹

¹Department of Physics, KAIST, Daejeon 34141, Korea

²Department of Materials Science and Engineering and KI for Nanocentury, KAIST, Daejeon 34141, Korea

Anisotropic Magnetoresistance (AMR) is a fundamental spin-orbit-coupling (SOC)-induced magneto-transport phenomena that describes the anisotropic charge conductivity depending on relative orientations of the current flow and the magnetization. The microscopic mechanisms of AMR have so far been attributed to either intrinsic [1,2] or extrinsic origin [3,4], yet the direct separating the origins have remained a challenge due to the experimental difficulties in direct accessing the electron scattering process. Here, we, for the first time, have clearly separated the extrinsic and intrinsic origin of AMR. Using terahertz (THz) time domain spectroscopy, we have independently probed the electron scattering time (τ) and the ratio of carrier density to the effective mass (n/m^*) in Permalloy films. The anisotropy ratio for τ , which corresponds to the extrinsic scattering-dependent effect, is about 2.4 ~ 3.0 % and decreases with increasing temperature. On the other hand, the anisotropy ratio for n/m^* , which reflects the intrinsic scattering-independent band-induced effect, is comparable to the extrinsic contribution and is almost independent of temperature. These results suggest that the intrinsic mechanism is increasingly important at higher temperature, and could be a significant for room-temperature applications, e.g., SOT devices utilizing the transverse AMR as a spin current source [5,6]. Our findings will stimulate further fundamental studies of SOC-induced phenomena, such as anomalous Hall effect, magnetic damping [7, 8], where identifying the intrinsic and extrinsic contributions is important.

References

- [1] Fert, A. & Campbell, I. A. Phys. Rev. Lett. 21, 1190-1192 (1968).
- [2] Kokado, S., Tsunoda, M., Harigaya, K. & Sakuma, A. J. Phys. Soc. Jpn. 81, 024705 (2012).
- [3] Velez, J., Sabirianov, R. F., Jaswal, S. S. & Tsymbal, E. Y. Phys. Rev. Lett. 94, 127203 (2005).
- [4] Zeng, F.L. et al. Phys. Rev. Lett. 125, 097201 (2020).
- [5] Taniguchi, T., Grollier, J. & Stiles, M. D. Phys. Rev. Appl. 3, 044001 (2015).
- [6] Safranski, C., Montoya, E. A. & Krivorotov, I. N. Nat. Nanotech. 14, 27-31 (2019).
- [7] Gilmore, K., Idzerda, Y. U. & Stiles, M. D. Phys. Rev. Lett. 99, 027204 (2007).
- [8] Berger L. Phys. Rev. B 83, 054410 (2011).

A large reduction in switching current in W/CoFeB heterostructures with W-N interfacial layers

Min Hyeok Lee^{a,1*}, Yong Jin Kim^{a,1}, Gyu Won Kim^a, Taehyun Kim^a, In Ho Cha^a,
Quynh Anh T. Nguyen^b, Sonny H. Rhim^b, Young Keun Kim^{a,*}

^aDepartment of Materials Science and Engineering, Korea University, Seoul 02481, Republic of Korea

^bDepartment of Physics, University of Ulsan, Ulsan 44610, Republic of Korea

A brand-new physical phenomenon called spin-orbit torque (SOT) is drawing attention from many researchers because it is suitable for the development of a memory device that is energy efficient and non-volatile. SOT refers to the torque generated by the angular momentum transferred to magnetization when the spin current generated in the nonmagnetic layer (NM) flows to the adjacent ferromagnetic layer (FM). By using this, it is possible to reverse the magnetization direction of the FM at higher driving speed and higher energy efficiency compared to the conventional spin-transfer torque (STT) [1]. However, in the case of operation using spin-orbit torque, the switching current is very large, so there is still a problem in application to memory or logic devices. The spin Hall angle (SHA) is defined as how much spin current can be generated compared to the injected current, and the magnitude of the switching current is inversely proportional to this SHA [2]. Therefore, recent studies have reported SHAs obtained from various NM (~ 0.33 for β -W [3], ~ 0.12 for Ta [4], ~ 0.10 for Pt [5]), but they have not been able to obtain high values that can be applied to devices. It is no longer possible to expect an improvement in the SHA with a single NM material, researches have been actively conducted in the direction of manipulating the NM/FM interface [6]. In this study, we would like to discuss how the SOT switching current can be greatly reduced by interfacial engineering in which a W-N ultra-thin film is inserted into the W/CoFeB interface. The W-N ultra-thin film was deposited by reactive sputtering using DC magnetron sputtering in an N_2 atmosphere, and the efficiency of SOT was measured while changing the N_2 composition and thickness of the W-N intercalation layer. When the thickness of the W-N insertion layer was 0.2 nm and the composition of N was 42 at%, a SHA of 0.54 was obtained. Accordingly, the SOT switching current was also reduced to one-fifth compared to that of W/CoFeB heterostructure. The results show that the SOT efficiency can be significantly changed even when the interface is manipulated using an ultra-thin film of 0.2 nm scale, and it can be confirmed that it is necessary to focus on the interface to increase the possibility that the SOT technology will be applied to the device.

References

- [1] I. M. Miron et al., Perpendicular switching of a single ferromagnetic layer induced by in-plane current injection, *Nature* 476 (2011) 189-193.
- [2] K.-S. Lee et al., Threshold current for switching of a perpendicular magnetic layer induced by spin Hall effect, *Appl. Phys. Lett.* 102 (2013) 112410.
- [3] C.-F. Pai et al., Spin transfer torque devices utilizing the giant spin Hall effect of tungsten, *Appl. Phys. Lett.* 101 (2012) 122404.
- [4] Q. Hao, G. Xiao, Giant spin Hall effect and magnetotransport in a Ta/CoFeB/MgO layered structure: A temperature dependence study, *Phys. Rev. B* 91 (2015) 224413.
- [5] H.L. Wang et al., Scaling of spin Hall angle in 3d, 4d, and 5d metals from Y3Fe5O12/metal spin pumping, *Phys. Rev. Lett.* 112 (2014) 197201.
- [6] H.-Y. Lee et al., Enhanced spin-orbit torque via interface engineering in Pt/CoFeB/MgO heterostructures, *APL Mater.* 7 (2019) 031110.

Electric-field control of deterministic spin-orbit torque switching via laterally modulated Rashba effect in Pt/Co/ AlO_x structures

Min-Gu Kang^{1*}, Jong-Guk Choi¹, Jimin Jeong¹, Jae Yeol Park¹, Hyeon-Jong Park²,
Jong Min Yuk¹, Kyung-Jin Lee³, Byong-Guk Park¹

¹Department of Materials Science and Engineering, KAIST, Daejeon 34141, Korea

²KU-KIST Graduate School of Converging Science and Technology, Korea University, Seoul 02841, Korea

³Department of Physics, KAIST, Daejeon 34141, Korea

Spin-orbit coupling effect in structures with broken inversion symmetry, known as the Rashba effect, facilitates spin-orbit torques (SOTs) in heavy metal/ferromagnet/oxide structures, along with the spin Hall effect [1,2]. Electric-field control of the Rashba effect is established for semiconductor interfaces [3], but it is challenging in structures involving metals owing to the screening effect. Here, we report that the Rashba effect in Pt/Co/ AlO_x structures is laterally modulated by electric voltages, generating out-of-plane SOTs. This enables field-free switching of the perpendicular magnetization and electrical control of the switching polarity. Changing the gate oxide reverses the sign of out-of-plane SOT while maintaining the same sign of voltage-controlled magnetic anisotropy, which confirms the Rashba effect at the Co/oxide interface is a key ingredient of the electric-field modulation. The electrical control of SOT switching polarity in a reversible and non-volatile manner can be utilized for programmable logic operations in spintronic logic-in-memory devices.

References

- [1] Liu, L. et al. Science 336, 555-558 (2012).
- [2] Miron, I. M. et al. Nature 476, 189-193 (2011).
- [3] Chen, L. et al. Nat. Electron. 1, 350-355 (2018)

Investigation of Weak Antilocalization Effect in Co-dusted Graphene films

Thi-Nga Do^{1,2*}, Sehee Lee³, Chanyong Hwang³, Taehee Kim^{1,2†}

¹IBS Center for Quantum Nanoscience, Ewha Womans University, Seoul, Korea

²Department of Physics, Ewha Womans University, Seoul, Korea

³Korea Research Institute of Standards and Science, Daejeon, Korea

The tunability of material properties is one of the fascinating and powerful advantages of quantum effects in nanoscale. In disordered two-dimensional system, weak antilocalization (WAL) appears due to the wave nature of electrons since interference effects double the classical probability for self-crossing paths and it slightly suppresses the conductance [1]. The observation of WAL effects requires the decrease of the classical signal by reducing the film thickness or the grain size. Furthermore, in the presence of strong spin-orbit coupling, the enhanced effect of WAL can be expected.

In this work, we have investigated magnetoresistance at different temperatures for the Co-dusted well-ordered layers grown on unetched silicon wafers. Co deposition ranging from 0.1 to 2 nm thick was performed at room temperature using the UHV-MBE deposition technique. The Pt Hall bars were also prepared simultaneously in order to study transport properties. We observed the enhanced WAL effect at low temperature as Co thickness decreases down to 0.1 nm.

References

- [1] Bergmann G., Phys. Rep., 107 (1984) 1.

Growth and analysis of novel A15 W_3Ta Heavy metal layer

Jeongwoo Seo^{1*}, Jeonghoon Shin, Woojong Kim², Jungyup Yang³, Jinpyo Hong^{1,2}

¹Department of Physics, Hanyang University, Seoul 2220-4770, Korea

²Division of Nanoscale Semiconductor Engineering, Hanyang University, Seoul, Korea

³Department of physics, Kunsan national University, Korea

Magnetization manipulation by a Spin Orbit Torque(SOT) phenomena has intense focus on the efficient operation of spintronic devices at extremely lower power. Recent theoretical paper suggested W_3Ta layer as one of candidate for heavy metal (HM)/ ferromagnet (FM) / Oxide (O) hetero-structure because of its large spin hall angle in A15 phase materials such as Tungsten(W). We address the SOT efficiency of A15 phase W_3Ta layer by RF sputtering approach. The growth key parameters adjusted in our work, such as RF power, working pressure and annealing temperature and roughness. We confirmed the conditions for A15 phase structure and measured W_3Ta A15 phase by XRD measurement, as shown in fig 1. To figure out spin orbit torque efficiency depend on crystal structure, we analyzed in-plane external magnetic field with DC and AC method to identify spin orbit torque-driven effective fields and confirmed improved spin orbit torque efficiency in W_3Ta based heterostructure.

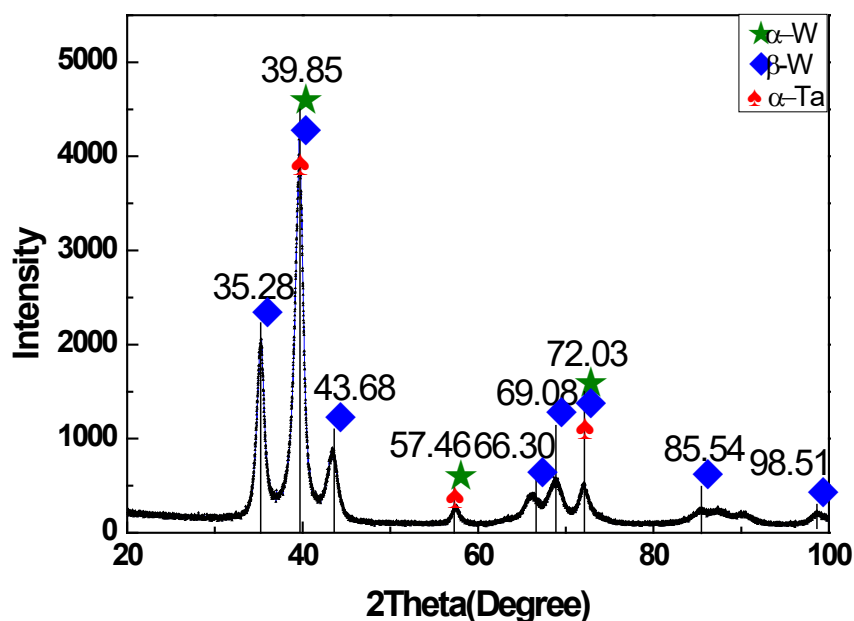


Fig. 1. W_3Ta XRD data

Manipulation of spin–orbit torque in HM/FM/Oxide frame by external gate voltage

Jeonghun Shin^{1*}, Jeongwoo Seo², Jungyup Yang³, Jinpyo Hong^{1,2}

¹Division of Nano-scale Semiconductor Engineering and Physics
Hanyang University, Seoul 133-791, South Korea

²Department of physics, Hanyang University, Seoul 133-791, South Korea

³Department of physics, Kunsan national University, South Korea 54150

Intentional manipulation of Spin-Orbit Torque (SOT) efficiency and its devices inevitably requires precise adjustment of heavy metal layer in a Heavy Metal (HM)/Ferromagnet Metal (FM)/oxide frame. The Rashba effect and SHE effect are mentioned as the origin of SOT. If find a parameter that can be control both effects, we search a way to control the SOT. One approach developed up to now is the possible displacement of the domain walls which are highly dependent on the angle between the direction of the current and domain wall motion, and asymmetric and nonlinear with respect to the current polarity. The other approach is the choice of other HM layer, topological insulator, or antiferromagnet/ferromagnet to provide the advancing SOT features. Here We present a parameter that could control the Rashba effect and SOT efficiency by external bias on the HM/FM/Oxide structure. PMA and Oxide characteristic and HK of FM are unchanged by external gate bias.

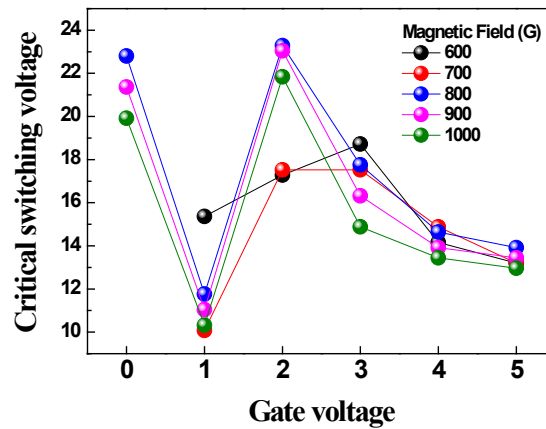


Fig 1. Critical switching voltage versus Gate voltage graph

Universality of stripe domain width change by an in-plane magnetic field

Seungmo Yang^{1*}, Kyoung-Woong Moon¹, Tae-Seong Ju^{1,2}, Changsoo Kim¹,
Byoung Sun Chun¹, Sungkyun Park², Chanyong Hwang¹

¹Quantum Spin Team, Korea Research Institute of Standards and Science, Daejeon 34113,
Republic of Korea

²Department of Physics, Pusan National University, Busan, 46241, Republic of Korea

In nature, diverse two-dimensional (2D) systems show stripe domain patterns of order parameters. The shape of stripe domain patterns in diverse physical systems have resembling forms, indicating a universal mechanism for forming the stripe domain patterns, which is the competing interaction between short- and long-range interactions in a two-fold symmetric potential. In particular, the magnetic stripe domain pattern with the Dzyaloshinskii-Moriya interaction (DMI) is an important issue due to its close connection to generation of magnetic skyrmions. Therefore, it can be required to understand how the specific form of a stripe domain is determined under diverse material parameters and environments. Here, we establish a reliable model for a stripe domain width change under a hard-axis magnetic field in a perpendicular magnetic anisotropy (PMA) system with DMI. The presence of hard-axis magnetic fields modulates the three critical parameters for stripe domain formation, which are a two-fold symmetric potential, short- and long-range interaction. The proposed model was confirmed to be well-matched with experimental results for various PMA samples of W/Co₂Fe₆B₂/MgO stacks. In addition, all curves of the stripe width under various hard-axis magnetic fields collapse into one single universal curve. Based on the universal curve, we derive a reliable approach to determine the DMI energy and a domain wall type.

Discovery of magnetoelectric coupling in a van der Waals compound CuCrP_2S_6

Chang Bae Park^{*}, Aga Shahee¹, Deepak R. Patil¹, Nikita Ter-Oganessian², Kee Hoon Kim^{1, 3}

¹Center for Novel States of Complex Materials Research, Department of Physics and Astronomy, Seoul National University, Seoul 08826, S. Korea

²Institute of Physics, Southern Federal University, Rostov-on-Don 344090, Russia

³Institute of Applied Physics and Department of Physics and Astronomy, Seoul National University, Seoul 08826, S. Korea

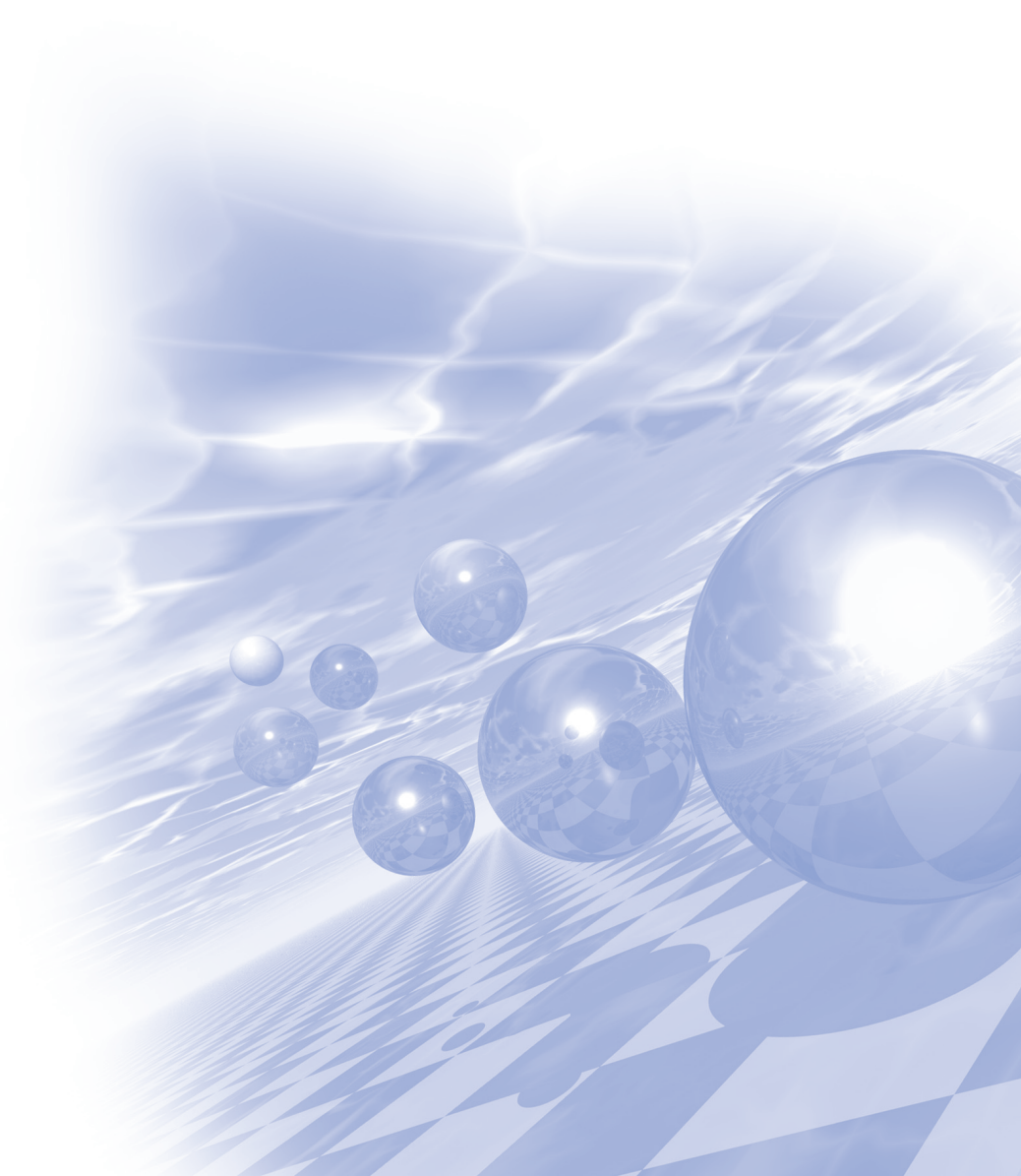
We have discovered magnetic-field-induced electric polarization that is closely associated with the p-d hybridization mechanism in CuCrP_2S_6 . We have observed that the electric polarization (P) occurs below antiferromagnetic ordering temperature, $T_N = 32$ K, and is modulated by magnetic field (H) while it is suppressed with the spin-flop transition located around 6.1 T. Furthermore, we could quantitatively explain the P-H curve with the symmetry analysis based on the P_c space group. The microscopic origin of the magnetoelectric coupling is a so-called spin direction-dependent p-d hybridization mechanism within the off-centered Cr^{3+} octahedral sites. It is further corroborated by the observation of vanishing electric polarization in the $\text{CuCrP}_2\text{Se}_6$ compound in which Cr^{3+} is positioned at the octahedral center, supporting that the off-centered cation plays an important role in the magnetoelectric coupling. Our results thus point to one general route to induce magnetoelectric coupling in 2D layered materials, i.e., via the off-centered cation.



KMS 2020 Winter Conference

Special Session IV

‘Theoretical magnetism and experiments’



Physical Properties of Rare–Earth f–electron Systems: Past and Present

Byung Il Min*

Department of physics, POSTECH, Korea

In the beginning, pioneers and achievements in the field of physics of magnetism in Korea are introduced. Then the interesting physical properties of rare-earth f-electron systems in the past and at present are briefly surveyed, which include permanent magnets, Kondo behavior, heavy fermion, mixed-Valence, and topological Kondo insulator. Our recent studies on Ce and Sm compounds are also presented.

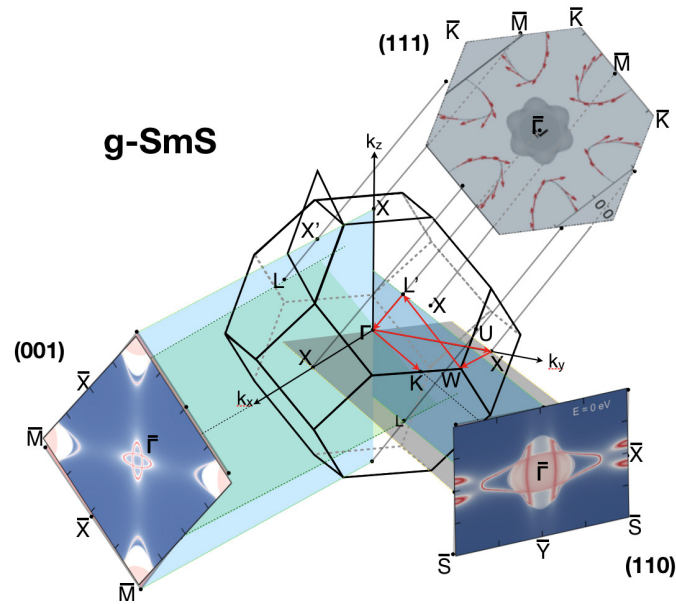


Fig. 1. Multiple topological Dirac cones
in a mixed-valent Kondo semimetal: g-SmS

MTG (Magnetism Theory Group) of Prof. B. I. Min at POSTECH and related academic genealogy

Young-Rok Jang^{1*}, Kicheon Kang²

¹Department of Physics, Incheon National University, Incheon 22012, Korea

²Department of Physics, Chonnam National University, Gwangju 61186, Korea

2021년 2월 정년퇴임 예정인 민병일 교수는 1987년 POSTECH 물리학과에 부임한 이후 지난 34년 동안 21명의 박사를 배출하며 자성 이론 분야의 교육과 연구에서 많은 기여를 하였다. 그가 학생들을 지도하며 학술지에 게재했던 논문들을 분석해서 국내 자성 이론 분야에 기여한 업적들을 살펴보고, 또한 그의 학문적 계보와 연관된 물리학자들에 대해서 간단하게 소개한다. 그의 석사과정 지도교수는 장희익(서울대)인데, 연관된 학문적 계보는 Joseph Callaway (Louisiana State University), Eugene Wigner (Princeton University), Michael Polanyi (TU Berlin) 등으로 거슬러 올라간다. 그의 박사과정 지도교수는 Arthur J. Freeman (Northwestern University)인데, 연관된 학문적 계보는 John Clarke Slater (MIT), Percy Williams Bridgman (Harvard University), Wallace Clement Sabine (Harvard University) 등으로 거슬러 올라간다. 그가 POSTECH에서 지도했던 박사과정 학생 21명 중 7명은 Many-body theory, 14명은 Electronic structure theory 분야로 분류할 수 있다. 박사 21명 외에도 (석사와 박사를 모두 지도한 학생들은 제외하고) 석사 4명을 배출하였으며, 함께 연구했던 박사후연구원 6명 중 4명은 외국인이었다. 그의 논문들 제목에서 키워드를 중심으로 분석하여 연구 주제 변화를 살펴보고, 이것을 바탕으로 해서 국내 자성 이론 분야의 발전 방향에 시사를 주는 사항들을 제시하고자 한다.

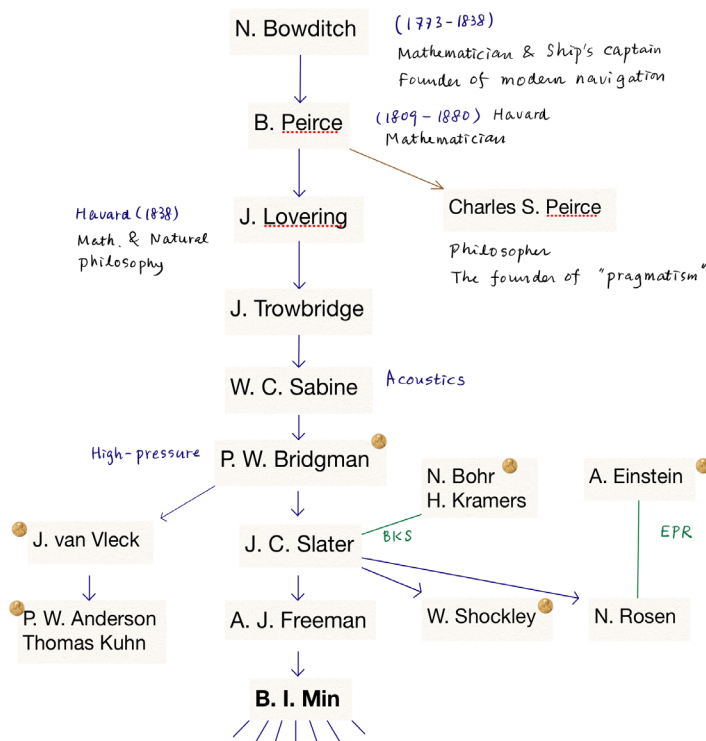


Fig. 1. Academic genealogy of Prof. B. I. Min

Valley magnetic domain: A new pathway to valleytronics

J.D. Lee^{*}

Department of Emerging Materials Science, DGIST, Daegu 42988, Korea

In the electron-doped monolayer (1L-) MoS_2 , an applied strain leads to the unbalanced Berry curvatures centered at K and $-K$ points and eventually the valley magnetization under an external electric field. This is shown to develop a novel concept of the valley magnetic domain (VMD), i.e., a real-space homogeneous distribution of the valley magnetization. A realization of VMD guarantees a sufficient number of stable valley-polarized carriers, one of the most essential prerequisites of the valleytronics. Further, we discover the anomalous electron dynamics through the VMD activation and achieve a manipulation of the anomalous transverse current with the uniaxial strain as a control parameter, directly accessible to the signal processing. The bilayer (2L-) MoS_2 has vanishing Berry curvatures at both K and K' valleys due to the inversion symmetry. When a vertical electric field is applied to 2L- MoS_2 , however, conduction bands are split due to a potential difference and become to restore the valley-selective Berry curvatures. In contrast to the uniaxial strain in 1L- MoS_2 , the vertical electric field can be employed as a control parameter to bring about the VMD activation and the anomalous transverse current in 2L- MoS_2 . This suggests a concept of VMD to provide a new physical insight to the valleytronic functionality and its manipulation to be a key ingredient of potential device applications

Time-dependent density functional theory calculations of spin-phonon dynamics and band topology of two-dimensional materials

Noejung Park^{*}, Mahmut Okyay, Bum Seop Kim

Department of Physics, UNIST, 44919, Ulsan, Korea

Topological states have commonly been cited as a new classification of materials, and global properties immune to local perturbations have been suggested in terms of topological invariants or associated quantities. For real materials, actual computations for them have been achieved through the theories of linear responses over the static ground electronic structure. In this talk, I first summarize our proposal for alternative ways of computation: calculating the real-time evolution of the Hamiltonian, letting the pumping parameter run periodically through the geometric space of the Hamiltonian. As test examples of this method, we present a trivial insulator, a spin-frozen valley-Hall system, a spin-frozen Haldane-Chern insulator, and a quantum spin-Hall insulators. In later part, we also demonstrate the spin precession dynamics of MoS_2 , in which the spin is strongly coupled to the optical phonon. This dynamical spin state can be resolved into discrete Floquet-phononic spectra, and once the phonon is pumped so as to break time-reversal symmetry, the resulting spin-Floquet structures induce net out-of-plane magnetizations in the otherwise non-magnetic 2D material.

Towards Rare–Earth and Rare–Earth–Free Permanent Magnets Designed Using First–Principles

Dorj Odkhuu^{1*}, T. Ochirkhuyag¹, D. Tuvshin¹, T. Tsevelmaa², S. C. Hong²

¹Department of Physics, Incheon National University, South Korea

²Department of Physics, University of Ulsan, South Korea

Permanent magnets are vital for future energy conversion and storage sectors such as electric vehicles, bullet trains, wind turbines, satellites, and to list a few. In order for permanent magnets to achieve large energy density product (BH_{\max}), magnetic materials with high saturation magnetization (M_s) and high uniaxial magnetic anisotropy (K_u) are essential. Not only those but also good thermal stability and high Curie temperature (T_c) are required to fulfill for practical applications. Furthermore, reducing the cost to produce the materials is also required. Optimization of the properties is so difficult that a new high performance permanent magnet is not realized yet since discovery of Nd-Fe-B magnets even though some materials such as R_2Fe_{17} , $R(Fe,M)_{12}$, $L1_0$ Mn-based alloys etc. Here R stands for rare-earth elements and M does for transition metals.

In this talk, first we will present what physical properties we should calculate by reviewing magnetic properties of a permanent magnet. Next, we will discuss our recent computational results of $Sm(FeCo)_{12}$, FeCo, FeNi, and some Mn-based alloys. Finally, we hope to suggest the way how to have a new optimal permanent magnet using first-principles design.

Supported by Future Materials Discovery Program (2016M3D1A1027831) through NRF funded by the Korea government (MSIT) and by the Korea Institute of Energy Technology Evaluation and Planning (KETEP) grant funded by the Korea government (MOTIE) (20192010106850, Development of magnetic materials for IE4 class motor).

Discovery of van der Waals magnets and beyond

Je-Geun Park^{1,2*}

¹Center for Quantum Materials, Seoul National University, Korea

²Department of Physics and Astronomy, Seoul National University, Korea

The discovery of graphene in 2004 took the scientific community by surprise and virtually transformed the research landscape of materials science and engineering by creating a then-new field of 2d materials. However, despite the unique properties of many van der Waals materials since discovered, it has certain limitations in exploring novel and new physical properties. Magnetism is a case in point.

Until I and a couple of other groups started to work on the much-neglected magnetic van der Waals materials, virtually nothing was known about it. However, with a series of publications, including those from my group [1-8], this field of magnetic van der Waals materials has become a fast emerging field in materials science. In this presentation, I would like to take you through the intellectual journey I made since 2010 and eventually discovering a novel quantum spin-entangled exciton NiPS_3 more recently [8]. I will end my talk by giving a personal view of the prospects for future research.

References

- [1] Je-Geun Park, J. Phys. Condens. Matter 28, 301001 (2016)
- [2] Cheng-Tai Kuo, et al., Scientific Reports 6, 20904 (2016)
- [3] Jae-Ung Lee, et al., Nano Lett. 16, 7433 (2016)
- [4] So Yeun Kim, et al., Phys. Rev. Lett. 120, 136402 (2018)
- [5] K. S. Burch, D. Mandrus, and Je-Geun Park, Nature 563, 47 (2018)
- [6] Kangwon Kim, et al., Nature Comm. 10, 345 (2019)
- [7] H Chu, et al., Phys. Rev. Lett. 124, 027601 (2020)
- [8] S. Kang, et al., Nature 583, 785 (2020)

ARPES study of a Multifold Fermionic Semimetal PdSb2

Woo-Ri Ju¹, Jinwon Jeong¹, En-Jin Cho¹, Han-Jin Noh^{1*}, Kyoo Kim², Byeong-Gyu Park³

¹Dep. Of Physics, Chonnam National University, Gwangju, Korea

²Korea Atomic Energy Research Institute, Daejeon, Korea

³Pohang Accelerator Laboratory, Pohang University of Science & Technology, Pohang, Korea

The experimental confirmation of the Dirac/Weyl fermions in topological semimetals invokes parallelism between particle physics and condensed matter physics. However, condensed matter physics has higher degrees of freedom because it is not limited by the Poincare symmetry. Type-II Dirac/Weyl fermions are the first example that shows such degrees of freedom. Recently, another type of unconventional quasiparticles that shows the flexibility has been proposed in several groups of materials, named multifold fermions. Multifold fermions are also called unconventional quasiparticles with a large Chern number, which have no high-energy counterpart. They are not only conceptually interesting, but also expected to have intriguing physical properties due to their topologically non-trivial nature. In this talk, we will present our recent ARPES data to confirm the multifold fermions in a semimetal PdSb2.

Textured Spin Singlets in an infinite layered nickelate

Kwan-Woo Lee*

Division of Display and Semiconductor Physics, Korea University, Sejong
Department of Applied Physics, Graduate School, Korea University, Sejong

Layered nickelates, pursued for three decades because of their similarity to high superconducting T_c cuprates, have received a strong boost from the discovery of superconductivity in strained nickelate thin films. Using correlated density functional methods, we study a new and highly unusual new nickelate, synthesized under pressure and with a strongly strained NiO_2 plane of “infinite layer” structure. It is, according to the experimental paper, a unique $d^8 \text{Ni}^{2+}$ ion showing magnetic behavior, although the peculiar susceptibility is unexplained. The susceptibility shows no evidence of a magnetic moment (no Curie-Weiss term), but a peak at 130K before return to the previous value, that has no obvious explanation.

The overriding features we find are (1) magnetic Ni but violation of Hund's rule, which is a rare occurrence, (2) unconventional spin-orbital polarization, leading to an unprecedented “off-diagonal singlet” (ODS) with textured magnetic internal structure of compensating $d(x^2-y^2)$ up spins with $d(z^2)$ down spins, but vanishing net spin. (3) We provide a minimal spin model for this system, which we propose to have a new type of phase transition. Finally, (4) we suggest that electron doping toward the d^9 regime will produce new phenomena (due to the singlet nature) and perhaps superconductivity. We anticipate that this work will stimulate many new investigations of this nickelate and related systems.

Acknowledgements

These researches were collaborated with Hyo-Sun Jin and W. E. Pickett. This research was supported by NRF of Korea Grants NRF-2019R1A2C1009588.

References

[1] H.-S. Jin, W. E. Pickett, and K.-W. Lee, Phys. Rev. Research 2, 033197 (2020).

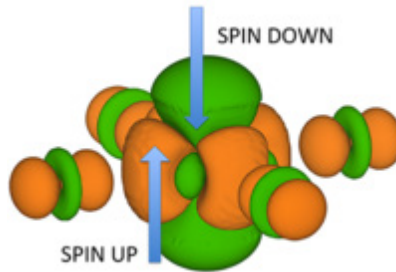


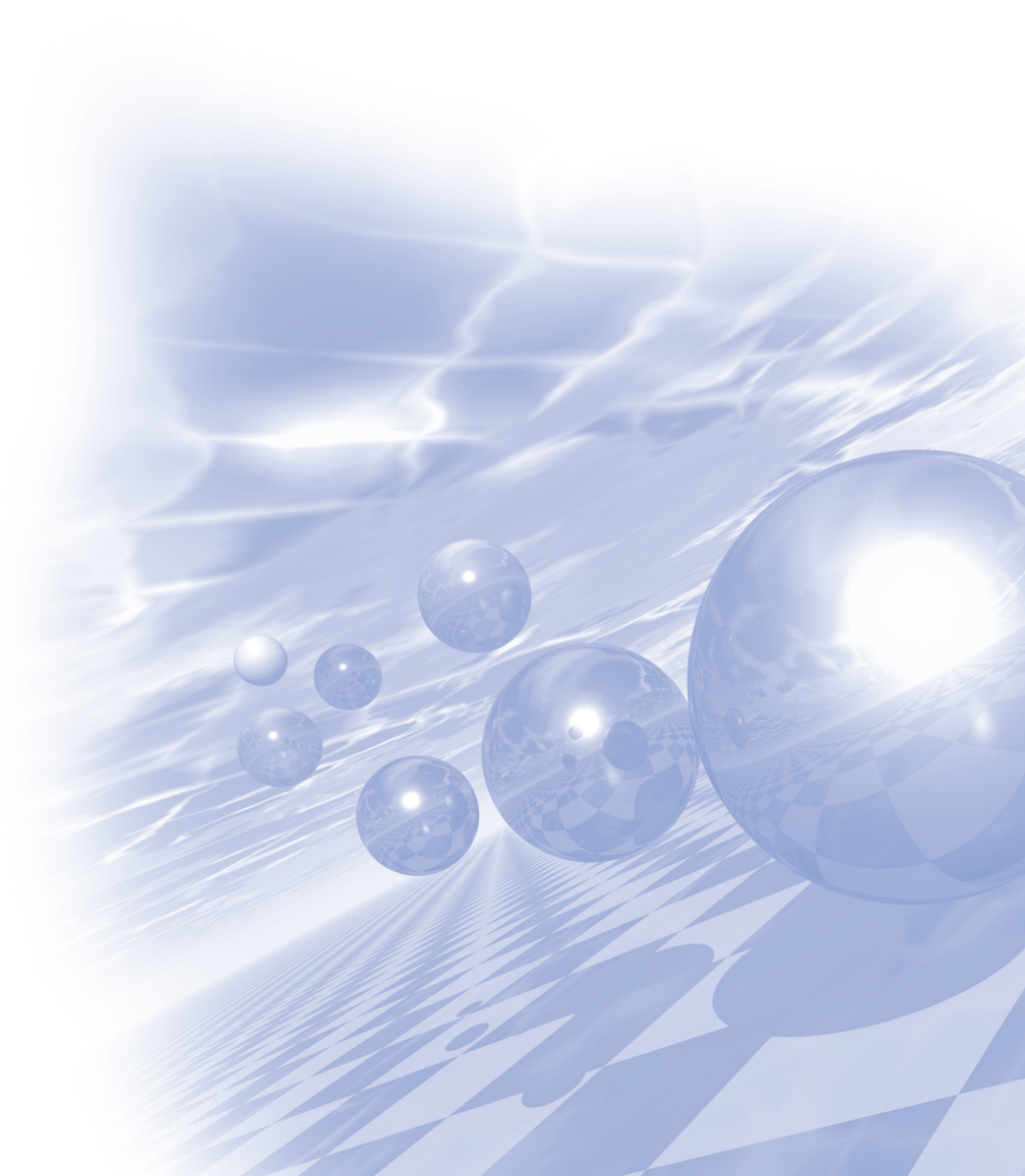
Fig. 1. Off-diagonal singlet



KMS 2020 Winter Conference

Special Session V

**‘Electro–Magnetic Energy
Convergence : MOTOR Session’**



Electromagnetic Force and Vibration Analysis of Outer Rotor Surface–Mounted Permanent Magnet Synchronous Motor

Jae-Hyun Kim¹, Soo-Hwan Park¹, Min-Ro Park², Soo-Gyung Lee¹,
Kyoung-Soo Cha¹, Myung-Seop Lim^{1*}

¹Department of Automotive Engineering, Hanyang University, Seoul, Korea

²Interactive Robotics R&D Division, Korea Institute of Robotics & Technology Convergence,
Pohang, Korea

*Corresponding author: myungseop@hanyang.ac.kr

Since electric motors with outer rotor have advantages such as higher torque density and less joule loss compared to electric motors with internal rotor, electric motors with outer rotor are widely used for various applications. The noise of the electric motor with outer rotor is one of the most important performance indicators especially when it is used for home appliances. Generally, the noise of the electric motor caused by the radial electromagnetic force acting on the outer part of the electric motor. As shown in Fig. 1, in the case of the electric motor with internal rotor, the radial force acts on the stator, which is a fixed part. On the other hand, in the case of the electric motor with outer rotor, since the radial force acts on the rotary part, the relative speed of the radial electromagnetic force and the rotor should be considered.

Therefore, in this paper, the frequency and spatial harmonic order of the radial electromagnetic force acting on the rotor of electric motor with outer rotor are analytically derived. The sources of the radial electromagnetic force are analytically derived by dividing it into permanent magnet (PM) magneto-motive force (MMF), armature reaction MMF, and slot effects. The frequency and the spatial harmonic order of the radial electromagnetic force acting on the rotor are summarized in Table I. Noise test of the prototype was conducted to validate the analytically derived results as shown in Fig. 2. The prototype is 48 pole 36 slot electric motor with outer rotor for direct drive system. The frequency of the radial electromagnetic force acting on the rotor is generated as multiple of $1.5f$, as can be derived from Table I. This result corresponds well with the noise test result as shown in Fig. 2. (b).

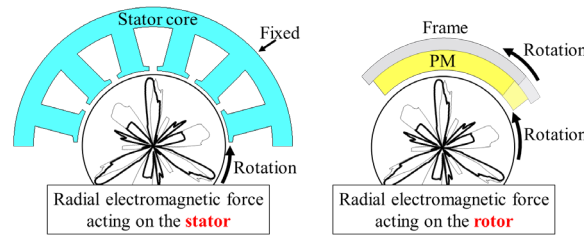
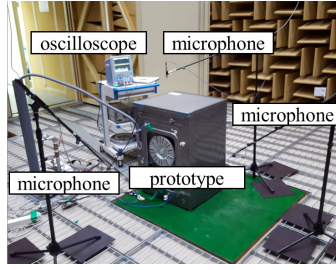


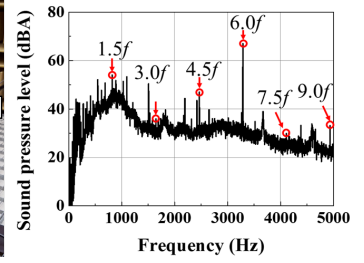
Fig. 1. Configuration of radial force in inner rotor and outer rotor

Cause	Spatial harmonic order	Frequency
PM MMF	$p(\mu_1 \pm \mu_2)$	0
Armature MMF	$p(v_1 \pm v_2)$	$\{(1 - v_1) \pm (1 - v_2)\}f$
PM MMF & armature MMF	$p(v \pm \mu)$	$(1 - v)f$
MMF & slot effects	$p(\mu_1 \pm \mu_2) - ks$	ksf / p
	$p(v_1 \pm v_2) \pm ks$	$\{(1 - v_1) \pm (1 - v_2) \pm ks / p\}f$
	$p(v \pm \mu) \pm ks$	$\{(1 - v) \pm ks / p\}f$

Table I. Frequency and spatial harmonic order of radial force



(a)



(b)

Fig. 2. Noise test setup and results.
(a) Noise test setup. (b) Noise test results.

*Corresponding author: myungseop@hanyang.ac.kr

토크밀도 향상을 위한 로봇 구동용 SPM 동기전동기 설계에 관한 연구

김광용^{1†}, 김동욱², 이근호², 김성일^{1*}

¹Hoseo University, Korea

²Kookmin University, Korea

본 논문에서는 로봇 구동용으로 적용되는 표면부착형 영구자석 동기전동기(Surface-Mounted Permanent Magnet Synchronous Motor, SPMSM)의 토크밀도 향상을 위한 설계 과정을 제시하였으며, 설계 모델의 다양한 특성들을 유한요소해석을 통해 비교 검토하였다. 최종적으로 제작된 설계 모델의 성능 평가를 통해 설계 과정에 대한 타당성을 검증하였다.

	기본 모델	설계 모델
극 수/슬롯 수	20/24	20/18
영구자석 Br [T]	1.0	1.4
영구자석 타입	링	세그먼트
영구자석 부피 [mm ³]	1600.38	1066.87
코일 선경 [mm]	0.5	0.7
상당 직렬 턴 수	114	132
권선 방식	집중권	
병렬 회로 수	4	2
고정자 적층 길이 [mm]	7 (회전자 12)	7
입력 전압 [Vdc]	48	
정격 속도 [rpm]	3500	

표 1. 기본 및 설계 모델 사양 및 제원

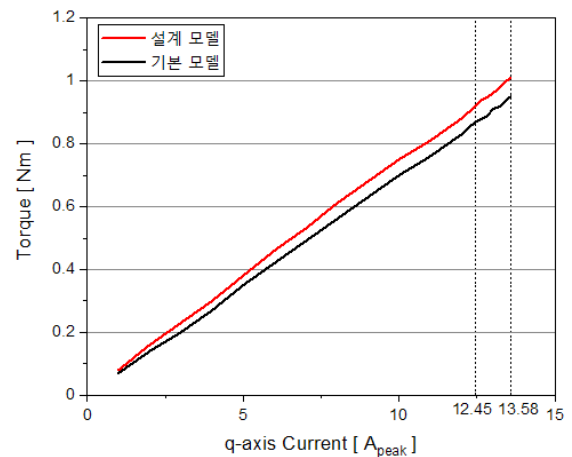
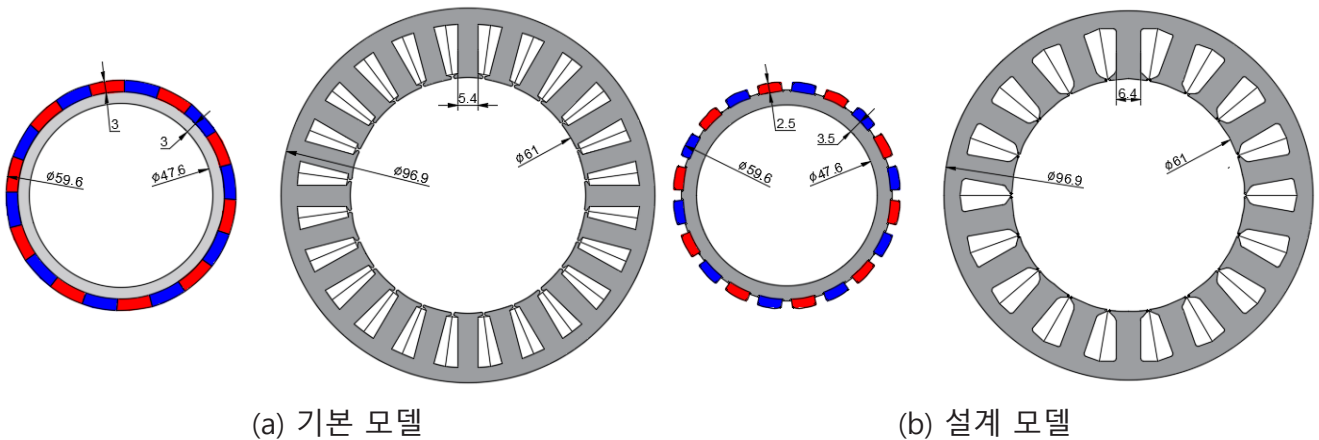


그림 1. 기본 및 설계 모델의 전류별 측정 토크



(a) 기본 모델

(b) 설계 모델

그림 2. 기본 및 설계 모델의 형상치수 비교

시간별 1일 부하변동을 고려한 에스컬레이터 시스템의 에너지 측정 및 추정

김해중^{1*}, 윤명환², 이정종²

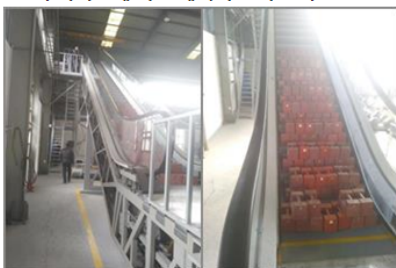
¹경남도립남해대학

²한국전자기술연구원

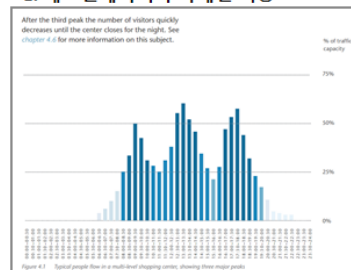
ISO 25745-1에서는 에스컬레이터의 전력 측정에 관해 규정하고 있고, ISO 25745-3에서는 에너지의 추정 방법 및 에너지 등급에 대해 규정하고 있다. 에스컬레이터의 전력 측정을 위해서는 우선 주 전원 결합지점에서 주 전원선에 에너지미터를 연결하여 주 전력을 측정하고, 보조 전원 결합지점에서 보조 전력을 측정한다. 전력의 측정은 에스컬레이터의 동작상태에 따라 각각 측정되어야 하는데, 승강기가 정지한 상태에서 전원을 켜고 스탠바이 상태의 전력이 측정되고, 정지상태에서 승객이 감지되면 자동으로 시작되는 조건에서 자동상태의 전력이 측정된다. 또한 승객을 태우지 않고 저속으로 가동하는 상태에서 저속상태의 전력이 측정되고, 승객을 태우지 않고 공칭속도에서 무부하상태의 전력이 측정된다. 이렇게 측정된 전력에 ISO 25745-1에서 제시하는 운전프로파일을 적용하여 무부하상태에서의 1일 총 에너지를 추정할 수 있다. 부하하중에 대한 1일 소비에너지 추정은 ISO 25745-3에서 제시하는 수식을 이용한다. 무부하상태의 1일 추정에너지와 부하하중에 대한 1일 추정에너지를 더하여 대상 에스컬레이터의 1일 소비에너지를 추정할 수 있다.

그런데 ISO 25745-3에서 제시하는 부하하중에 대한 1일 소비에너지 추정은 1일 승객 수와 이동 거리 및 높이, 마찰계수와 에스컬레이터 시스템 효율을 단순화 하여 계산한다. 그로 인해 에너지의 추정에 있어서 큰 오차를 가질 수 밖에 없다. 본 논문에서는 이러한 오차를 줄이기 위해 에스컬레이터의 부하패턴을 고려하여 에너지를 추정하였다. 우선 대상 에스컬레이터에서 분동을 이용하여 부하하중 별로 소비에너지를 측정하였다. 부하하중에 대한 소비에너지를 선형보간하여 1일 부하패턴에 적용하였다. 이를 통해 시간대별 30분당 승객 수를 산정하고, 상승 및 하강 1회당 부하하중을 산정하였으며, 산정된 결과를 이용하여 1인당 부하하중 소비에너지를 추정하였다. 30분당 승객 수와 1인당 부하하중 에너지를 고려하여 1일 상승/하강 소비에너지를 추정하였다. ISO 규정과 제시한 방법의 추정결과를 비교하여 오차를 확인하였다.

1. 부하하중에 따른 에너지 소비량 측정



2. 에스컬레이터 부하패턴 적용



3. 1일 부하상태 에너지 소비량 계산

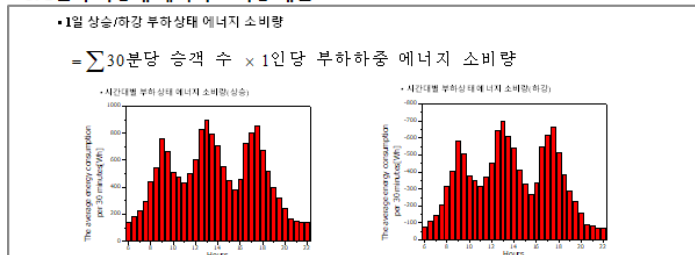


그림. 1. 부하패턴을 고려한 부하하중 에너지 소비량 추정 개념

A Design of Halbach Cylinder Shape Sintered Nd-Fe-B Magnets for Servo Motors

김효준*, 김상면

자화전자(주)

브러시리스 DC (BLDC) 모터의 설계에 있어서, Halbach 배열과 같은 높은 공극 자속 밀도를 갖는 영구 자석 로터가 관성과 무게를 줄이고 더 높은 전력 대 부피 비율을 얻기에 더 매력적이다. 현재까지 문헌에 제시된 Halbach 로터 디자인은 미리 자화된 여러 개의 분할 자석을 사용해 하나의 실린더 형태를 구성해야하기 때문에, 로터를 제조하는 것은 복잡한 과정을 거쳐야하는 불편함이 있을 뿐만 아니라 그 공극 자속밀도가 이상적인 정현파형을 나타내지 못하는 문제점이 있다. 본 연구에서는 Nd-Fe-B소결 자석을 성형하는 단계에서 자석 분말을 Halbach 배향을 갖도록 하는 자기장 시스템의 새로운 설계가 제안되었다. 주요한 설계 매개 변수의 영향은 2-D 유한 요소 분석에 의해 조사되고, 결과는 실험적으로 검증해 소개하고자 한다.

해석적방법을 이용한 표면부착형 영구자석 기기의 가진원 해석

이훈기[†], 최장영^{*}

Department of Electrical Engineering, Chungnam National University, 99 Daehak-ro,
Yuseong-gu, Daejeon 34134, Korea

에너지 밀도가 높은 회로류계 영구자석의 사용으로 표면부착형 영구자석 기기는 산업 전반에 필수적인 요소가 되었다. 이에 따라 제품의 소음, 진동에 대한 소비자의 요구조건이 늘어나게 됨으로써 동력을 발생시키는 전동기의 소음, 진동 특성에 대한 연구가 활발히 진행되고 있으며 설계 단계에서 전자기적인 가진원을 고려하여 보다 소음 및 진동에 대한 강건한 설계 및 특성에 대한 관심이 높아지고 있다. 영구자석 기기의 전자기적 가진원은 역기전력 THD, 코깅토크, 토크 리플, 그리고 공극에서 발생하는 불평형 전자기력으로 나타나며 이와 같은 전자기적 가진원 특성을 해석하는 방법으로 유한요소법과 해석적방법이 있다. 유한요소법의 경우 수치해석적인 방법 중에 하나로 해석 시 상용 툴을 이용하여 해석 수행을 할 수 있어 해석의 용이성이 높으나 사용되는 상용 툴 마다의 사용 방법을 익혀야 하고, 해석 모델의 형상이 복잡할수록 요소 분할이 어려워져 설계자의 경험에 의존하게 된다는 단점을 가지고 있다. 해석적방법은 맥스웰 방정식을 이용한 전자계 특성을 해석하는 것으로 정확도가 높고 빠른 해석이 가능하지만 이를 위해서는 푸리에 급수를 이용한 자화모델링의 정의, 맥스웰 방정식과 자기 벡터 포텐셜을 통해 도출되는 편미분 방정식을 기기의 형상에 맞는 다양한 경계조건을 고려하여 해를 도출하는 것이 선행 되어야하며 자기포화현상을 고려할 수 없는 단점이 있다. 해석적 방법은 유한요소법과 비교했을 때 빠른 해석 시간의 장점이 있고 설계 파라미터에 직관적으로 특성 변화를 예측할 수 있기에 꾸준한 연구가 수행되고있다. 먼저 해석적 방법의 초기 연구는 슬롯리스 형태의 전기기기에 대한 많은 2 차원 해석 모델이 제안되었으며 대부분이 개방 회로 해석에 중점을 두었다. 철의 비투자율을 무한하다고 가정한다면, 슬롯리스 영구자석 기기는 매우 간단하며 단순한 영역에서 프아송 및 라플라스 방정식을 계산하면 공극에서의 자기장을 예측 할 수 있다. 슬롯리스 영구자석 기기에 대한 또 다른 해석 방법은 해석 영역을 나누고 지배방정식으로부터 각 영역의 포텐셜을 계산하고 경계 조건을 이용하여 미정계수를 계산함으로써 해석적 방법의 연구가 활발히 진행되었다. 해석적 방법을 이용한 영구자석 기기의 해석 시 어려운 문제 중 하나는 고정자 측 슬롯의 존재로 인한 슬롯팅 효과를 고려하는 것이다. 영구자석 기기는 회전자와 고정자 사이 공극에서 자기장을 통한 에너지 변환이 발생하고 이는 전자기적 가진원의 원인이 되므로 정확한 공극 자계의 예측이 필수적이다. 고정자 및 회전자 슬롯의 존재는 공극 자계 분포를 왜곡시킨다. 그러므로 슬롯 현상을 고려하지 않고 영구자석 기기를 해석하게 된다면 전자기 특성에 대한 정확한 결과를 예측하기 어렵게 되므로 슬롯의 형상을 고려하여 자계 특성을 도출하고 이를 이용하여 가진원 분석을 수행하여야한다.

따라서 본 논문에서는 해석적 방법을 이용하여 영구자석 기기의 자계 특성 및 가진원 특성 도출을 수행하였다. 일반적으로 많이 사용되는 치집중권의 극/슬롯 조합인 8극12슬롯, 8극9슬롯, 10극12슬롯, 그리고 10극9슬롯 모델을 서브도메인 방법을 통해서 각 영역에 대해서 자기벡터포텐셜을 기반으로 지배방정식 도출하였으며, 도출한 일반해를 통해서 자속밀도를 계산하고 이를 이용하여 가진원 특성을 계산하였다. 해석적 방법을 통해서 도출된 유한요소 해석 결과와 비교함으로써 검증하였다.

A Study on the Electromagnetic Field Design of BLDC Motor For Electric Outboard Propulsion

Ho-Joon Lee*, Jae-Sung Woo, Dong-Hyun Kim

Converged Electronic Engineering, Cheongju University, Korea

Abstracts All of the outboard units of small ships in use in domestic depend on imports, and most of them are obsolete and the need for repairs is increasing. In addition, the supply and demand of replacement parts is difficult, and additional cost and time are required, so the development of high-power motors for electric outboard motors is essentially needed. Therefore, this paper manufactured a prototype through a study to improve the power density of a 4HP-class electric outboard BLDC motor, and verified its performance through a test.

Table. 1. Performance Comparison of BLDC Motor Models

Parameter	Outer Rotor#1	Outer Rotor#1	Inner Rotor	Final Model
DC Link Voltage	32.3	26	34	27
Average Torque [Nm]	9.30	8.86	8.68	8.59
Core Loss [W]	38.76	122.35	89.44	31.1
Eddy Current Loss [W]	152.03	129.64	154.13	52.94
Copper Loss [W]	141.37	37.0	52.89	48.63
Winding Resistance [ohm]	0.004876	0.001085	0.00481	0.004969
Efficiency [%]	89.7	90.5	90.2	95.3
Current Density [A/mm ²]	12.22	4.28	5.96	3.77



Fig. 1. Prototype of BLDC motor for Electric Outboard Propulsion

Torque Improvement Design of Interior Permanent Magnet Synchronous Motor considering Saturation of Rotor Core

Myung-Hwan Yoon*, Ki-Deok Lee, Se-Hyun Rhyu, Jeong-Jong Lee

Intelligent Mechatronics Research Center, Korea Electronics Technology Institute, Korea,
yoonmh@keti.re.kr

Synchronous motors applying interior permanent magnet have many merits such as high torque density, efficiency and a wide speed range which is very important issue. Therefore, the IPMSM motors are used in various field for example cars, military, and home application. However, there is a problem of the IPMSM which is torque ripple. The torque ripple is necessary to be reduced to the zero because the torque ripple affect vibration and acoustic noise. The total resultant instantaneous torque is composed of three components which are magnetic torque, reluctance torque and cogging torque. The magnetic torque is generated by interaction of the permanent magnet, or rotor field, and the armature which may be the stator part. However, the reluctance torque is occurred by the variation of self-inductance of the phase windings which are affected by unequal permeances of the d-axis and q-axis. Final one is the cogging torque which is generated by the interaction of permanent magnet and stator slots. Therefore, there can be three reasons for the torque ripple which are the non-sinusoidal flux density distribution around the air gap, reluctance torque and cogging torque. Many methods are tried to reduce torque ripple and there are two concepts. One is the point view of design side and the other one is the control. This paper suggests the design method of designing the saturation of rotor core to make the flux distribution around the air gap more sinusoidal. This method is helpful to reduce torque ripple and increase the average torque at the same time. The optimized model of using this method is obtained by response surface method which is presented in Fig. 1. The shape of original model of rotor core and the improved model is shown in Fig.2.

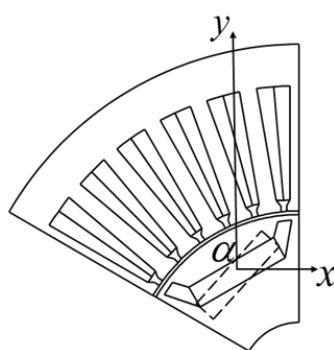


Fig. 1. Setting of Response Surface Methodology

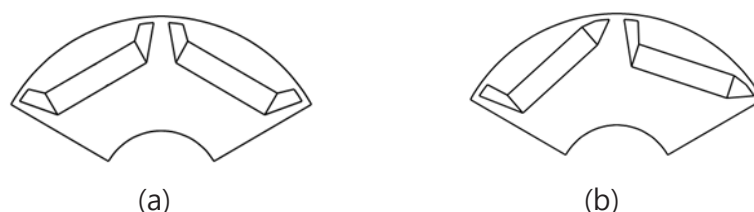


Fig. 2. Shape of Rotor Core (a) Original Model (b) Improved Model

Rotor Design of Ultra-high-speed Motor for Electric Turbo Charger Considering Mechanical Stiffness

Sung-Hyeok Wi[†], Soo-Gyung Lee, Jun-Yeol Ryu, Sung-Woo Hwang, Soo-Hwan Park, Myung-Seop Lim^{*}

Department of Automotive Engineering, Hanyang University, Seoul, Korea

^{*}Corresponding author: myungseop@hanyang.ac.kr

Recently, turbo chargers have been used to improved efficiency and power of the powertrain. The turbo chargers increase the charging efficiency of the mixed gas by driving the turbine using exhaust energy. However, turbo lag can occur due to small exhaust energy when engine speed is low. To reduce the turbo lag, ultra-high-speed motor is necessary to drive the turbine at low speed of the engine. As a result, research on ultra-high-speed motors for turbochargers has been studied. As the ultra-high-speed motor is driving at much high speed than the other motors, the rotor is affected by high centrifugal force due to its high speed. Therefore, to analyze which part of the rotor is fragile at high speed is important. For this purpose, the stress on each part of the rotor should be analyzed when designing the ultra-high-speed motor. The stress can be calculated by finite element method but it is inefficient because it requires much time to compute the partial differential equations. Thus, it is better to use the analctic method for calculating the stress of the rotor. Since the rotor shape of the ultra-high-speed motor has a simple shape, such as Fig. 1., the stress analysis is carried out using an analytical method.

In this paper, we designed the ultra-high-speed motor that satisfy mechanical stiffness and electromagnetic performance in consideration of design specifications. Analytical methods are used to select the rotor outer diameter range. The design process is as shown Fig. 2. Finally, proceed with verification of the mechanical stiffness and electromagnetic performance. Fig. 3. shows the results of the verification of mechanical stiffness by using FEM. The torque that satisfies the target is shown in the Fig. 4.

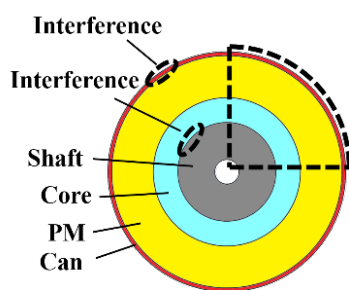


Fig. 1. Analysis model

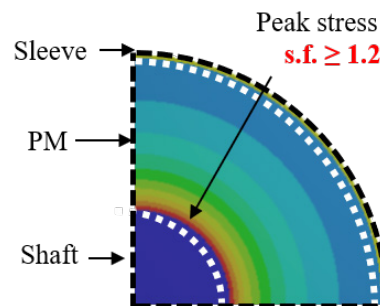


Fig. 2. Stress of the rotor

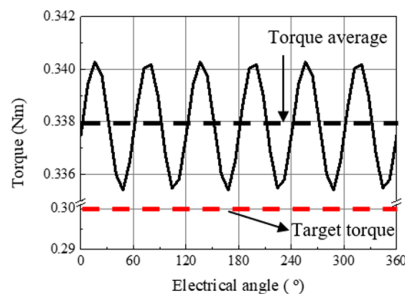


Fig. 3. Torque

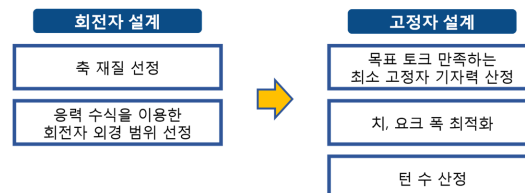
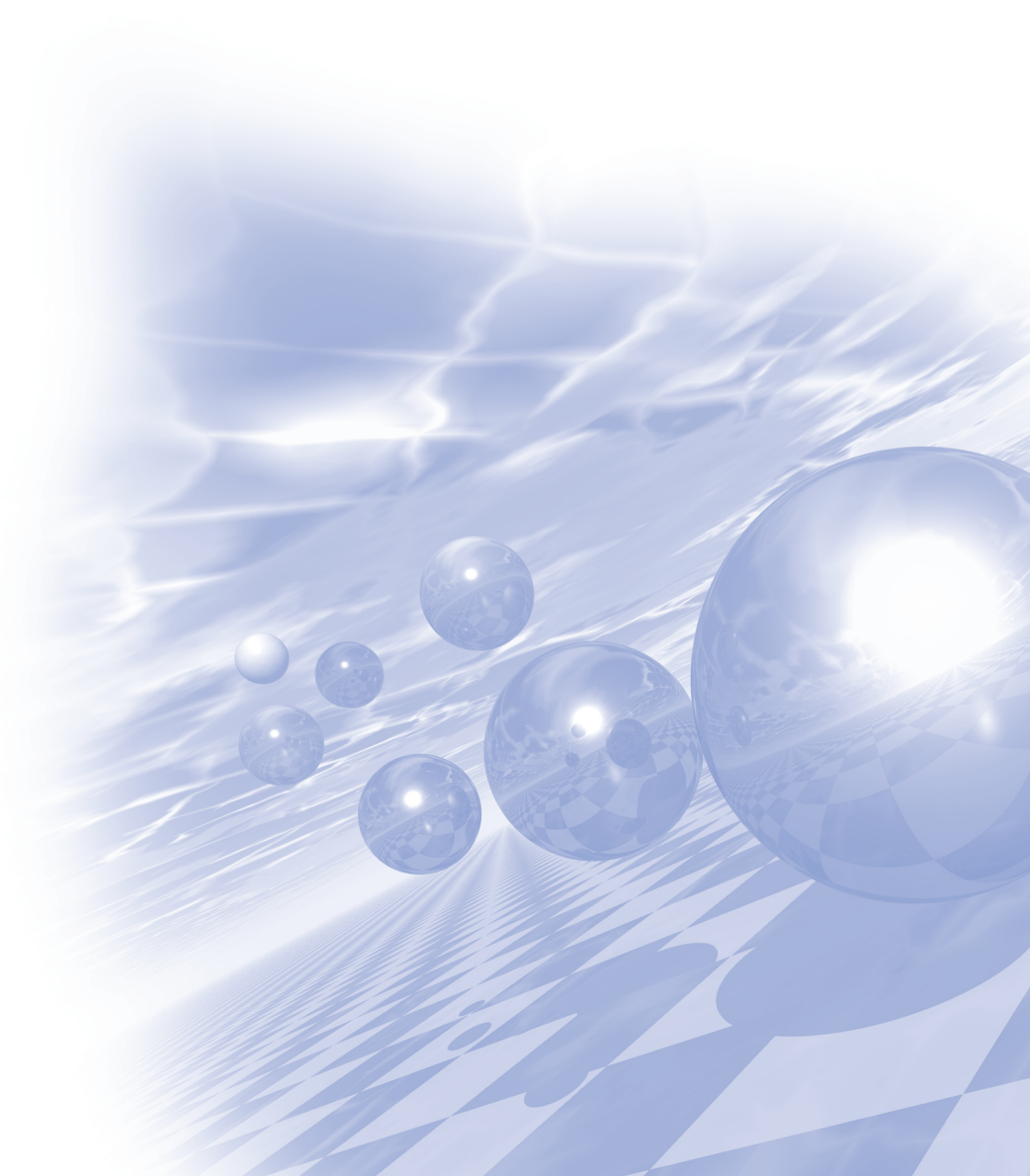


Fig. 4. Design process



KMS 2020 Winter Conference

스핀트로닉스 초청강연



Thermoelectric energy conversion utilizing spin degree of freedom

Hyungyu Jin (진현규)

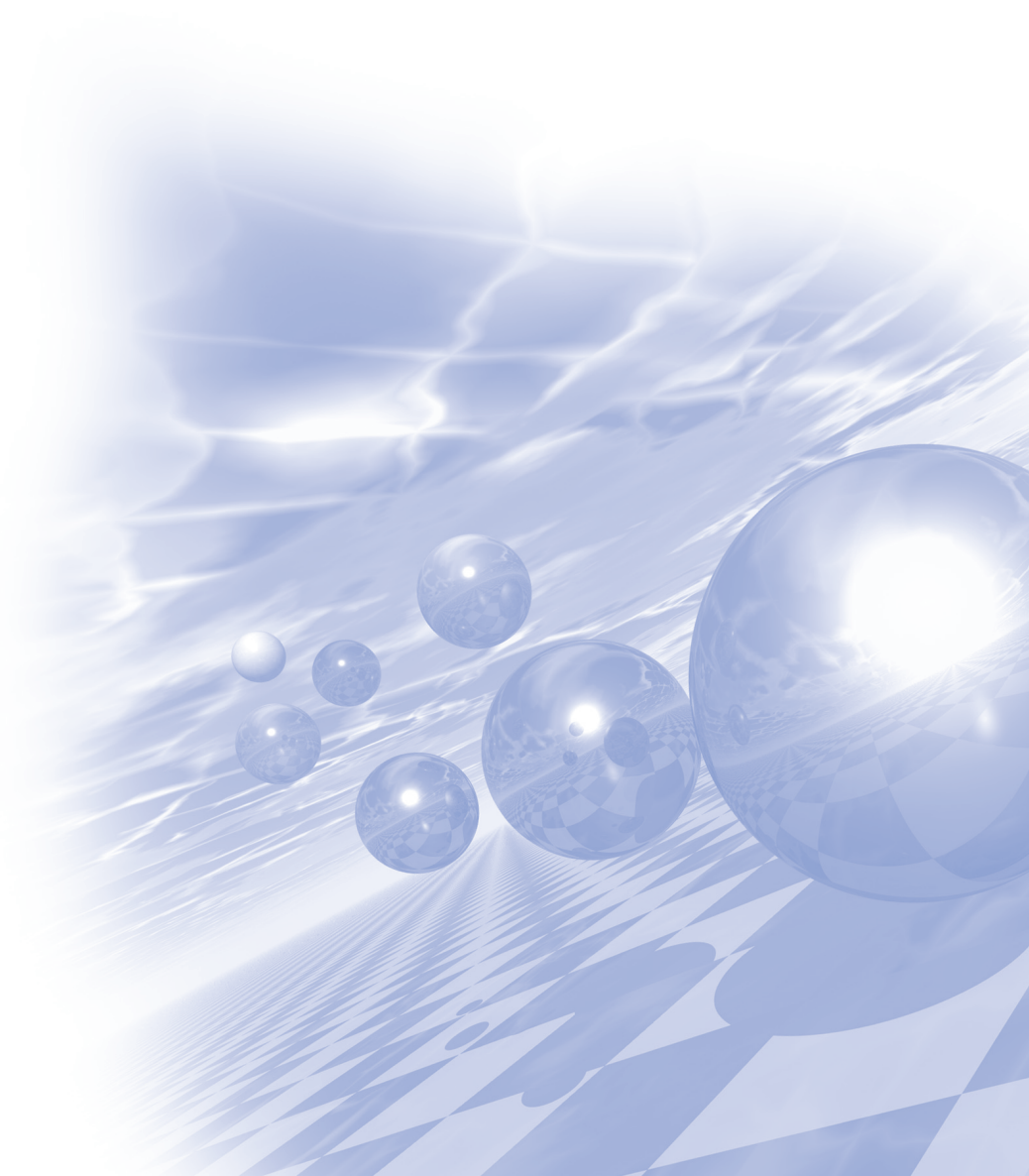
Department of Mechanical Engineering, Pohang University of Science and Technology
(POSTECH), Pohang, South Korea

The burgeoning field of spin-caloritronics studies interaction between electron spin and heat, and has led to the discovery of various novel phenomena such as spin-Seebeck effect, spin-Peltier effect, etc. In a broader context, the research field encompasses other spin-dependent thermomagnetic effects such as anomalous Nernst effect, anomalous thermal Hall effect, etc. Among those, the spin-Seebeck effect (SSE) and anomalous Nernst effect (ANE) have drawn particular interest due to their potential as a new solid-state heat-to-electricity conversion mechanism. In the SSE, a temperature gradient on a spin-polarized material creates a spin current that is driven into an adjacent material (Pt). There, the injected spin current is converted into a transverse electric field by the inverse spin-Hall effect via spin-orbit interactions. On the other hand, the ANE utilizes various skew scattering mechanisms of spin polarized electrons, which lead to a transverse electric field perpendicular to both of the applied temperature gradient and magnetization directions. A thermoelectric device based on SSE or ANE could have several advantages over that based on the conventional charge Seebeck effect. In this talk, a general introduction to SSE and ANE as well as our relevant research directions will be given, through which we show that the spin degree of freedom is emerging as a new design tool that adds to thermoelectrics research.



KMS 2020 Winter Conference

총회초청강연|



강일구박사님의 생애와 업적

김희중

한국과학기술연구원

1990년에 한국자기학회 창립을 주도하고 초대 회장과 2대 회장을 역임하신 학회의 원로 강일구박사님을 추도하는 특별한 모임을 학회 주관으로 가지게 되었습니다.

강일구박사님은 1931년 2월에 출생하셔서 서울대학교 금속공학과(학사), 영국 맨체스터대학교 임페리얼 칼리지에서 수학하신 후 귀국하셔서 서울대학교 금속공학과에서 박사학위를 받으셨습니다.

1961년부터 69년까지 영국 텔콘금속회사 연구원으로 재직할 때 개발하신 50-50 Permalloy합금 ‘Satmumetal’은 상품으로 출시되기도 하였습니다.

1969년에 귀국하여 1996년 은퇴하실 때까지 한국과학기술연구원에 근무하시면서 자성재료와 전기재료의 연구개발에 매진하여 많은 업적을 이루셨습니다. 동복강선(일진전기), 내열 알루미늄 송전선(LS전선, 대한전선), 반도체용 금본딩와이어(MK전자)가 대표적으로 상업화에 성공한 업적들이며 비정질과 나노결정 자성합금을 선도적으로 연구하셨습니다.

1990년 한국자기학회를 창립하신 후 학회 발전에 큰 기여를 하셨으며 1995년 ISPMM 1995, 1999년에 세계 최대의 자기학 학술행사인 Intermag 국제학술행사의 চে어맨을 맡으셔서 성공적으로 행사를 추진시켜 한국 자기학회의 위상을 국제적으로 크게 높이는 데도 큰 공헌을 하셨습니다.

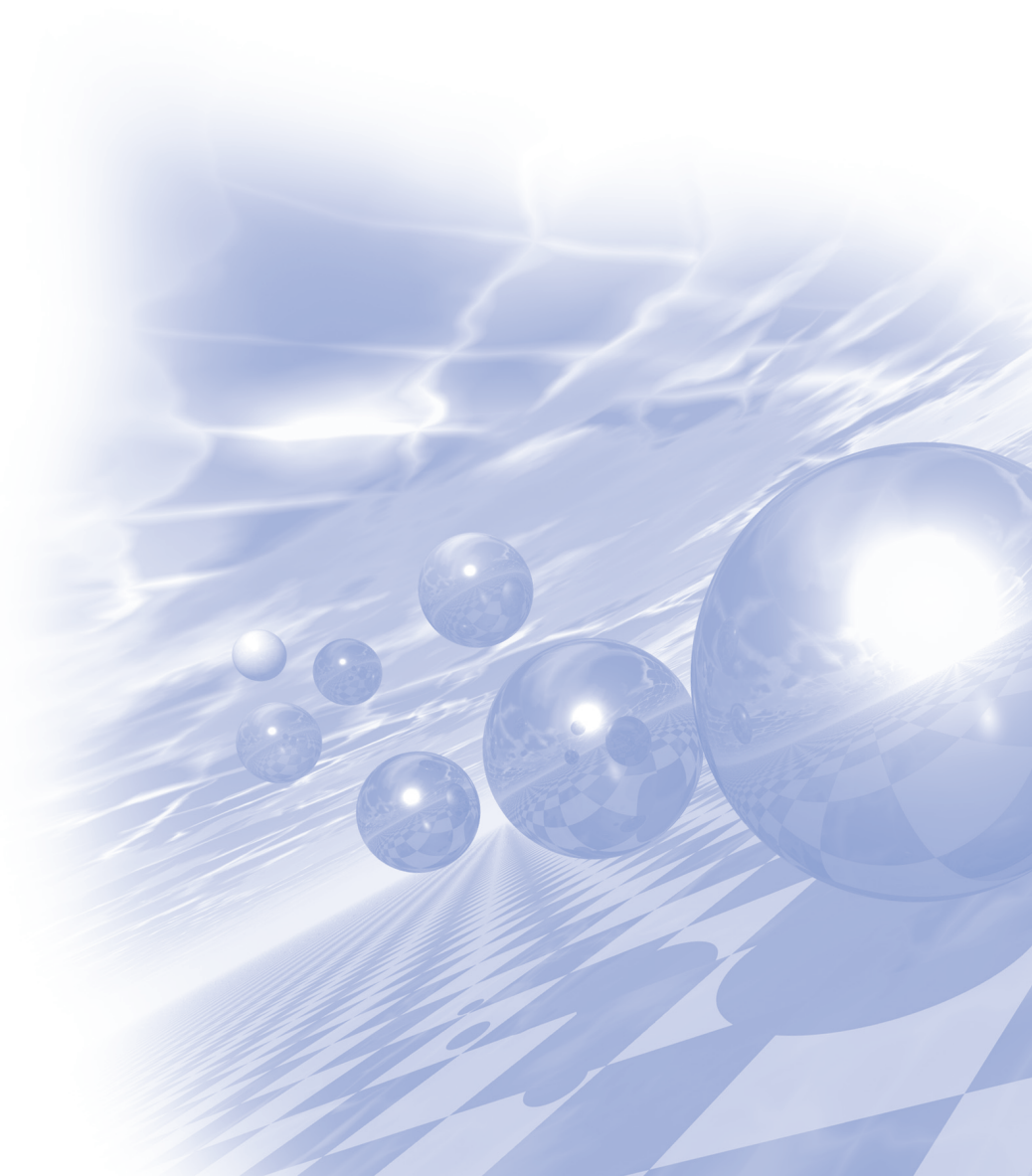
정부로부터 국민훈장 석류장(1981년)과 대한민국 과학기술상(1989년)을 받으셨으며 학술원으로부터 학술원상(1996년)도 수상하셨습니다.

이번 추도모임을 통해 강일구박사님의 업적을 기리고, 박사님의 공헌이 한국자기학회의 미래발전을 위한 초석이 되기를 기대합니다.



KMS 2020 Winter Conference

총회초청강연II



**2021년 이후 소재 · 부품분야 과학기술정보통신부
/ 연구재단 국책연구사업 소개**

이영국

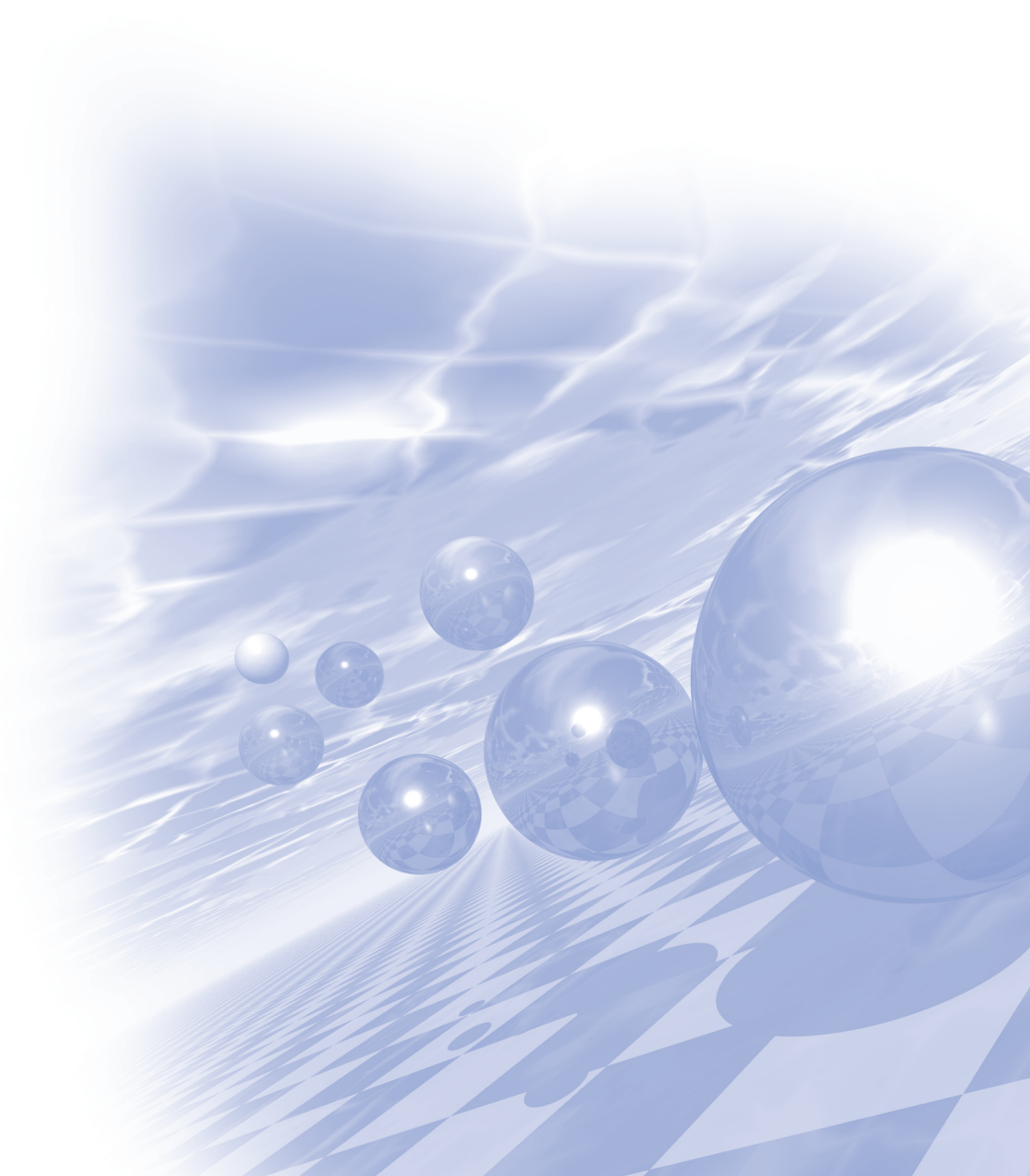
한국연구재단



KMS 2020 Winter Conference

Oral Session III

‘Hard & Soft Magnetics’



Coercivity improvement of Nd–Cu infiltrated Nd–Fe–B hot–deformed magnets by microstructure modification of initial HDDR powders

Jae–Gyeong Yoo^{1,2*}, Hee–Ryoung Cha¹, Tae–Hoon Kim¹, Yang–Do Kim^{2†}, Jung–Goo Lee^{1†}

¹Powder & Ceramics Division, Korea Institute of Materials Science, Changwon, Korea

²Department of Materials Science and Engineering, Pusan National University, Busan, Korea

The hot-deformed Nd-Fe-B magnets produced from ultra-fine grained melt-spun (~50nm) or HDDR (~300nm) powders have a great potential to obtain high coercivity and better temperature dependence of coercivity without using heavy rare earth elements. However, the hot-deformed magnets still have lower coercivity than that expected from their intrinsic properties because of high concentration of ferromagnetic Fe and Co in the Nd-rich intergranular phase. In order to reduce Fe and Co concentration in the intergranular phase, infiltration process using low melting non-ferromagnetic material such as Nd-Cu, Pr-Cu, or Nd-Al is necessary. However, in the case of hot-deformed magnets produced from the melt-spun ribbons, there is a limit to the increase of infiltration depth because the infiltration temperature is restricted below 700° C. An abnormal grain growth occurred during the infiltration above 700°C due to very fine nature of grains in the magnets fabricated using the melt-spun ribbons as an initial powder. If the HDDR powders, which have much bigger grains than melt-spun ribbons, are used as an initial alloy, such a rapid grain growth during the infiltration would be prevented. Then we can expect that the infiltration temperature could be increased thereby increasing the infiltration depth. The microstructure and chemistry of intergranular phases in the initial alloys is also very important to leads the formation of non-ferromagnetic intergranular phases in the final Nd-Fe-B hot-deformed magnets. In order to investigate the dependence of the microstructure of the Nd-rich intergranular phases and the infiltration behavior of hot-deformed magnets on the microstructure of initial powders, in this study, we fabricated the hot-deformed magnets using 2 kinds of HDDR powders having different microstructure, i.e., un-treated HDDR powders(SC_HDDR) and annealed HDDR powders(SC_PA_HDDR). Then, the hot-deformed magnets made from different initial HDDR powder were subjected to infiltration using NdHx-Cu. The microstructure and magnetic properties of hot-deformed and subsequently infiltrated magnets were analyzed by FE-SEM and VSM. For the characterization of elemental distribution in the hot-deformed magnets, field emission transmission electron microscopy, FE-TEM was used. As an interesting result, the coercivity of hot-deformed magnet produced from annealed HDDR powders increased more than that of produced from un-treated HDDR powder after infiltration process. Especially, the large coercivity increment of hot-deformed magnet using annealed HDDR powders approximately 8 kOe was achieved after 6 wt%. Nd-Cu infiltration at 800°C for 1h.

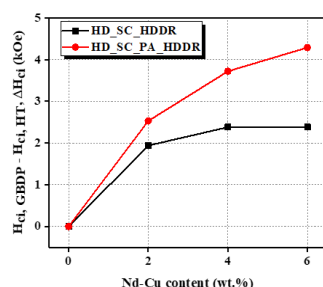


Fig. 1. The coercivity increment as a function of diffused Nd-Cu contents.

Coercivity enhancement of (Nd, M)–Fe–B hot-deformed magnet by post-annealing treatment

Ga-Yeong Kim^{1,2*}, Hee-Ryoung Cha¹, Tae-Hoon Kim¹, Dong-Hwan Kim³, Yang-Do Kim^{2*},
Jung-Goo Lee^{1†}

¹Powder&Ceramics Division, Korea Institute of Materials Science, Changwon, Korea

²Department of Materials Science and Engineering, Pusan National University, Busan, Korea

³Research Center of SG Tech., Star Group Ind. Co., Daegu, Korea

Nd-Fe-B magnets are technologically important for the applications in the electric motors, acoustics devices and hybrid vehicle. In general, 30-33 wt.% of rare earth elements are consumed to produce Nd-Fe-B magnets. Especially, heavy rare-earth (HRE) elements such as Dy or Tb have been added to achieve high coercivity despite their high price. Therefore, developing high coercivity Nd-Fe-B permanent magnets without HRE elements have drawn a great deal of attention. However, Nd element is also less abundant in the natural rare earth resources compared to other light rare-earth (LRE) elements such as Ce and La which is the most abundant and cheapest rare earth elements. However, the magnetic properties of Nd-Fe-B magnets could be drastically deteriorated after replacing Nd with Ce and La due to inferior intrinsic magnetic properties of $\text{Ce}_2\text{Fe}_{14}\text{B}$ ($4\pi M = 11.7$ kG, $H_a = 26$ kOe) and $\text{La}_2\text{Fe}_{14}\text{B}$ ($4\pi M = 13.8$ kG, $H_a = 20$ kOe) compared to $\text{Nd}_2\text{Fe}_{14}\text{B}$ ($4\pi M = 16$ kG, $H_a = 73$ kOe).

It is well known that the modification of the microstructure by post-annealing is the most effective way to improve the coercivity of Nd-Fe-B magnets without degradation of their remanence. For the Nd-Fe-B sintered magnet, post-sinter annealing process is performed at a temperature ranging from 773 K to 873 K in order to improve Nd-rich grain boundary phase for high coercivity. However, although many studies have reported on the role of intergranular phases on the coercivity, the annealing effects of Nd-Fe-B hot-deformed magnet have not been well understood. The hot-deformed magnet is subjected to high stress during process. Therefore, it is expected that considerable residual stress caused during hot-deformation process, exists in the hot-deformed magnet. In our previous study, the coercivity of Nd-Fe-B hot-deformed magnet was increased about 2.4 kOe by post-annealing at 873 K, which was attributed to that residual stress or defects caused during hot deformation have been removed after post-annealing.

In this study, post-annealing effects on the magnetic properties and microstructure of (Nd, M)–Fe–B hot-deformed magnets, were investigated. Initial ribbons with the nominal compositions of $(\text{Nd}_{1-x}\text{M}_x)_{13.6}\text{Fe}_{61}\text{B}_{5.6}\text{Ga}_{0.6}\text{Co}_{0.6}$ ($x=0$, $x=0.2/\text{M}=\text{Ce}$, $x=0.3/\text{M}=\text{Ce}$ and $x=0.3/\text{M}=\text{Ce}+\text{La}$, wt.%, named as ND, CE0.2, CE0.3 and CELA0.3, respectively) were prepared by melt-spinning technique and then pulverized into powders. The powders were hot-pressed at 973 K under 100 MPa and then subjected to die-upsetting at 973 K with a deformation rate of $\dot{\epsilon} = 0.1 \text{ s}^{-1}$. From SEM and TEM observation, it was confirmed that the RE-rich phase distribution along grain-boundaries is quite different. The triple junction phase increased when increasing the content of Ce and La substituted for Nd. Especially, the grain boundary phase of CELA0.3 magnet was quite indistinct in almost grain boundary area. The post-annealing effect was different depending on the substitution elements. The post-annealing effect was highest in CELA0.3 magnet at 973K. After post-annealing at 973 K, the coercivity was largely enhanced about 3.4 kOe in CELA0.3 magnet. Based upon these results, the post-annealing effects on coercivity and microstructure of (Nd, M)–Fe–B hot-deformed magnets will be discussed.

Phase transformation and magnetic properties of $\text{Sm}(\text{Fe}_{0.8}\text{Co}_{0.2})_{11}\text{Ti}$ bulk magnets

Hui-Dong Qian^{1,2*}, Jung Tae Lim¹, Yang Yang^{1,2}, Jong-Woo Kim¹, Su Yeon Ahn¹, Hankuk-Jeon¹, Tian Hong Zhou¹, Kyung Mox Cho², Jihoon Park^{1*}, Chul-Jin Choi^{1†}

¹ Powder & Ceramic Division, Korea Institute of Materials Science, Changwon, Gyeongnam, 51508, South Korea

² School of Materials Science and Engineering, Pusan National University, Busan, 46241, South Korea

As early as the 1980s, Fe-rich compounds with a ferromagnetic tetragonal ThMn_{12} -type structure were known to be a promising hard magnetic materials [1]. However, owing to the rapid development of Nd-Fe-B permanent magnets with large magnetic moments and strong anisotropies, ThMn_{12} -type Fe-rich compounds were not given enough attention at that time. Recently, ThMn_{12} -type $\text{Sm}(\text{Fe}_{1-x}\text{Co}_x)_{12}$ compound films with a saturation magnetization (M_s) of 1.78 T, an anisotropy field of 12 T, and a Curie temperature (T_c) of 586 °C, all of which are superior to those for $\text{Nd}_2\text{Fe}_{14}\text{B}$ [2], were successfully produced. However, the coercivity (H_c) of the $\text{Sm}(\text{Fe}_{1-x}\text{Co}_x)_{12}$ film is as small as that of soft magnetic materials according to the magnetic hysteresis loops shown in Ref. 2. In addition, phase decomposition and grain growth during sintering and high-pressure compaction degrade the magnetic properties of bulk samples. So, we still need to develop a stable process to prepare bulk magnet for production. In this work, we have developed a process to prepare a fully dense(>99%) $\text{Sm}(\text{Fe}_{0.8}\text{Co}_{0.2})_{11}\text{Ti}$ bulk magnet.

High density sintered $\text{Sm}(\text{Fe}_{0.8}\text{Co}_{0.2})_{11}\text{Ti}$ bulk magnets were successfully produced using a newly developed high pressure pressing fabrication method. Amorphous $\text{Sm}(\text{Fe}_{0.8}\text{Co}_{0.2})_{11}\text{Ti}$ ribbons were prepared by arc-melting raw material pieces and melt-spinning. The melt-spun ribbons were ground and pressed to produce green bodies, and the green bodies were annealed at 800°C for various times ranging from 10 to 20 min, followed by quenching as shown in Fig. 1. The purity of the hard magnetic ThMn_{12} phase in the bulk magnet reached to higher than 97 wt.%. The phase transformation behavior from amorphous to ThMn_{12} phase during heat treatment was systematically investigated by transmission electron microscopy. The remanent magnetization and maximum energy product of a bulk magnet were 96.0 emu/g and 12.22 MGOe, respectively.

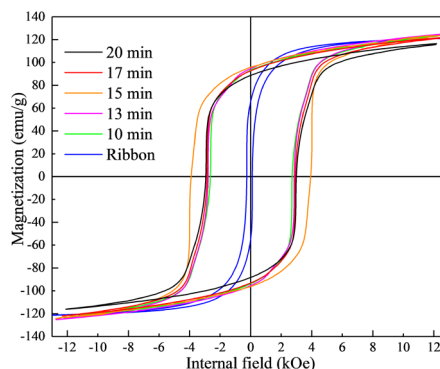


Fig. 1. Magnetic hysteresis loops of $\text{Sm}(\text{Fe}_{0.8}\text{Co}_{0.2})_{11}\text{Ti}$ bulk magnets

References

- [1] G.C. Hadjipanayis, A.M. Gabay, A.M. Schönhöbel, A. Martín-Cid, J.M. Barandiaran, D. Niarchos, Engineering 6 (2020) 141-147.
- [2] Y. Hirayama, Y.K. Takahashi, S. Hirose, K. Hono, Scr. Mater. 135 (2017) 62-65.

First-Principles Study of Magnetic Properties of MnBi with Bi-site Substitutes

Dorjsuren Tuvshin^{1*}, Tumentsereg Ochirkhuyag¹, Soon Cheol Hong^{2,†}, Dorj Odkhuu^{1,†}

¹Department of Physics, Incheon National University, Incheon 22012, South Korea

²Department of Physics, University of Ulsan, Ulsan 44610, South Korea
*schong@ulsan.ac.kr, †odkhuu@inu.ac.kr

Due to today's huge demand of many applications including motors of an electric vehicle, high-speed bullet trains, satellites and sustainability difficulty of the rare-earth (RE) elements, there have been intensive research interests recently centered at rare-earth free permanent magnetic materials and various methods to improve their uniaxial magnetic anisotropy (K_u) to at least half of the RE included magnets. MnBi alloys have recently received lots of attention due to their cheap cost, moderate saturation magnetization ($\mu_0 M_s$) of 1 T, and large K_u of 1.6 MJ/m³ at room temperature. Unlike well-known permanent magnet Nd₂Fe₁₄B, K_u of MnBi increases with temperature, making it more suitable in high-temperature applications such as motors. In this study, we conduct systematic first-principles electronic structure calculations to further enhance the structural stability, $\mu_0 M_s$, and K_u by replacing Bi with p-block elements (Sn and Sb) and Mn with 3d transition metal elements (Fe and Co). Furthermore, we reveal that K_u can even reach up to 3.3 MJ·m⁻³ in MnBi_{0.75}Sn_{0.25} while simultaneously improving $\mu_0 M_s$. These results demonstrate the feasibility of possible enhancements on the magnetic anisotropy and energy product of already potent magnet, making it best candidate of plugging the gap between RE and RE-free permanent magnetic materials.

This work is supported by Future Materials Discovery Program through the National Research Foundation of Korea (NRF) funded by the Ministry of Science and ICT (2016M3D1A1027831) and by the Korea Institute of Energy Technology Evaluation and Planning (KETEP) grant funded by the Korean government (MOTIE) (20192010106850, development of magnetic materials for IE4 class motor).

Control of magnetic properties of MnBi by elements doping

Yang Yang^{*}, Hui-Dong Qian, Jung Tae Lim, Jihoon Park, Jong-Woo Kim[†], Chul-Jin Choi

Powder & Ceramics Division, Korea Institute of Materials Science, Changwon 51508, Republic of Korea

MnBi has attracted much attention due to its large crystal anisotropy, coercivity and positive temperature behavior. To enhance its magnetic properties, doping on MnBi as well as chemical composition control has been widely employed so far. In this work, in order to obtain high purity of low-temperature phase (LTP) MnBi, various nominal compositions and 3rd elements substitution on the crystal structure and magnetic properties of MnBi were studied systematically. The alloys with high portion of LTP were prepared by conventional induction melting method with subsequent temperature annealing and post ball milling process. The Mn₅₆Bi₄₄ powder crushed from annealed ingot showed remarkably high magnetic property, i.e. saturation magnetization of 70.2 emu/g with a coercivity of 4381 Oe. In the meantime, it was found that the Ga-doping increased the Curie temperature of Mn₅₅Bi_{45-x}Ga_x for $x \leq 5$ and the phase transformation temperature of LTP-MnBi to HTP-MnBi. The Curie temperature is elevated by ~25 K for 5 at.% doped Ga. In this presentation, fabrication and optimization process for MnBi compositions and magnetic property variations according to the transition metal elements doping on MnBi will be discussed in detail.

Enhancement of magnetic properties of Fe-rich compounds with tetragonal ThMn_{12} structure by mixing non-magnetic materials

Jung Tae Lim^{*}, Hui-Dong Qian, Jihoon Park, Chul-Jin Choi[†]

Powder & Ceramic Division, Korea Institute of Materials Science, Changwon 51508, Korea

Among rare earth (R)-Fe-X compounds, it is well known that the Fe-rich compounds with tetragonal ThMn_{12} structure are potential as next generation permanent magnet materials because of high anisotropy field, saturation magnetization (M_s), and Curie temperature (T_c). In addition, the ratio of rare earth elements is very small as about 8%. Very recently, cobalt doped $\text{SmFe}_{11}\text{Ti}$ alloys have been extensively studied due to the enhanced M_s and magnetic anisotropy by Co substitution. However, the Fe-rich compound with ThMn_{12} structure showing theoretically excellent properties has not yet realized the full potential of the magnet, since the ThMn_{12} structure is not stable and has a very small domain size about 20 - 50 nm. Therefore, grain refinement and grain boundary control are well-known methods for obtaining high coercivity. In this study, to increase the coercivity, we have synthesized the Fe-rich $\text{Sm}(\text{Fe}_{0.8}\text{Co}_{0.2})_{11}\text{Ti}$ bulk by mixing non-magnetic grain boundaries diffusion materials. The crystallographic and magnetic properties were characterized by using x-ray diffractometer (XRD) with Cu-K α radiation source, scanning electron microscopy (SEM), and vibrating sample magnetometer (VSM). The $\text{Sm}(\text{Fe}_{0.8}\text{Co}_{0.2})_{11}\text{Ti}$ compound was synthesized by using arc-melting and melt-spinning methods. The $\text{Sm}(\text{Fe}_{0.8}\text{Co}_{0.2})_{11}\text{Ti}$ powder was sintered at 800 °C, followed by quenched to prevent any phase transition. The non-magnetic grain boundaries diffusion materials were synthesized by using induction-melting. The as-prepared sample mixed with a non-magnetic grain material by using ultra-sonication in ethyl alcohol and annealed at various temperatures ranging from 600 to 900 °C in high vacuum. The phase identity and volume fraction were determined by using the Rietveld refinement method. In order to improve the magnetic properties, the grain boundary diffusion process was performed and all samples were formed a thick and continuous grain boundary phase with non-magnetic materials. With increasing annealed temperature, $\text{Sm}(\text{Fe}_{0.8}\text{Co}_{0.2})_{11}\text{Ti}$ phase was decomposed and H_c decreased rapidly due to the α -Fe phase.

References

- [1] Y. Hirayama, Y. K. Takahashi, S. Hirosawa, and K. Hono, *Scr. Mater.* 138, 62 (2017).
- [2] K. Hono and H. Sepehri-Amin, *Scr. Mater.* 67, 530 (2012).

A Development of the coating technique on Soft-magnetic Composite Powders for a motor device

Kim youngmin^{1*}, Kim shingyu¹, Chung yeonjun¹, Kim jongryul²

¹Hyundai Motor Group, Korea

²Hanyang University Erica Campus, Korea

최근 모터의 고속화, 경량화에 대응하여 고주파수 작동을 위한 새로운 모터용 저손실 코아재료 개발이 필요하다. 기존의 실리콘 전기강판은 강판 두께 조절 및 형상 조절의 제약으로 인하여, 고주파에서 손실이 높으며, 다양한 형태의 코아 제작이 어려운 점이 있어 형상자유도가 높은 분말 소재의 필요성이 대두되고 있다. 일부 샌더스트, 규소강, 연자성 페라이트 분말을 활용한 인덕터 코어에 대한 연구 및 제품 생산을 하고 있으나, 순철 분말에 비해 자기 특성이 낮고 원자재 가격이 비싸 큰 경쟁력을 가지지 못하는 실정이다. 특히, 포화 자화가 높은 순철 분말 소재를 활용할 경우 자기 특성이 등방성이기 때문에 3차원 자기 회로 구성이 가능하며, 출력 향상, 다양한 코어형상 제조, 소형 제조 등에 장점이 있다.

본 연구에서는 현대제철에서 제조된 순철분말을 활용하였고, 순철분말의 기본적인 자성특성 향상을 위해 분말 입도 및 형상을 제어하였다. 먼저, 분말 입도를 키워 성형체 밀도를 개선하였고, 이는 $H_{ci}(p)=H_{ci}(0)(1-p)$ 에 따라 철손(Coreloss)을 높이는 보자력(H_{ci})을 9.45 Oe에서 8.94 Oe로 낮춰 철손을 개선할 수 있었다. 그리고, 분말 밀링을 적용하여 수분사 분말 특유의 요철부를 감소시켜 정자기에너지를 낮출 수 있을 뿐만 아니라, 성형밀도 증가에도 큰 효과를 보았다.

또한, 순철분말의 절연특성을 향상시키기 위해, 생산단가가 낮으며 접착특성이 우수한 인산염을 코팅재로 선정하여 분말코팅을 진행하였다. 특히, 인산화철 코팅은 코팅층 조절이 비교적 용이하여 박형의 코팅층을 형성할 수 있어, SMC 분말의 자속밀도 향상에 유리하다. 그 결과, 상용SMC분말 제품인 회가내스 소말로이 5P분말과 동등한 수준인 자속밀도 1.68 T(5P : 1.70 T), 철손 36.96 W/kg(5P : 34.66W/kg)을 달성하였다. 상기 분말 코팅 기술을 바탕으로, 당사에서는 EWP (Electric Water Pump) 와 구동모터용 고정자 코어 개발을 진행하고 있다.

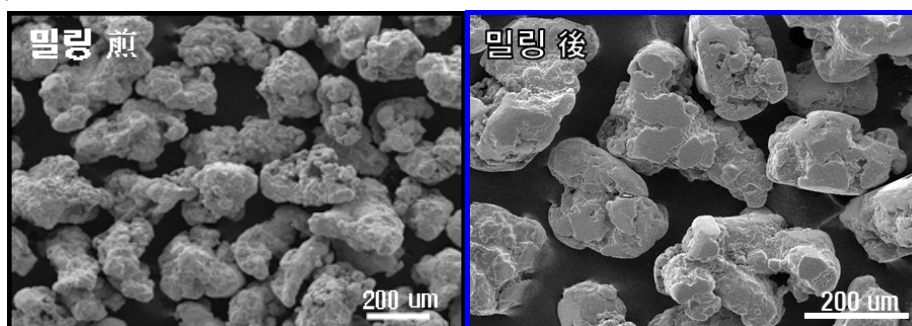


Fig.1 순철분말 밀링 전(左)과 밀링 후<右> 분말

Table.1 SMC양산품 및 개발품 평가 결과

구분	양산품 (H社 5P)	개발품 (Fe-P)
성형밀도 (g/cc)	7.566	7.501
포화자속밀도 (T)	1.70	1.68
철손 (W/kg)	34.66	36.96

Structural and magnetic properties of rare earth doped Fe by ion beam implantation

Joonhyuk Lee^{1*}, Jinhyung Cho², Hyoungeen Jeon^{1,†}

¹Department of Physics, Pusan National University, Busan 46241, Korea

²Department of Physics Education, Pusan National University, Busan 46241, Korea

With the development of automation technology, use of motors is increasing, and various studies are being conducted to secure the performance of permanent magnets. In order to develop a permanent magnet, a lot of research is being conducted to increase the maximum energy product and try to improve the performance by including a small amount of rare earth elements in iron. Recently, the first-principles calculation predicted that CeFe_{12} compounds would have a good candidate for magnetism study. (Y. Harashima et.al., Scripta Materialia, 179 (2020), 12) In this presentation, we show effect of nitrogen implantation on magnetic property of CeFe_{12} . Mo capped (110) CeFe_{12} thin films on (110) Mo buffered (0001) Al_2O_3 were deposited by RF magnetron sputtering. N^+ implantation was taken place to tune magnetism. The beam conditions are 50 and 100 keV as beam energy and 10^{16} ions/ cm^2 of fixed dose. We specially designed thickness of capping layer to minimize the effect of recoiling due to high energy implant. The prepared samples with different thickness of capping amorphous Mo: 10, 50, and 100 nm. The implanted films were analyzed using X-ray diffraction and SQUID magnetometer. The results show in limited condition enhanced magnetism is clearly seen.

Keywords: CeFe_{12} , Nitrogen ion implantation, Magnetism

Spin-thermoelectric energy conversion based on molecule-based magnetic thin film

Inseon Oh^{1*}, Jungmin Park², Deaseong Choe¹, Junhyeon Jo¹, Hyeonjung Jeong¹,
Mi-Jin Jin¹, Younghun Jo², Joonki Suh¹, Byoung-Chul Min³, Jung-Woo Yoo¹

²Department of Materials Science and Engineering, Ulsan National Institute of Science and Technology, Ulsan, 44919, Korea

³ Center for Spintronics, Korea Institute of Science and Technology, Seoul, 02792, Korea.

Spin thermoelectrics (STE), an emerging thermoelectric technology, offers energy harvesting from waste heat with advantages of large-area capability and potential advance in energy conversion efficiency, thanks to orthogonal paths for heat and charge flow. However, magnetic insulators used for STE pose challenges for scale-up due to high temperature processing and difficulty in large-area deposition. Here, we introduce a molecule-based magnetic film for STE applications because it entails versatile synthetic routes in addition to weak spin-lattice interaction and low thermal conductivity. Thin film of $\text{Cr}^{\text{II}}[\text{Cr}^{\text{III}}(\text{CN})_6]$ grown on a Cr electrode via room temperature electrochemical deposition shows effective spin thermoelectricity associated with strong excitations of low energy spin waves. Moreover, the ferromagnetic resonance studies exhibit low Gilbert damping constant $\sim (2.4 \pm 0.67) \times 10^{-4}$, indicating low loss of heat-generated magnons. The demonstrated STE applications of a new class of magnet will pave the way for versatile recycling of ubiquitous waste heat.

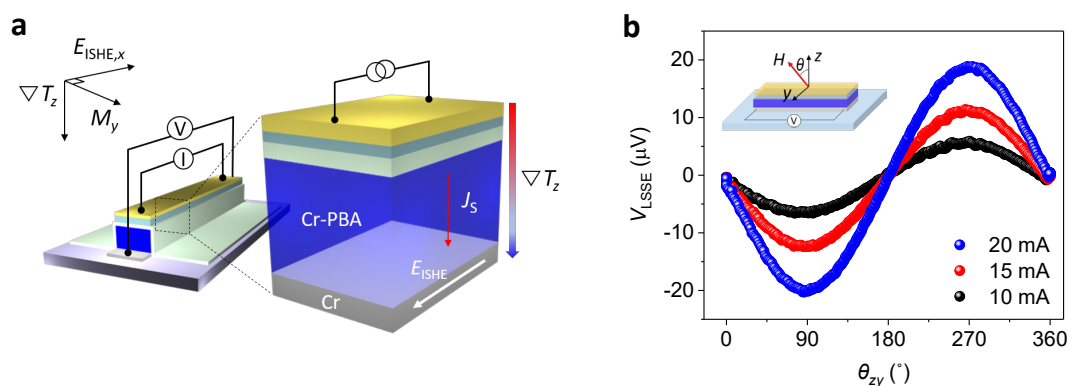


Fig. 1. Longitudinal spin Seebeck effect in molecule-based magnet/Cr metal heterojunction

First-principles prediction of enhancing magnetic anisotropy and stability of α'' -Fe₁₆N₂ phase

Tumentsereg Ochirkhuyag¹, Dorjsuren Tuvshin¹, Soon Cheol Hong^{2,*†}, Dorj Odkhuu^{1,†}

¹Department of Physics, Incheon National University, Incheon 22012, South Korea

²Department of Physics, University of Ulsan, Ulsan, South Korea

E-mail: *schong@ulsan.ac.kr, †odkhuu@inu.ac.kr

Rare-earth based magnetic materials are widely used in permanent magnet applications. Recently, rare-earth free permanent magnets have received much attention for their earth abundance and cheap materials price. Herein, systematic first-principles density functional calculations are used to reveal possible improvements of uniaxial magnetic anisotropy (K_u) and thermal stability of α'' -phase Fe₁₆N₂ by replacing Fe with a series of 3d metal elements (Ti to Zn). Among the 9 substitute elements, the V and Zn (or, V and Co) co-substitute stabilizes the α'' phase of Fe₁₆N₂ and enhances its K_u up to $2.9 \text{ MJ} \cdot \text{m}^{-3}$, which is nearly 5 times that of $0.6 \text{ MJ} \cdot \text{m}^{-3}$ in α'' -phase Fe₁₆N₂. These results provide an instructive guideline for simultaneous enhancement of the structural stability and energy product in 3d-only rare-earth free permanent magnets.

Keywords: Rare-earth free permanent magnets, First-principle calculations, Uniaxial magnetic anisotropy

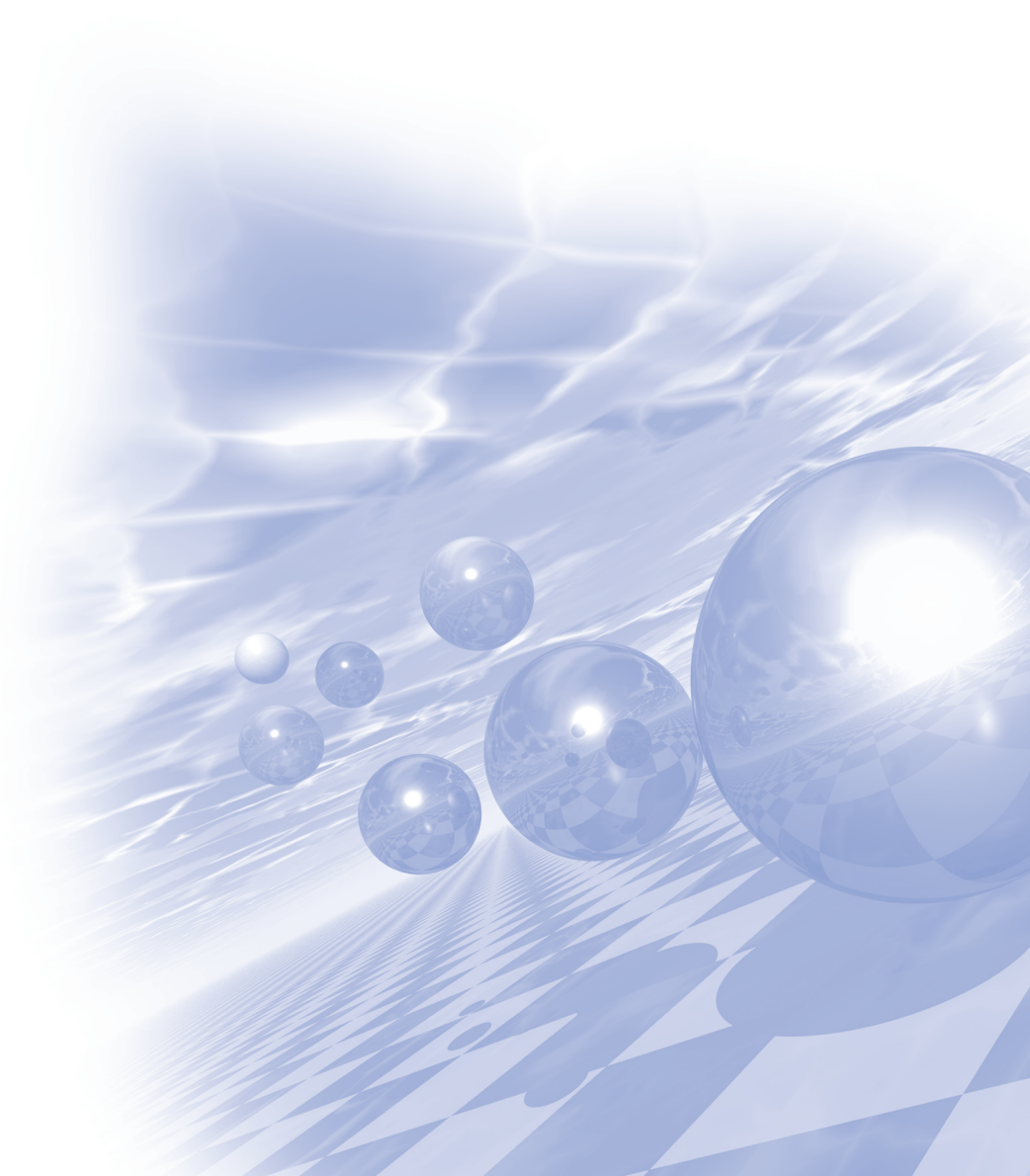
This work is supported by Future Materials Discovery Program through the National Research Foundation of Korea (NRF) funded by the Ministry of Science and ICT (2016M3D1A1027835) and by the Korea Institute of Energy Technology Evaluation and Planning (KETEP) grant funded by the Korean government (MOTIE) (20192010106850, development of magnetic materials for IE4 class motor).



KMS 2020 Winter Conference

Special Session VI

‘Medical Magnetism’



Transcranial Magnetic Stimulation for the Treatment of Multiple Neurologic Conditions; Focused on Clinical Application

Jung-Woo Jeong^{1*}, Bo-Kyoung Song²

¹Dept. Emergency Medical Rehabilitation Graduate School, Kangwon National University, Korea

²Dept. of Occupational Therapy, Kangwon National University, Korea

Purpose of Review

Transcranial magnetic stimulation (TMS) has found its way into the mainstream in the areas of non-invasive therapy for multiple neurological and psychiatric disorders. TMS is a method of non-invasive brain stimulation that is based on electro-physical principles discovered by Michael Faraday. A TMS device is made of one or two copper coils, positioned superficially to a site of interest in the brain, to non-invasively produce a brief magnetic pulse to an estimated depth from the surface of the scalp with the following axonal depolarization. This axonal depolarization activates cortical and subcortical networks with multiple effects. There are different methods of TMS used, all with different mechanisms of action. Depending on the frequency of stimulation, low frequency (< 1 Hz) or high frequency (> 5-20 Hz), we will obtain a specific result, long-term depression or potentiation, respectively. TMS became a safe and non-invasive method to study the brain, a process that could be done inexpensively and repeatedly.

Recent Findings

TMS is now approved for major depression disorder and obsessive-compulsive disorder. There is significant data to consider approval of TMS for many neurological disorders. This is a review of the uses of TMS in diverse neurological conditions, including stroke and spasticity, migraine, and dementia.

Summary

TMS is a device that utilizes non-invasive brain stimulation, and it has shown promising results with objective clinical and basic science data. Its ability to trigger neuronal plasticity and potentiating synaptic transmission gives it incredible therapeutic potential.

There are diverse mechanisms of action, and this could be troublesome in elaborating clinical trials and standardization of therapy.

Image Quality Assessments According to the Angle of Tilt of a Flex Tilt Coil Supporting Device: An ACR MRI Phantom Study

Ji-Sung Jang^{1*}, Ho-Beom Lee^{1,2}, Sung-min Kim²

¹Department of Radiology, Asan Medical Center, Korea

²Department of Medical Device Industry, Dongguk University,

The purpose of this study was to assess the effects on image quality of different angle of tilt created by a flex tilt coil supporting device during the MRI examination. All images were analyzed using an automatic assessment method following the ACR MRI accreditation guidance. Image quality was compared between acquisitions grouped according to the angle of tilt of the coil supporting device: group A (Flat mode), group B (10°), and group C (18°). All measured image qualities were within the ACR recommended criteria, regardless of the angle of tilt coil supporting device. There were no statistically significant differences in geometric accuracy, high contrast spatial resolution, percent signal ghosting, and low contrast object detectability ($p > 0.05$). However, statistically significant differences between the three groups were found for slice thickness, position accuracy, and image intensity uniformity ($p < 0.05$, ANOVA). The flex tilt coil device can provide sufficient image quality, passing the criteria of the ACR MRI guideline, despite differences in slice thickness, slice position accuracy, and image quality uniformity according to the angle of tilt.

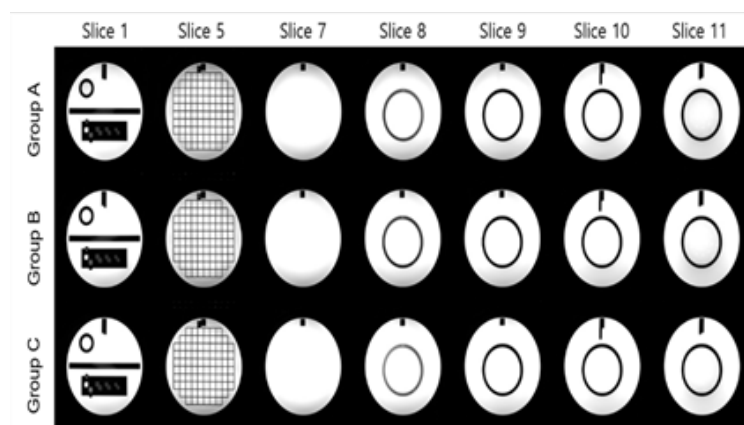


Fig. 1. Representative images acquired with the flex tilt coil, displayed using their default contrast level and window. Group A, flat; Group B, tilt 10°; Group C, tilt 18°.

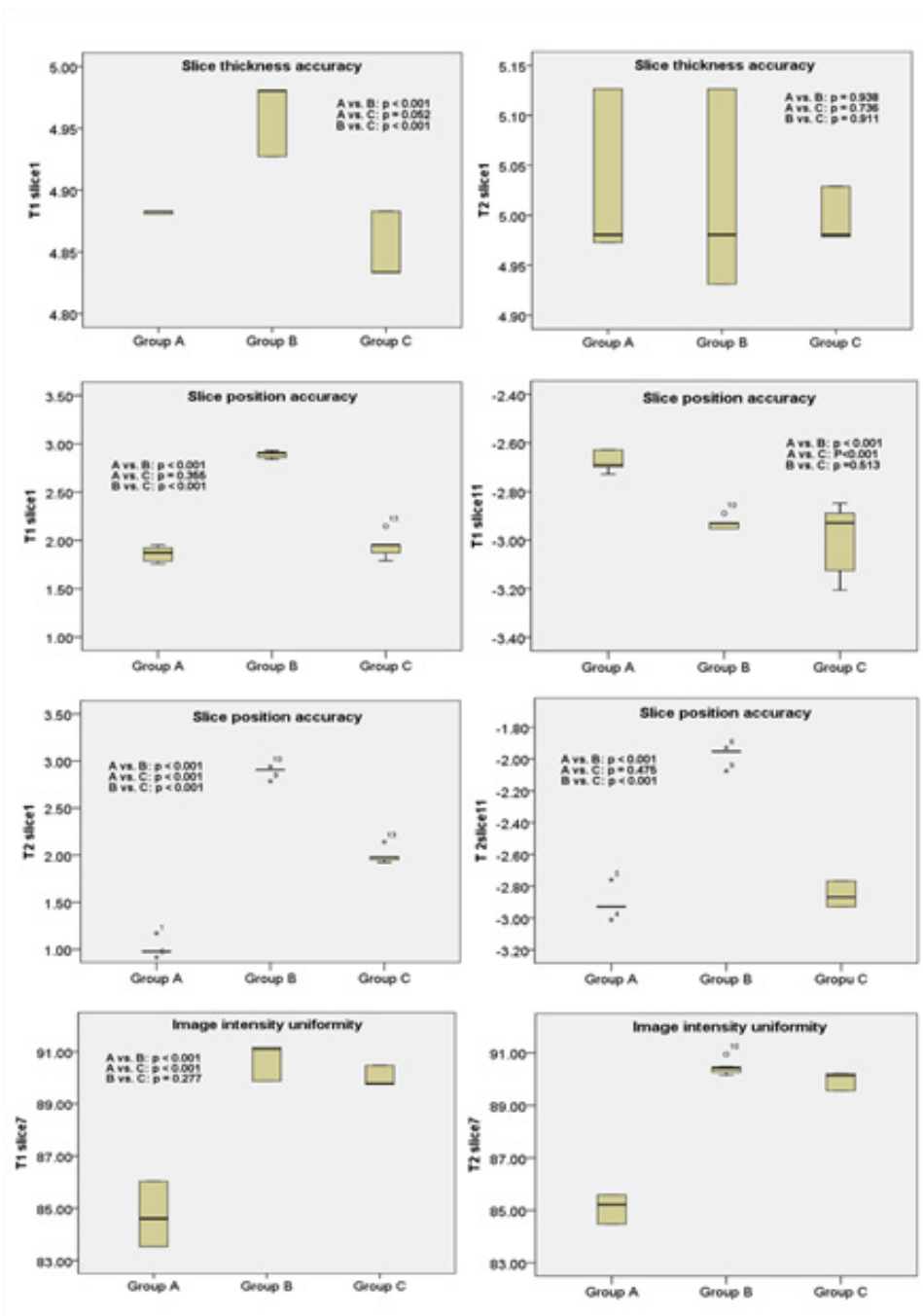


Fig. 2. Box-plots showing statistically differences in image quality categories between groups A, B, and C.

MRI 보어 구경에 따른 검사 시 실효 단면적 분석

유재원¹, 배규성¹, 배서현¹, 김성호¹, 유세종¹, 전민철², 고현철², 정현근^{1*}

¹HK리서치센터 의생명공학연구소 (Biomedical Engineering Lab, HK Research Center Inc.)

²서울성심병원 마취통증의학과 (Department of Anesthesiology and Pain Medicine, Seoul Sacred Heart General Hospital)

I. 서론

실제 임상에서는 보어 구경을 늘리는 방향으로만 경쟁이 진행되어 왔지만 실제 테이블과 피검사자가 보어 안으로 진입한 이후 내부의 실효 단면적에 대해서는 고려해 본 적이 없다. 분명 테이블 사이즈 및 최대 높이에 따라 보어 안에서의 공간면적이 다를 것으로 추론되며, 이는 피검사자가 보어 내부에 위치할 때 느끼는 안정감에 분명히 영향을 미친다. 이에 따라 본 연구에서는 각 MRI 모델에 따른 보어 구경을 확인 및 측정해보고, 테이블이 차지하는 면적을 계산하여 검사 시 정확한 보어 구경 내의 실효 단면적을 구해보고자 하였다. 이를 위하여 각 업체의 3.0T MRI장비사에서 제공하는 메뉴얼과 임상현장에서 사용하는 해당 장비를 실제 측정하여 분석을 진행하였다.

II. 실험방법과 결과

MRI 모델 및 보어 구경은 표 1에 기록된 각각의 3.0 T 초전도 MRI를 대상으로 하였고, 보어 구경은 각 업체에서 공식적으로 배포하는 장비 매뉴얼을 기본자료로 활용하였으며 현장에 설치된 MRI 장비를 20회 이상 실측하여 도면과 비교하였다. 실효면적 계산 방법은 보어 반지름에 따른 전체면적에서 테이블로 인해 닫히는 면적을 빼서 구하였다. 각 MRI 시스템의 ACSA (Actual Cross-Sectional Area), ACSA%를 결과로 나타냈다. 실제 면적은 Ingenia CX, Elition X, uMR 780, Omega, Vida, Lumina, Architect, Premier 순으로 171230, 232150, 242100, 309332, 230760, 230760, 229380, 235990 mm² 이며, uMR 780, Omega 장비가 73.0%, 70.0%로 높은 실효면적비를 나타냈다.

III. 고찰

통상적으로 임상에서는 보어사이즈가 피검사자가 내부에 놓였을 때 느끼는 실제 공간면적으로 오인하고 있다. 하지만 본 연구를 통하여 보어 구경과 실효 단면적이 꼭 비례하지 않는다는 것을 알 수 있었다. 보어 구경 사이즈가 당연히 보어 내부의 단면적에 영향을 미치기는 하지만, 임상에서 사용 중인 여러 MRI시스템의 실효 단면적이 꼭 보어구경에 의해 결정되는 것은 아니라는 의미이다. 오히려 피검사자의 편의성 목적이라면 보어구경 보다는 내부의 실효 단면적을 우선시하는 것이 적당하다고 보이며, 더불어 동일 사이즈의 내부 면적이라면 검사 시간을 더 단축하는 것이 의미가 있을 수도 있다.

IV. 결론

결론적으로, 본 연구를 통하여 여러 MRI시스템에서의 보어 내부 실효 단면적을 정량화 할 수 있었다. 그 결과는 각 업체에서 제작된 MRI시스템에 따라 모두 다른 공간면적을 지니고 있었다. 이 의미는 각 MRI제조업체에서 강조하고 있는 보어구경 으로서만 검사 시 공간면적을 논하는 것이 크게 의미를 부여하기 어렵다. 통상적으로 전 세계에 판매 중인 임상용 MRI시스템은 작게는 60 cm부터 크게는 75 cm의 보어사이즈를 지니고 있다. 그리고 보어 구경이 클수록 그 내부 검사 면적도 클 것이라는 고정관념을 지니고 있었다. 그러나 본연구에서는 실효 단면적을 통하여 사실과 다르다는 것을 정량화 하였으며, 이러한 부분을 감안 후 피검사자의 입장을 고려한다면, 더 넓은 현장 매니징과 더불어 궁극적으로는 진단 정확도로 더 유용한 검사가 가능하다고 사료된다.

References

- [1] HK Jeong, KH Lee, MH Kim, SH Kim, MG Kim and HC Kim "Signal Intensity of Contrast Enhancement according to TE in 3.0T MRI T1 Imaging" by Journal of Applied Science, 2018, 8, 1138;

- [2] SH Kim, SY Kwon, CH Kang, HK Jeong, SW Kim, YJ Park, DK Han, JW Hong and YC Heo “Analysis of Peak Velocity and Mean Velocity According to Shimming Technique in 2D Phase Contrast : Comparison of 1.5T Tesla and 3.0 Tesla” by Journal of Magnetism, 23(2), 201-206(2018).
- [3] E. Hagberg, and K. Scheffler, “Effect of r(1) and r(2) relaxivity of gadolinium-based contrast agents on the T1-weighted MR signal at increasing magnetic field strengths” , Contrast Media Mol Imaging vol.8,no.6, pp. 456 – 65, Nov-Dec,2013.
- [4] Z. Seidl, J. Vymazal, M. Mechl, M. Goyal, M. Herman, C. Colosimo, M. Pasowicz, R. Yeung, B. Paraniak-Gieszczyk, B. Yemen, N. Anzalone, A. Citterio, G. Schneider, S. Bastianello, and J. Ruscalleda, “Does higher gadolinium concentration play a role in the morphologic assessment of brain tumors? Results of a multicenter intraindividual crossover comparison of gadobutrol versus gadobenate dimeglumine (the MERIT Study)” , AJNRAmJNeuroradiol, vol.33, no.6, pp.1050 –8, Jun, 2012.
- [5] Bloembergen N, Purcell EM, Pound RV “Relaxation effects in nuclear magnetic resonance absorption” , Phys Rev vol.73,pp. 679,1948.
- [6] Bloembergen N, “Proton relaxation times in paramagnetic solution” , J Chem Phys vol.27,pp. 572,1957.
- [7] Just, M.; Thelen, M. Tissue characterization with t1, t2, and proton density values: results in 160 patients with brain tumors. Radiology 1988, 169, 779-785. DOI:10.1148/radiology.169.3. 3187000.

Feasibility of fast non-local means algorithm for T1-weighted MR images using BrainWeb: A simulation study

Seong-Hyeon Kang*, Youngjin Lee

Department of Radiological Science, Gachon University, Korea

The purpose of this study was to analyze the efficiency of the fast non-local means (FNLN) algorithm in T1-weighted MR images. For this purpose, we simulated the References image and noise image based on T1-weighted images, which Gaussian noise added with 0% and 5%, respectively, using the BrainWeb. In addition, the FNLN algorithm with kernel size, search window size, and sigma values set to 5 x 5, 11 x 11, and 0.05, respectively, was modeled and applied in noisy image. To evaluate the noise level and similarity, we used the coefficient of variation (COV), contrast to noise ratio (CNR), root mean square error (RMSE), and peak signal-to-noise ratio (PSNR). Moreover, the conventional noise reduction methods such as median filter, Gaussian filter, and Wiener filter were additionally applied. As a result, FNLN algorithm was showed the most improved value for all evaluation factors. Especially, compared to the noisy image, the COV, CNR, RMSE, and PSNR were improved about 11.24, 13.01, 1.34, and 1.03 times, respectively. In conclusion, we demonstrated that the FNLN algorithm can effectively remove the noise, which generated in the T1-weighted MR image.

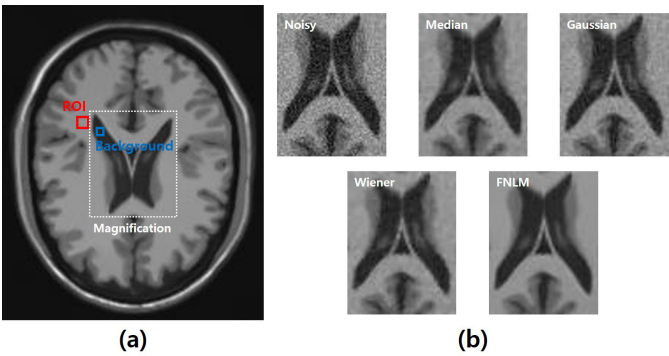


Fig. 1. (a) The References image of the T1-weighted MR image with ROIs for quantitative evaluation and (b) reconstructed images with noise reduction algorithms

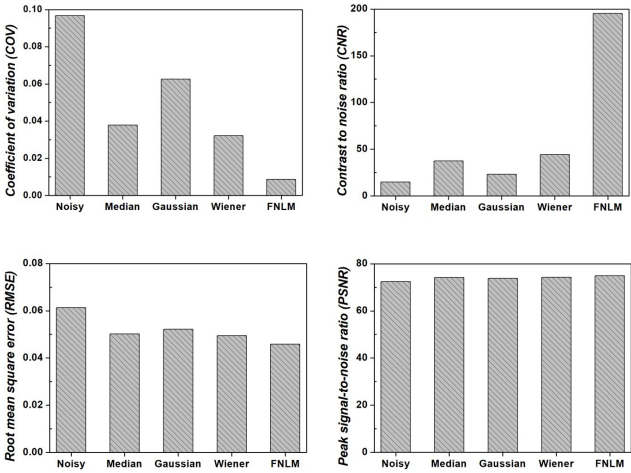


Fig. 2. Results of the COV, CNR, RMSE, and PSNR of the reconstructed images with noise reduction algorithms for evaluation of the noise level and similarity.

A Study on the Evaluation of Dose Distribution Error According to the Spacing and Angle of Bolus in Electromagnetic Radiation

Kim Jeong Ho^{1*}, Seo Jeong Min², Kim Gap Jung³

¹Department of Radiology, Sunlin University, Pohang, Republic of Korea

²Department of Radiological Science, Catholic University of Pusan, Pusan, Republic of Korea

³Department of Radiology, Songho University, Gangwon, Republic of Korea

The purpose of the radiation therapy bolus is to move the dose distribution in the body to the surface using electromagnetic radiation. To do this, the exact position of the bolus is necessary. However, there are many cases in which the reproducibility of the position of the bolus is not maintained in clinical practice, so it is necessary to evaluate the change in dose for this. For the 6MV and 10MV of the linear accelerator (Varian, RapidArc), PDD was measured for an interval from 0 cm to 9cm, and a slope from 0° to 30° degrees under irradiation field 10x10cm² conditions. For radiometric measurement, PDD was measured using an ion ionizer, and D5 (percentage of 5mm depth) to D50 (percentage of 50mm depth) were compared. The difference in the index according to the gap difference was from -0.7% to 3.1% when using a 6MV and 5mm bolus. When using a 10MV and 5mm bolus, there was a difference of -0.2% to 11.3%. When 6MV and 10mm bolus was used, the difference was -0.6% to 0.4%. When 10MV and 10mm bolus was used, the difference was -0.3% to 5.6%. In addition, the difference in the index according to the difference in inclination was -0.1% to 1.3% when using a 6MV and 5mm bolus. When using a 10MV and 5mm bolus, there was a difference of -4.2% to 1.5%. When 6MV and 10mm bolus was used, the difference was -0.1% to 1.7%. When 10MV and 10mm bolus was used, the difference was -1.5% to 1.5%. And the change according to the gap difference showed a big difference only in the vicinity of the surface, whereas the change according to the inclination showed an overall change. If the bolus is attached to the side or rear direction of the body part, or if the bolus is inappropriately attached due to the fixing mechanism, the redesign of the treatment plan should be determined considering the error.

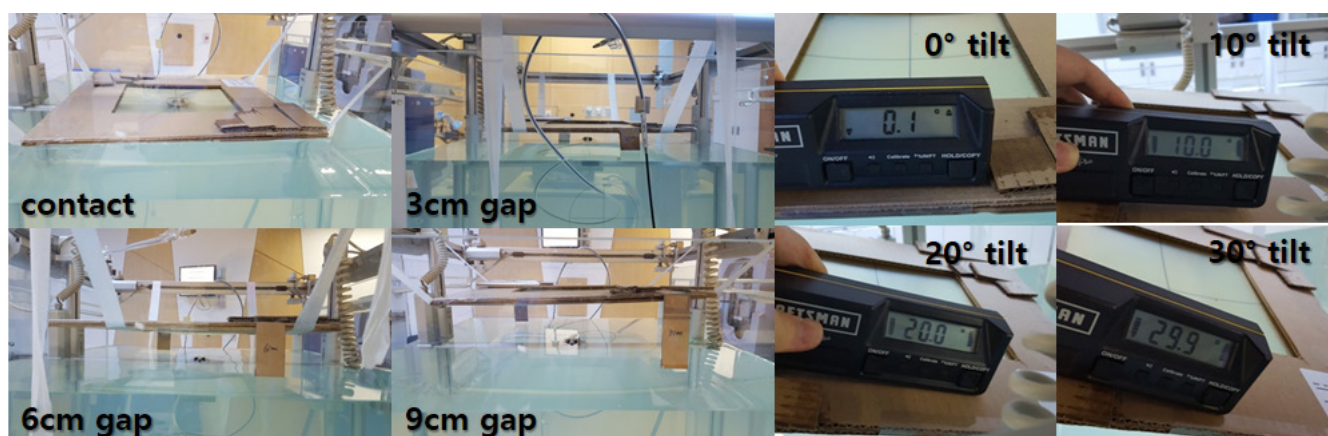


Fig. 1. Comparison of gap and tilting angle

Feasibility of Customized 3d Bolus for H&N cancer: Applied to Oral Cavity and Supraclavicular Area

Seunghyeop Baek^{1,3*}, Eunbin Ju^{1,2}, Woo Sang Ahn⁴, Nuri Hyun Jung¹, Sohyun Ahn¹

¹Department of Radiation Oncology, Kangwon National University Hospital, Kangwon 24289, Korea,

²Department of Bio-medical Science, Graduate School of Korea University, Sejong 30019, Korea,

³Department of Radiological Science, School of Yonsei University, Wonju 26493, Korea

⁴Department of Radiation Oncology, Gangneung Asan Hospital, University of Ulsan College of Medicine, Gangneung 25440, Korea

Purpose

The side effects such as dry mouth, skin change and a sore throat still remain when the oral cavity or head and neck (H&N) cancer were treated by the intensity-modulated radiotherapy (IMRT).

To alleviate these side effects, a customized 3d bolus was recently used during IMRT instead of a commercial bolus.

So, this study is aimed at reviewing a novel method of manufacturing a customized bolus for patients with head and neck (H&N) cancer and evaluating the target coverage and normal tissue sparing.

Materials and Methods

For H&N cancer patient, a 3D bolus structure was created from an extended planning target volume (PTV) and transmitted to DICOM file type. Then, the 3d bolus was manufactured using PLA material with 3d printer (3DWOX, Sindoh) after the type was converted to STL file type.

For oral cavity (hard palate) patient, a balloon was inserted into a patient's mouth to secure space, and then the area surrounding the balloon was designed into a 3D bolus structure so that the patient could comfortably handle a dose buildup.

These manufactured 3d boluses were applied during treatment of each patient, and the in-vivo dosimetry was performed using EBT3 film to evaluate dose of the tumor and surrounding normal tissue.

Results

The skin dose of H&N patients using a 3D bolus was 14.4% lower than the skin dose when using a commercial bolus.

This bolus enables effective performance of skin sparing procedures and full coverage of the target skin area.

For oral cavity patients, the PTV dose was 93.8% of the prescribed dose and the tongue dose was sufficiently sparing at 8% of the prescribed dose.

Conclusion

In this study, we found that creating a local 3D bolus structure using an extended PTV can improve target coverage and reduce unnecessary skin dose for irregular skin. In addition, for the oral cavity, this method not only improves target coverage, but also allows achieving a tongue immobilization effect. Thus, our proposed method can use a clinical field.

The effect of patient size on radiation with size-specific dose estimates for computed tomography dose index

Pil-Hyun Jeon^{1*}, Cheol-Ha Baek²

¹Department of Radiology, Yonsei University, Wonju Severance Christian Hospital, Wonju, Korea

²Department of Radiological Science, Kangwon National University, Korea

CT scanners typically display standard dose metric with two indices. CT dose index (CTDIvol) and dose length product (DLP) based on two of standard cylindrical PMMA phantoms (16 and 32 cm diameter) were used in the calculation of radiation dose. CTDIvol represented with the radiation provided by a CT scanner is not accurately matched to the radiation dose to an individual patient. At this moment, CT dose a pediatric patient (an average diameter less than 32 cm) may be underestimated without adjusting dose data for body size and shape. In according to AAPM 204 report, the size specific dose estimate (SSDE) described a method for adjusting dose index values based on effective diameter with the geometric means of measurement. To calculate the effective diameter is computed as the diameter of the circle whose area is the same as that of slice at the fixed level of T12-L1. Image of scanning CT was imported into software MATLAB version 7.7.0. to convert the pixel values of DICOM (Digital imaging and communication in medicine) files from oval to circle shape for calculating effective diameters. Patient effective diameter by image-based empirical used to a threshold of 1000 HU for sampling the image pixels. Number of pixels whose Hounsfield Unit (HU) value exceeded a set threshold. This pixel count was multiplied by the area of a single pixel to give an estimate of the cross-sectional area. In compare with the effective diameter, the root square error was 8.269 with changing pixel in threshold value of effective diameter slightly higher than the manually measured effective diameter. This study is to find a practical and physical method for changing pixel in threshold value calculation of effective diameter with reconstructed axial abdominal CT images for radiation dose with CTDIvol. Our research will improve to evaluate the measurement of effective diameter on a CT image appropriate and useful to normalize CT dose data for body shape and size.

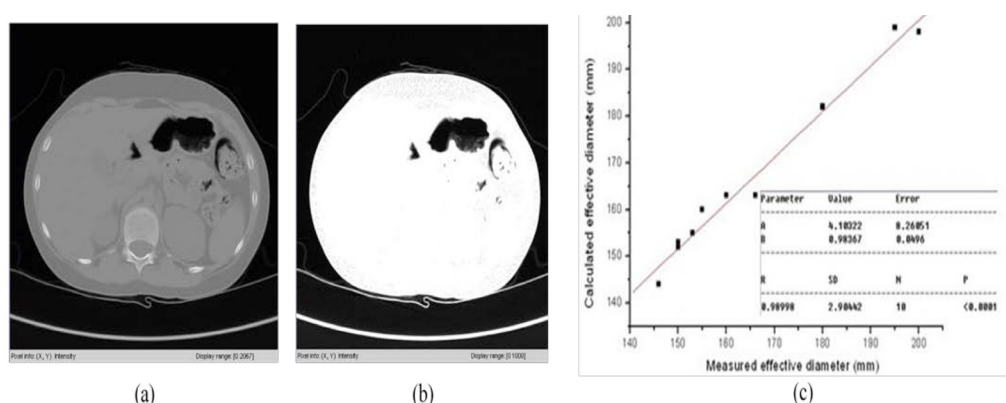


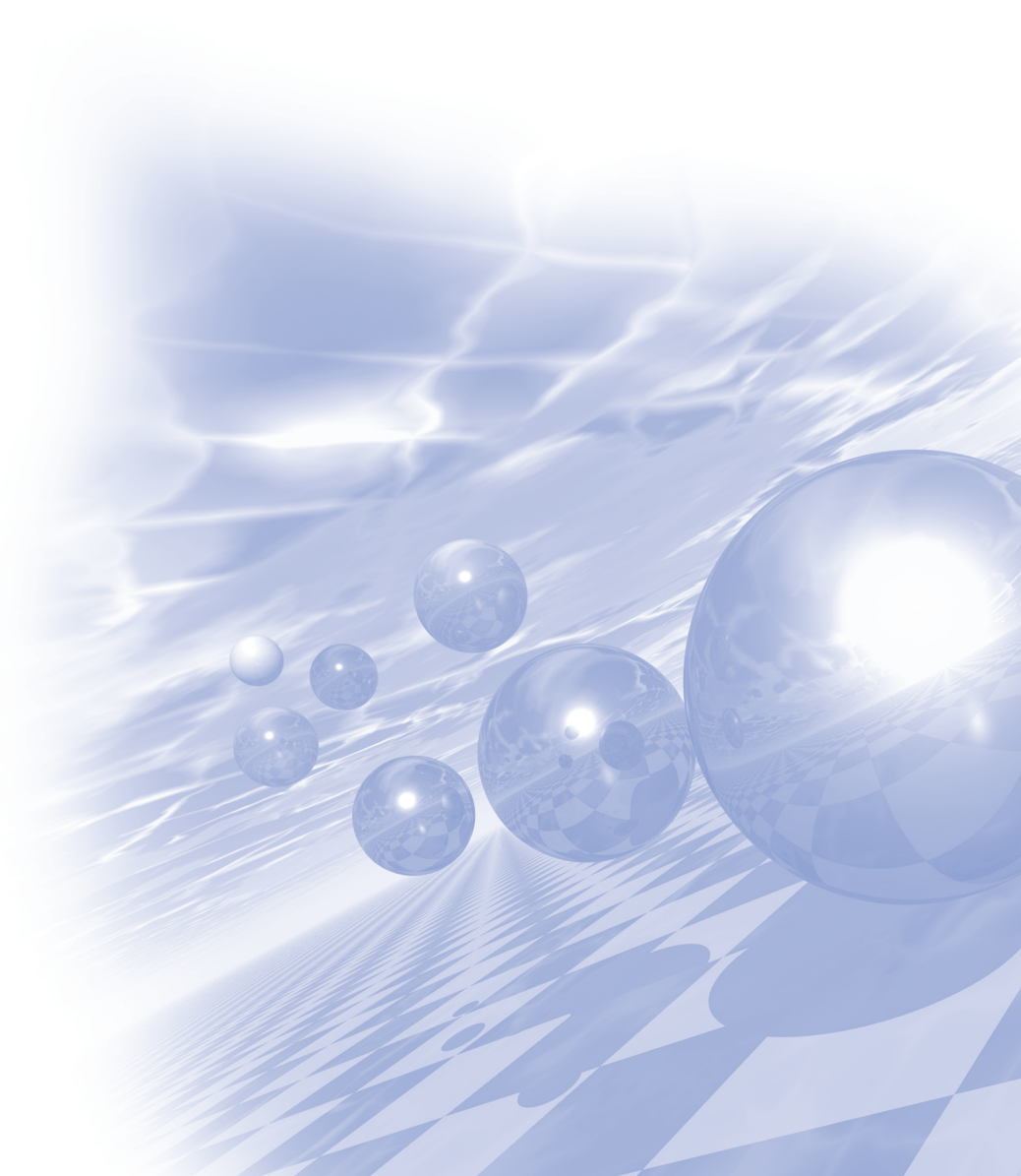
Fig. 1 Illustration of DICOM file images using pixel values for the effective diameter (a) The original abdomen CT image to convert the DICOM file (b) Changing pixel in threshold value of colored white, with remaining pixels colored black. (c) Comparison of calculated and measured effective diameters for the patient cross section area.



KMS 2020 Winter Conference

Special Session VII

‘Bio–Med–Magnetics convergence’

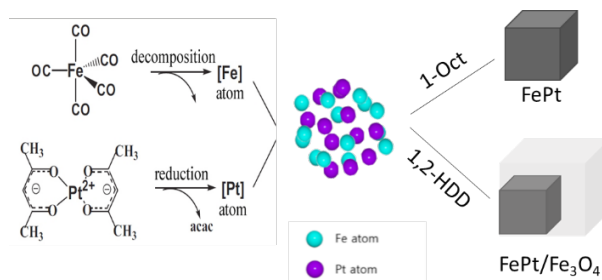


FePt–Ferrite heterogeneous nanoparticles: One–pot synthesis with controlled phase and their enhanced biocompatibility

Yunji Eom^{*}, Yumin Kang, Satish Kasturi, Sri Ramulu Torati, CheolGi Kim[†]

Department of Emerging Materials Science, DGIST, Daegu-42988, Republic of Korea

During the last decade, the synthesis of multifunctional magnetic nanoparticles has been received a great attention due to their flexibility for simultaneous various multi-applications such as drug delivery, magnetic resonance imaging, immuno-detection etc. Particularly, bimagnetic FePt/Fe₃O₄ nanoparticles are more interesting for simultaneous magnetic and biological applications^{1,2,3}. The synthesis method is very important for the controlled formation of bimagnetic particles. Although, few techniques are available for the synthesis of FePt/Fe₃O₄ nanoparticles, the time-consuming two-steps and longer reaction time remains a challenge for wider applications. Hence, we developed a one-pot synthesis technique for the synthesis of the composition controlled FePt and phase-controlled FePt/Fe₃O₄ nanocubes (NCs) by using 1, 2-hexadecanediol and 1-octadecene as a reducing agent, respectively. When 1, 2-hexadecanediol was used as a reducing agent with varying source ratio of Fe:Pt, the homogeneous FePt NCs were formed while by using 1-octadecene as a reducing agent with Fe:Pt ratio 4:1, heterostructure of FePt/Fe₃O₄ NCs were obtained. The FePt/Fe₃O₄ heterostructure shows two phases i.e., FePt with (111) facet of the fcc and Fe₃O₄ with inverse cubic spinel structure. Both FePt and FePt/Fe₃O₄ NCs shows typical superparamagnetic behavior with negligible coercivity. Also, the cell viability of FePt and FePt/Fe₃O₄ NCs were investigated, and found that the NCs shows excellent biocompatibility. Hence, the NCs could be useful for various biomedical applications including MRI contrast agents, hyperthermia, and as a label in magnetic biochips^{4,5}.



Schematic of FePt nanoparticles formation from decomposition of Fe(CO)₅ and reduction of Pt(acac)₂.

References

- [1] Hongwei Gu, Pak-Leung Ho, Kenneth W. T. Tsang, Ling Wang, and Bing Xu, J. Am. Chem. Soc. 2003, 125, 51, 15702-15703
- [2] Shang-Wei Chou, Yu-Hong Shau, Ping-Ching Wu, Yu-Sang Yang, Dar-Bin Shieh and Chia-Chun Chen, J. AM. CHEM. SOC. 2010, 132, 13270-13278
- [3] Teruaki Fuchigami, Ryo Kawamura, Yoshitaka Kitamoto, Masaru Nakagawa, Yoshihisa Namiki, Biomaterials, 2012, 33, 5, 1682-1687
- [4] Jung-tak Jang, Hyunsoo Nah, Jae-Hyun Lee, Seung Ho Moon, Min Gyu Kim, and Jinwoo Cheon, Angew. Chem. Int. Ed. 2009, 48, 1234 -1238
- [5] N. K. Sahu, J. Gupta, and D. Bahadur, Dalton Transactions, 2015, 44, 19, 9103-9113

생체기능화 된 자성입자의 프로그래밍 가능한 이송을 위한 다중 전송 게이트

임병화*, 후싱하오, 토라티라무, 김현설, 윤종환, 김철기†

신물질과학전공
DGIST

대구 달성군 테크노중앙대로333

*cgkim@dgist.ac.kr

프로그래밍 가능한 세포 및 생체물질의 이송과 이를 이용한 대규모 배열은 생화학, 생물학 및 의학 응용 분야에서 매우 큰 활용도를 가집니다. 미세 전류선과 자기영동 회로에 의해 단일세포에 대한 프로그래밍 된 조작방법이 구현되었지만 여러 단계의 제작공정과 복잡한 전류인가체계는 대규모 생체물질배열에 대한 실제 적용을 어렵게 합니다. 이 연구에서는 복잡한 미세 전류 와이어 대신 시간에 따른 펄스 자기장에 의해 동작하는 다양한 통과 게이트를 사용하여 편리하게 조작가능한 생체 기능화 된 자성입자의 프로그래밍 가능한 조작 방식을 제안합니다. 자성입자의 프로그래밍 가능한 조작을 위해 복귀, 지연 및 저장 L-게이트와 분할, 역전 및 정류 T-게이트를 포함한 다양한 통과 게이트가 이론적, 실험적으로 조사되었습니다. 그 결과 다중 전송 게이트에서 펄스자기장이 적절한 시간과 각도로 인가되었을 때 자성입자의 동작이 프로그래밍 된 것과 같이 구현되어 생체분자 및 세포에 대한 대규모배열을 위한 유용한 방법임을 확인할 수 있었습니다.

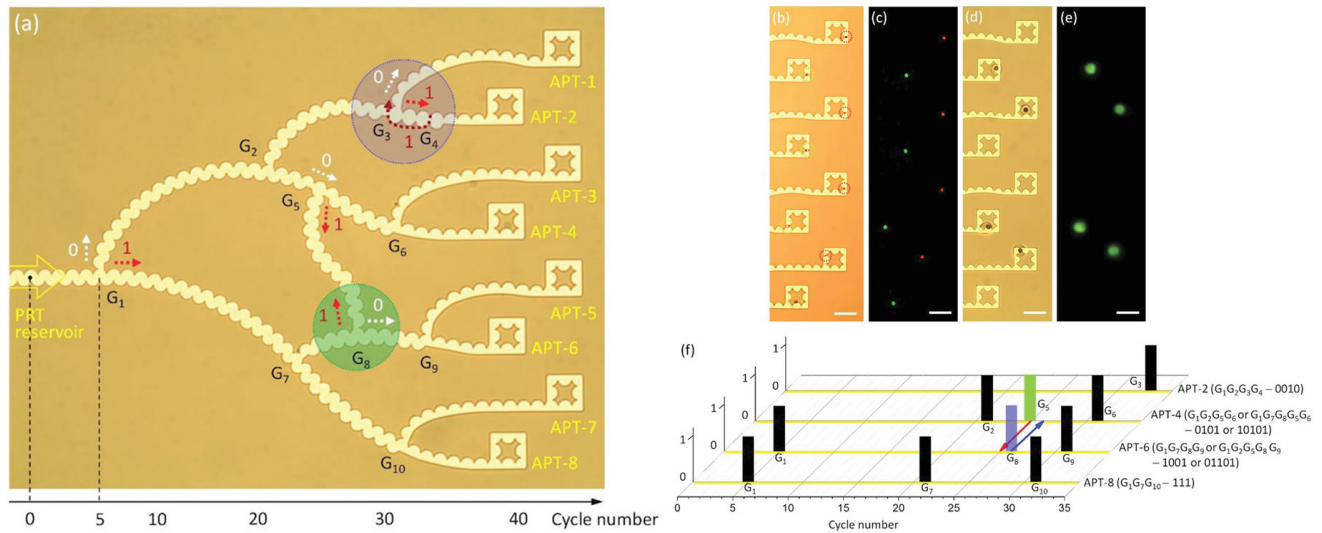


그림 1 다중 전송 게이트에 의한 프로그래밍 가능한 조작 및 자성입자의 배열:

- 미세로봇 입자의 위치를 파악하기위한 아파트를 포함한 복귀 L-게이트, 지연 L-게이트, 저장 L-게이트, 분할 T-게이트, 역 T-게이트 (녹색 원) 및 정류 T-게이트 (파란색 원)의 통합 명시야 이미지. 자성입자의 프로그래밍 된 조작을 보여주기 위해 설계된 다중전송게이트이다.
- a) 아파트에 저장된 생체기능화 된 자성입자의 명시야 및 형광 이미지.
- b) 아파트에 저장된 단일세포의 명시야 및 형광 이미지, 스케일 바는 25μm이다.
- c) 자성입자를 아파트 APT-2, 4, 6 및 8로 이동하도록 조작하기 위한 프로그래밍 된 펄스자기장에 대한 다이어그램.

Label-free electrochemical biosensor for miRNA-122 biomarker detection based on naturally reduced rGO/Au nanocomposite.

Satish Kasturi^{*}, Yun Ji Eom, Sri Ramulu Torati, CheolGi Kim[†]

Department of Emerging Materials Science, DGIST, Daegu-42988, Republic of Korea

Viruses are obligate intracellular parasites and can easily interact with the pathways in the infected host. DNA viruses such as polyomaviruses, adenoviruses, and herpesviruses express viral microRNAs (miRNAs) and use the miRNA levels to observe the growth to regulate both host and viral RNAs [1]. Early detection of this type of miRNA's is very important to reduce the people who get affected and keep these types of diseases in control [2]. In this work, we have fabricated a novel and simple miRNA-122 electrochemical sensing platform biosensor fabrication to detect the microRNA-122 (miRNA-122) with high resolution by using reduced gold nanoparticles dotted on reduced graphene oxide (rGO/Au) synthesized via natural soapnut solution. The successful synthesis of naturally reduced rGO/Au nanocomposite were confirmed through various characterization techniques like XRD, HR-TEM, RAMAN, etc [3]. Next the rGO/Au nanocomposite was coated on to the gold electrode and checked the electrochemical performance, the nanocomposite shows excellent bio-analytical performance to detect microRNA-122. The probe DNA was immobilized onto the binding sites of rGO/Au nanocomposite using covalent bond of thiol-Au and detected the target miRNA-122, the successful formation of DNA-RNA duplex and the recognition of target miRNA-122. The developed rGO/Au based electrochemical biosensor demonstrated an excellent wide linear range from 10 μ M to 10 pM with a detection limit of 1.73 pM. In conclusion, the developed biosensor shows good stability and reproducibility, could be used for the detection of miRNA-122 and can be used for the potential basic research and clinical studies related to cancer biomarker [4].

References

- [1] Selena et.al, Journal of Virology 2013, 87, 13
- [2] S.R. Torati et.al, Biosens. Bioelectron. 2016, 78, 483
- [3] Zhuo Guo et.al, Materials Science and Engineering C 2015, 57, 197
- [4] Satish Kasturi et.al, Journal of Industrial and Engineering Chemistry 2020, (article in press <https://doi.org/10.1016/j.jiec.2020.09.022>)

Development of magnetic–based pressure sensor for pulse pattern detection

Mijin Kim^{1*}, Sang-Hoon Shin², Sunjong Oh^{3†}, Cheolgi Kim^{1†}

¹DGIST, Emerging Materials Science

²Sangi University, Oriental Medical engineering

³Korea Institute of Machinery and Materials, Nature Simulation Application

[†]ssun@kimm.re.kr, cgkim@dgist.ac.kr

The pulse pattern appears as a superposition of the traveling wave and the reflected wave generated during the contraction and diastolic phase of the heart. Vascular diseases such as cardiovascular, cerebrovascular, coronary artery, and peripheral vascular disease are caused by the increase in stiffness as the elastic tissue of blood vessels decreases or destroys, the rate of pulse wave transmission increases and the maximum systolic blood pressure increases. Diagnosis is possible through pulse pattern analysis. Therefore, in this study, based on the existing high-resolution magnetic-based sensor, a pressure sensor for pulse pattern analysis was developed that precisely senses the pulse pattern while varying the external applied pressure applied to the object to be measured, and measures and analyzes the physical characteristics of blood vessels. In addition, a single pulse pattern measurement system was developed based on the development of a portable precision measurement electronic circuit that can monitor the exact physical blood vessel characteristics according to the patient's health status and static/dynamic pressure sensing element technology. It aims to develop a single system that can analyze the shape of the pulse pattern and infer the stiffness of blood vessels. This can be applied to the existing medical diagnosis monitoring electronics and sensor markets, and is expected to be applicable in markets such as next-generation medical equipment and sensors, flexible displays, and robotics.

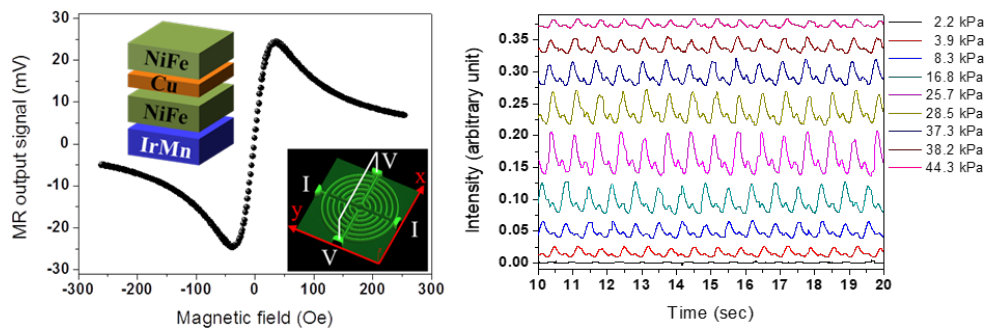


Fig. 1. Pulse signal according to applied pressure.

Author Index

Name	Abstract ID	Page	Name	Abstract ID	Page
Aga Shahee	MD17	56	Changsoo Kim	MD12	51
Aga Shahee	O-II-10	160	Changsoo Kim	O-II-9	159
A. G. Kolesnikov	츠S-I-1	3	Changsoo Kim	츠S-I-8	10
A. G. Kozlov	츠S-I-1	3	Chang-woo Cho	NS03	96
Akshay Kumar	MD09	48	Chang-Woo Cho	HM07	63
Albert M. Park	NS06	99	Chan-Kang Lee	MD04	42
Ara Go	츠S-II-6	126	Chan-Kang Lee	SO01	82
A. S. Samardak	츠S-I-1	3	Chanyong Hwang	HM07	63
A.S. Samardak	SM06	71	Chanyong Hwang	MD12	51
A. V. Davydenko	츠S-I-1	3	Chanyong Hwang	O-II-6	156
A. V. Gerasimenko	츠S-I-1	3	Chanyong Hwang	O-II-9	159
A. V. Ognev	츠S-I-1	3	Chanyong Hwang	츠S-I-8	10
A.V. Ognev	SM06	71	Cheolgi Kim	츠S-VII-4	224
A. V. Sadovnikov	츠S-I-1	3	CheolGi Kim	츠S-VII-1	221
A.V. Telegin	SM06	71	CheolGi Kim	츠S-VII-3	223
A. Yu. Samardak	츠S-I-1	3	Cheol-Ha Baek	MM01	105
Bappaditya Pal	츠S-I-1	3	Cheol-Ha Baek	SA01	111
B. -C. Min	MD15	54	Cheol-Ha Baek	츠S-VI-7	217
B. -C. Min	MD16	55	Chul-Jin Choi	HM06	62
Beom Hyun Kim	츠S-II-5	125	Chul-Jin Choi	O-III-3	199
B.I. Min	MT09	29	Chul-Jin Choi	O-III-5	201
B. Koteswara Rao	MD17	56	Chul-Jin Choi	O-III-6	202
Bo-Kyoung Song	츠S-VI-1	209	Chul-Jin Choi	츠S-III-2	144
Bon Heun Koo	MD09	48	Chung yeonjun	O-III-7	203
Bon Heun Koo	SM03	68	Chun-yeol You	MD11	50
Brahim Marfoua	O-I-5	135	Chun-Yeol you	MD04	42
Brahim Marfoua	O-I-9	139	Chun-Yeol You	MD03	41
Bum Seop Kim	츠S-IV-4	166	Chun-Yeol You	MD08	46
Byeong-Gyu Park	츠S-IV-7	169	Chun-Yeol You	MT04	24
Byeong-Kwon Ju	SO09	92	Chun-Yeol You	NS04	97
Byong-Guk Park	O-II-3	153	Chun-Yeol You	SO01	82
Byong-Guk Park	O-II-5	155	Chun-Yeol You	SO02	84
Byong-Guk Park	SO04	86	Chun-Yeol You	츠S-I-10	12
Byong-Guk Park	SO08	90	C. Won	MT17	37
Byong-Guk Park	SS06	80	Dae-Han Jung	MT13	33
Byong-Guk Park	츠S-I-2	4	Dae-Han Jung	MT15	35
Byong Sun Chun	츠S-I-8	10	Dae-Han Jung	MT16	36
Byoung-Chul Min	O-II-2	152	Dae-Han Jung	O-I-3	133
Byoung-Chul Min	O-III-9	205	Daeseong Choe	O-II-2	152
Byoung Sun Chun	O-II-9	159	Dae-Yun Kim	MD02	39
Byung Il Min	츠S-IV-1	163	Dae-Yun Kim	MT01	21
Chang Bae Park	O-II-10	160	David Muller	NS06	99
Chang-Bin Song	SM08	73	D. B. Lee	MT17	37
Changgu Lee	SO10	93	D. D. Cuong	ST01	100
Changhoon Lee	츠S-II-7	127	D. D. Cuong	츠S-I-7	9
Chang-Jin Yun	O-I-1	131	Deaseong Choe	O-III-9	205
Chang-Jin Yun	O-II-1	151	Deepak R. Patil	O-II-10	160

Name	Abstract ID	Page
D. H. Yun	MD15	54
D. H. Yun	MD16	55
D. J. Lee	MD15	54
D. J. Lee	MD16	55
Do Duc Cuong	O-I-8	138
Dohyoung Kim	SS06	80
Dohyoung Kim	츠S-I-2	4
Dong-Hee Han	MM01	105
Dong-Hwan Kim	MT08	28
Dong-Hwan Kim	O-III-2	198
Donghyeon Lee	MT12	32
Dong-Hyun Kim	츠S-V-6	179
Donghyun Lee	SO02	84
Dong-Kwan Kim	츠S-III-6	148
Dongryul Kim	MD11	50
Dong-Soo Han	SO07	89
Dongwon Choi	SO09	92
Dong-Woo Kang	MT08	28
Dongwook Go	츠S-I-2	4
Dong-Woo Nam	SA02	112
Dooyong Lee	HM07	63
Dorj Odkhuu	O-III-4	200
Dorj Odkhuu	O-III-10	206
Dorj Odkhuu	츠S-IV-5	167
Dorjsuren Tuvshin	O-III-4	200
Dorjsuren Tuvshin	O-III-10	206
D. Tuvshin	츠S-IV-5	167
Duc Duong Viet	MO01	102
Duck-Ho Kim	MD02	39
En-Jin Cho	츠S-IV-7	169
Eunbin Ju	츠S-VI-6	216
Eunchong Baek	MD04	42
Eunchong Baek	MD11	50
Eunchong Baek	츠S-I-10	12
Eun-Gook Moon	츠S-II-6	126
Eunkang park	SO03	85
Eunkang Park	MT04	24
Eunkang Park	MT12	32
Eunkang Park	SO02	84
Eunkang Park	SO04	86
Eunkang Park	SO05	87
Eunsook Lee	SS07	81
Eun-su An	MD10	49
Ganghwi Kim	O-I-3	133
Garam Park	NS04	97
Ga-Yeong Kim	O-III-2	198
Ga-Yeong Kim	츠S-III-6	148
Geun-Hee Lee	SO06	88
G Hye Kim	MT06	26
Gi-Ryeon Jo	HM02	58
Gi-Ryeon Jo	HM03	59
Gregory D. Fuchs	NS06	99

Name	Abstract ID	Page
Guihyun Han	MT03	23
Guihyun Han	MT05	25
Gukcheon Kim	MD08	46
Gyu Won Kim	O-II-4	154
Gyu Won Kim	SM06	71
Haein Choi-Yim	HM01	57
Haein Choi-Yim	SM01	66
Hae-Woong Kwon	츠S-III-6	148
Han-Jin Noh	츠S-IV-7	169
Hankuk-Jeon	O-III-3	199
Ha Yeong Ahn	HM09	65
H. C. Koo	MD15	54
H. C. Koo	MD16	55
Heechan Jang	MT12	32
Heechan Jang	SO02	84
Heechan Jang	SO03	85
Heechan Jang	SO05	87
Heejung Kim	MT09	29
Hee-Lack Choi	HM02	58
Hee-Ryoung Cha	O-III-1	197
Hee-Ryoung Cha	O-III-2	198
Hee-Ryoung Cha	츠S-III-6	148
Hee-Sung Han	MT10	30
Hee-Sung Han	MT13	33
Hee-Sung Han	MT14	34
Hee-Sung Han	MT15	35
Hee-Sung Han	MT16	36
Hee-Sung Han	NS01	94
Hee-Sung Han	O-I-3	133
Hee-Sung Han	SM02	67
Hee-Sung Han	SM07	72
H. G. Yoon	MT17	37
Ho-Beom Lee	츠S-VI-2	210
Ho-Joon Lee	츠S-V-6	179
Hongjae Moon	HM08	64
Ho-Sang Jung	MM02	106
Ho-Sang Jung	MM03	109
Hosub Jin	O-II-2	152
Howon Lee	츠S-II-3	123
Hui-Dong Qian	O-III-3	199
Hui-Dong Qian	O-III-5	201
Hui-Dong Qian	O-III-6	202
Hwi-Jun Kim	츠S-III-5	147
Hyegyung Kim	HM07	63
Hye-Jin Ok	NS01	94
Hye-Jin Ok	SM02	67
Hye-Jin Ok	SM07	72
Hyeon-Jong Park	O-II-5	155
Hyeonjung Jeong	O-III-9	205
Hyeonjung Jung	MD13	52
Hye-Won Ko	O-II-3	153
H. Y. Kwon	MT17	37

Name	Abstract ID	Page
Hyo-bin Anh	SO10	93
Hyoungjeen Jeon	O-III-8	204
Hyun Cheol Koo	O-II-2	152
Hyun Cheol Koo	SS02	75
Hyun Cheol Koo	SS03	76
Hyung-Jin Choi	O-II-2	152
Hyung-jun Kim	SS02	75
Hyung-jun Kim	SS03	76
Hyungyu Jin	츠O-I-1	185
Hyun-Joong Kim	MD12	51
Hyun-Jo Pyo	SA02	112
Hyunjun Shin	츠S-II-3	123
Hyun-Seok Whang	MT01	21
Hyun-Seok Whang	츠S-I-9	11
Hyunsol Son	SM01	66
Hyun-Sook Lee	HM08	64
Hyun-Woo Lee	O-II-2	152
Imran Khan	O-I-5	135
In Ho Cha	O-II-4	154
In-Ho Kim	SM08	73
In-Hwan Oh	NS04	97
Inseon Oh	MD13	52
Inseon Oh	O-II-2	152
Inseon Oh	O-III-9	205
Jae-Gyeong Yoo	O-III-1	197
Jae Hoon Kim	츠S-II-3	123
Jae-Hoon Park	MT09	29
Jaehun Cho	MD08	46
Jaehun Cho	NS04	97
Jaehun Cho	SO01	82
Jae-Hyun Kim	츠S-V-1	173
Jae-Sung Woo	츠S-V-6	179
Jae-Won Lee	MM02	106
Jae-Won Lee	MM03	109
Jae Yeol Park	O-II-5	155
J.D. Lee	츠S-IV-3	165
Je-An Yu	SM08	73
Jeehoon Jeon	SS02	75
Je-Geun Park	츠S-IV-6	168
Jeonghoon Shin	O-II-7	157
Jeonghun Shin	O-II-8	158
Jeong-Jong Lee	츠S-V-7	180
Jeong Kyu Lee	SM06	71
Jeong-Mok Kim	O-II-3	153
Jeongwoo Seo	O-II-7	157
Jeongwoo Seo	O-II-8	158
Jeong-Yeon Min	SA02	112
J.H. Shim	MT09	29
Ji Eun Lee	MD09	48
Ji Eun Lee	SM03	68
Ji Heon Seong	츠S-II-6	126
Jiho Kim	O-I-1	131

Name	Abstract ID	Page
Jiho Kim	O-II-1	151
Jihoon Kang	O-I-10	140
Jihoon Park	HM06	62
Jihoon Park	O-III-3	199
Jihoon Park	O-III-5	201
Jihoon Park	O-III-6	202
Jihoon Park	츠S-III-2	144
Ji Hoon Shim	츠S-II-7	127
Ji-Ho Park	O-II-3	153
Jimin Jeong	O-II-5	155
Jimin Jeong	SO08	90
Ji-Min Yu	MM02	106
Ji-Min Yu	MM03	109
Jin-A Kim	MD03	41
Jin-A Kim	츠S-I-10	12
Jingyu Yang	O-I-10	140
Jinhyung Cho	O-III-8	204
Jinki Hong	SS02	75
Jinpyo Hong	O-II-7	157
Jinpyo Hong	O-II-8	158
Jinwon Jeong	츠S-IV-7	169
Jinwon Jung	MD08	46
Jinyong Jung	NS04	97
Jisang Hong	O-I-5	135
Jisang Hong	O-I-9	139
Jiseok Yang	NS05	98
Ji-Seok Yang	MT04	24
Jisu Kim	MT04	24
Jisu Kim	SO02	84
Ji-Sung Jang	츠S-VI-2	210
Jisung Lee	HM07	63
Jisung Lee	NS03	96
Ji-Sung Yu	MD02	39
Ji-Sung Yu	MD05	43
Ji-Wan Kim	MD14	53
Jiwoong Kim	NS03	96
Jiyoung Jang	NS05	98
Jong-Guk Choi	O-II-5	155
Jong-Han Won	HM07	63
JongHee Han	HM01	57
Jong-Hwan Cho	MT08	28
Jongill Hong	츠S-I-3	5
Jongmin Lee	SO03	85
Jong Min Yuk	O-II-5	155
Jong-Ryul Jeong	HM09	65
Jong-Ryul Jeong	MO01	102
Jong-Ryul Jeong	SO06	88
Jong-Seok Byeon	MM01	105
Jongsun Park	츠S-I-4	6
Jong-Woo Kim	HM06	62
Jong-Woo Kim	O-III-3	199
Jong-Woo Kim	O-III-5	201

Name	Abstract ID	Page
Jong-Woo Kim	츠S-III-2	144
Joomin Kim	O-I-10	140
Joong-Woo Lee	MD17	56
Joonhyuk Lee	O-III-8	204
Joonki Suh	O-III-9	205
Joon Moon	MD02	39
Joon Moon	MD05	43
Joonwoo Kim	NS04	97
Joonwoo Kim	SO01	82
Joonyeon Chang	SS03	76
Joonyoung Choi	NM01	101
Jooyoon Kim	츠S-I-4	6
Jouhahn Lee	HM07	63
J. -S. Kang	SS07	81
Ju-Hyeong Moon	MT08	28
June-seo Kim	MD08	46
June-Seo Kim	NS04	97
June-Seo Kim	SO01	82
Jung Dae Kim	SO10	93
Jung-Goo Lee	O-III-1	197
Jung-Goo Lee	O-III-2	198
Jung-Goo Lee	츠S-III-4	146
Jung-Goo Lee	츠S-III-6	148
Jung-Hyun Park	MT01	21
Jung-Il Hong	MD12	51
Jung-Il Hong	SO05	87
Jungmin Park	MD01	38
Jungmin Park	O-II-2	152
Jungmin Park	O-III-9	205
Jungmin Park	SO10	93
Jung Tae Lim	HM06	62
Jung Tae Lim	O-III-3	199
Jung Tae Lim	O-III-5	201
Jung Tae Lim	O-III-6	202
Jung-Woo Jeong	츠S-VI-1	209
Jung-Woo Yoo	MD13	52
Jung-Woo Yoo	O-II-2	152
Jung-Woo Yoo	O-III-9	205
Jungyup Yang	O-II-7	157
Jungyup Yang	O-II-8	158
Jun-Ho Kang	SS06	80
Junho Park	HM05	61
Junho Park	SM06	71
Junho Seo	MD10	49
Junhyeon Jo	O-II-2	152
Junhyeon Jo	O-III-9	205
Jun-Seok Lee	MM02	106
Jun-Seok Lee	MM03	109
Jun-Su Kim	MD08	46
Jun Sung Kim	MD10	49
Jun Sung Kim	츠S-II-1	121
Jun-Yeol Ryu	츠S-V-8	181

Name	Abstract ID	Page
Jun-Young Chang	MD02	39
J. W. Choi	MT17	37
Kab-Jin Kim	MT04	24
Kab-Jin Kim	NS05	98
Kab-Jin Kim	O-I-4	134
Kab-Jin Kim	O-II-3	153
Kab-Jin Kim	SO06	88
Kab-Jin Kim	SS06	80
Kab-Jin Kim	츠S-I-2	4
Kang-Hyuk Lee	HM05	61
Kanguk Jin	O-I-10	140
Kee Hoon Kim	MD17	56
Kee Hoon Kim	O-II-10	160
Keesung Kim	츠S-I-3	5
Kicheon Kang	츠S-IV-2	164
Ki-Deok Lee	츠S-V-7	180
Kim Gap Jung	츠S-VI-5	215
Kim Jeong Ho	츠S-VI-5	215
Kim jongryul	O-III-7	203
Kim shingyu	O-III-7	203
Kim youngmin	O-III-7	203
Kiran Shinde	MD07	45
Ki-seung Lee	MD11	50
Ki-Seung Lee	MD03	41
Ki-Seung Lee	MD04	42
Ki-Seung Lee	MT04	24
Ki-Seung Lee	츠S-I-10	12
Ki-Suk Lee	MT10	30
Ki-Suk Lee	MT13	33
Ki-Suk Lee	MT14	34
Ki-Suk Lee	MT15	35
Ki-Suk Lee	MT16	36
Ki-Suk Lee	NS01	94
Ki-Suk Lee	O-I-3	133
Ki-Suk Lee	SM02	67
Ki-Suk Lee	SM07	72
Ki-Yeon Kim	NS04	97
Ki-Young Lee	SO09	92
K. -J. Lee	MD15	54
K. -J. Lee	MD16	55
Kungwon Rhie	O-I-1	131
Kungwon Rhie	O-II-1	151
Kwanghyun Chung	츠S-III-2	144
KwangHyun Lee	SO01	82
Kwangsuk Kim	SO02	84
Kwangsuk Kim	SO10	93
Kwang-Tak Kim	MD17	56
Kwang-Yong Choi	츠S-II-4	124
Kwan-Woo Lee	츠S-IV-8	170
Kwnojin Park	NS04	97
Kyoo Kim	MT09	29
Kyoo Kim	츠S-IV-7	169

Name	Abstract ID	Page
Kyoung-Soo Cha	츠S-V-1	173
Kyoung Soon Choi	HM07	63
Kyoung-Woong Moon	MD12	51
Kyoung-Woong Moon	O-II-9	159
Kyoung-Woong Moon	츠S-I-8	10
Kyung-Hwan Jung	MM01	105
Kyung Ik Sim	츠S-II-3	123
Kyung Jae Lee	NS05	98
Kyung-Jin Lee	O-II-3	153
Kyung-Jin Lee	O-II-5	155
Kyung-Jin Lee	츠S-I-5	7
Kyung Mee Song	SO10	93
Kyung Mox Cho	O-III-3	199
Kyusung Hwang	츠S-II-6	126
Lijun Zhu	NS06	99
Mahmut Okyay	츠S-IV-4	166
Mariam Omran	NM01	101
Mi-Jin Jin	O-II-2	152
Mi-Jin Jin	O-III-9	205
Mijin Kim	츠S-VII-4	224
Min-gu Kang	SO04	86
Min-Gu Kang	O-II-5	155
Min-Gu Kang	SO08	90
Min-Gu Kang	츠S-I-2	4
Mingu Kim	O-I-1	131
Min Gyu Park	O-I-4	134
Min Hyeok Lee	O-II-4	154
Min-Jae Jeong	SA02	112
Min-Ji Pyo	HM02	58
Min-Ji Pyo	HM03	59
Min Ji Shin	MD09	48
Min Ji Shin	SM03	68
Minkyu Park	MT03	23
Minkyu Park	MT05	25
Minkyu Park	O-I-8	138
Min-Ro Park	츠S-V-1	173
Min-Woo Lee	츠S-III-5	147
Mi-Young Im	NS01	94
Mi-Young Im	O-I-3	133
Mi-Young Im	SM02	67
Mi-Young Im	SM07	72
Moojune Song	O-I-4	134
Myeonghwan Kang	NS01	94
Myeonghwan Kang	O-I-3	133
Myeonghwan Kang	SM02	67
Myeonghwan Kang	SM07	72
Myung-Hwan Yoon	츠S-V-7	180
Myung Joon Han	츠S-II-2	122
Myung-Seop Lim	츠S-V-1	173
Myung-Seop Lim	츠S-V-8	181
Namkyu Kim	MT10	30
Namkyu Kim	MT13	33

Name	Abstract ID	Page
Namkyu Kim	MT14	34
Namkyu Kim	MT15	35
Namkyu Kim	MT16	36
Namkyu Kim	NS01	94
Namkyu Kim	O-I-3	133
Namkyu Kim	SM02	67
Namkyu Kim	SM07	72
Nguyen Thi Thanh Huong	SO05	87
Nguyen Van Quang	SO05	87
Nikita Ter-Oganessian	O-II-10	160
Noejung Park	츠S-IV-4	166
Nuri Hyun Jung	츠S-VI-6	216
Nyun Jong Lee	MT04	24
Nyun Jong Lee	MT12	32
Nyun Jong Lee	SO02	84
Nyun Jong Lee	SO03	85
Nyun Jong Lee	SO05	87
Nyun Jong Lee	SO10	93
O. J. Lee	MD15	54
O. J. Lee	MD16	55
Oleg A. Tretiakov	츠S-I-1	3
OukJae Lee	SS02	75
Phuoc Cao Van	HM09	65
Phuoc Cao Van	MO01	102
Phuoc Cao Van	SO06	88
Pil-Hyun Jeon	츠S-VI-7	217
Qurat ul Ain	MT06	26
Quynh Anh T. Nguyen	O-II-4	154
Quynh Anh T. Nguyen	ST01	100
Quynh Anh T. Nguyen	츠S-I-7	9
Sanghan Lee	SO03	85
Sanghoon Kim	MT02	22
Sanghoon Kim	MT04	24
Sanghoon Kim	MT12	32
Sanghoon Kim	SO02	84
Sanghoon Kim	SO03	85
Sanghoon Kim	SO04	86
Sanghoon Kim	SO05	87
Sanghoon Kim	SO10	93
Sanghoon Kim	SS06	80
Sanghoon Kim	츠S-I-2	4
Sanghoon Lee	NS05	98
Sang-Hoon Shin	츠S-VII-4	224
Sang-Im Yoo	HM05	61
Sang-Koog Kim	츠S-III-3	145
Sang-Uk Kim	SM08	73
Sang Wook Han	SS07	81
S. A. Nikitov	츠S-I-1	3
San Ko	O-I-4	134
Satish Kasturi	츠S-VII-1	221
Satish Kasturi	츠S-VII-3	223
S. C. Hong	MT02	22

Name	Abstract ID	Page
S. C. Hong	O-I-8	138
S. C. Hong	ST01	100
S. C. Hong	츠S-I-7	9
S. C. Hong	츠S-IV-5	167
Seen-Young Kang	MM02	106
Seen-Young Kang	MM03	109
Sehee Lee	O-II-6	156
Sehwan Song	NS03	96
Se-Hyun Rhyu	츠S-V-7	180
Seiji Yunoki	츠S-II-5	125
Se-Jeong Park	HM07	63
Se Kwon Kim	O-II-3	153
Seo-Hee Yang	SA02	112
Seo Jeong Min	츠S-VI-5	215
Seok Hwan Huh	SM03	68
Seong Been Kim	SS02	75
Seong Been Kim	SS03	76
Seongboo Park	MT04	24
Seonghoon Woo	SO09	92
Seong-Hyeon Kang	츠S-VI-4	214
Seong-Hyub Lee	MD02	39
Seong-Hyub Lee	MD05	43
Seulgi Koo	MD01	38
Seungho Seong	SS07	81
Seunghyeop Baek	츠S-VI-6	216
Seung-Hyub Baek	O-II-2	152
Seung-Jae Lee	SA01	111
Seungmo Yang	HM07	63
Seungmo Yang	MD12	51
Seungmo Yang	O-II-9	159
Seungmo Yang	츠S-I-8	10
Seung-Youl Lee	MM02	106
Seung-Youl Lee	MM03	109
Seung-Young Park	MD01	38
Seyeob Jeong	SO10	93
Seyeop Jeong	SO02	84
SeYeop Jeong	SO03	85
Seyeop Jung	MT12	32
Seyeop Jung	SO05	87
Seyeop Jung	SS06	80
Shigetoshi Sota	츠S-II-5	125
Shin-Ik Kim	O-II-2	152
S. H. Rhim	MT02	22
S. H. Rhim	MT03	23
S. H. Rhim	MT06	26
S. H. Rhim	O-I-8	138
S.H. Rhim	MT05	25
S. M. Park	MT17	37
Sohyun Ahn	츠S-VI-6	216
Songhyup Kang	O-I-10	140
Sonny H. Rhim	O-II-4	154
Sonny H. Rhim	ST01	100

Name	Abstract ID	Page
Sonny H. Rhim	츠S-I-7	9
Soogil Lee	SO04	86
Soogil Lee	SS06	80
Soogil Lee	츠S-I-2	4
Soo-Gyung Lee	츠S-V-1	173
Soo-Gyung Lee	츠S-V-8	181
Soo-Hwan Park	츠S-V-1	173
Soo-Hwan Park	츠S-V-8	181
Soon Cheol Hong	MT05	25
Soon Cheol Hong	MT06	26
Soon Cheol Hong	O-III-4	200
Soon Cheol Hong	O-III-10	206
Soon Cheol Hong	SS07	81
Soon Cheol Hong	츠S-III-2	144
Soong-Geun Je	MD12	51
Soong-Geun Je	NS01	94
Soong-Geun Je	SM02	67
Soong-Geun Je	SM07	72
Sooran Kim	MT09	29
Sooseok Lee	MT13	33
Sooseok Lee	NS01	94
Sooseok Lee	O-I-3	133
Sooseok Lee	SM02	67
Sooseok Lee	SM07	72
SooSeok Lee	MT10	30
SooSeok Lee	MT14	34
Sri Ramulu Torati	츠S-VII-1	221
Sri Ramulu Torati	츠S-VII-3	223
Stefano Sanvito	T-2	16
Sug-Bong Choe	MD02	39
Sug-Bong Choe	MD05	43
Sug-Bong Choe	MT01	21
Sug-Bong Choe	츠S-I-9	11
Suhyeok An	MD03	41
Suhyeok An	MD04	42
Suhyeok An	MD11	50
Suhyeok An	츠S-I-10	12
Sujin Jo	SO09	92
Suk Hee Han	SS02	75
Suk-Min Hong	O-II-2	152
Sumin Kim	HM08	64
Sung-Gu Lee	MT08	28
Sung-Hyeok Wi	츠S-V-8	181
SungJoon Choi	HM05	61
Sung Kyu Jang	O-I-4	134
Sungkyun Park	HM07	63
Sungkyun Park	NS03	96
Sungkyun Park	O-II-9	159
Sunglae Cho	SO05	87
Sung-min Kim	츠S-VI-2	210
Sung-Woo Hwang	츠S-V-8	181
Sungyu Park	MD10	49

Name	Abstract ID	Page
Sunjong Oh	츠S-VII-4	224
Su Yeon Ahn	HM06	62
Su Yeon Ahn	O-III-3	199
Su Yeon An	MT05	25
Suyeong Jeong	MT13	33
Suyeong Jeong	O-I-3	133
Suzuki Ippei	MT12	32
Tae-Eon Park	SO10	93
Tae-Haeng Lee	SM08	73
Taehee Kim	O-II-6	156
Tae Heon Kim	SO03	85
Tae-Hoon Kim	O-III-1	197
Tae-Hoon Kim	O-III-2	198
Tae-Hoon Kim	츠S-III-4	146
Taehwan Kim	츠S-I-4	6
Taehyun Kim	O-II-4	154
Taekhyeon Lee	MT04	24
Taekhyeon Lee	츠S-I-2	4
Tae-Seong Ju	HM07	63
Tae-Seong Ju	O-II-9	159
Tae-Seong Ju	츠S-I-8	10
Taeyueb Kim	SS02	75
Taiwoon Eom	MD01	38
Takahashi Yukiko	MT12	32
Takasada Shibauchi	츠S-II-6	126
Thi Huynh Ho	MT02	22
Thi-Nga Do	O-II-6	156
Thu-Thuy Hoang	O-I-8	138
Tian Hong Zhou	O-III-3	199
Tien Van Manh	MD07	45
T. Ochirkhuyag	츠S-IV-5	167
Tomonori Shirakawa	츠S-II-5	125
Trinh Nguyen Thi	HM09	65
Trinh Nguyen Thi	MO01	102
Trinh Thi Ly	SO10	93
T. Tsevelmaa	츠S-IV-5	167
Tumentsereg Ochirkhuyag	O-III-4	200
Tumentsereg Ochirkhuyag	O-III-10	206
V.B. Bessonov	SM06	71
Viet Dongquoc	MO01	102
Voma Uday Kumar	MD17	56
Weilun Chao	NS01	94
Weilun Chao	SM02	67
Weilun Chao	SM07	72
Won-Chang Choi	MD12	51
Won-Ho Kim	SA02	112
Won Seok Yun	SS07	81
Woojong Kim	O-II-7	157
Woo-Ri Ju	츠S-IV-7	169
Woo Sang Ahn	츠S-VI-6	216
Woo-Yeong Kim	MD04	42
Woo-Yeong Kim	MD08	46

Name	Abstract ID	Page
Woo-yeoung Kim	MD11	50
Wooyoung Lee	HM08	64
Wooyoung Lee	츠S-III-1	143
Xiyue S. Zhang	NS06	99
Yang-Do Kim	O-III-1	197
Yang-Do Kim	O-III-2	198
Yang Yang	HM06	62
Yang Yang	O-III-3	199
Yang Yang	O-III-5	201
Y. J. Choi	츠S-II-3	123
Yong Jin Kim	O-II-4	154
Yooleemi Shin	MD14	53
Young-Guk Son	HM03	59
Young-Han Shin	MT04	24
Younghun Jo	MD01	38
Younghun Jo	O-III-9	205
Youngjin Lee	츠S-VI-4	214
Young Keun Kim	O-II-4	154
Young Keun Kim	SM06	71
Youngkuk Kim	T-3	17
Young-Rok Jang	츠S-IV-2	164
Young-Sang Yu	SM02	67
Young-Sang Yu	SM07	72
Young-Woo Son	츠S-II-5	125
Younjung Jo	NM01	101
Youn-Kyoung Baek	HM02	58
Youn-Kyoung Baek	HM03	59
Yumin Kang	츠S-VII-1	221
Yune-Seok Nam	MT01	21
Yunho Jang	츠S-I-4	6
Yunji Eom	츠S-VII-1	221
Yun Ji Eom	츠S-VII-3	223
Zhen Chen	NS06	99
강동우	SA03	115
강범승	SS01	74
강예빈	SM04	69
강지훈	O-I-7	137
고현철	츠S-VI-3	212
공선희	SM04	69
권철민	O-I-7	137
김경모	O-I-2	132
김경원	SA04	117
김광용	츠S-V-2	175
김규원	츠S-I-1	3
김기성	SS01	74
김동영	NS02	95
김동욱	츠S-V-2	175
김동현	MD07	45
김민구	O-I-6	136
김상면	츠S-V-4	177
김상우	SM04	69
김성일	츠S-V-2	175

Name	Abstract ID	Page
김성호	초S-VI-3	212
김양도	HM04	60
김영래	SS04	78
김영래	초S-I-6	8
김예래	SM05	70
김용진	초S-I-1	3
김재민	O-I-2	132
김주란	SS05	79
김지호	O-I-6	136
김창수	MT11	31
김철기	초S-VII-2	222
김태훈	HM04	60
김해중	초S-V-3	176
김현설	초S-VII-2	222
김현중	MT11	31
김효준	초S-V-4	177
김희중	초O-I-1	189
노태성	HM04	60
문경웅	MT11	31
박경배	초S-I-6	8
박덕근	O-I-2	132
박창배	SS05	79
방승환	BM01	103
배규성	초S-VI-3	212
배서현	초S-VI-3	212
서호건	O-I-2	132
손대락	T-1	15
신광호	SA04	117
신정우	O-I-2	132
안지훈	SM04	69
양승모	MT11	31
우혁준	SM05	70
유성초	MD07	45
유세종	초S-VI-3	212
유재원	초S-VI-3	212
윤명환	초S-V-3	176
윤석수	NS02	95
윤종환	초S-VII-2	222
윤창진	O-I-6	136
이근호	초S-V-2	175
이금원	O-I-6	136
이동열	SA03	115
이민영	SM05	70
이민호	O-I-7	137
이보화	SM04	69
이보화	SM05	70
이상선	SS05	79
이상호	SS01	74
이승훈	MD06	44
이영국	초O-II-1	193
이정구	HM04	60
이정중	초S-V-3	176

Name	Abstract ID	Page
이준규	MT07	27
이현숙	BM01	103
이훈기	초S-V-5	178
임병화	초S-VII-2	222
임상호	SS04	78
임상호	초S-I-6	8
임성현	MT07	27
전민철	초S-VI-3	212
정우현	SM05	70
정지윤	O-I-7	137
정현근	초S-VI-3	212
정효연	MD06	44
차인호	초S-I-1	3
차희령	HM04	60
최광수	MD06	44
최원창	MT11	31
최유경	BM01	103
최장영	초S-V-5	178
트라티라무	초S-VII-2	222
허희선	O-I-7	137
홍순철	MT07	27
홍정일	MT11	31
홍종일	SS01	74
황찬용	MT11	31
황찬용	SS05	79
후싱하오 초	S-VII-2	222



Digests of the KMS 2020 Winter Conference
The Korean Magnetics Society
사단법인 한국자기학회

2020년도 동계학술연구발표회 논문개요집

제 30권 2호

(06130) 서울특별시 강남구 테헤란로 7길 22(역삼동635-4) 한국과학기술회관 신관 905호

TEL. (02)3452-7363, **FAX.** (02)3452-7364

E-mail. komag@unitel.co.kr, **Home-page.** www.komag.org



New Cryogen Free 7 Tesla Magneto-Optical Cryostat



Cryogen Free

Temperature Range: 1.7 K to 350 K

7 T Split-Coil Conical Magnet

Low Vibration: <10 nm Peak-to-Peak

89 mm x 84 mm Sample Volume

Automated Temp. & Magnet Control



Quantum Design